

Impact of Three-dimensional Photovoltaic Structure on Solar Power Generation



Mafimidiwo Olufunmilayo Alice

212562244

A thesis submitted in fulfilment of the academic requirements
for the degree of Doctor of Philosophy in Electrical Engineering

In the

School of Engineering
University of KwaZulu-Natal
Durban, South Africa

**IMPACT OF THREE-DIMENSIONAL PHOTOVOLTAIC
STRUCTURE ON SOLAR POWER GENERATION**

SUBMITTED BY

Olufunmilayo Alice Mafimidiwo

IN FULFILMENT OF THE DEGREE OF

**Doctor of Philosophy in Electrical Engineering from the University of KwaZulu-
Natal**

Durban, South Africa

DATE OF SUBMISSION

November, 2016

SUPERVISED BY

Dr. Akshay Kumar Saha

As the candidate's Supervisor, I agree to the submission of this thesis.

Signed:

Name:

Date:

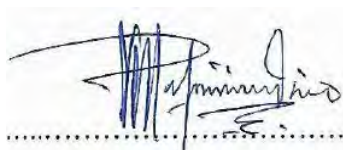
UNIVERSITY OF KWAZULU-NATAL
COLLEGE OF AGRICULTURE, ENGINEERING AND SCIENCE

DECLARATION 1 - PLAGIARISM

I, OLUFUNMILAYO ALICE MAFIMIDIWO, declare that:

1. The research reported in this thesis, except where otherwise indicated, is my original research.
2. This thesis has not been submitted for any degree or examination at any other university.
3. This thesis does not contain other persons' data, pictures, graphs or other information, unless specifically acknowledged as being sourced from other persons.
4. This thesis does not contain other persons' writing, unless specifically acknowledged as being sourced from other researchers. Where other written sources have been quoted, then:
 - a. Their words have been re-written but the general information attributed to them has been referenced.
 - b. Where their exact words have been used, then their writings have been placed in italics and inside quotation marks, and referenced.
5. This thesis does not contain text, graphics or tables copied and pasted from the Internet, unless specifically acknowledged, and the source being detailed in the thesis and in the References sections.

Signed:

A handwritten signature in blue ink, appearing to read 'Olufunmilayo Alice Mafimidiwo', is written over a horizontal dotted line.

UNIVERSITY OF KWAZULU-NATAL
COLLEGE OF AGRICULTURE, ENGINEERING AND SCIENCE

DECLARATION 2 - PUBLICATIONS

DETAILS OF CONTRIBUTION TO PUBLICATIONS AND CONFERENCE PRESENTATIONS that form part and/or include research presented in this thesis (include publications in preparation, submitted, *in press* and published and give details of the contributions of each author to the experimental work and writing of each publication)

Published Journal for May 2016 Publication:

O.A. Mafimidiwo and A.K. Saha “Incorporating three dimensional Photovoltaic structure for optimum solar power generation - the effect of height” in DOHET, *Journal of Energy in Southern Africa (JESA)*. ISSN: 1021 447X, Volume 27 Number 2 • May 2016

Publication 2:

O.A. Mafimidiwo and A.K. Saha “The Challenges of Sustainable Energy Development In Developing Nation – A Case Study of Nigeria”, Proceedings of the 21st *Southern African Universities Power Engineering Conference (SAUPEC)*, 31 January and 1 February 2013, North-West University, Potchefstroom, South Africa, pp. 294-300; print ISBN: 978-1-86822-631-3

Publisher: Southern African Universities Power Engineering Conference.

Publication 3:

O.A. Mafimidiwo and A.K. Saha “Improving Solar Energy Generation Through the use of Three-dimensional Photovoltaics Technology, Proceedings of the 22nd *Southern African Universities Power Engineering Conference (SAUPEC) – Digital Edition*, 30 – 31 January 2014, University of KwaZulu-Natal, Durban, South Africa, pp. 294-300; print ISBN: 978-1-86840-619-7

Publisher: Southern African Universities Power Engineering Conference.

Publication 4:

O.A. Mafimidiwo and A.K. Saha “Impact of Solar Power Generation on Economic Growth – The Role of Three-dimensional Photovoltaic Structure” Proceedings of the 24th *Southern African Universities Power Engineering Conference (SAUPEC)*, 26 - 28 January 2016, Vaal University of Technology and South African Institute of Electrical Engineers, Vereeniging, South Africa, pp. 570-575 (6B-3); print ISBN: 978-1-77012-386 , Publisher: Southern African Universities Power Engineering Conference.

Conference Presentation: 2014 Postgraduate Research Day

O.A. Mafimidiwo and A.K. Saha “Three-Dimensional Photovoltaic Structure – Its Impact on Solar Power Generation” being a conference paper presented at the *Postgraduate Research Day, College of Agriculture, Engineering and Science, University of KwaZulu-Natal, Durban, South Africa Howard College Campus* in October, 2014.

ADDITIONAL JOURNAL PAPERS ALREADY SUBMITTED:

Submitted Journal 1 – Undergoing corrections

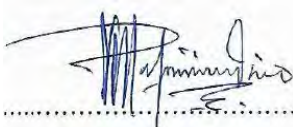
O.A. Mafimidiwo and A.K. Saha “Generating optimum solar output energy with Three-dimensional Photovoltaic system - the effect of solar radiation” being a submitted Manuscript for DOHET Journal publication, *African Journal of Science, Technology, Innovation and Development (AJSTID)*.

Date of submission: 2nd September, 2015.

Submitted Journal 2:

O.A. Mafimidiwo and A.K. Saha “Optimising thermal photovoltaic energy system for green and sustainable energy generation” being a submitted Manuscript for DOHET Journal publication, *Journal of Energy in Southern Africa (JESA)*.

Date of submission: May, 2016.

Signed: 

DEDICATION

This work is dedicated as follows:

First and foremost, to the Glory of God Almighty through His only begotten son Jesus Christ, who grants the Grace and enablement and makes everything possible for me, according to the faithfulness of His promise and Glory of His name.

To my loving husband, my confidant, trusted, proven and best friend, Mr Bamidele Adeniyi Mafimidiwo, for his unflinching love and support at all times and for his encouragement all along. I thank you for believing in me, for standing by me at all times, for continuously being a loving husband and a caring father to our children – Olugbenga, Oluwaseyi, Ololade and Omotunde who also have shown great understanding and have given their support all through these years.

To the cherished memories of my late parents, Pa Michael Ariyibi Soyebi and Mrs Janet Amoke Modupeola Soyebi for the legacy they left behind. The teachings and discipline they instilled in me have propelled me thus far. My late sister, Esther Oluranti Folami, I will ever appreciate the motherly role you took over and did perfectly well. Your memories remain evergreen.

To Dr. Samuel Ayodele Iwarere – for your immense supports in every way possible and your encouragement all through to the completion of this work. You are part of my testimonies.

PREFACE

This research was carried out by Olufunmilayo Alice Mafimidiwo under the supervision of Dr. Akshay Kumar Saha in the school of Engineering, the Discipline of Electrical, Electronic and Computer Engineering, University of KwaZulu-Natal (UKZN), Durban, South Africa.

This thesis was designed to determine the impact of three-dimensional photovoltaic structure on solar power generation. The research into this area of power generation is very appropriate particularly at this time when the fossil energy source faces the risk of being exhausted, coupled with its negative impact on the environment and the worldwide call for alternative energy sources.

Solar energy is not only a renewable and alternative energy source but it is also sustainable, freely-given, on-the-spot available and accessible, thereby reducing generation cost particularly for a stand-alone system. While solar power is generated, the heat which could have otherwise been lost is available for harnessing for use in other areas of needs such as in geysers, steam washing and the like.

While expectation is high on the use of solar power, it is yet to be widely used due to its low efficiency and relatively high cost. Various researches have been carried out on solar energy optimisation and utilization and research is still on-going. The recent research work on solar energy incorporates the use of three-dimensional analysis. Three-dimensional study into solar power generation is an innovation to enable multiple source collection of solar energy for optimum power generation.

More awareness has been called for in order to promote effective use of solar energy and continuous research and development has translated into reduced-cost of photovoltaic solar energy, wider acceptability and integration into major power projects. Over the years, photovoltaic energy cost has reduced but the levelised cost of electricity (LCOE) still requires more attention. At present, PV energy costs stands at less than 1% of what it used to be in the past. Solar energy cost is indicated in this work in South African Rand for better evaluation since the research work is carried out in South Africa and examined by South African readers.

Different technologies to harness solar energy for human utilisation are available but the technology involving the concentrated thermal photovoltaic (CTPV) system or the direct photovoltaic (PV) use for power generation, rank high in importance due to the fact that they are the two most developed and most commonly used solar energy technologies. This has been the motivation to research into this area of study. Improving on their present status will represent a significant contribution to solar energy utilization.

The essence of this thesis was to model the PV power systems (the concentrated and non-concentrated) in three-dimensions and to be able to establish the conditions under which the thermal system of the photovoltaic study would maximise the input energy source, the optical radiation and heat transfer that would be required to improve the efficiency and output power of the solar power generation.

Six publications have been generated and submitted from this thesis. One has been accepted for publishing in May, 2016 while three have been published in peer reviewed conference proceedings. These include one article being accepted for publishing in May 2016 in the *Journal of Energy in Southern Africa* (JESA), three articles already published in peer reviewed conference proceedings of *Southern African Universities Power Engineering Conference* (SAUPEC) and two additional papers are already

submitted, one to the *African Journal of Science, Technology, Innovation and Development* (AJSTID) and the other one to *the Journal of Energy in Southern Africa* (JESA).

ACKNOWLEDGEMENTS

First and foremost, my acknowledgement goes to God Almighty, the Creator of ALL THINGS in heaven and on earth and to whom ALL power belongs – for His faithfulness, grace, love, enablement and provision in all ways and at all times and for walking with me and strengthening me all through the journey to the completion of my PhD programme. He has seen me through it all, encouraged me when challenges stood in the way and strength was at a low ebb. He has been with me and seen me through them ALL. HE is indeed God of ALL possibilities - Jeremiah 32:17, Luke 1:37.

I express my appreciation to my Supervisor, Dr Akshay Kumar Saha for his efforts, advice, and supervision. For being available for consultation and his valuable suggestions from time to time. In addition to all these, for his concern for my general welfare and wellness. Thank you sir.

I also express my appreciation to the Academic leader for the discipline of Electrical, Electronic and Computer Engineering, Professor Thomas Joachim Odhiambo Afullo, for his encouragement, motivation and for constantly reminding every student including me, of the reason for being in school and of the need for finishing in good time. That has always been a motivation for me and has kept me on my toes at all times. I appreciate your contribution, sir.

I acknowledge and appreciate Mrs Kehinde Akinsanya, whom God used as a link to this noble University of KwaZulu-Natal and who provided me with the necessary information that kick-started me on this journey to the story that is being told today, thank you so much. In addition, I acknowledge all my dear friends for your love, encouragement, generous support and prayers - Professor (Mrs) Olubola Babalola, Dr. (Mrs) Lauretta Ofodile, Mrs Olubunmi Falilat Idowu, Mrs Omolara Ogunmola, Mrs Olusina Taiwo, Mrs Chinyere Atta, Mrs Victoria Amaka Okeke, Mrs Yetunde Olaitan Idowu, Mrs Olabisi Lawson, Mrs Adeola Dosunmu, Mrs T. Olubunmi Adegbile and Mrs Bose Christiana Dacosta to mention but a few. For others not listed, I hold you all dear to my heart and appreciate you all a great deal – Thank you all.

My special acknowledgement goes to Professor Matthew Biodun Dayomi, who whole-heartedly took everything upon himself to provide all logistical support, advice, guidance, other support in so many ways during my admission processes and all through the period of my study at the University and for his continuous interest in my safety, well-being and general welfare from time to time. In addition, due acknowledgement is rendered to Dr. Abubakar Mobolaji Olaseni for his interest, encouragement and guidance during my admission processes and thereafter. Thank you sir.

I greatly appreciate the Rector, Dr (Mrs) Margaret Kudirat Ladipo and the entire management staff, Yaba College of Technology, Yaba Lagos Nigeria, for granting me the permission for study leave and for supporting me throughout the period of my doctoral programme. In particular, I acknowledge the encouragement received from the College Registrar, Mrs Biekoroma Charity Amapakabo, the Deputy Rector, Academic, Mr Innocent Akhuemonkhan and the Dean of Engineering, Dr. Engr. W.O. Adedeji. I acknowledge every member of staff and student of the Department of Electrical/Electronic Engineering, for their love and comradeship.

I express my profound acknowledgement and appreciation to the management of Tertiary Education Trust Fund (TETFund) Nigeria, for the financial grant extended to me on this programme. I am very grateful.

My dear uncle, Mr Babarinu Adeeye Falode, I can never forget you. You singled me out and gave me every support for my education. You have been my motivator and given me much encouragement. I thank God for your influence in my life. God bless and reward you abundantly. My sincere acknowledgement also goes to my uncle and aunty, Professor James Adewuyi Akinwumi and Mrs Eniola Akinwumi for your mentorship, encouragement and the leadership role you played in my life. I appreciate you both.

Due acknowledgement is rendered to my uncle and his wife, Mr Joseph Oluyomi Nadi and Mrs Victoria Folake Nadi. You have both been wonderful. Thank you for your love, prayers, encouragement and unflinching support to my family. You are highly appreciated.

I appreciate you, Elder Isaac Oluwatosin Famurewa and Deaconess Esther Eniola Famurewa for your love, support, prayers and inspiration to me and my entire family. I bless God for your exemplary lives, your affection and impact on me and my family and for us having the same heritage in Christ Jesus. You have both been a source of blessings to me and my family. You are both appreciated.

I acknowledge my Spiritual mentor, the Senior Pastor, Foursquare Gospel Church (The Sanctuary of Praise), YabaTech Area - Pastor (Mrs) Gladys Adenike Ariyibi, the Pastorate, the Church arm and my family members in the Lord. I appreciate you all for your unflinching support, prayers, for keeping in constant touch with me, for your words of encouragement at all times and for being there for me and my family at all times. I appreciate everyone.

I appreciate all my friends at the University of KwaZulu-Natal, Durban, consisting of my colleagues from Yaba College of Technology, Yaba Lagos, Nigeria and those from various other Universities. Our coming closer together has really impacted on one another for the better. Your interesting views and opinions have shed light on my perspectives and given me encouragement even up till now. Coming together is really a privilege which I cherish. I appreciate all of you.

My unreserved appreciation to Dr Samuel Ayodele Iwarere and his family. You have had a positive impact on me in no small measure. You are a blessing to me. I really appreciate you. The Lord will bless you in return beyond measure. Thank you.

My acknowledgement is rendered to every Scholar and Researcher whose work has been referenced in my thesis. My acknowledgement is also rendered to Sunpower and Yingli Solar PV panel manufacturers for making the electrical parameters of their solar panels available for use. Thank you all.

Due acknowledgements are rendered to all my siblings particularly my sisters, Mrs Felicia Adebisi Esuruoso, Mrs Comfort Olubunmi Kehinde Adegbite, Mrs Dorcas Olukemi Olubode and Mrs Victoria EbunOluwa Moyosore Owwoeye, for your love, prayers and generous, unfailing support – Thank you all.

Finally, my unparalleled appreciation goes to the love of my life, my husband and the very best friend I could ever have, Mr Bamidele Adeniyi Mafimidiwo, for standing by me at all times, encouraging me all along, standing in the gap for me in prayers, in responsibilities and representing my interests at all times and everywhere. I appreciate you for being a faithful husband and a caring father to all our children – the biological, spiritual and adopted – all of them. All our children are acknowledged and appreciated in

particular Olugbenga, Oluwaseyi, Ololade and Omotunde, I say thank you all, for your understanding and support at home, for giving me reasons to be at peace with myself and my studies and for the good reports I received concerning you all, Thank you and God bless you all.

ABSTRACT

Solar power is obtained through conversion of sunlight into electricity, either directly using photovoltaic solar cells, or indirectly using concentrated solar panel. The various forms of solar energy – solar photovoltaic, solar thermal electricity, solar heat and solar fuels offer a clean, climate-compliant, free, abundant and in-exhaustive energy resource for mankind.

Solar energy has huge potential but it is presently not fully harnessed. There exist concerns about its costs and efficacy of meeting and sustaining energy needs economically. This is further compounded by the strong dependency of the power output of photovoltaic device on the latitude and weather.

Three-dimensional technology is considered as an option to address some of these problems and improve on present solar energy generation. Photovoltaic solar energy generation in three dimensions is an emerging technology that mimics the natural collection of sunlight in three-dimensions in structures which is in contrast with the planar method. The technology of collecting light in three-dimension offers advantages of multiple orientations with absorbers for effective capturing of off-peak sunlight and re-absorption of reflected light within a structure. Furthermore, the ability to harness and calculate optical, electrical, material absorption analysis and the physics of the solar material is of interest.

Performance predictions and optimisation strategies require simulation tools that can efficiently and accurately compute thermal and electrical parameters of intricate three-dimensional geometrical structures.

The aims and objectives of this thesis are to explore three-dimensional technology in solar energy with the expectation that models and simulations developed will serve as important tools in performance predictions and early validation of newly designed cells, modules and arrays for optimal performance that will contribute to accelerated adoption of a carbon-free society.

This thesis investigated the effect of using three-dimensional technology in enhancing the generated solar output power. The investigation carried out was for solar photovoltaic and concentrated thermal photovoltaic systems in particular. The issues involved in the generation of quality and reliable solar power for future applications were investigated and reported on. The approach used utilizes the tool flow in COMSOL Multiphysics, Version 5.1 to build three-dimensional and two-dimensional models. The relevant physical and material properties of these models are then used as variables and expressions to apply directly to the solid domains, boundaries, edges, and points independently for their computational meshes. The three-dimensional and two-dimensional geometries of solar photovoltaic were then simulated and their performances were evaluated.

The output results in both the three-dimensional and the two-dimensional systems are analysed, compared and reported on. The key findings reveal that heat generated in solar system is a major issue to be tackled in solar power generation. Through the different 1D, 2D and 3D study, modelling and simulation carried out, the research has been able to use 3D structure to explore the space in greater dimensions and analyse the heat distribution, thermal behaviour, physics of material selected, the system geometry and configuration as important parameters for consideration in solar design systems. The analysis and the results obtained were found useful in predicting the performance behaviour of the solar systems under study for power generation optimization.

TABLE OF CONTENTS

DEDICATION.....	iv
PREFACE.....	v
ACKNOWLEDGEMENTS.....	vii
ABSTRACT	x
LIST OF FIGURES	xv
LIST OF TABLES.....	xix
LIST OF ABBREVIATIONS.....	xxi
LIST OF ENGINEERING AND MATHEMATICAL SYMBOLS	xxii
LIST OF NOMENCLATURE	xxv
CHAPTER ONE.....	1
INTRODUCTION	1
1.1 Introduction.....	1
1.2 Statements of the problem.....	2
1.3 Research questions	3
1.4 Significance / Aims & Objectives of the study	3
1.5 Contribution to knowledge.....	4
1.6 Scope of study.....	4
1.7 Thesis outline	5
CHAPTER TWO	7
LITERATURE REVIEW	7
2.1 Introduction.....	7
2.2 Brief on solar energy generation	7
2.3 Solar technologies	8
2.4 Major solar power generation techniques	9
2.4.1 Photovoltaics Techniques	9
2.4.1.1 Basic representation, equations and electrical behaviour of a PV system	10
2.4.1.2 Electrical characteristic behaviour of solar PV/cells	12
2.4.2 Concentrated photovoltaics technology	15
2.4.3 Dye-sensitized solar cell	16
2.4.4 Solar thermoelectricity	16
2.4.5 Concentrated solar power (CSP).....	16
2.5 Limitation to solar energy generation	19
2.5.1 The use of the automatic tracking system (ATS).....	19
2.5.2 The use of the maximum power point tracking (MPPT) system.....	20
2.5.3 The scientific storage battery charging approach.....	20
2.6 Three dimensional photovoltaic (3DPV) structure.....	20
2.6.1 Review of literatures on 3DPV structure	21
2.6.1.1 Fibonacci PV module (FPM).....	21
2.6.1.2 Spherical solar technology (SST).....	22
2.6.1.3 3D Nanopillar-based cell modules	22
2.6.1.4 Solar energy generation by 3D method, using Fibonacci PV module (FPM).	22
2.6.1.5 Three-dimensional modelling and simulation of P-N junction spherical silicon solar cells	22
2.6.1.6 Three-dimensional nanopillar-array PV on low-cost and flexible substrates	23
2.7 The need for modelling and simulation of solar cells	23
2.8 Thermal CTPV modelling	25
2.8.1 The implementation of the thermal model	25

2.9	Non-concentrating solar PV modelling.....	27
2.9.1	Electrical modelling.....	28
2.9.1.1	Series resistance.....	28
2.9.1.2	Shunt resistance.....	28
2.9.1.3	Series and Shunt resistances.....	28
2.9.2	Irradiation and temperature effect on PV modules.....	29
2.9.3	Consideration for environmental parameters and cell parameters in PV modelling.....	29
2.10	3DPV thermal modelling.....	29
2.10.1	PV model materials.....	30
2.10.2	Meshing of material.....	31
2.11	Chapter summary.....	31
CHAPTER THREE.....		32
METHODOLOGY.....		32
3.1	Introduction.....	32
3.2	Three-dimensional modelling of the photovoltaic system.....	33
3.3	Three-dimensional modelling of a concentrated thermal photovoltaics energy system.....	34
3.3.1	Basic Modelling consideration for CTPV model, using COMSOL Multiphysics software.....	34
3.3.2	Governing equations for the CTPV model.....	35
3.3.3	Properties of CTPV materials.....	36
3.3.4	The three-dimensional CTPV model.....	36
3.4	Non-concentrating solar PV energy system and modelling.....	37
3.4.1	Basic modelling workflow equations in 3DPV.....	37
3.4.2	Thermal load equations and boundary conditions.....	38
3.4.3	PV model materials and consideration for selection.....	38
3.5	Selection of material properties.....	39
3.5.1	Front surface materials – Material 1.....	40
3.5.2	Rear surface – Material 4.....	40
3.5.3	Solar cell – Material 3.....	41
3.5.4	Finger – Material 6.....	41
3.5.5	Frame – Material 5.....	41
3.6	Meshing of modelled PV panel.....	44
3.7	Electrical characteristics of the system.....	44
3.8	Chapter conclusion.....	44
CHAPTER FOUR.....		45
MODELLING AND SIMULATION OF THERMAL PHOTOVOLTAIC ENERGY SYSTEM.....		45
4.1	Introduction.....	45
4.2	Concentrating solar thermal energy conversion.....	45
4.3	Energy analysis of a concentrating thermal photovoltaic system.....	47
4.4	Electrical and thermal energy.....	48
4.5	Solar thermal electricity – present status.....	50
4.6	Modelling and simulation of the concentrating thermal photovoltaic module.....	50
4.6.1	Energy conversion process - Brief description.....	50
4.7	Modelling and simulation of solar cells.....	51
4.8	Concentrated thermal photovoltaic modelling.....	52
4.9	The implementation of the thermal model, using COMSOL Multiphysics.....	53
4.9.1	Thermal modelling and simulation.....	54
4.9.2	Materials specifications.....	54
4.9.3	Governing equations for the heat transfer.....	55

4.10	2D modelling and simulation of a CTPV system for optimum performance	56
4.11	3D Thermal modelling and simulation of a CTPV system for optimum performance	60
4.12	Comparison of the 2D and 3D models for the CTPV system	62
4.13	Results and Discussions.....	66
4.14	Findings and analysis of simulations of modelled CTPV different configurations	69
4.15	Comparison of 2D and 3D six mirror configurations of the CTPV system	70
4.16	Chapter conclusion	73
CHAPTER FIVE		74
THE EFFECT OF HEIGHT IN INCORPORATING THE 3DPV STRUCTURE FOR OPTIMUM SOLAR POWER GENERATION		74
5.1	Introduction.....	74
5.2	Present status of solar power generation	74
5.3	Three dimensional nature of photovoltaic (3DPV) structure	75
5.3.1	Solar energy generation in 3D.....	75
5.3.2	3DPV module assembly by Fibonacci number	76
5.3.3	Spherical silicon solar technology	76
5.3.4	3D Nanopillar-based cell modules.....	76
5.4	Effect of height in the Fibonacci method of 3DPV generation	76
5.5	3DPV structure effect on solar radiation intensity	78
5.6	Energy per unit volume	78
5.7	Computation of solar energy in three-dimensions.....	79
5.7.1	3D Configuration of the solar panel.....	81
5.8	2D Configuration of the solar panel.....	81
5.9	Results and discussions	82
5.10	Chapter conclusion.....	83
CHAPTER SIX.....		85
ONE DIMENSIONAL SIMULATION OF PHOTOVOLTAIC MODULE FOR PERFORMANCE PREDICTION.....		85
6.1	Introduction.....	85
6.2	1D Modelling of photovoltaic module/performance analysis determination	85
6.3	Mathematical modelling of PV cells and Module	87
6.3.1	Consideration for environmental and cell parameters in PV modelling	88
6.4	Matlab modelling of a PV Module.....	89
6.5	Simulation and results	91
6.6	Conclusion	105
CHAPTER SEVEN		106
THREE-DIMENSIONAL MODELLING AND SIMULATION OF PHOTOVOLTAIC ENERGY SYSTEM		106
7.1	Introduction.....	106
7.2	The need for PV modules design, modelling and optimization	107
7.3	Three-dimensional (3D) modelling of the PV panel system	107
7.3.1	Details of the modelled thermal PV system	109
7.3.2	Implementation of solar thermal PV panel model in COMSOL Multiphysics	111
7.3.3	Physics and materials selection and applicable boundary conditions	111
7.3.4	Theory and governing equations	112
7.3.5	The variables to be determined as the output	113
7.3.6	Material composition description.....	113
7.3.7	Meshing	114
7.4	Model validation	115

7.5	Results and discussion	115
7.5.1	Effect of ambient temperature on panel performance	115
7.6	Conclusions	119
CHAPTER EIGHT		120
SUMMARY AND CONCLUSION		120
8.1	Conclusion	120
8.2	Recommendation for further research	122
REFERENCES		123
APPENDIX A.....		131
APPENDIX A-1: COMSOL generated report on 2D CTPV system with 6 mirrors configuration.....		131
APPENDIX A-2: COMSOL generated report on 2D CTPV system with 10 mirrors configuration....		137
APPENDIX A-3: COMSOL generated report on 3D CTPV system with 8 mirrors configuration.....		143
APPENDIX B.....		152
APPENDIX B-1: Top 50 solar PV module efficiency		152
APPENDIX B-2: YINGLI MONO 260 SERIES SOLAR PANEL.....		154
APPENDIX B-3: SUNPOWER SOLAR PV ELECTRICAL SPECIFICATIONS.....		157
APPENDIX B-4: YINGLI SOLAR PANEL SIMULATION REPORT		159
APPENDIX C.....		176
APPENDIX D.....		181

LIST OF FIGURES

Figure 2-1: Electric energy consumption as percentage of total energy production in 2008	7
Figure 2-2: Overview of solar technologies.....	8
Figure 2-3: The expectation of photovoltaics efficiency improvement in future	10
Figure 2-4: Simplified equivalent circuit of a photovoltaic cell	11
Figure 2-5a: Different curves for a photovoltaic module at varying irradiance and temperature	13
Figure 2-5b: I –V and P-V curves indicating maximum power point of a PV solar system.....	13
Figure 2-6: Different basic CSP technologies	18
Figure 2-7(a): Parabolic trough system of concentrated solar power	18
Figure 2-7(b): Solar tower system of concentrated solar power	18
Figure 2-8: Energy plot comparison between GA optimized 3DPV structures and a flat panel	21
Figure 2-9: Basic modelling workflow in COMSOL Multiphysics	24
Figure 2-10: Surface temperature distribution at T _{heater} =1400 K in 2D configuration for the CTPV system.....	27
Figure 2-11: Plot showing the trend of (a) PV cell voltaic efficiency, (b) PV cell temperature, and (c) PV cell electric output power versus the operating temperature.....	27
Figure 2-12(a): Materials structure in solar module	31
Figure 2-12(b): Materials list in solar module	31
Figure 3-1: A typical structure of a c-Si solar cell	38
Figure 3-2(a): Solar panel make-up	39
Figure 3-2(b): Materials layout in solar module	39
Figure 3-3: EVA browning in field PV modules	41
Figure 3-4: Severe EVA browning on mirror-enhanced PV arrays	42
Figure 3-5: Irregular PVB browning - water ingress and corrosion	42
Figure 3-6: Degraded modules	43
Figure 3-7: Degraded Thin film module at NREL OTF	43
Figure 4-1(a): Parabolic dish collectors	46
Figure 4-1(b): Parabolic trough	46
Figure 4-1(c): Central receiver with heliostats.....	46
Figure 4-1(d): Linear Fresnel reflector	46
Figure 4-2: Operating principle of a concentrating thermal photovoltaic system	53
Figure 4-3: Geometry and dimensions of the modelled thermal PV system]	53
Figure 4-4: Stationary temperature distribution at operating conditions for (a) eight mirrors, (b) six mirrors, and (c) 10 mirrors.....	57
Figure 4-5: The point graph of the PV cell temperature versus the heater temperature for (a) eight, (b) six, and (c) ten mirrors respectively.	58
Figure 4-6: Plot showing the voltaic efficiency against temperature for 2D CTPV configuration with (a) eight mirrors, (b) six, (c) ten mirrors	59

Figure 4-7: Plot showing the electric output power against the heater temperature for the CTPV with (a) eight mirrors, (b) six mirrors, and (c) ten mirrors	60
Figures 4-8(a): Modelled insulation for 2D CTPV geometry with eight mirrors	62
Figures 4-8(b): Modelled insulation for 3D CTPV geometry with eight mirrors	62
Figures 4-8(d): Modelled PV cells for 3D CTPV geometry with eight mirrors	62
Figures 4-8(c): Modelled PV cells for 2D CTPV geometry with eight mirrors.....	62
Figures 4-8(f): Modelled mirrors for 3D CTPV geometry with eight mirrors.....	63
Figures 4-8(e): Modelled mirrors for 2D CTPV geometry with eight mirrors	63
Figures 4-8(g): Modelled emitter for 2D CTPV geometry with eight mirrors.....	63
Figures 4-8(h): Modelled emitter for 3D CTPV geometry with eight mirrors.....	63
Figures 4-8(j): Modelled air for 3D CTPV geometry with eight mirrors	63
Figures 4-8(i): Modelled air for 2D CTPV geometry with eight mirrors	63
Figures 4-8(k): Meshed result of 2D CTPV thermal PV system with eight mirrors.....	64
Figures 4-8(l): Meshed result of 3D CTPV thermal PV system with eight mirrors.....	64
Figures 4-8(m): Stationary temperature distribution of modelled 2D CTPV system with eight mirrors ...	64
of modelled 2D CTPV system with eight mirrors	64
Figures 4-8(n): Stationary temperature distribution of modelled 3D CTPV system with eight mirrors	64
Figure 4-9(d): Voltaic efficiency versus temperature in a 2D CTPV for eight mirrors	65
Figure 4-9(c): Electric power output versus temperature in a 2D CTPV for eight mirrors.....	65
Figure 4-9(e): Voltaic efficiency versus temperature in a 2D CTPV for eight mirrors	65
Figure 4-9(b): Point graph - temperature in a 3D CTPV for eight mirrors	65
Figure 4-9(a): Point graph - temperature in a 2D CTPV for eight mirrors	65
Figure 4-9(f): Electric power output versus temperature - in a 2D CTPV for eight mirrors.....	65
Figure 4-10(a): Temperature distribution of modelled 2D CTPV with six mirrors	71
Figure 4-10(b): Temperature distribution of modelled 3D CTPV with six mirrors	71
Figure 4-11(b): Point temperature of modelled 3D CTPV with six mirrors	71
Figure 4-11(a): Point temperature of modelled 2D CTPV with six mirrors	71
Figure 4-12(b): Voltaic efficiency against temperature of modelled 3D CTPV with six mirrors.....	72
Figure 4-12(a): Voltaic efficiency against temperature of modelled 2D CTPV with six mirrors.....	72
Figure 4-13(a): Electric output power against temperature of modelled 2D CTPV with six mirrors	72
Figure 4-13(b): Electric output power against temperature of modelled 3D CTPV with six mirrors	72
Figure 5-1: Leaf arrangement on plants by phyllotaxis	77
Figure 5-2: A 500 Watts solar-powered tree at tourism London, Ontario Canada	78
Figure 5-3: Solar irradiance components to a cube.....	79
Figure 5-4: Multilevel panels arranged as a volume	81
Figure 5-5: Planer (2D) arrangement of solar panels.....	81
Figure 5-6: Energy optimization by 'area' in a planar system.....	83
Figure 5-7: Energy optimization by 'volume' in a 3DPV system.....	83
Figure 5-8: Energy optimization by 'volume' in a 3DPV and by area in a planar systems	83
Figure 6-1(a): Image of Sunpower X21- 345 PV panel.....	86

Figure 6-1(b): Dimension (mm) of Sunpower X21 1,559 x 1,046 x 46.....	86
Figure 6-1(c): Image of Yingli YL260C- PV panel.....	86
Figure 6-1(d): Dimension (mm) of Yingli PV panel 990 x 1,650 x 50.....	86
Figure 6-2(a): I-V Characteristics for series resistance (R_s) variation for SunPower PV panel	92
Figure 6-2(b): P-V Characteristics for series resistance (R_s) variation for SunPower PV panel	92
Figure 6-3(a): I-V Characteristics for series resistance (R_s) variation for Yingli PV panel	93
Figure 6-3(b): P-V Characteristics for series resistance (R_s) variation for Yingli PV panel	93
Figure 6-4(a): I-V Characteristics for shunt resistance (R_{sh}) variation for SunPower panel.....	94
Figure 6-4(b): P-V Characteristics for shunt resistance (R_{sh}) variation for SunPower panel.....	94
Figure 6-5(a): I-V Characteristics for shunt resistance (R_{sh}) variation for Yingli panel.....	95
Figure 6-5(b): I-V Characteristics for shunt resistance (R_{sh}) variation for Yingli panel.....	95
Figure 6-6(a): I-V Characteristics for ideality (N) variation for SunPower PV panel	96
Figure 6-6(b): P-V Characteristics for ideality (N) variation for SunPower PV panel	96
Figure 6-7(a): I-V Characteristics for ideality (N) variation for Yingli PV panel	97
Figure 6-7(b): P-V Characteristics for ideality (N) variation for Yingli PV panel	98
Figure 6-8(a): I-V Characteristics for temperature variation for SunPower PV panel.....	98
Figure 6-8(b): P-V Characteristics for temperature variation for SunPower PV panel.....	98
Figure 6-9(a): I-V Characteristics for temperature variation for the Yingli PV panel	99
Figure 6-9(b): P-V Characteristics for temperature variation for the Yingli PV panel	99
Figure 6-10(a): I-V Characteristics for irradiation (G) variation for the SunPower PV panel	100
Figure 6-10(b): P-V Characteristics for irradiation (G) variation for the SunPower PV panel.....	100
Figure 6-11(a): I-V Characteristics for irradiation (G) variation for the Yingli PV panel	101
Figure 6-11(b): P-V Characteristics for irradiation (G) variation for the Yingli PV panel.....	101
Figure 6-12(a): I-V characteristic for modelled SunPower solar panel @ STC.....	104
Figure 6-12(b): P-V characteristic for modelled SunPower solar panel @ STC	104
Figure 6-12(c): I-V characteristic for modelled Yingli solar panel @ STC.....	104
Figure 6-12(d): I-V characteristic for modelled Yingli solar panel @ STC	104
Figure 7.1: Sources of heat loss in a PV device	109
Figure 7-2: The Yingli YL260C-30b panel	110
Figure 7-3: 3D modelled Yingli of 5 cells arranged in a 1x5 rectangle.....	110
Figure 7-4 : Principle of a crystalline module assembly	114
Figure 7-5a: Free tetrahedral meshing of PV cell	114
Figure 7-5b: Normal meshing of PV fins.....	114
Figure 7-5c: Extra-fine meshing of PV edges.....	115
Figure 7-6a: 3D Solar PV 40 cells @ 298.15 K.....	116
Figure 7-6b: 3D Solar PV 40 cells @ 348.15 K.....	116
Figure 7-6c: 3D Solar PV 40 cells @ 368.15 K.....	116
Figure 7-6b: 3D Solar PV 40 cells @ 348.15 K.....	116
Figure 7-7: Sun's energy converted to heat (kW/m^2)	117
Figure 7-8: PV cell efficiency temperature dependence	117

Figure 7-9: Thermal efficiency	118
Figure 7-10: Voltaic efficiency.....	118
Figure 7-11: Overall efficiency.....	119
Figure 7-12: Electric output power (kW/m ²)	119
Figure A-1.1: Geometry of the concentrated thermal photovoltaics system in two-dimension.....	131
Figure A-1.2: Geometry of the modelled 2D CTPV system with six cells and insulation around the PV cells.....	132
Figure A-1.3: Geometry of the modelled 2D CTPV system showing the PV cells (six in number).....	132
Figure A-1.4: Geometry of the modelled 2D CTPV system showing the mirrors (six in number)	133
Figure A-1.5: Geometry of the modelled emitter for the 2D CTPV system	133
Figure A-1.6: Geometry of the modelled air for emitter cooling in a 2D CTPV system with six mirrors.....	134
Figure A-1.7: Geometry of the meshing of various domains in CTPV system.	134
Figure A-1.8: Stationary temperature distribution of modelled 2D CTPV system with six mirrors/PV cells	135
Figure A-1.9: The isothermal contours in 2D geometry with six mirrors and PV cells.....	135
Figure A-1.10: Line surface radiosity of the modelled 2D, six mirrors CTPV system.....	136
Figure A-2.1: Geometry of the concentrated thermal photovoltaics system in two-dimensions	137
Figure A-2.2: Geometry of 2D CTPV system with ten cells and insulation around the PV cells.....	138
Figure A-2.3: Geometry of 2D CTPV system showing the PV cells (ten in number)	138
Figure A-2.4: Geometry of the 2D CTPV system showing the mirrors (ten in number).....	139
Figure A-2.5: Geometry of the emitter for the thermal photovoltaics system	139
Figure A-2.7: Geometry of the meshing of various domains in 2D CTPV system with ten mirrors.	140
Figure A-2.8: Stationary temperature distribution of modelled 2D CTPV system with ten mirrors/PV .	141
Figure A-2.9: The isothermal contours in 2D geometry with ten mirrors and PV cells	141
Figure A-2.10: Line surface radiosity of the modelled 2D CTPV system with ten pair mirrors/PV cells	142
Figure A-3.1: Geometry of modelled 3D CTPV system showing the mirrors (eight in number)	143
Figure A-3.2: Geometry of the modelled 3D CTPV system.....	144
Figure A-3.3: Geometry of insulation of modelled 3D CTPV system in three-dimension.....	144
Figure A-3.4: Geometry of modelled 3D CTPV system.....	145
Figure A-3.5.: Geometry of the modelled 3D CTPV system showing the mirrors (eight in number)	145
Figure A-3.6.: Geometry of the modelled 3D CTPV system showing the modelled air/fluid area	146
Figure A-3.7.: Geometry of the modelled CTPV system showing the modelled insulation	146
Figure A-3.8: Geometry of the meshed mirrors in the 3D CTPV system with eight mirrors	147
Figure A-3.9: Geometry of the meshed emitter in the 3D CTPV system with eight mirrors.....	147
Figure A-3.10: Stationary temperature distribution of modelled 3D CTPV system with eight mirrors ..	150
Figure A-3.11: Line surface isothermal of the modelled 3D, CTPV system with eight mirrors/PV cells	150
Figure A-3.12: Line surface radiosity of the modelled 3D, CTPV system with eight mirrors/PV cells ..	151

LIST OF TABLES

Table 2-1: Various categories of concentrated photovoltaic energy system	16
Table 2-2: Summary and comparison of different solar energy generation techniques	19
Table 2-3: Global definition for the heater	26
Table 2-4: Global definition for the PV cell	26
Table 2-5: Basic materials property summary for CTPV	26
Table 3-1: Material properties summary	36
Table 3-2: Summary list of materials for solar photovoltaics	39
Table 4-1: Progress in concentrating solar plants (CSP) since 2009	46
Table 4-2: Operating characteristics of concentrating solar power technologies	47
Table 4-3: Global definition for the heater	54
Table 4-4: Global definition for the PV Cell	54
Table 4-5: Material properties used in the CTPV modelling	55
Table 4-6: The summary of domain selection for the selected materials	61
Table 4-7: Geometry statistics of two-dimensional and three-dimensional geometries	61
Table 4-8: Results of comparative analysis of the 2D CTPV geometry with different number of mirrors	66
Table 4-9: Results of comparative analysis of 2D CTPV with eight mirrors and 3D CTPV with six mirrors	67
Table 4-10: Case one summary of the results of 2D CTPV modelling with different mirror configurations	68
Table 4-11: Case two summary of the results on 2D and 3D CTPV modelling with eight mirrors.....	69
Table 4-12: Summary of the results on 2D and 3D CTPV modelling with six mirrors	73
Table 5-1: Power output data for the 2D and 3D solar installations	82
Table 6-1: Establishing the series and shunt resistances for Sunpower and Yingli PV Panels	90
Table 6-2: 1D Simulation of SunPower X21-series-345 solar panel for series resistance	92
Table 6-3: 1D Simulation of Yingli Mono PV 260 Series 60 solar panel for series resistance	93
Table 6-4: 1D simulation of SunPower X21-Series-345 solar panel for shunt resistance	94
Table 6-5: 1D Simulation of Yingli Mono PV 260 Series c-60 solar panel for shunt resistance.....	95
Table 6-6: 1D Simulation of the SunPower X21-Series-345 solar panel for Ideality factor.....	96
Table 6-7: 1D Simulation of the Yingli Mono PV 260 Series 60 solar panel for Ideality factor.....	97
Table 6-8: 1D Simulation of the SunPower X21-Series-345 solar panel for Temperature variation.....	98
Table 6-9: 1D Simulation of Yingli Mono PV 260 Series c-60 solar panel for Temperature variation.....	99
Table 6-10: 1D Simulation of the SunPower X21-Series-345 solar panel for irradiation variation	100
Table 6-11: 1D Simulation of the Yingli Mono PV 260 Series 60 solar panel for irradiation variation..	101
Table 6-12: Derived optimum operating parameters for the SunPower X21-Series panel at STC	102
Table 6-13: Validated electrical parameters for the SunPower X21-Series-345 solar panel at STC	102
Table 6-14: The 345 W Sunpower_X21-Series- solar panel at STC	102

Table 6-15: Derived optimum PV operating parameters for the Yingli Mono PV 260 Series 60 c-Si solar panel at STC	103
Table 6-16: Validated electrical parameters for the Yingli Mono PV 260 Series 60 c-Si solar panel	103
Table 6-17: The Yingli 260 Series 60 c-Si, Monocrystalline solar panel at STC	103
Table 6-18: Compared calculated/validated values for the SunPower and the Yingli PV panels	105
Table 7-1: Electrical parameters from 1D modelling of the Yingli 260 series PV panel as input parameters for the 3D modelling of the same PV panel	108
Table 7-2: Modelled material properties for 3D modelling and simulation	111
Table 7-3: Geometric entries for output variables to be determined	113
Table C-1: Governing physics for the 2D and 3D CTPV models, using heat transfer with surface-to-surface radiation	176
Table D-1: Governing physics for the 3D PV model using heat transfer by surface-to-surface radiation	181

LIST OF ABBREVIATIONS

1D	:One-dimensional
2D	:Two-dimensional
3D	:Three-dimensional
ATS	:Automatic tracking system
BiPV	:Building-integrated photovoltaics
CLFR	:Concentrated linear Fresnel reflector
CPV	:Concentrated Photovoltaics
CSP	:Concentrating solar panels
CTPV	:Concentrated thermal photovoltaic)
LCOE	:Levelised cost of electricity (LCOE)
MJ	:Multi-junction
MPPT	:Maximum power point transmitter
NCSP	:Non-concentrating solar panels
OPV	:Organic Photovoltaics
PV	:Photovoltaics
SSST	:Spherical Si solar technology
SST	:Spherical solar technology
STC	:Standard Test Conditions
STE	:Solar thermal energy
STT	:Solar thermal technology
TPV	:Thermal photovoltaic

LIST OF ENGINEERING AND MATHEMATICAL SYMBOLS

h_c	:Convective heat transfer coefficient of the process, (W/(m ² K) or W/(m ² °C))
A_{panel}	:PV panel front area (A)
C_p	:Specific heat capacity of the fluid (J/kg K)
E_g	:Band-gap of the semiconductor material
F_{amb}	:Geometric factor for the ambient
G_{amb}	:Ambient irradiation (W/m ²)
G_{ref}	:The reference intensity of solar irradiance (1000 W/m ²)
$I_{0,cell}$:Saturated reverse current or leakage current (A)
I_0	:Reverse saturation current (A)
I_D	:Diode current modeled by the equation for a Shockley diode (A)
I_{or}	:Reverse saturation current at reference temperature at T_r (A)
$I_{ph,cell}$:Photocurrent, the current produced by the incident light and function of irradiation level and junction temperature (A)
I_{ph}	:Photocurrent, The photovoltaic current (A)
$I_{scr,cell}$:Short circuit current of photovoltaic cell (A)
K_i	:Temperature coefficient of the short circuit current
N_p	:Number of parallel cells branches
N_s	:Number of series cells
P_{mod}	:Electric energy supplied by the module (J)
Q_{vd}	:Viscous dissipation (W/m ³)
R_s	:Series resistance of the cell (Ω)
R_{sh}	:Shunt resistance of the cell (Ω)
T_a	:Ambient air temperature (K)
T_{amb}	:Ambient temperature (K)
T_c	:Cell operating temperature (K)
T_{ext}	:External or ambient temperature (293.15 K)
T_o	:Environment temperature (K)
T_{pv}	:Temperature for the surface of the module (K)
T_r	:Reference cell operating temperature (25 °C) or (298.13 K)
$V_{0c,Cell}$:Open circuit voltage of photovoltaic cell (V)
$V_{oc}(T_c, C)$:Open circuit voltage function of the cell temperature and concentration factor (V)
$V_{pv,cell}$:Volume of the PV cells in the panel (m ³)
V_t	:Thermal voltage (V)
k_{cond}	:Thermal conductivity (W/m K)
q_0	:Heat flux (W/m ²)
β_{ref}	:Thermal coefficient of the PV module
η_{Tref}	:PV module efficiency at reference conditions

η_{elec}	:Efficiency of the PV module
η_{pv}	:Voltaic efficiency of the PV panel
η_r	:Reference efficiency corresponding to the concentration factor chosen.
μ_T	:Turbulent viscosity (Pa s)
ρ_{ground}	:Reflectivity of the ground
AK_0	:Temperature coefficient of the open circuit voltage
A_i	:Anisotropy index factor
b	:Tilt angle of the PV panels
C_p	:Specific heat capacity of the material (J/ (kg.K))
η_{pv}	:Voltaic efficiency for PV cell
F	:Geometric factor
G	:Irradiation flux (W/m ²)
G_a	:absorbed solar radiation (W/m ²)
G_b	:Beam solar radiation (W/m ²)
G_d	:Diffuse solar radiation (W/m ²)
G_g	:Ground reflected solar radiation (W/m ²)
G_h	:Horizontal plane solar radiation (W/m ²)
I_{sc}	:Short circuit current (A)
k	:Thermal conductivity of the fluid (W/m K)
k	:Turbulent kinetic energy (J)
M	:Air mass modifier
MW	:Megawatts
n	:Surface normal
p	:Pressure of the fluid (Pa)
q	:Heat transferred by conduction (W)
Q	:Internal Heat Generation (W)
q	:Heat transferred by conduction (J)
q	:Reflectivity of the ground
q_{out}	:Electric output power (W)
R_{beam}	:Ratio of beam radiation on tilted plane to that on horizontal plane,
T	:Temperature, (25 °C) or (298.13 K)
t	:Time, (sec, min or hour)
T_{heater}	:Temperature for emitter inner boundary (25 °C) or (298.13 K)
T_c	:Cell temperature, (25 °C) or (298.13 K)
T_o	:Environment temperature (25 °C) or (298.13 K)
TWh	:Terawatt-hour
u	:Velocity of the fluid (m/s)
V_{oc}	:PV cell's terminal operating voltage (V)
$V_{oc}(T_c, C)$:Open circuit voltage function of the cell temperature and concentration factor (V)

$V_{oc}(T_o, C_o)$:Open circuit voltage function of the environment temperature and concentration factor equal to 1
$\beta(C)$:Voltage thermal coefficient
ε	:Emissivity of the material
ρ	:Density
ρ	:Density of the material
A	:Heat transfer area of the surface (m ²)
G	:The intensity of solar irradiance W/m ²
I	:PV cell output current (A)
N	:PN junction ideality factor
$NOCT$:Nominal operating cell temperature
V	:PV cell output voltage (V)
$V_{oc}(T_o, C_o)$:Open circuit voltage function of the environment temperature with concentration factor of 1
dT	:Temperature difference between the surface and the bulk fluid (K or °C)
k	:Boltzman's constant (1.38065 x 10 ⁻²³ J/°k)
q	:Electronic charge (1.602 x 10 ⁻¹⁹ C)
q	:Heat transferred per unit time (W)
β	:Tilt angle of the PV panels
$\beta(C)$:Voltage thermal coefficient
ε	:Surface emissivity
μ	:Dynamic viscosity of the fluid on the front face of the PV module (Pa s)
ρ	:Density of film of the fluid on the front face of the PV module (kg/m ³)
σ	:Stefan-Boltzman constant (5.67x10 ⁻⁸ W/m ² K ⁴)

LIST OF NOMENCLATURE

These terms are come across or found in this thesis.

APSYS	:Advanced physical models of semiconductor devices
A-Si	:Amorphous Silicon
CdTe	:Cadmium telluride
CdS	:Cadmium Sulphide
CIGS or CIS	:Copper indium gallium di-selenide
CTE	:Coefficient of thermal expansion
DMA	:Dynamic mechanical
DSSC, DSC or DYSC	:Dye-sensitized solar cell
EVA	:Ethylene vinyl acetate
FPM	:Fibonacci photovoltaic module
GaAs	:Gallium Arsenide
Ge	:Germanium
GHG	:Greenhouse-gas emissions
InGaAs	:Indium gallium arsenide
InGaP	:Indium gallium phosphide
PET	:Polyethylene terephthalate
PVF	:Polyvinyl fluoride
T_g	:Glass transition temperature
TGA	:Thermo gravimetric analysis
UV	:Ultra violet

CHAPTER ONE

INTRODUCTION

1.1 Introduction

Global energy demand is daily on the increase due to economic development. This has resulted in high consumption of fossil fuels with adverse environmental consequences such as environmental degradation, global warming, acid rain, and the depletion of the ozone layer [1]. This then led to calls for alternative energy resources diversification in order to overcome these negative impacts of fossil fuel energy technologies that threaten the ecological stability of the earth. Furthermore, the growing scarcity of fossil fuel and the consequential rising fuel costs have their increasing negative impacts on economic development of many countries that need to be curtailed. A global solution reached on this crisis is the use of alternative renewable energy systems [2, 3].

Of all renewable energy sources, solar energy is considered to be practically unlimited in the long-term, and it is a very abundant energy resource in the developing world [4, 5]. Photovoltaic (PV) solar technology has gained recognition in both application and economics as a renewable energy source over the past years through research into and development of this technology. However, the technology still requires improvement in developing higher efficiency PV cells and modules, reducing the cost of manufacturing processes, improving the numerous components states of the PV systems etc. Different PV technologies have emerged to improve upon solar energy output but the conversion efficiency of the solar radiation into useful energy has not improved appreciably [6]. In order to address this problem, various research findings have been made and are still being made on solar energy generation.

According to [7] ground-based PV panels, otherwise known as the convectional PV panels that are commonly installed in harvesting solar power, have lower generated energy, which is further worsened by strong dependency of the generated power of this PV device on the latitude and conditions of the weather [4]. These features have particularly obstructed the adoption of PV in various countries particularly in the north European countries with record of hazy climates. On the other hand, areas with high solar irradiances, particularly in major parts of Africa, are either far-off from most PV solar energy users and the challenges of long distance losses over connecting miles of cables, the meagre generated energy output compared with the huge associated overall costs involved and the associated political issues involved in such a large project, heavily minimizes the economic benefits; or in most cases, are not even tapped for adequate use [8]. The convectional use of solar energy has been in two-dimensional structures whereby solar energy generation is considered only in x and y co-ordinates only and is faced with limitations such as changing weather conditions, losses due to solar radiation adsorption and reflection [9].

According to [10], research has proved that three-dimensional photovoltaic (3DPV) structures can increase the density of the generated energy (energy in per footprint area, Wh/m^2) in a linear proportion to the configuration height, for a specified day and place. These 3D structures include shapes like an open cubic box (at the top), a funnel-like shaped cubic box, a trapezium, sphere, a

parallelepiped or any other 3D shape which are in principle found capable of increasing the daily energy generation [11].

Research findings have revealed the ability of 3D nature advantage of the biosphere to permit large collection of solar energy on plane structures contrary to what obtains in planar or two-dimensional method of energy collection on flat structures. Three-dimensional collection of sunlight radiation enables multiple orientations of the absorbers to allow for the effective capture of off-peak sunlight and the re-absorption of reflected light inside the 3D structure [11]. This then informs the application of 3DPV technology as an engineering approach to optimising solar power generation through 3D modelling and simulation of the PV devices and the design of the PV systems. Based on the above facts, it is necessary for a simple, cost-effective and accurate simulation application or tool, which can handle commercially available solar panels to be designed and modelled and this is the motivation behind this research [12, 13].

To enhance the pre-study of solar power systems, many studies have been developed on methods of simulating and building prototype solar panels and solar cells. These studies involve techniques like software simulation which models solar cells in 1D and 3D and making use of different mathematical models [13-15]. Nevertheless, the motive of these studies was to establish accurate modelling techniques of simulating solar panels for performance prediction and it was not aimed at commercial production. As an alternative, some attempts have been directed towards assembling power supplies similar in performance to solar cells by using innovative power electronic topologies. These are programmable power supplies which exhibit similar properties to commercial solar panels when the input source is energized. However, these power supplies are equally expensive to date and are no better substitute for solar power, there is therefore a need for more improvement [16].

In this work, two and three dimensional concentrated thermal PV and normal PV models were developed and modelled to forecast the thermal and electrical behaviours of PVs and as well used in determining the impact of 3DPV structures on PV power generation. The systems are fixed with radiation and electrical models to form multi-physics models capable of determining the thermal and electrical performances of the PV panels. In addition, 1D modelling using MATLAB R2014b was used to determine the PV electrical characteristics which were used as input for the performance determination of the panel which includes efficiency, the electrical power output, and PV cell temperatures. Consideration was given to careful selection of the materials which to a large extent affect the solar panel's overall performance. Using this model, effects of atmospheric changes and operating conditions on the performance of the PV systems were studied.

1.2 Statements of the problem

1. Efficient conversion of the abundant solar energy radiated to the earth into affordable electricity has been a major task. Over the years, PV conversion has faced the problem of low energy conversion. Hence, optimizing the solar energy conversion to electricity remains the world's focus for attaining the future energy economy. The challenge is in finding the

appropriate technology in optimizing the converted solar photons into conducting electrons in order to improve the solar device efficiency and overall energy output.

2. Three-dimensional arrangement of the solar structure has been researched to improve the generated solar energy more than that which is currently achievable through the conventional planar arrangement. However, the task of establishing the best arrangement of solar panels in three dimensions to make a 3DPV device able to optimize the energy generated in a given base area (energy density) is still a challenge.
3. There is also the challenge of understanding the correlation between the performance of the materials, the performance of the module and the ability to select the materials appropriately.
4. The challenge remains of determining the impact the 3DPV structure could have on efficiency in solar power generation.

1.3 Research questions

1. How can 3D complex design and fabrication be realized and incorporated into sustainable installations on a global scale for optimal solar power generation?
2. In what ways has 3DPV impacted on the efficiency and power generated in comparison with the planar method of roof or ground installation?
3. Temperature increase is known to mitigate against solar energy generation with the planar configuration. In what ways has 3DPV addressed or resolved this problem?

1.4 Significance / Aims & Objectives of the study

1. Significance

This study is significant since advancement in renewable energy technologies particularly on solar power generation over the past decades is yielding results in both improved performance and lower costs. The world believes that renewable resources are already cost-effective in some locations and for some applications. It is expected that with appropriate research and invention of improved and appropriate technology, cost should become increasingly more competitive with other traditional forms of energy generation within the next few years, even for bulk generation purposes for economic and green-environmental advantages.

2. Aim and Objectives

The objective of the work is in two parts.

- a. To determine the influence of 3D structures on the solar PV generated output power for the concentrated thermal PV system by modelling, simulating and comparing the 2D and 3DPV structures for their thermal and operating performances (Temperature effect, efficiency and output power).
- b. To determine the influence of 3D structures on the solar PV generated output power for the normal (non-concentrated) solar PV system by modelling 1D and 3D models, and simulating and comparing their electrical and operating performances (Temperature effect, efficiency and output power).

The electrical and thermal properties of these modules were realized through appropriate materials and physics selection and evaluation to enable determination of the structure effects on the output power generation. With the success of the simulation, it is believed that the obtained results could be used to predict PV system performances for technical advice.

1.5 Contribution to knowledge

Hitherto, research work on solar energy generation has mainly been by one-directional methods and occasionally by two-directional method. This research work is unique because the research method utilized involved developing, designing and modelling of a PV panel for the study of power generated in both the concentrated and non-concentrated solar systems. It presents detailed information on the modelling approaches of PV systems and the challenges encountered. Chapters four, five and six present in a clear way, the different techniques that could be used to model PV systems, particularly the concentrated thermal PV and the solar PV systems.

In chapter four, a modelled prototype two dimensional CTPV with eight number PV cells and mirrors with associated materials was successfully modelled. A new knowledge contribution was added to this as new CTPV with different configurations such as decreased PV cells from eight to six cells as well as increased same from eight cells to ten cells were developed and modelled in order to determine the effects on the CTPV efficiency and generated output power. Furthermore, the three dimensional model of the CTPV was successfully developed and modelled, a study approach rare to come across. The electrical performances of the modelled two and three dimensional configurations were analysed, compared and interpreted.

In chapter seven, the PV panel was modelled in 1D and validated in agreement with the manufacturer's electrical data sheet. The output of the 1D simulation was used to model and simulate the 3D photovoltaic system successfully to predict the impact of a three-dimensional photovoltaic structure on solar power performance.

The findings in this thesis could provide insights that could help other researchers avoid long-term switching cost in the future and contribute to making the solar power systems performance more efficient, less expensive and sustainable towards the goals of Tera-Watt solar power generation and a free-carbon emission environment.

1.6 Scope of study

The study gives a general overview of various forms of solar power sources and technologies but more specifically of thermal concentrated and solar Photovoltaics. It investigates the impact of both the 2D and the 3DPV structure on thermal concentrated PV while it utilises the 1D modelling and simulation to investigate the impact of 3D structure on the solar PV systems. The study was carried out by modelling and simulation, the solar devices in one dimension, using MATLAB as well as in two-dimension and three-dimension geometrics, using COMSOL Multiphysics and analysing their material and physical effects on the efficiency and power outputs. The study enables the investigation, analysis and prediction of heat distribution in the solar devices, choice and physics of

materials selection and the effect of different system configurations in determining and establishing the global definitions required to predict solar configuration for optimum power generation.

1.7 Thesis outline

The subsequent chapters in this study are indicated below. The outline shows the theoretical framework of the research, the review of existing studies and the methods adopted in improving the existing work to evolve new variants of the study. The findings and application to global optimization problems with empirical results are also presented. The summary of the organization of the remaining part of the thesis is given below:

1. Chapter 2: Gives a general review of the literatures on solar energy technologies and recent development in those areas. This is followed by review of the 2D and 3D modelling and simulation of solar cells, using the engineering software, COMSOL Multiphysics.
2. Chapter 3: This chapter presents the methodology or the approaches used for modelling and simulation of both the concentrated and non-concentrated thermal PV systems in determining the impact of 2D and/or 3D structures on solar power systems, and why the approach was preferred. Two different scenarios were considered. The first scenario was on concentrated thermal PV systems while the second scenario was on solar photovoltaics system (non-concentrated). In both cases, the method used involved the application of COMSOL Multiphysics engineering software, version 5.1.
3. Chapter 4: Presents the various thermal energy technologies available and updates on their status to date. The 2D and 3D structures of the thermal PV structures were modelled and simulated. The operating conditions were varied to determine the effects on the system performance and the effect of 2D and 3D configurations on the system were compared, and analysed. The results were interpreted and conclusions drawn.
4. Chapter 5: Presents the effects of height on solar energy generation in three and two dimensions with consideration for a single tree because more complex equations would be required to describe all figurations when more solar trees are involved. Hence, it was adequate to utilize Mathematical analysis and Matlab programming to demonstration that energy collection occurs in the volumetric biosphere. It was established that 3DPV structures are capable of generating more power from the same base area when compared to the conventional flat solar panels. The other variable parameters, such as weather conditions, time of the day and such were assumed constant. This chapter discusses the methodologies for computation and analysis of the effect of height per unit volume compared with a plain surface arrangement and the obtained results are discussed. The reports on the remarkable effects of height on the generated power for both the two-dimensional and three-dimensional structures are given.
5. Chapter 6: Presents the 1D method of PV electrical modelling to determine the electrical output of PV panels at any given operating condition. The electrical behaviour of the PV system is non-linear and variation effects could only be determined by varying a parameter

while others parameters were fixed, using a 1D modelling with MATLAB programing. The electrical properties modelled for in 1D included the parasitic resistances (series resistance R_s , parallel/shunt resistance R_{sh}), temperature T , irradiation G , and ideality factor N . The obtained results were used as electrical properties to model for the 3D. The generated results in 3D were compared with the electrical parameters generated in 1D modelling.

6. Chapter 7: Presents the 3DPV methods of solar power generation. The PV structure was modelled and simulated in 3D. The performance forecast of the PV panel employed involved a radiation model, a thermal model and an electrical model. Both the radiation and thermal modelling were carried out by using COMSOL Multiphysics on the 3D geometry to determine the temperature distribution, electrical power output and the efficiency of the system while MATLAB was used for the 1D electrical modelling to determine the electrical output of PV panels at any given operating condition. The results were interpreted and conclusions drawn.
7. Chapter 8: Presents the summary of findings of work carried out in this Thesis. Conclusions were drawn on these findings and recommendations for future research were also proposed.

Finally, some of the modelling and simulation outputs in this work and some referenced materials, data and records used in the study are presented as Appendices.

CHAPTER TWO

LITERATURE REVIEW

2.1 Introduction

This chapter provides a general review of the literature. It explains why solar energy study and application is of interest and presents a broad review of the fast-developing solar technology industries. It reviews the challenges facing the solar energy industry and various research studies being made for improving solar energy generation. It further presents various technological approaches utilized in improving solar cell efficiency for the conventional solar system. Furthermore, it reviews the new technology of three-dimensionality of solar power generation in particular for thermal and solar photovoltaics. It critically reviews previous modelling and simulation of solar cells and panels to highlight the motivations, viewpoints, limitations, advances, contributions and their relevance to the current study. Lastly, it provides an overview of the key issues identified from the literature and how they provide leverage for the modelling success in the current research.

2.2 Brief on solar energy generation

Solar energy is one of the most significant sources of renewable energy that promises to grow its share in the near future. An international energy agency study, which examined world energy consumption, estimates that about 30 to 60 Terawatt of solar energy per year will be needed by 2050 [17, 18]. Solar energy is one of the key answers to energy demand of the world [18, 19]. The sun has the most abundant energy source for the earth and apparent surface temperature around 6,000K (10,340°F) [20] [16]. The atmosphere transmits extra-terrestrial solar energy by about 70 per cent on a very clear day to nearly 10 percent on a very cloudy day. As a result of the losses in the atmosphere and the fraction of photons being converted into electricity, the collection of solar energy and its conversion to electrical energy is just about 30% as shown in Figure 2-1 [21]. Solar energy has wide application as all other energy sources such as wind, fossil fuel, hydro and biomass energy have their origins in it.

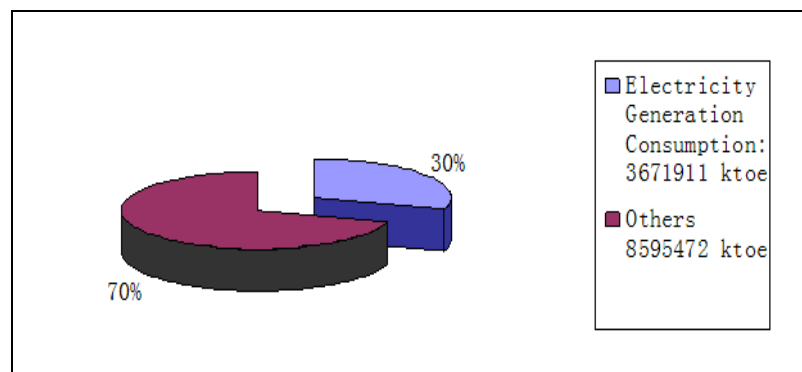


Figure 2-1: Electric energy consumption as percentage of total energy production in 2008 [21]

According to [22], the demand for energy worldwide is expected to keep rising at the rate of 5 percent each year, consequently, it behooves researchers and developers to find a way of meeting up with this challenge and to find solutions through suitable technologies that can meet up with the energy

demand. Solar energy is acknowledged as the most suitable choice that satisfies such a large and progressively increasing demand [19, 23, 24].

2.3 Solar technologies

Various solar technologies are at different levels of maturity, each with a significant potential for improvement. Continuous and sustained research, development and demonstration efforts are still ongoing over the long term in order to improve power generation output, accelerate cost reductions, existing mainstream technologies transfer, medium-term cell and system technologies development and improvement, and designing of novel concepts in order to bring them to industrial use. The overview layout of solar technologies is given in Figure 2-2 [21]. On a general note, non-concentrated solar panels (NCSP) and concentrated solar power (CSP) are the two most matured technologies and most commercialized and these are captured under non-concentrating photovoltaics (PV) solar and concentrated solar power respectively [19, 21].

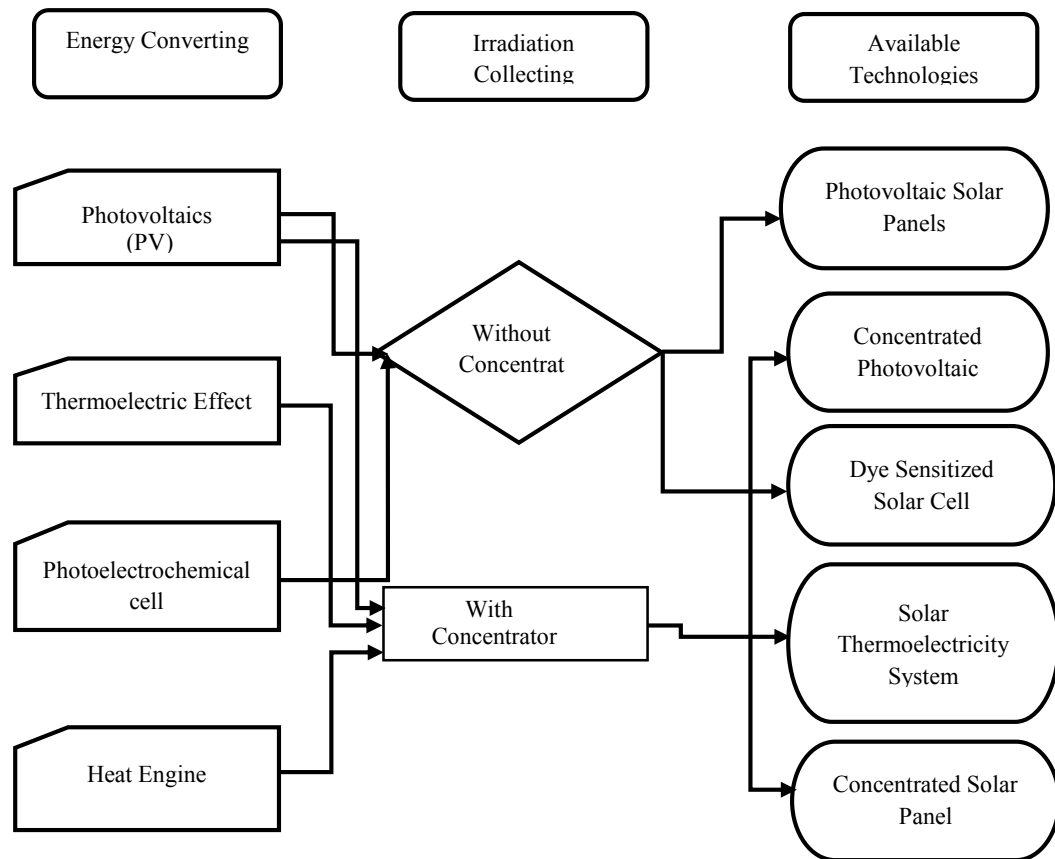


Figure 2-2: Overview of solar technologies [21]

Due to increasing demand for clean energy, particularly solar energy, crucial steps are being taken in the industry so as to keep up with solar energy's growing demands in the market. Identifying and improving on the appropriate technology is paramount to boosting solar energy generation.

2.4 Major solar power generation techniques

Different solar power generation techniques available and presented in this work are photovoltaics (PV) solar panel, concentrated photovoltaic (CPV) systems, Dye sensitized solar cell, solar thermoelectric effect and concentrated solar power (CSP) [19, 21]. A brief review of each technology is presented below.

2.4.1 Photovoltaics Techniques

One of the means of harvesting solar energy is by using PV cells but the problem with solar energy is its non-availability at all times due to weather variations and the problem that its demand for use coincides mostly with the times when it is cloudy or the sun is not available for direct energy conversion, mainly at night. These then negatively affect the efficiency of the PV system by reducing its output power. PV energy accumulated during high insolation times is therefore stored in a battery, not only to maintain power supply during low-irradiation times or cloudy periods, but also to provide a continuous electrical output when required. A battery is an electro-chemical device for storing electrical energy. PV energy sources can be used as stand-alone systems, hybrid system or grid-connected systems.

PV technology is classified into three generations of wafer-based crystalline silicon technology, thin-film PV technology and CPV / organic PV (OPV) technology, depending on the basic material being used and the amount of commercial maturity involved [19, 21]. The types of semiconductor materials being used for PV power generation are monocrystalline silicon, polycrystalline silicon, amorphous silicon, cadmium telluride, and copper indium gallium selenide/sulfide. The type of semiconductor materials used in PV energy generation determines its power output to some extent [9, 19].

(a) Crystalline Silicon

PV modules are mainly of wafer-based crystalline-silicon, constituting between eighty-five percent and ninety percent of the overall annual market. They are either mono-crystalline or multi-crystalline. Mono-crystalline is made of single or uniform crystalline silicon so its efficiency is highest and it is the most expensive. Multi-crystalline silicon modules are of lower atomic structure, hence they have reduced efficiency but are less expensive and are more resistant to degradation as a result of irradiation and hence, more durable [19]. As indicated in Figure 2-3, the modules currently use silicon as single sc-Si or mc-Si. Commercial single silicon sc-Si modules have greater conversion efficiency of about 14 to 20 percent [25]. Crystalline silicon PV modules dominate the PV market for now and may continue to do so until about the year 2020 based on results of their proven and reliable technology, longer lifespan, and abundant primary resources [26]. However, its efficiency and marketability still require improvement which is achievable through reduction in materials, cell concept improvement and manufacturing automation [27]. Si is the most common and popular semiconductor material used for solar cells manufacturing because its fabrication is easy to process and it is economically feasible for mass production. There are other materials that can yield greater efficiency conversion but they are either health hazards or economically unattractive [28].

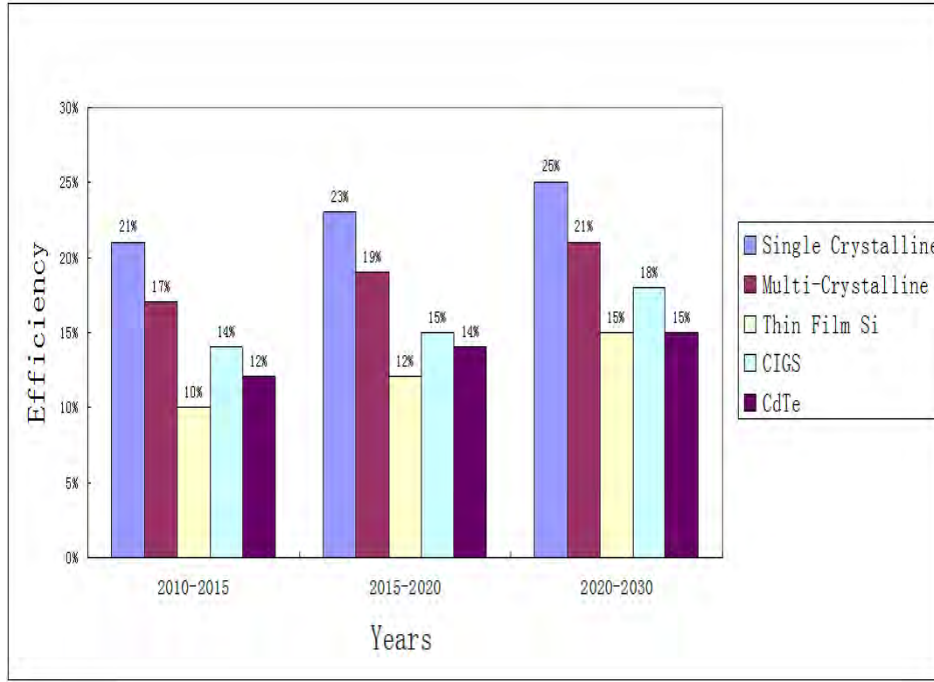


Figure 2-3: The expectation of photovoltaics efficiency improvement in future [29]

(b) Thin Films

Thin films are produced by making a deposit of a thin layer of semiconductor material (with respect to the thickness of a crystalline cell) on a substrate and then etching that semiconductor material into cells and wiring them together as a module [30]. There are three most important thin film materials available, namely: amorphous silicon (a-Si), cadmium telluride (Cd-Te), and copper indium gallium diselenide (CIGS or CIS) and each of these materials has its own properties. However, they have lower efficiency records and shorter lifespan durability [6]. Furthermore, their energy output is less due to their lower efficiency and would then require extra land for utility production than what crystalline silicon technology would require in order to reach the same capacity. Hence, land availability and cost are major factors for consideration when thin film technology is being considered [31].

(c) II-VI Semiconductor Thin Films

CdTe cells are semiconductor thin film technology with a comparatively simpler production process and lower production costs. The technology has attained higher production levels than any other thin film technology available. Similarly, it has attained a leading position in the thin film technology, and it has the most competitive cost-per watt and the least energy payback period of eight months among all other existing PV technologies [21]. However, CdTe cells are known to be toxic and less in abundance than silicon cells, hence, they are least suitable as recommendable semiconductor materials [22, 32].

2.4.1.1 Basic representation, equations and electrical behaviour of a PV system

The PV panel model is electrically represented by the equivalent circuit model shown in Figure 2-4:

Practical Cell

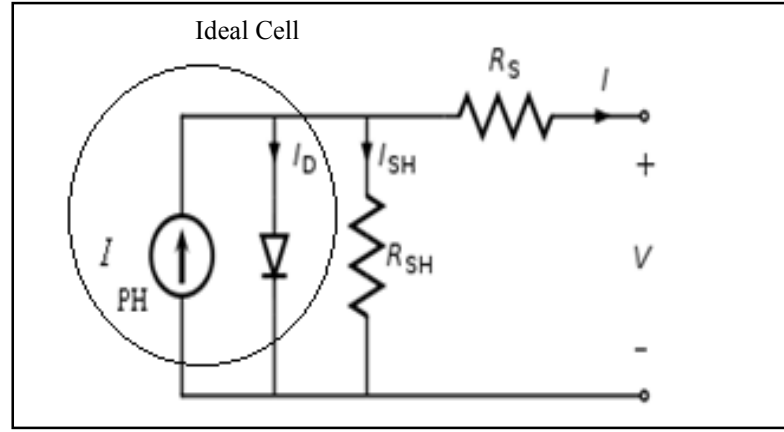


Figure 2-4: Simplified equivalent circuit of a photovoltaic cell

For an ideal PV cell

$$I = I_{ph} - I_d \quad (2.1)$$

Shockley diode equation is given by:

$$I_d = I_s \left[\exp\left(\frac{qV}{NKT}\right) - 1 \right] \quad (2.2)$$

For a practical cell,

$$I = I_{ph} - I_d - I_{sh} \quad (2.3)$$

and

$$I_{sh} = \left[\frac{V + IR_s}{R_{sh}} \right] \quad (2.4)$$

Hence:

$$I = I_{ph} - I_s \left[\exp\left(\frac{qV}{NKT}\right) - 1 \right] - \left[\frac{V + IR_s}{R_{sh}} \right] \quad (2.5)$$

R_s is more dominant in operation when PV is in the voltage source region. R_{sh} is the diode reverse voltage current and it is more dominant in operation when PV is in the current source region.

The presence of series resistance is brought about as a result of poor solar cell design. Its presence reduces the fill factor (FF), while excessively high values may cause further reduction in the short-circuit current. The equivalent circuit current equation then becomes:

$$I = I_L - I_o \exp\left[\frac{q(V + IR_s)}{nKT}\right] - \left(\frac{V + IR_s}{R_{SH}}\right) \quad (2.6)$$

The presence of shunt resistance is due to manufacturing defects and its presence causes appreciable power losses. The effect of low shunt resistance is largely severe at low light levels, since the impact of diverted current will be severe on the light-generated current. Furthermore, the impact is also greatly felt at lower voltages where the effective resistance of the solar cell is high.

$$I = I_L - I_o \exp\left[\frac{qV}{nkT}\right] - \frac{V}{R_{SH}} \quad (2.7)$$

In the presence of both series and shunt resistances, the IV curve of the solar cell is described by the equation:

$$I = I_L - I_o \exp\left[\frac{q(V+IR_s)}{nkT}\right] - \left(\frac{V+IR_s}{R_{SH}}\right) \quad (2.8)$$

The reverse saturation current, I_s , was determined by considering open circuit condition where (when) $I_{cell} = 0$ and at short circuit condition where (when) $I_{cell} = I_{sc}$. This implies that I_{sc} is equal to light generated current I_{ph} given by:

$$I_s = \left[\frac{I_{sc}}{\left(\frac{V_{oc}}{e(NKT)} - 1\right)} \right] \quad (2.9)$$

Series resistance (R_s) lower and upper limits are obtained from [28]

$$R_s < \frac{0.1 \times V_{oc}}{I_{sc}} \quad (2.10)$$

and

$$R_{sh} > \frac{10 \times V_{oc}}{I_{sc}} \quad (2.11)$$

For a PV module with N_s numbers of cells serially connected,

$$I_m = I_{ph} - \left[I_s \left(\frac{V_m + I_m R_s N_s}{e N_s V_t} - 1 \right) \right] - \left[\frac{(V_m + I_m R_s N_s)}{N_s R_{sh}} \right] \quad (2.12)$$

and,

$$V_t = \frac{NKT}{q} \quad (2.13)$$

$$P = V * I$$

$$\eta = \text{Efficiency} = \frac{\text{Maximum output power}}{\text{Incident light power}} = \frac{P_m}{EA_c} \quad (2.14)$$

and

$$\text{Fill Factor (FF)} = \frac{V_{mp} I_{mp}}{V_{oc} I_{sc}} \quad (2.15)$$

2.4.1.2 Electrical characteristic behaviour of solar PV/cells

A typical PV plot of current or power versus its voltage at standard temperature and pressure (STC) of (1000 W/m² irradiance, air mass (AM) 1.5, 25° C) is as represented below in Figure 2-5a [28]. The pink curve represents the Current-Voltage curve while the blue curve represents the Power-Voltage curve. The point I_{sc} on the Current axis is the PV short circuit current and the V_{oc} on the voltage axis is the open circuit voltage.

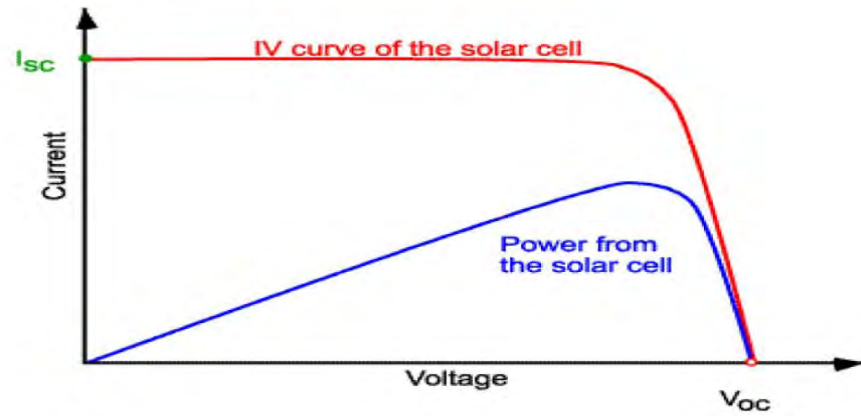


Figure 2-5a: Different curves for a photovoltaic module at varying irradiance and temperature [33]

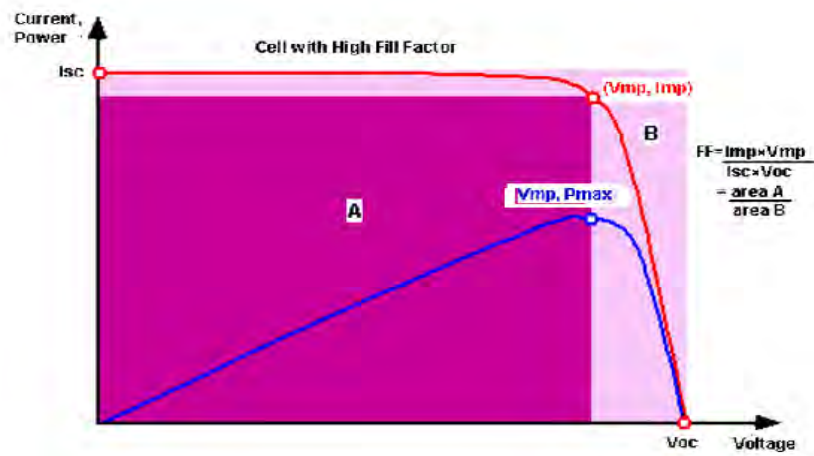


Figure 2-5b: I –V and P-V curves indicating maximum power point of a PV solar system[33]

In Figure 2.5b, I_{sc} is the maximum current from a solar cell which occurs at the point when the device voltage is zero, while V_{oc} is the maximum voltage from a solar cell which occurs at the point when the device current is zero.

Hence, when the device current = 0, Equation (2-13) becomes:

$$V_{oc} = \frac{nKT}{q} \ln \left(\frac{I_L}{I_o} + 1 \right) \quad (2.16)$$

At the operating point on the two graphs in Figure 2-5a and Figure 2-5b, where A (V_{mp}, P_{max}) and B (V_{mp}, I_{max}), the power from the solar cell is zero. The fill factor, FF, combines (I_{sc}) and (V_{oc}) to determine the solar cell maximum power such that:

The following attributes can be deduced from the behaviour of the PV graphs:

- The PV panel behaviour is non-linear as shown in Figures 2-5 as the operating system always changes and deviates from maximum power point (MPP) when atmospheric conditions change [16, 34, 35].
- The output power and current of the PV panel depend on solar irradiance G , the temperature T , and the cell's terminal operating voltage, V_{oc} [12, 13, 36].

- iii. Variations in temperature affect V_{oc} more than I_{sc} and V_{oc} diminishes with increasing T when G is kept constant as seen in from Figures 2-5. Furthermore, I_{sc} of the PV panel increases parallel to an increase in T , whereas the maximum power output decreases. The net power will continue to decrease at high temperatures in as much as the rise in I_{sc} is smaller than the reduction in V_{oc} [9, 37, 38].
- iv. Increase in solar irradiance G , also raises the panel output current as well as the output power whilst T remains unchanged as shown in Figures 2-5. This is borne out of the fact that I_{sc} is directly proportional to G while V_{oc} is logarithmically dependent on G [9, 37, 39].

Due to the non-linearity behaviour of the PV panel and non-availability of solar energy at all times, a maximum power point transmitter (MPPT) system or automatic tracking system (ATS) could be employed to deliver maximum power during the operation of the solar panel so as to track the changes in power due to changes in atmospheric conditions [9, 40]. The electrical behaviour of the solar panel as regards collecting of electric charges generated by light could be determined with fill factor (FF). It is an expression that describes the behaviour of the IV curve marked-out by the rectangle established by (V_{oc}) and (I_{sc}) and portrays the feature of the cell/module's junction [33].

$$FF = \frac{\text{Maximum power from the solar cell}}{\text{Product of } (I_{sc}) \text{ and } (V_{oc})} \quad (2.17)$$

This is the geographical rectangular area under the IV, PV graphs.

FF can also be defined as [33]

$$FF = \frac{V_{oc} - \ln(V_{oc} + 0.72)}{V_{oc} + 1} \quad (2.18)$$

where,

$$V_{oc} \text{ becomes normalised as } V_{oc} = \frac{q}{nKT} V_{oc} \quad (2.19)$$

And N = Ideality factor, where $1 < N < 2$

N determines the quality of the junction and recombination type.

FF is most commonly determined from IV measurement graphs as:

$$FF = \frac{V_{mp} I_{mp}}{V_{oc} I_{sc}} \quad (2.20)$$

The performance of solar cells from one to the other is rated by the cell's efficiency. Efficiency is the PV cell's effective attribute of the ratio of the solar cell energy output to the solar irradiation falling upon it. The spectrum and intensity of the incident light (sun) and the solar cell temperature, all affect the cell's efficiency. As a result the operating condition of the solar cell must be carefully controlled when determining its efficiency in order to enable performance comparison of one device to the other. For

control purposes, terrestrial solar cells are measured under standard conditions of Air mass (AM) of 1.5 and temperature of 25 °C or 298 K and solar irradiation of 1000 W/cm² or 1 KW/m²

From equation (K1),

$$V_{mp}I_{mp} = P_{max} = V_{oc}I_{sc}FF \quad (2.21)$$

The efficiency is defined as

$$\eta = \frac{V_{oc}I_{sc}FF}{P_{in}} \quad (2.22)$$

Where the parameters are as earlier defined and P_{in} = input power for efficiency calculation and it is also known as the in-coming solar irradiation with the value as given earlier.

By obtaining the area (A) of the PV cell/module from the PV manufacturers' data sheet, the efficiency of the PV cell/module could similarly be obtained by combining Equations (2.1) and (2.2) together to get the efficiency as indicated in equation (2.3) as:

$$\eta = \frac{P_{max}}{P_{in} \times A} \quad (2.23)$$

2.4.2 Concentrated photovoltaics technology

CPV is a PV technology that generates electricity directly from sunlight energy, using the PV effect. In contrast to conventional PV systems, lenses and mirrors are used to focus sunrays onto small, but highly efficient solar cells [41] with multi-junctions (MJ). Furthermore, CPV systems could use solar trackers or a cooling system to further increase their efficiency. Continuous research and development is speedily improving their acceptability in the utility-scale segment and particularly in the aspect of high solar insolation. This type of solar technology is therefore very appropriate for use in smaller areas [30, 42].

CPV systems are classified according to the amount of solar concentration involved as indicated in Table 2-1. During the concentrating process, energy is lost but in spite of it, CPV can still attain the highest efficiency among all kinds of other solar technologies. Commercial CPV modules with silicon-based cells offer efficiency in the range of 20% to 25% [32]. Other materials such as Ge (0.67 eV), GaAs or InGaAs (1.4 eV), and InGaP (1.85 eV) could also be employed. Since optics are employed to concentrate incoming solar radiation, CPV modules rely on direct sunlight to operate by using reflectors to concentrate direct solar radiation onto a solar receiver. Hence CSP collectors need to be used in regions with clear skies and high direct solar irradiation to maximize performance [19].

At the moment, CPV is not as common as conventional PV systems and it is not used in the PV rooftop installation. For locations with a high annual insolation of 2000 kilowatt-hour (kWh) per square meter or more, the levelized cost of electricity is in the range of R1.20 to R2.24 per kWh [41]. Different CPV energy systems are presented below:

Table 2-1: Various categories of concentrated photovoltaic energy system [41]

Part	Class CPV	Typical Concentration Ratio	Type of Converter
i	High-concentration, MJ cells	>400X	Multi-junction
ii	Medium-concentration, cells	$\sim 3X - 100X$	Silicon or other cells
iii	Enhanced concentration, modules	<3X	Silicon Modules

2.4.3 Dye-sensitized solar cell

The dye-sensitized solar cell (DSSC, DSC or DYSC), is also known as the Grätzel cell. It is an electronic device formed between a photo-sensitized anode and an electrolyte system. The dye converts the absorbed photons into free electrons in the TiO_2 , but only photons absorbed by the dye produce electric current [21, 22]. The rate of photon absorption is a function of the spectrum absorbed by the sensitized TiO_2 layer and as well of the solar flux spectrum. The maximum possible photocurrent is determined by the overlap between these two spectra. Normally, silicon has better absorption in the red part of the spectrum than the dye molecules, meaning that in sunlight fewer of the photons can be used for electrical current generation in dye molecules. These features limit the current generated by a DSSC. For example, a traditional silicon-based solar cell offers about 35 milli-ampere per square centimetre (mA/cm^2) while current DSSCs offer about 20 mA/cm^2 [43].

2.4.4 Solar thermoelectricity

In solar thermoelectricity, the concentrator beams and focuses the irradiation on a small area of lenses (absorbers) which increases the temperature of the receiver to very high temperature. Then, heat flows from the hot side to the cold side through thermoelectric material to generate voltage between the two ends [21]. Solar thermoelectricity employs parabolic disc technology to receive thermal energy based on the thermoelectric effect. A concentrator thermoelectric generator which is driven by low grade heat energy produces electricity, but the thermoelectric material (Bismuth telluride) still has very low efficiency of about $1.3 \sim 2.0$ [44, 45]. Like the other solar technologies with concentration requirements, this system collects only direct radiation. Hence high temperatures are required for it to work efficiently (~ 2000 , based on Carnot or thermal efficiency) and in order to have sufficient output. At present, solar thermoelectricity is considered not mature enough to meet the market requirements and besides thermoelectric material like Bismuth telluride is toxic and expensive [21]. However, due to the use of its low grade thermal energy, combining thermoelectricity generator with other solar technology systems as a hybrid system will enable it to achieve higher final overall efficiency [46].

2.4.5 Concentrated solar power (CSP)

CSP, also known as concentrated solar thermal, employs optical reflectors, such as lenses or mirrors, to focus direct solar radiation onto a very small area and using highly efficient solar cells made of a semiconductor material [21, 42]. Energy conversion from sunlight to electricity by CSP systems is based on application of heat engine instead of the PV effect which transfers photon energy directly from sun radiation into electricity, similar to what is obtained in PV solar cells. Electricity

generated in CSP is mainly by heat engines driven by burning of fossil fuels or hydropower. Solar power is generated by using mirrors or lenses to concentrate a large area of sunlight, or solar thermal energy, onto a small area of the mirrors or lenses. CSP utilizes the heat from the sun's radiation to drive a heat engine which is usually a steam turbine which is connected to an electrical power generator, to drive a turbine that produces electricity.

The conversion efficiency η of the incident solar radiation into mechanical work is a function of thermal radiation properties of the solar receiver and the heat engine (e.g. steam turbine) of the system. The solar receiver first converts the irradiation falling on it into heat with the efficiency $\eta_{Receiver}$ and thereafter, using Carnot's principle, it is then converted into work by the heat engine with the, η_{Carnot}

For a solar receiver supplying a heat source at temperature T_H and with a heat sink at room temperature T_0 , the overall conversion efficiency is expressed as:

$$\eta = \eta_{Receiver} \cdot \eta_{Carnot} \quad (2.24)$$

$$\eta_{Carnot} = 1 - \frac{T_0}{T_H} \quad (2.25)$$

with

$$\eta_{Receiver} = \frac{Q_{absorbed} - Q_{lost}}{Q_{solar}} = \quad (2.26)$$

Equation 2.26 is the ratio of the difference between flux absorbed by the system's solar receiver and flux lost by the system solar receiver to the incoming solar flux.

$$Q_{solar} = \eta_{Optics} ICA \quad (2.27)$$

$$Q_{absorbed} = \alpha Q_{solar} \quad (2.28)$$

For simplicity, it can be assumed that for high temperatures, the losses are only radiative. Hence, for a re-radiating area A and an emissivity ϵ , applying the Stefan-Boltzmann law yields:

$$Q_{lost} = A\epsilon\sigma T_H^4 \quad (2.29)$$

By considering the perfect optics ($\eta_{Optics} = 1$) and simplifying Equation (2.26) to Equation (2.29), collecting and reradiating areas equal and maximizing absorptivity and emissivity ($\alpha = 1, \epsilon = 1$), then substituting these equations in equation (2.25) gives

$$\eta = \left(1 - \frac{\sigma T_H^4}{IC}\right) \cdot \left(1 - \frac{T_0}{T_H}\right) \quad (2.30)$$

where,

T_H, T_0, I , and C are as earlier defined in the list of Engineering and Mathematical notations.

The efficiency obeys the laws of thermodynamics and the theoretical maximum efficiency achievable is determined by Carnot's cycle. The cycle declares that the heat engine efficiency is determined by the difference between the lowest and highest temperatures reached in one cycle as shown in equation (2.31) [21, 47]. Hence equation (2.30) can be re-written as:

$$\eta_{max} = 1 - \frac{T_c dS_c}{-T_h dS_h} = 1 - \frac{T_c}{T_h} \quad (2.31)$$

There are four basic CSP technologies as indicated in Figure 2-6. The first two (Linear Fresnel and Central receiver) are stationary devices which are independent of the plant's focusing device and enables the conveyance of collected heat to the power block. The second two (parabolic dish and Solar Trough) are mobile receivers which move along with the focusing device and mobile receivers to collect more energy in both line and point focus designs [21]. The main CSP technologies are shown below:

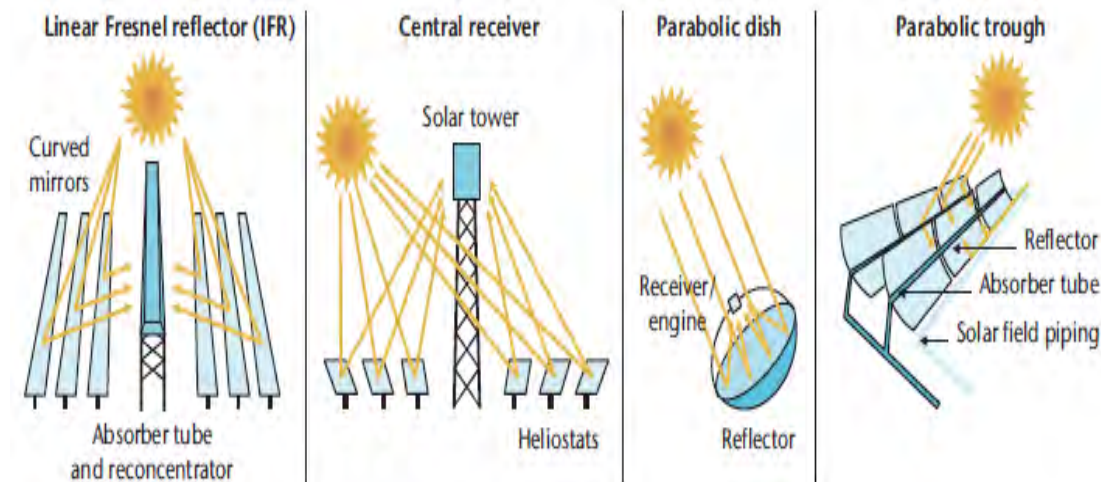


Figure 2-6: Different basic CSP technologies [32]

Most current CSP plants are based on trough technology as shown in Figure 2-7(a), but tower technology in Figure 2-7(b) is advancing and linear Fresnel installations are emerging more and more due to their advantages in terms of higher efficiency, reduced operating costs and promising prospects [21, 42]. The comparison of these different solar energy generation techniques is summarized in Table 2-2.

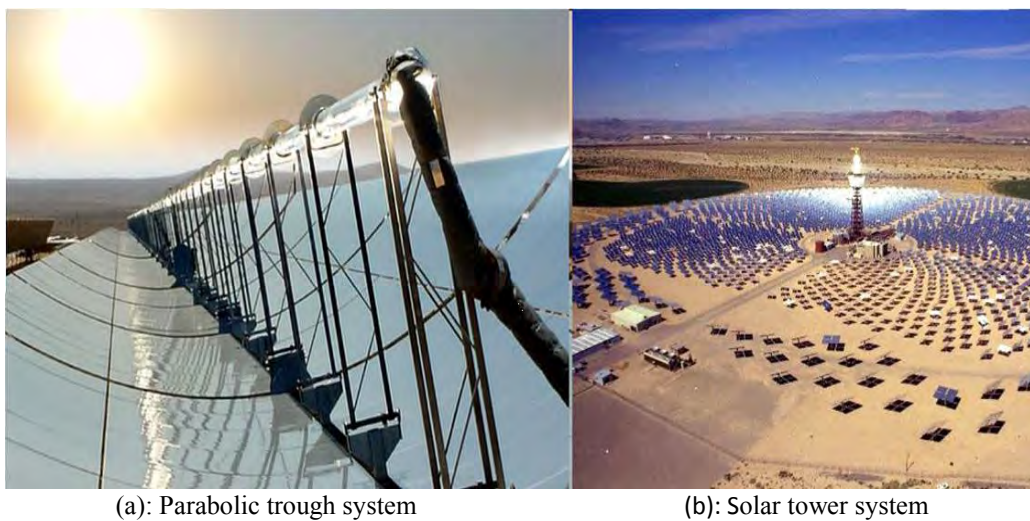


Figure 2-7(a): Parabolic trough system of concentrated solar power [21]

Figure 2-7(b): Solar tower system of concentrated solar power [21]

Table 2-2: Summary and comparison of different solar energy generation techniques

Solar energy generation	Techniques
Photovoltaic Solar Panels (without Concentrators)	Generates electrical power by direct conversion of solar radiation using PV solar panels. Most commonly used techniques in today's solar market.
Concentrated Photovoltaic Systems (with Concentrators)	CPV technology uses optics, such as mirrors or lenses to concentrate a large amount of sunlight onto a small area of solar PV semiconductors to generate electricity. Energy conversion is based on PV effect which directly transfers photon energy into electric energy with no heat involvement. This is recorded to be the highest efficiency ever achieved in laboratory.
Dye Sensitized Solar Cell (no Concentrators)	Generates electrical power Biomimics techniques based on cheap organic materials using Photo-electrochemical system.
Solar Thermoelectric Effect (with Concentrators)	Generates electricity using semiconductors (parabolic disc technology) to capture thermal energy based on the thermoelectric effect.
Concentrated Solar Power(with Concentrators)	Concentrated solar power uses optics, such as mirrors or lenses to concentrate a large amount of sunlight or solar thermal energy, onto a small area of solar PV semiconductors. Electrical power is produced by the conversion of concentrated light first to heat (thermal energy) and then to electrical energy through an electrical power generator connected. Energy conversion is based on the application of heat engine.

2.5 Limitation to solar energy generation

Solar energy conversion into electricity as a viable, clean and sustainable energy source and security against the gloomy global energy crisis is limited in its energy generation capacity. The conversion efficiency of solar cell to electrical energy is very low at present. The world's solar cell efficiency levels are: silicon cell panel up to 23.7%, poly cell panel up to 18.6%, and amorphous silicon cell panel up to 12.8% [6]. Hence, the technologies still require improvement in developing higher efficiency PV cells and modules, establishing lower cost manufacturing processes, improvements in the various components of PV systems, etc.

Different technological approaches to improving solar cell efficiency have been exploited and some of these approaches are briefly indicated below:

2.5.1 The use of the automatic tracking system (ATS)

An ATS system is an electronic device that operates the PV system in such a way that can enable the PV to deliver the maximum power it is capable of generating [9, 38]. Tracking is needed to improve electric power generation. Presently, there exists technology for collection of solar energy in the range of 600° F which favours solar energy generation which utilizes a three-dimensional auto-tracking system in order to attain the high temperature output needed by central station power plants for power

production in the multi-megawatt range [21]. There is the need for accurate tracking devices that are able to track under extreme weather conditions and in varying high wind forces on large three-dimensional concentrators [48].

2.5.2 The use of the maximum power point tracking (MPPT) system

The results indicated that generally, maximum power point tracking (MPPT) can be adopted to track the maximum power point in the PV system. The output power of the PV system varies, depending on the load current, temperature and insolation. The efficiency of the PV module was found to depend on both the MPPT control algorithm and the MPPT circuit. The MPPT control algorithm is usually applied in the DC-DC converter, which is normally used as the MPPT circuit [6] [49].

2.5.3 The scientific storage battery charging approach

A proper battery charge controller is required to balance the power flow from a PV system to a battery and to load this in such a way that PV power is utilized effectively. Whether solar energy is used as a stand-alone or particularly as grid-connected, to avoid losses of transmission and in contributing to reductions to CO₂ emission in urban centres, such a system needs to be available to provide electrical support whenever called upon to do so. The obtained energy from the PV system depends on the voltage produced in the PV module, the temperature of the cell and the solar irradiation [6].

The various approaches used in improving the solar cell efficiencies for optimum power generation are yet to yield appreciable improvements. That is why research interest is shifting in other directions. One of these directions is the area of new technology called three-dimensional photovoltaic (3DPV) structures. A conventional solar PV system is limited in its power generation, hence, the need for establishing improved technology in order to optimize power generation per installation area. Research studies are employing 3D technology for energy optimization and designing new 3D structures that can generate between 2 to 20 times the power output from the same base area when compared to using conventional flat solar panels [11, 50].

2.6 Three dimensional photovoltaic (3DPV) structure

3DPV technology is a new approach for achieving optimum solar energy that will yield a cost-effective, more reliable and more economically friendly alternative energy source. In 3DPV systems, the absorbers have multiple orientations that allow effective capturing of off-peak sunlight, and the re-absorption of reflected light within the 3D structure [11, 13]. It utilizes 3D nature of structures such as the spherical or cubic system, etc., to absorb power in the entire volume of that material. Hence, power is measured in Watts per unit volume as against per area measurement as is the case in the planar or two-dimensional (2D) system. Furthermore, the impact of height in system efficiency for the 3DPV has been found to be remarkable [4, 51, 52].

The plot of energy obtained in a day by the Genetic Algorithm (GA) optimized 3DPV structures compared with that of a flat panel under the same conditions was found to be much higher as shown in Figure 2-8: The insertion in the figure illustrates the power generated during the day for the flat panel as against what was obtained in the 3DPV structure at height of 10 meter [11, 53].

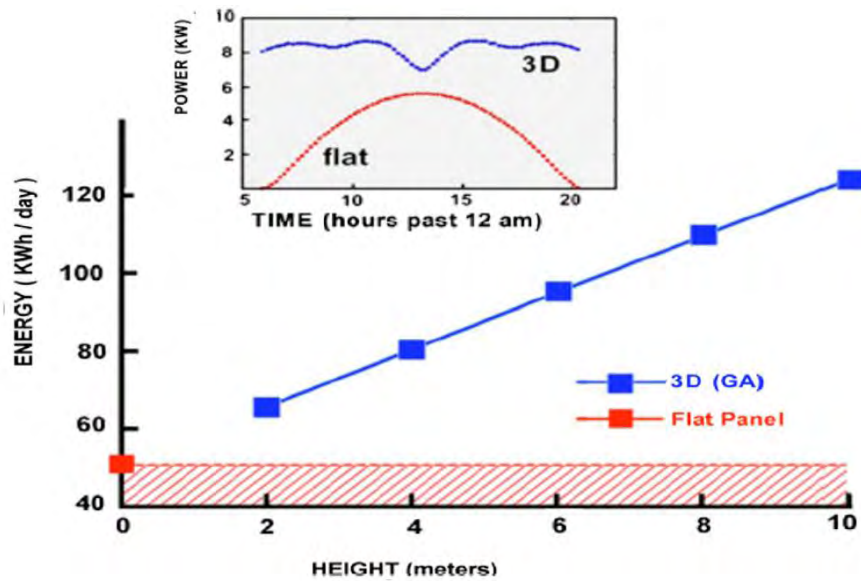


Figure 2-8: Energy plot comparison between GA optimized 3DPV structures and a flat panel [11]

These are major advantages of 3DPV over the planar arrangement. These are in contrast to the popular flat design of PV systems [54, 55].

2.6.1 Review of literatures on 3DPV structure

Various research findings have been made and are still on-going on solar energy generation. Research has proved that 3DPV structures are able to increase the generated energy density (energy per footprint area, Wh/m^2) in a linear proportion to the configuration height, for a given day and location [10, 56]. Some of these assertions on 3DPV technology are as stated below:

2.6.1.1 Fibonacci PV module (FPM)

The mathematical work of Leonard of Pisa, popularly known as Fibonacci, played a major role in utilizing the nature advantage of the abundant intake of sunlight energy. Fibonacci revealed through his analytical numbers that the leaf grows vertically upwards the stem in the direction of the sun so as to absorb more sunlight energy for its photosynthesis and this growth follows a spiral arrangement called 'phyllotaxis' [57]. Another research group, carried out a test on a 3DPV module whose configuration was based on Fibonacci numbers. The results of simulations on the test device revealed that the power generation characteristics of the solar cells depend on the shape and spacing of the solar cells for the most effective use of sunlight energy.

Some other researchers carried out some work on 3DPV technology based on Fibonacci's phyllotaxis:

1. The absorbers and reflected method - By using self-supporting 3D shapes, taller and more complex shapes - such as the open parallelepiped, cubes, trapezium and ridged tower for increased energy density that could enable the use of cheaper thin film material [10].
2. The Fibonacci PV module (FPM) - By using Fibonacci numbers to obtain the shape and spacing arrangement in a 3DPV structure for most effective solar radiation conversion into optimized output solar energy [8].

3. The Fibonacci PV module (FPM) - By using Fibonacci numbers to increase the number of solar module stages (height) in the FPM for volumetric energy output [51].
4. 3D nanopillar-based cell modules - By using new device structures and materials processing, such as embedded 3D single-crystalline n-CdS nanopillars in polycrystalline thin films of p-CdTe to facilitate high absorption of light and efficient collection of the carriers for acceptable efficiencies [55].

2.6.1.2 *Spherical solar technology (SST)*

Accurate 3D technology has been found to enable innovative and improved device design which can result in overall cost-effectiveness, improved material processing and system utilization. Of particular interest is the spherical Si solar technology (SSST) which has been found to be attractive because it uses low-cost Si feedstock and the fabrication process is found simple and inexpensive. Similarly, new innovation in PV installation exploits the use of cheaper, thin film materials on 3D shapes self-supporting structures to facilitate increased energy density generation. Hence, utilizing solar energy in three dimensions can open new avenues towards large-scale power generation [11, 54, 58].

2.6.1.3 *3D Nanopillar-based cell modules.*

In recent years, tremendous progress has been made in developing PV that can, potentially, be mass deployed. An example of this is in the use of 3D Nanopillar-based cell modules, with the aim to reduce solar cells cost by using novel device structures and materials processing for obtaining acceptable efficiencies. This enables the highly regular, single-crystalline nanopillar arrays of optically active semiconductors to be directly grown on aluminium substrates which are then configured as solar-cell modules. An example is a PV structure that incorporates three-dimensional, single-crystalline n-CdS nanopillars that is embedded in polycrystalline thin films of p-CdTe to enable high absorption of light and efficient collection of the carriers. Various other experiments and modelling have demonstrated the potency of this approach for enabling highly versatile solar modules on both rigid and flexible substrates. These display enhanced carrier collection efficiency that arises from the geometric configuration of the nanopillars [59].

2.6.1.4 *Solar energy generation by 3D method, using Fibonacci PV module (FPM).*

In Fibonacci PV Module, (FPM), the aim is to maximize solar power generation per installation area. Low-cost solar cells (Thin-film with conversion efficiency of 10%) were assembled in modules in 3D structures. The PV modules were arranged in the shape of a tree based of Fibonacci's sequence [51]. Eight solar cells make up a single stage in the module. As the number of stages increases, the total power generated also increases accordingly. For a single-stage FPM, the maximum power generated is about 75% [15], thus a two stage or three stage FPM maximum power output doubles or triples in values accordingly. In addition, the amount of generated power increases with increases in solar altitude. Thus a FPM will yield more power generation per installation area than a conventional plane module.

2.6.1.5 *Three-dimensional modelling and simulation of P-N junction spherical silicon solar cells*

Another new promising technology for PV energy conversion is the Three-dimensional simulated spherical p-n junction spherical silicon solar cells (SST). The simulation is based on models

using finite-difference method. It has been proved that the efficiency of a spherical solar cell is slightly lower than a conventional planar device but this is being compensated-for in terms of cost advantage. Furthermore, the materials being used are low-cost based, the device design gives optimal performance and the device processing technology is quite simple and affordable.

The spherical solar technology involves the use of tiny inexpensive Si spheres which are used as feed stock in the form of irregular shaped particles. These are melted and solidified into minute single crystalline spheres. The impurities are segregated to the outer layer to be removed, thereby improving their quality and purity and making them ideal for use for low-cost PV modules. Accurate Three-Dimensional (3D) modelling is necessary for advanced device design and material processing optimization [54].

The Three-Dimensional numerical approach has been used to overcome the modelling challenges. Simulation results in device quantum efficiency and the model is found to be useful in device design and simulation and in process optimization.

2.6.1.6 Three-dimensional nanopillar-array PV on low-cost and flexible substrates

In this technology, solar-cell modules are configured by growing optically active, highly regular single-crystalline nanopillar arrays of semiconductors directly on aluminium substrate [59]. The geometric configuration of the nanopillars enables highly versatile solar modules on the substrates achieved improved efficiency of the carrier charges. This method was reported not to be cost-effective. When nanowires are grown non-epitaxially on amorphous substrates, their random orientation on the growth could also limit the explored device structure. This is reported to be an improvement on the hitherto-common approach being used for the coating of the epitaxial growth of thin films by using single-crystalline substrate as the template.

The success of the technology is in the ability to produce high density, single-crystalline nanopillar arrays on an amorphous substrate with fine geometrical control. The reliance on epitaxial growth from single-crystalline substrates has been overcome. Reduced reflectivity from CdS nanopillar arrays was observed for small inter-pillar distance indicating that the light absorption properties in 3D nanopillar-based cell modules could be improved while enhancing the carrier collection[59].

In spite of the various technological improvements being made so far on solar power generation, its effect on costs has only marginally improved. The cost is still comparatively higher than conventional energy technologies. Furthermore, the effect of the high variation in solar panel electrical parameters such as output voltages, currents and powers due to environmental conditions such as temperature and solar irradiance are not favourable to solar power generation [13, 21]. Hence, it is paramount to decide on the feasibility or otherwise of installing a solar power plant at a location for a particular project before actually investing in constructing the plant. There will otherwise be a high risk of project abandonment or unsustainability. In order to avoid this risk, there is the need to carry out pre-analysis of the solar plant by carrying out modelling and simulation of the solar panels and solar cells.

2.7 The need for modelling and simulation of solar cells

Modelling and simulation of the solar cells and modules requires the use of appropriate software simulation techniques. This process is critical to the design and development of PV devices and systems.

One-dimensional simulations are usually employed but are inadequate for conventional geometry solar cells [60]. At high intensities, many cell designs with high efficiency require 2D simulations or even 3D simulations for correct interpretation of 2D/3D finite element analysis of electrical, optical and thermal properties of silicon semiconductor devices as well as for achieving accurate results [61].

There are numerous solar cell programs and commercial simulation tools used by researchers from all over the world for solar cells modelling. A few among them are SILVACO, TFT [16] and In Crosslight, APSYS, Advanced Physical Models of Semiconductor Devices, [17], Synopsys and COMSOL Multiphysics [14, 62].

COMSOL Multiphysics is an engineering software for modelling and simulating prototype scientific and engineering systems or structures. It enables the environment for building model geometries in 3D, 2D-Axisymmetry, 2D, 1D axisymmetry and/or 1D. It is possible to extend conventional models easily for one type of physics into Multiphysics models that solve coupled physics phenomena. However, a good knowledge of physics and material properties is required to enable the user develop the mesh for the finite elements, parameters and variables used within a model. The user could generate the required physics for the model design or select and add from COMSOL Multiphysics [63]. A basic modelling workflow is thus represented in Figure 2-9.

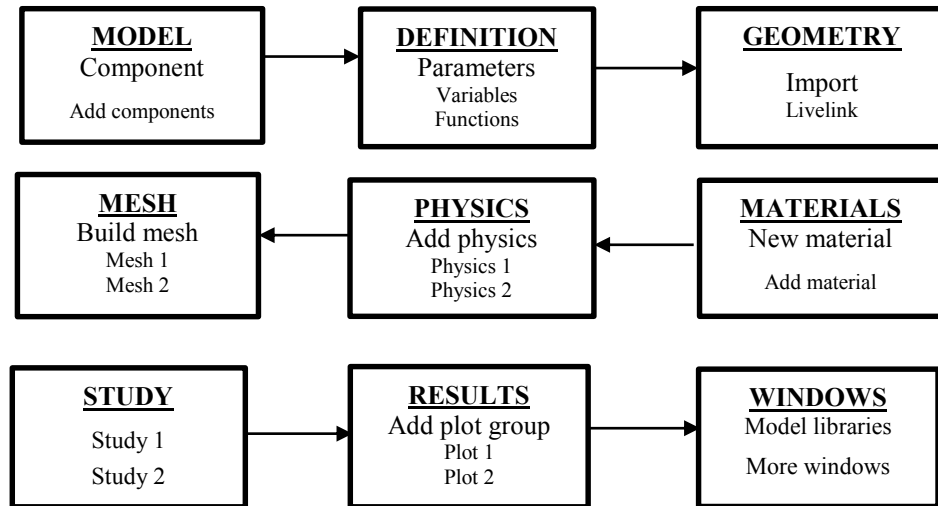


Figure 2-9: Basic modelling workflow in COMSOL Multiphysics

The built models define the relevant physical quantities such as material properties, loads, boundaries, sources, and variations which are often defined by the underlying equations. The variables, expressions, or numbers could be directly applied to solid and fluid domains, boundaries, edges, and points independently of the computational mesh. The control of COMSOL Multiphysics is enhanced through a graphical user interface (GUI) or by script programming in Java or the MATLAB language, using LiveLink. COMSOL Multiphysics Version 5.1 is used for the modelling and simulation in this work [63]. The objective is to determine the physics and materials for designing and developing innovative TPV and solar PV models and to simulate them for varying operating conditions for consequential effects. Their results are then interpreted and validated. The study of the models was first carried out in 2D and thereafter converted to 3D geometries.

2.8 Thermal CTPV modelling

In 3D modelling, the temperature distribution in the PV panel is calculated by using the thermal model. Factors determining the temperature distribution in the PV systems are the materials of the PV module, the cell type, the panel configuration, the electrical load attached to that PV system and the subjected environmental conditions. The thermal modelling could be with or without cooling and this also affects the temperature distribution. When cooling is involved, the heat exchanger attribute is also a factor.

There are different channels of energy transfer in the PV panel. The panel absorbs energy from the incoming solar radiation and loses energy by convection and radiation to the environment, by energy relocation experienced by the fluid in the heat exchange unit and also in the electrical energy delivered to the electrical load. The quantity of electrical energy loss from the system depends on the load characteristics and this determines the I–V characteristics, the electrical power output and efficiency of the PV panel.

There is need for TPV systems to maximize radiation heat falling upon them in order to enhance efficiency. However, the fraction of radiation not converted to electric power contributes to increased temperature in the PV cells and this is undesirable. Similarly, heat exchange through conduction causes increased cell temperature. On the other hand, the operating temperature range in a PV cell has its limit and this depends on the type of materials used. In general, solar cells are limited to temperatures below 80 °C, but semiconductor materials with high-efficiency can withstand as much as 1000 °C [64]. The temperature range in favour of PV efficiency has to do with some temperature at maximum above ambient. The temperature range utilized in this work varied between 500 °C and 2000 °C.

2.8.1 The implementation of the thermal model

The thermal implementation of the PV system is of importance since the temperature of the panel is constantly subjected to fluctuating temperature. Hence, the thermal model enables the study and estimation of the 3D temperature distribution of the PV system. COMSOL is therefore utilized in this work to carry out the study and calculations. The geometry, definition, dimensions and meshing for the 2D model already exists in COMSOL Multiphysics as seen in Figure 2-9. However, the model was positively revalidated against the existing one. Contributions were made to the existing 2D configuration by developing other 2D system configurations such as CTPV systems with six and eight mirrors respectively. Further contributions made were converting the existing and newly developed 2D models of the thermal PV into their corresponding 3D models as carried out and reported in Chapter four of this work.

The defined geometric, definition, dimensions and meshing were initiated in the 2D model using COMSOL Multiphysics as seen in Figure 2-9. The global definition for the heater is given in Table 2-3. The PV efficiency and solar electric output power were defined under global definition in Table 2-4. The thermal properties used in the model of the various materials are as given in Table 2-5. The electrical behaviours of the PV cell are characterised as indicated in Figure 2-10 (a, b and c).

Table 2-3: Global definition for the heater

Parameters Name	Expression	Value	Description
T_heater	1000 [K]	1000 K	Temperature, emitter inner boundary

Table 2-4: Global definition for the PV cell

Name	Expression	Unit	Description
eta_pv	if(T<1000[K], 0.2*(1 - (T/800[K] - 1)^2), 0)		Voltaic efficiency, PV cell
q_out	ht.Gm*eta_pv	W/m^2	Electric output power

The equations for the exchange of heat for solid and fluid domains are contained in equations (2.2) and (2.3) respectively [13] as:

$$\rho C_p u \cdot \nabla T + \nabla \cdot q = Q + Q_{ted} \quad (2.32)$$

$$q = -k \nabla T \quad (2.33)$$

The materials below, the emitter, mirror, PV cell and insulation described the materials used for the modelling and simulation of 2D geometry [64]. The emitter has a specific temperature, T_{heater} , as described in Table 2-3. Radiation was taken into account on all mirrors inner boundaries and low emissivity was applied to both the mirrors and the insulation while high emissivity was applied to the PV cells as indicated in Table 2-5.

Table 2-5: Basic materials property summary for CTPV [64]

Component	Thermal conductivity, k [W/(m·K)]	Density, ρ [kg/m ³]	Heat capacity at Constant Pressure, C_p [J/(kg·K)]	Emissivity, ϵ
Emitter	10	2000	900	0.99
Mirror	10	5000	840	0.01
PV Cell	93	2000	840	0.99
Insulation	0.05	700	100	0.1

Presented in Figure 2-10 is the temperature distributions in CTPV for the 2D geometry having the same number of PV cells and mirrors. The system in Figure 2-10 is a 2D CTPV subjected to heater temperature of 1.4×10^3 K. The 2D geometry experienced great heat distribution and consequently has a high temperature gradient. Further work shall be carried out in this thesis in order to determine the temperature distribution pattern of the 3D in comparison to that of the 2D PV system.

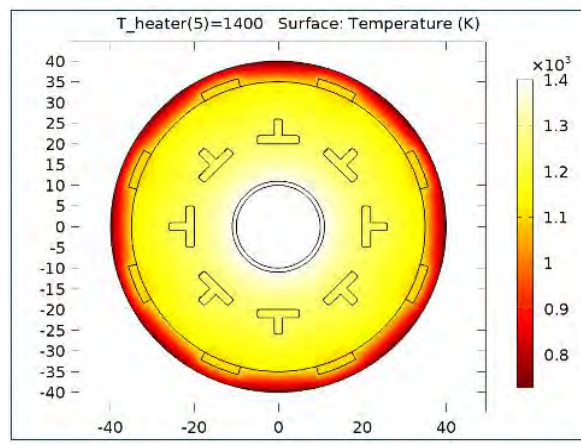


Figure 2-10: Surface temperature distribution at $T_{\text{heater}} = 1400$ K in 2D configuration for the CTPV system

The standard electrical behavioural pattern of the 2D CTPV system in Figure 2-10, when plotted against the temperature, reveal the behavioural pattern for the efficiency, PV cell temperature and the electric output power respectively as shown in Figures 2-11 (a, b and c).

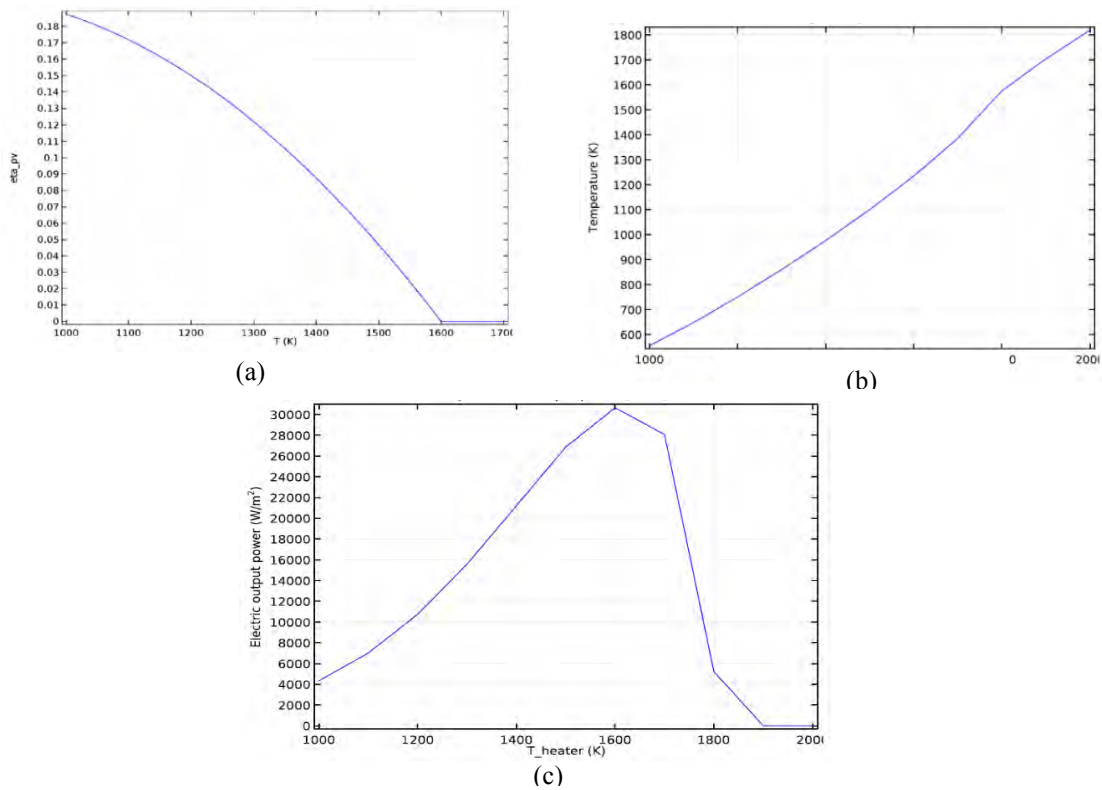


Figure 2-11: Plot showing the trend of (a) PV cell voltaic efficiency, (b) PV cell temperature, and (c) PV cell electric output power versus the operating temperature.

2.9 Non-concentrating solar PV modelling

Review was carried out on the other section of this work which is the modelling and simulation of the non-concentrating solar PV otherwise known as the direct solar PV system. In direct PV systems, the source of energy is sun and solar irradiation is directly converted to electricity with the aid of the electronic semiconductor material known as solar cell(s), module(s) or array(s). Due to different types of losses experienced by a PV system and coupled with the high cost of solar cells and the problem of weather and season variations, the need to optimize the generated output power in order to make the project worthwhile becomes necessary.

Solar PV study to predict the behaviour and performances of PV system are considered in two parts, namely, the electrical (1D) modelling and the thermal modelling (3D) modelling [13]. The electrical model in 1D is required as input to the 3D system to enable the investigation of the effects of varying operating conditions on the electrical parameters and to investigate the effect of variation in one parameter while the others are fixed constants. These type of graphs are not obtainable from the 3D plot but from the 1D plots [13]. The obtained parameters are required for verified against the manufacturers' data and then input them as electrical parameters for the thermal modelling.

2.9.1 Electrical modelling

The 1D modelling of the PV cells and Module is very crucial to the 3D modelling for the prediction of the panel operation. The PV nature or electrical behaviour is not constant as obvious from its characteristic electrical equations. The manufacturers' specifications at standard test conditions are used to determine and predict the behavioural patterns of the I - V , P - V graphs for varying T , G , R_s , R_{sh} and N . Information obtained from the PV manufacturers' datasheet such as open circuit voltage V_{oc} , the short circuit current I_{sc} , maximum power current I_{mp} , maximum power voltage V_{mp} are used in validating test or simulated results. This aspect has been extensively covered in section 2.4.1.1 and further reference on basic characteristics and equations of solar cell can be made to that section.

However, the effect of the cell parameters (R_s and R_{sh} and ideality factor) on the design and modelling of the solar cell or panel are worthy of note in solar cell/panel design and modelling.

2.9.1.1 Series resistance

The presence of series resistance is brought about as a result of poor solar cell design. Its presence reduces the fill factor, while excessively high values may cause further reduction in the short-circuit current. The equivalent circuit current equation then becomes [65]:

$$I = I_L - I_o \exp \left[\frac{q(V + IR_s)}{nkT} \right] - \left(\frac{V + IR_s}{R_{SH}} \right) \quad (2.34)$$

2.9.1.2 Shunt resistance

The presence of shunt resistance is due to manufacturing defects and its presence causes appreciable power losses. The effect of low shunt resistance is mainly significant at low light levels, since the impact of diverted current will be significant on the light-generated current. Furthermore, the impact is also greatly felt at lower voltages where the effective resistance of the solar cell is high and given as [65]:

$$I = I_L - I_o \exp \left[\frac{qV}{nkT} \right] - \frac{V}{R_{SH}} \quad (2.35)$$

2.9.1.3 Series and Shunt resistances

In the presence of both series and shunt resistances, the IV curve of the solar cell is described by the equation [65]:

$$I = I_L - I_o \exp \left[\frac{q(V + IR_s)}{nkT} \right] - \left(\frac{V + IR_s}{R_{SH}} \right) \quad (2.36)$$

where the electrical quantities are as defined before.

2.9.2 Irradiation and temperature effect on PV modules.

The variation in solar radiation reaching the ground is caused by some factors such as the distance travelled by the irradiation, time and seasonal variations, climatic conditions, apparent motion of the sun and tropospheric conditions. The proportion of the solar irradiation getting to a typical commercial PV panel is about 13 to 20% while the rest is converted to heat which is not useful to the PV system. All these variants affect the PV module performance [28] and to what extent they affect the performance need to be verified.

The light-emitted current is given by the equation [28]:

$$I_{ph} = [I_{sc} + K_i(T - T_{ref})] \left[\frac{I_r}{100} \right] \quad (2.37)$$

The equation above is used in modelling and determining the effects of irradiance. The effect of varying temperature is seen in the diode reverse saturation current, $I_s(T)$, and they are related as [28]

$$I_s(T) = I_s \left(\frac{T}{T_{ref}} \right)^3 \exp \left[\frac{E_g}{NV_t} \left(\frac{T}{T_{ref}} - 1 \right) \right] \quad (2.38)$$

2.9.3 Consideration for environmental parameters and cell parameters in PV modelling

The effect of environmental parameters on PV performances which are irradiance and temperature play crucial roles in PV study. According to [66],

$$I_{ph} = (G_k) [I_{sc} + K_1(T_{op} - T_{ref})] \quad (2.39)$$

This implies that the photo current, I_{ph} is a function of ambient irradiation, G in W/m^2 . As the G increases, I_{ph} also increases. The symbol K_1 is the change in panel short-circuit current, ΔI_{sc} in per $^{\circ}C$ at temperatures different from $25^{\circ}C$ or $298 K$. The value of K_1 increases as the operating temperature differs from the standard temperature of $25^{\circ}C$ or $298 K$, that is where $T_{op} \neq T_{ref}$ ($25^{\circ}C$ or $298 K$)

Similarly,

$$V_{oc} = V_t \ln \left(\frac{I_{ph}}{I_s} \right) \quad (2.40)$$

As the operating temperature, T increases, the open circuit voltage decreases indicating that the operating temperature of the PV cell, T in kelvin, linearly decreases with open circuit voltage, V_{oc} under standard test conditions of irradiation value, $G = 1 KW/m^2$ air mass, $AM = 1.5$ and operating temperature, $T_{op} = 25^{\circ}C$ or $298 K$, $I_{ph} = I_{sc}$. This is known to be the greatest current value condition.

2.10 3DPV thermal modelling

3D thermal modelling of the PV system is of great importance because the thermal modelling enables the temperature distribution study within a typical PV system. Temperature distribution within the PV system and its study, analysis and effects are vital to the system optimal performance. The 3D also is a representation of a process, concept, or operation of a system or structure which is often executed by a computer program for validating real-world measurements [67, 68]. It is recognised as a very important

part of any engineering practice. With the current use of computers and powerful software, extremely complex systems can be simulated for performance prediction and monitoring. Availability of models of all various components of the PV system at all stages is very important in system sizing, cost analysis and monitoring. Furthermore, such models could be tested together with other distributed system models in order to evaluate and predict the overall system performance [33].

The techniques in modelling PV systems stress the importance and the need for design considerations that are required to be undertaken in the course of modelling the 3DPV system. Environmental conditions are known to have a huge influence on the characteristics and performance of a PV module [28]. Contrary to the common practice of modelling in one-dimension (x and y planes) only, due to the complex nature of capturing the light sources in three-dimension and in order to obtain more accurate results, three-dimensional structure is usually utilized. One of the 3DPV model software programs to study the performance of the PV system is COMSOL Multiphysics. Materials selection choices in making-up the solar panel were studied and are as indicated in Table 2-5. Likewise the need for defining the physics selection for the selected materials is important and could either be user-defined or selected from the bank of physics equations from COMSOL Multiphysics. The use of appropriate meshing sizes are also important to successful modelling.

Removing the generated heat or turning it to useful energy is a viable solution to the negative effect of heat generation in PV energy system by converting the heat into useful energy and applying the appropriate heat transfer coefficients [13]. Heat transfer coefficients are a variant for determining the feasible method of drawing heat away from the cell. A forced method (water cooling method) offers the best results, bringing the cell temperature nearly back to ambient air temperature. Another method of cooling could be the free method (using air) [69]. These methods are promising solutions to the PV heat/efficiency problem and they provide the opportunity for the heated water or the extracted heat to be used for other applications and consequently increase the overall energy generation of the PV panel.

2.10.1. PV model materials

Modelling of the PV panel is composed of different layers of materials (depending on the photovoltaic technology used) such as the glass covering Corning 7059 Barium-Borosilicate, the encapsulants (for top and bottom layer of the PV cells) which are anti-reflective coating (ARC) for PV cells protection such as ethylene vinyl acetate (EVA), the PV cells, the metallic conducting Fingers and the metal back sheet/frame which is the final structural component support embedding the PV module.

These materials equally required modelling for optimum PV system operation performance [71]. The various layers are briefly reviewed in this chapter and illustrated in Figure 2-12a and Figure 2-12b but more details on them are presented in Chapters 3 and 7.

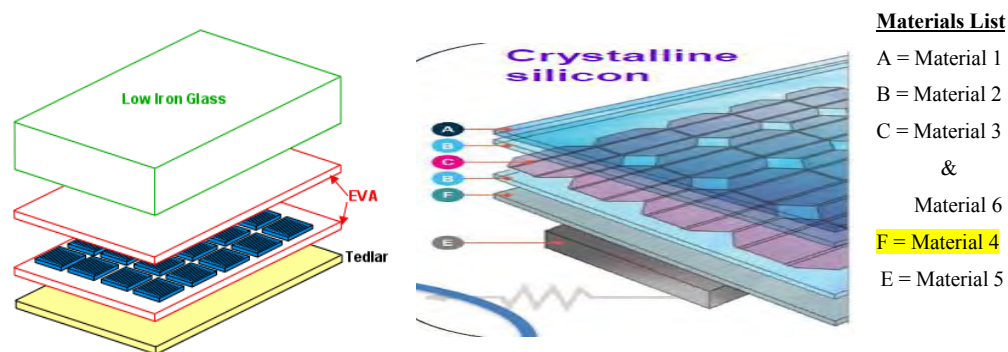


Figure 2-12(a): Materials structure in solar module [70]

Figure 2-12(b): Materials list in solar module [70]

2.10.2 Meshing of material

Meshing is an important aspect in modelling and simulation and it goes with experience on the job. There are no strict rules to meshing as variations in mesh size are necessary to determine how small or large a mesh size could be used without it affecting the results [72]. The temperature results in the model of the solar cell are not affected by the mesh size, however the process is important especially in models that are more complex because while smaller mesh sizes are more accurate, they result in longer computation times or may even run out of memory and therefore terminate the simulation, thereby yielding no results. A rather coarse meshing will more likely successfully complete running the simulation but may also compromise the results. Therefore, a proper mesh sizing (in-between) is necessary for a result yielding, non-compromising simulation [72]. A mesh size of 'Normal' when used for computations results in multiple rows of slices throughout the thickness of the cell.

2.11 Chapter summary

This Chapter presents various solar technologies with particular attention on concentrated thermal photovoltaic system (CTPV) and the non-concentrated photovoltaic (PV) system. Various literature materials that reported on these technologies were reviewed. Continuous research and development was reported to be on-going in order to improve the efficiency and acceptability of the solar energy in the segment of the utility scale. Attention was stated to be shifting in the direction of three-dimensional photovoltaic research in order to achieve power generation optimisation. The objective of building the 2D and 3DPV power system was reviewed to be for developing innovative PV and thermal models. A review was also carried out on the CTPV system modelling in 2D. This was given to be necessary in order to determine the impact of geometry on the electrical performance of multi-dimensional PV solar panels. For the non-concentrated PV systems, various practical electrical equations guiding the PV operation were also reviewed. Various materials used in modelling any or both of the PV technologies were reviewed as well as the factors affecting the operating performance and optimum output power generation of a typical commercial PV system. Such factors were given as the environmental, the PV internal and the electrical parameters. The materials composition of a typical solar cell was reviewed and the need for accurate meshing was revealed as well.

CHAPTER THREE

METHODOLOGY

3.1 Introduction

This chapter presents the methods and approaches used in determining the impact of 3D structure on solar power generation. There are two aspects to it. The first part handles the impact of 3D structure on the CTPV system while the other aspect has to do with the solar photovoltaic system (non-concentrated), simply referred to as the PV system. In this work, for the CTPV system, modelling and simulation in two and three-dimensions were carried out to investigate and predict the influence of the flame or emitter temperature (operating conditions) on the system efficiency, the output power and the temperature distribution within a typical CTPV system, using the engineering software package of COMSOL Multiphysics, version 5.1.

On the other hand, for the PV system, the 3D geometry of the solar panel was imported from solidworks website into COMSOL environment, using the livelink interface. The domains, boundaries, edges and points were set and materials properties defined and the geometry then modelled, meshed and simulated to study and predict the temperature distribution in the PV system and its thermal effect on the system efficiency and the output power generated while MATLAB programing was used in predicting the system's electrical performance for optimum power output. MATLAB was used for the electrical validation due to the complexities of modelling the electrical circuit in three-dimensions.

Most of the research methods commonly used in modelling and simulation of solar photovoltaic panels involve using simulation programs such as genetic algorithm [73], particle swarm optimization (PSO) method motivated by flocking and swarming behaviour of insects and animals [34], MATLAB programming, swarm intelligence (SI) motivated by the social behaviour of animals and insects [74], and colony optimization (ACO) motivated by trail-following behaviour of ant species and cockroach swarm optimization (CSO), to mention but a few. These conventional approaches are good in programing and simulating mainly 1D models. However, 1D simulations are usually inadequate for typical commercial solar panels but could pass for PV, especially at low solar intensities and for semiconductor materials that are not well formed. At high intensities, many PV cell designs with high efficiency require 2D simulations or even 3D simulations for correct interpretation of 2D/3D finite element analysis of temperature, efficiency, power and thermal properties of silicon semiconductor devices. Likewise, 2D/3D simulations are required for achieving accurate results due to the fact that their problems which are rather complex involve the use of increasingly large solution space. This has led to the use of more efficient engineering tools and software [13, 34].

There are numerous solar cell programs and commercial simulation tools used by researchers from all over the world for solar cells modelling in three-dimensions. A few among them are TFT, a device simulator in SILVACO, which contains physical models and specialized numerical techniques required to simulate amorphous or polysilicon devices and it is also used for thin film transistors [34]. Other programs include Crosslight, Synopsis and Advanced Physical Models of Semiconductor Devices (APSYS). The use of APSYS is centered on 2D/3D finite element analysis of electrical, optical and

thermal properties of compound and silicon semiconductor devices. Synopsis software is noted to have some solar cell simulation capabilities. Inclusion of various optical modules in the software makes the simulation package attractive for light dependent applications such as photosensitive or light emitting devices and solar cells. The Si rear-contacted cells (RCC) with textured front surface and using real-time (RT) techniques are recorded to compute enhanced optic absorption coefficients. Conversion efficiency is recorded as being improved upon with about 20.7 percent for certain textured devices and these are recorded to be in good agreement with the obtained experimental results [34].

For the PV system, the objective was to design and develop a practical technique of using complex geometries in 3D structures with various material properties in COMSOL Multiphysics without the challenge of physically assembling the multiple parts. The proposed method involved the use of COMSOL Multiphysics to define the parameters, variables and functions. The basic solar panel was imported from Solidworks website into COMSOL environment using the livelink but the building of the geometries were modelled in the COMSOL environment.

Multiphysics modelling of complex 3D geometries requires adequate knowledge and understanding of physics to enable the selection of material properties as well as to define and establish the global definitions required to model the 3D geometry. A proper understanding of the materials is required to enable the correct settings for the domain, nodes, boundaries and other necessary points in order to construct the entire geometry as a unit with each of its parts representing different materials. The Matlab program is a simpler practical alternative to modelling solar PV cells but it is restricted in modelling PV panel performances as far as 3D modelling is concerned, especially when dealing with multipart geometries that require assembling [13]. A custom algorithm was developed to enable the labelling of geometry nodes with corresponding materials. Then, interpolation functions of COMSOL Multiphysics were utilized to define material properties as a function of mesh coordinates. This method enabled incorporating two or 3D geometries with various material properties in COMSOL Multiphysics without the difficulties that may arise if the complex multipart geometries were to be physically assembled [75].

3.2 Three-dimensional modelling of the photovoltaic system

The impact of 3DPV technology and its promising potential is tremendous, especially in high altitude and adverse climate locations. It has been investigated and found that 3DPV technology is suitable for power generation in adverse weather conditions and for a more constant power generation across the day and at off-peak hours at high altitudes [4]. The innovative and potentially promising nature of this technology can be applied at multiple dimensional scales, such as small 3DPV towers acting as compact foldable power generators and to optimized integration of 3DPV towers in metropolitan settings. 3DPV technology when fully developed will ultimately pave the way for the integration of 3DPV with architectural and urban design for improved efficiency in energy generation at grid scale [76, 77]. The tremendous potential for the exploitation of 3DPV at different levels can be achieved only through extensive fundamental and technological, computational and experimental investigations of 3DPV technology. 3DPV technology is able to address problems regarding light reflection, incident angle, position with respect to the sun, panel arrangement with respect to one another and a number of other

issues defined as part of the complicated optimisation problems [50]. It is possible to optimize solar energy collection by incorporating 3DPV structure into the system in order to maximize the collection of indirect, reflected and diffuse insolation.

The first part of this work is the thermal modelling of a concentrated PV system in two and three geometries with water cooling, using COMSOL Multiphysics software and this is given in full details in chapter four of this thesis. A 2D modelling has already been achieved by COMSOL [64] with eight PV cells and an equal number of mirrors. This work was further remodelled in 3D with the same eight PV cells and equal number of mirrors and the results were validated against the one built by COMSOL. The validated results agreed with the COMSOL results. However, further contributions were made to already existing work by COMSOL by modelling in 3D and developing further models in 2D and 3D but with varying geometries with six and ten number PV cells and equal number of mirrors in order to investigate their effects on temperature distribution, efficiency and generated output power. The findings are detailed in Chapter four of this work.

The second part of the thesis is on thermal and electrical modelling of the non-concentrated PV system in three geometries with air cooling. Electrical modelling in 1D, using Matlab R2014b, was first carried out. It was necessary to carry out the 1D simulation of the electrical properties as these could not be determined by the 3D modelling. The study of the effects of environmental variations such as the temperature and irradiation on electrical parameters was undertaken one at a time, while others are kept constant. This is only possible with 1D modelling and simulation. The simulated results were then validated against the manufacturers' data sheet. Since these were positively verified within limits of acceptable tolerance, these validated parameters were then used as part of the simulation input for the 3D simulation on COMSOL Multiphysics, version 5.1. The details on this are given in chapter 6 of this thesis.

3.3 Three-dimensional modelling of a concentrated thermal photovoltaics energy system

The 2D existing model for the CTPV with COMSOL was re-modelled and the results were validated against COMSOL's results. The results were validated and in agreement with the existing results. In the re-modelling and simulation of the CTPV system, the 2D model of the CTPV was modelled for every segment of the CTPV system such as the heater, the mirrors, the PV cells and insulation. The CTPV geometry was modelled with its other different components. Selections were developed for the domains and boundaries which were used in implementing materials settings and boundaries conditions, using the COMSOL software.

The selected physics was heat transfer with surface-to-surface radiation interface. Thereafter, the CTPV model in 3D was developed from the 2D CTPV model, using the same approach. This ensured that the modelling parameters for 2D and the 3D of the CTPV could be compared directly one to the other.

3.3.1 Basic Modelling consideration for CTPV model, using COMSOL Multiphysics software

The basic simulation workflow for the 2D model of the CTPV, using COMSOL Multiphysics software, follow the same pattern as already shown in the chart in Figure 2-9. The heat radiated on the PV

cells is not fully converted into electric power but it is wasted away as radiation, conduction and/or convection and most often raises the temperature of the PV material and the material becomes hot. This heat reduces the efficiency of the solar material.

To lessen the temperature effect, the PV cells were cooled with water on their rear surfaces by free convective heat transfer (at the interface with the insulation). All the different boundaries experienced heat by conduction. The model simulated the emitter with a definite temperature, T_{heater} , on the inner boundary. At the outer emitter boundary, radiation (surface-to-surface) was taken into account in the boundary condition. The mirrors were simulated by taking radiation into account on all boundaries and applying a low emissivity. Both the inner boundaries of the PV cells and that of the insulation, used radiation boundary conditions. Nonetheless, the PV cells had a high emissivity while the insulation had a low emissivity. Furthermore, the PV cells converted a fraction of the irradiation to electricity and the remaining part remained as heat loss.

3.3.2 Governing equations for the CTPV model

Heat sinks installed on their inner boundaries simulated this condition by accounting for a boundary heat source, the heat transferred per unit time, q , is defined by in Equation (3.1) [64]:

$$q = -G\eta_{pv} \quad (3.1)$$

For water-cooling of the PV cells by natural or free convective heat transfer took effect and was as represented in Equation (3.2). According to Newton's law of cooling, the equation for convection (heat transfer per unit surface through convection) is expressed as:

$$q = h_c A dT \quad (3.2)$$

where q , A , h_c and dT are as defined in the list of Engineering and Mathematical symbols.

The convective heat transfer coefficient (h_c) is dependent on the type of medium, liquid or gas, the flow properties such as velocity and viscosity, and any other flow and temperature-dependent properties. The typical free convective heat transfer coefficient for water and liquids ranges from 50 - 3000 ($W/(m^2K)$) as referenced in the Appendix. In this work, h value of 50 was used.

The PV cell's voltaic efficiency is a function of the local temperature, having a maximum of 0.2 at 800 K and it is mathematically expressed as:

$$\eta_{pv} = \begin{cases} 0.2 \left[1 - \left(\frac{T}{800 K} - 1 \right)^2 \right] & T \leq 1600 K \\ 0 & T > 1600 K \end{cases} \quad (3.3)$$

where,

800 K is the PV cell maximum temperature.

At the outer boundary of the PV cells, water cooling by convection was applied to the model which satisfied the convective heat transfer with the water cooling equation defined as:

$$q_0 = h \cdot (T_{ext} - T) \quad (3.4)$$

where,

The heat flux is q_0 and the heat flux is for any fluid which can be liquid or gas/air.

$$h = h_{water}(D, T_{ext}) \quad (3.5)$$

For water, h takes value, h_{water} between 500 and 10,000 W/m^2K

T_{ext} = external or ambient temperature = 293.15 K

Lastly, at the outer boundary of the insulation, convective cooling for air with h set to 5 $W/(m^2 \cdot K)$ and T_{amb} to 293 K, were applied.

3.3.3 Properties of CTPV materials

The materials definitions used in the model are listed below. Their references and relevant material properties are attached in the Appendices.

Table 3-1: Material properties summary [64]

Component	k [W/(m·K)]	ρ [kg/m ³]	C_p [J/(kg·K)]	ϵ
Emitter	10	2000	900	0.99
Mirror	10	5000	840	0.01
PV Cell	93	2000	840	0.99
Insulation	0.05	10	100	0.1

The parametric solver was used by the model to calculate the stationary solution for a list of emitter temperatures (1000 K to 2000 K). The graph in Figure 2-10 shows the temperature distribution that changed with the operating condition within the CTPV system. The upper (right side) of the graph in Figure 2-11(b) investigates what the optimal operating temperature would be and illustrates the stationary distribution at working conditions with an emitter temperature of 2000 K. Further various parameters changes could be effected and investigated; such as the number of mirrors used, the number of PV cells used, the type of coolants used and so many other changes could be investigated to predict the CTPV performances with those changes. The results were post-processed and various graphs plotted, analysed and discussed.

3.3.4 The three-dimensional CTPV model

The 3D CTPV model was developed by determining and selecting the physics, using the same material properties for the 2D configuration. The materials physics could be chosen from COMSOL library or could be user-defined. This was followed by meshing and simulation, the details of which are given in Chapter four. As the materials selection and definitions are the same for the 2D and 3D models, the same physics on selected materials apply for the 2D and 3D models.

The same procedure of modelling and simulation as illustrated in the basic modelling workflow in Figure 2-9 was similarly followed for the 3D after importing the modelled 2D geometry into the COMSOL environment. The obtained results were post-processed, analysed and discussed. However, the number of points generated for the domain, boundaries, edges and points in the 3D modelling were greater than in the 2D model.

3.4 Non-concentrating solar PV energy system and modelling

The non-concentrating photovoltaic technology is simply referred to in this work as PV technology. PV technology provides the direct method of converting solar energy into electricity through the use of semiconductors. Modelling and simulation play vital roles in the development of PV devices as well as in the design of PV systems [13].

The 3DPV model was implemented in the COMSOL Multiphysics environment. The geometric model was 3-dimensional and was prepared and meshed using COMSOL Multiphysics mechanical code. The model consisted of four solid domains for the PV panel namely: front cover, back sheet, encapsulants (up and down) and the PV cells. The electrical properties used in the model for the various material are given in details in Chapter five.

In solar PV, the PV module materials, such as PV cell type, configuration of the panel, the electrical load attached to the PV system [13] and the prevailing conditions in the surrounding environment, all do affect the temperature distribution. The panel receives the incoming solar radiation and loses energy from it by convection and radiation to the surrounding environment, transferring energy to the working fluid in the heat exchanger and also delivering electrical energy to the connected electrical load.

The load characteristics determine the prevailing current–voltage (I–V) point and consequently the electrical power output of the PV panel. Usually, maximum power point trackers can be connected to the PV panel to ensure that the panel performs close to the maximum power point on the I–V curve [78]. The use of maximum power point trackers connection to the PV was not utilized in this thesis. The materials and the operating physics of the 3DPV model were determined and selected and successfully meshed and simulated in COMSOL Multiphysics while the electrical modelling and validation were carried out using Matlab.

3.4.1 Basic modelling workflow equations in 3DPV

The 3D model was developed by importing the 3D geometry into the COMSOL environment, using Livelink interface as earlier described. The materials and physics properties were defined, exported and developed in 3D geometry as earlier described and thereafter analysed and compared with the manufacturer's specifications.

The heat transfer equations [79] for solid domains respectively are:

$$\rho_i C_{p,i} \frac{\partial T_{i(x,y,z)}}{\partial t} = \nabla \cdot (q_i) + Q_i \quad \text{for } i=1,2,3 \dots \dots n \quad (3.6)$$

$$\rho C_p \frac{\partial T}{\partial t} + \rho C_p u \cdot \nabla T(x,y,z) = \nabla \cdot (q) + Q_{vh} \quad (3.7)$$

$$q = k_{cond} \nabla T \quad (3.8)$$

3.4.2 Thermal load equations and boundary conditions

According to [13], the absorbed solar radiation was determined by using the incoming solar radiation from the radiation model which is defined as :

$$\frac{G_a}{G_{ref}} = M \left(\frac{G_b + A_i + G_d}{G_{ref}} \right) \cdot R_{beam} K_{\tau\alpha,b} + M \left(\frac{(1-A_i) \cdot G_d}{G_{ref}} \right) \cdot K_{\tau\alpha,d} \left(\frac{1+\cos\beta}{2} \right) \times \left(1 + f \sin^3 \left(\frac{\beta}{2} \right) \right) + M \frac{G_h}{G_{ref}} \rho_{ground} K_{\tau\alpha,g} \left(\frac{1-\cos\beta}{2} \right) \quad (3.9)$$

and

$$S_{ref} = (\tau\alpha)_n G_{ref}$$

where, all the parameters in the equations are as defined in the list of Engineering and Mathematical notations.

The absorptivity of the PV cells, α , could be assumed to be 0.9 [13]

Only the absorbed portion of solar irradiation was transformed to electrical energy. Applying the heat transfer equation to this absorbed portion of the PV cell layer (as an internal heat generation, Q), as in [13] gives:

$$Q = (1 - \eta_{pv}) \cdot \left(\frac{G_a \times A_{panel}}{V_{pv,cell}} \right) \quad (3.10)$$

The PV panel electrical efficiency, η_{pv} , is then given as:

$$\eta_{pv} = 1 - \left(\frac{Q \cdot V_{pv,cell}}{G_a \times A_{panel}} \right) \quad (3.11)$$

3.4.3 PV model materials and consideration for selection

The PV cell is a p-n device that produces current when irradiated upon. The various material components of the semiconductor interface, from the top-layer material coat to the back cover of a typical semiconductor are as represented in Figure 3-1 and Figure 3-2(a) and Figure 3-2(b).

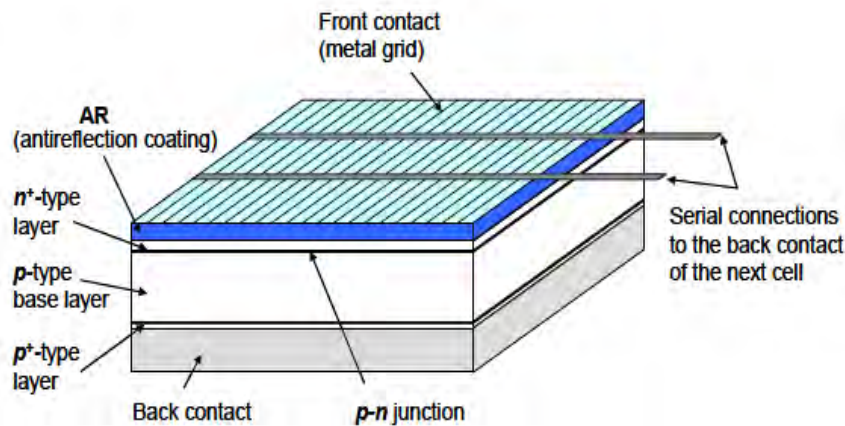


Figure 3-1: A typical structure of a c-Si solar cell [80]

The full details of the materials used 3D PV thermal modelling and their properties are described in Chapter seven. The general list of materials used in the 3D PV model are as indicated in Figures 3-2, Figure 3-2(a) and Figure 3-2(b) and are as listed in Table 3-1. However, there could be slight variation from manufacturer to manufacturer in material composition. Their references and relevant material properties are attached in the Appendices. The geometry of the model majorly consist of four solid domains for the PV panel namely: front cover, back sheet, encapsulants and the PV panel.

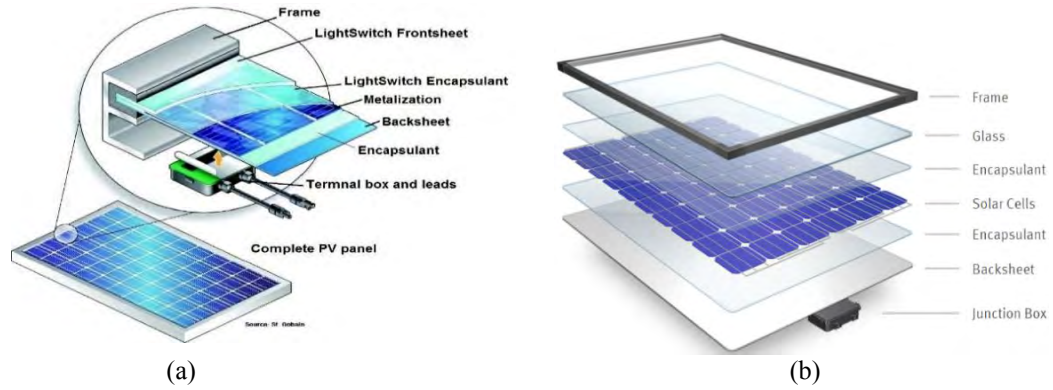


Figure 3-2(a): Solar panel make-up

Figure 3-2(b): Materials layout in solar module [82]

3.5 Selection of material properties

New material methods are being harnessed to pave way for solar cells as emerging power resources for the world to reckon with. According to the literature, for a typical PV module operating at its maximum power potential, about 75 to 80 percent heat is generated and the output power of the PV system drops to as high value as 0.4 percent for every 1°C rise in temperature [72]. Furthermore, temperature increase has been noted to adversely affect solar panels causing several failures and material degradation of PV modules due to associated stresses from thermal expansion due to elevated temperatures. Consequently, PV materials need to be selected in such a way that they do not have the chances of increasing the module temperature. In addition, adequate attention and analysis of temperature distribution in the solar panel needs to be properly interpreted for a good commercial PV panel operating at its maximum power potential. The properties of the material selected and used for modelling the PV panel were taken from literature as well as from the COMSOL Multiphysics material library and are as indicated below:

Table 3-2: Summary list of materials for solar photovoltaics

List of materials	List of materials	Location
Material 1	Corning 7059 [solid]	Frontsheet materials
Material 2	Elvax 250 (28% VA, 25 MI) [solid]	Module encapsulant sheets
Material 3	Silicon	Silicon semiconductor
Material 4	Elvax 250 (28% VA, 25 MI) [solid]	Module encapsulant sheets
Material 5	PET (polyethylene terephthalate or Mylar) [solid]	Backsheet materials
Material 6	Copper	Cell metallization pastes on silicon

The materials selection in the design of the PV module was carefully done to ensure optimum power output and durability. Most PV bulk silicon PV modules consist of a transparent top surface, encapsulant, a rear layer and a frame around the outer edge. In most modules, the top surface is glass, the encapsulant was EVA (ethyl vinyl acetate) and the rear layer was Tedlar. Below are the brief descriptions of each of these materials for expected electrical performance.

3.5.1 Front surface materials – Material 1

The top surface of the PV module possessed high light transmission of appropriate wavelengths. The transmission wavelength for silicon solar cells, range from 350 nm to 1200 nm [22]. In addition, the front surface reflection was ensured to be low but was not made rough so as not to attract dust and particles. Furthermore, the top surface material was ensured to be waterproof, having good bearing resistance, ensured to tolerate prolonged ultraviolet (UV) exposure and possessed small thermal resistivity as water or moisture migrate into the PV panel would oxidise the metal contacts and all interconnects, and consequently lower the lifetime of the PV module. The top surface and the rear surface were ensured to be mechanically strong and firm so as to provide support to the solar cells and the electrical wiring. Available options good for consideration for a top PV surface material were acrylic, polymers and glass. The most commonly used is the tempered, low iron-content glass because it is low cost, strong, stable, highly transparent, impervious to water and gases and has good self-cleaning properties. The one considered in this work for this purpose was Corning 7059 Barium-Borosilicate Glass and it is tagged Material 1 [83]. This was extracted from [84] as at 1st December, 2015 at 1:51 PM].

An encapsulant was used to give bond and protection between the solar cells at the top surface and also for the rear surface of the PV module. The encapsulant was ensured to be safe at high temperatures and to high UV exposure. It was ensured to be optically transparent and possessed a low thermal resistance. EVA (ethyl vinyl acetate) is the most regularly used encapsulant material and it was the one considered for this work. EVA comes in thin sheets and the solar cells normally are inserted between the top and bottom encapsulants as a sandwich. This sandwich was then heated to 150 °C to polymerize the EVA and bond the module together. So there exists ‘encapsulant up’ and ‘encapsulant down’. In this work, these are materials 2 and 4 respectively while obviously, material 3 is absolutely PV solar cell. The material used for this purpose in this work was Elvax 250 UP.

3.5.2 Rear surface – Material 4

It is important and it was ensured that the rear surface of the PV module possessed low thermal resistance and is capable of ensuring the protection of water or water vapour into the PV module. In most PV panels, a thin polymer sheet is often used as the rear surface such as Tedlar. Some PV modules, known as bifacial modules are designed to accept light from either side of the solar cell. In bifacial modules both sides are ensured to be optically see-through. The rear surface material used in this work is Elvax 250 Down.

3.5.3 Solar cell – Material 3

Material 3 is the solar cell that is sandwiched between the upper and lower Encapsulants. The details are given in Chapter five of this Thesis.

3.5.4 Finger – Material 6

The finger is the metallic lines of good electrical properties that run through the surface of the solar cell in convectional solar panels. This could be made of Copper, Silver or Gold. The recently manufactured solar panels no longer have Fingers on them. More details about this are given in Chapter seven of this work.

3.5.5 Frame – Material 5

The frame is the final structural part of the panel used for enclosing the module. A typical PV module casing is made of aluminium due to its strength and non-corrosion. The frame structure needed to be free of any entanglement from water lodgement, dust or other matter. The material used in this case is Mat 5 - PET (Polyethylene terephthalate or Mylar).

Improper selection and modelling of suitable and quality materials will ultimately jeopardize the integrity of the overall aim and intended purpose of the designed solar panel. Some of these effects of improper materials selection are presented in this work. EVA and PVB are types of commonly used encapsulants for PV systems. They provide bond and protection between the upper and lower surfaces holding the solar cells together. Figures 3-6 and 3-7 show the breakdown of this encapsulant, thereby leading to browning EVA in PV modules, indicating an error or improper material selection.



Figure 3-3: EVA browning in field PV modules [85]

Figure 3-3 and Figure 3-4 shows the 1990 EVA Browning Crisis at Carrisa PV Power Plant, California, USA, where the annual power output got degraded by over 45 percent from 1986-1990 as a result of encapsulant browning.



Figure 3-4: Severe EVA browning on mirror-enhanced PV arrays [85]

Figure 3-5 shows irregular browning in PVB encapsulant, caused by water ingress and consequently leading to corrosion. This encapsulant has failed in its intended service of optimum power generation.

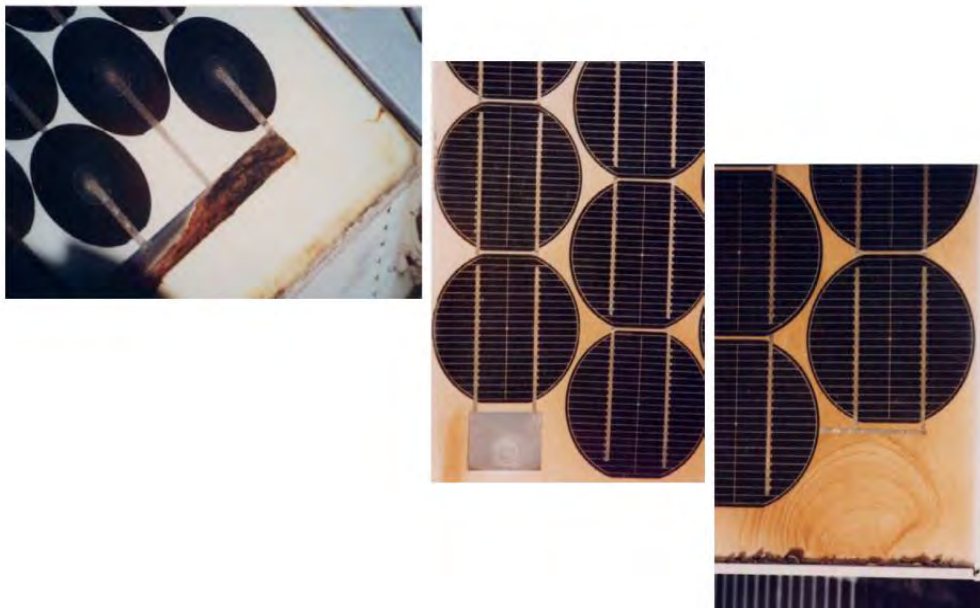


Figure 3-5: Irregular PVB browning - water ingress and corrosion [85]



Figure 3-6: Degraded modules [85]

Figure 3-6 and Figure 3-7 are additional pictures showing a degraded PV module as a result of materials failure, thus stressing the importance of proper material selection in the modelling of PV panels for optimum power generation and durability.

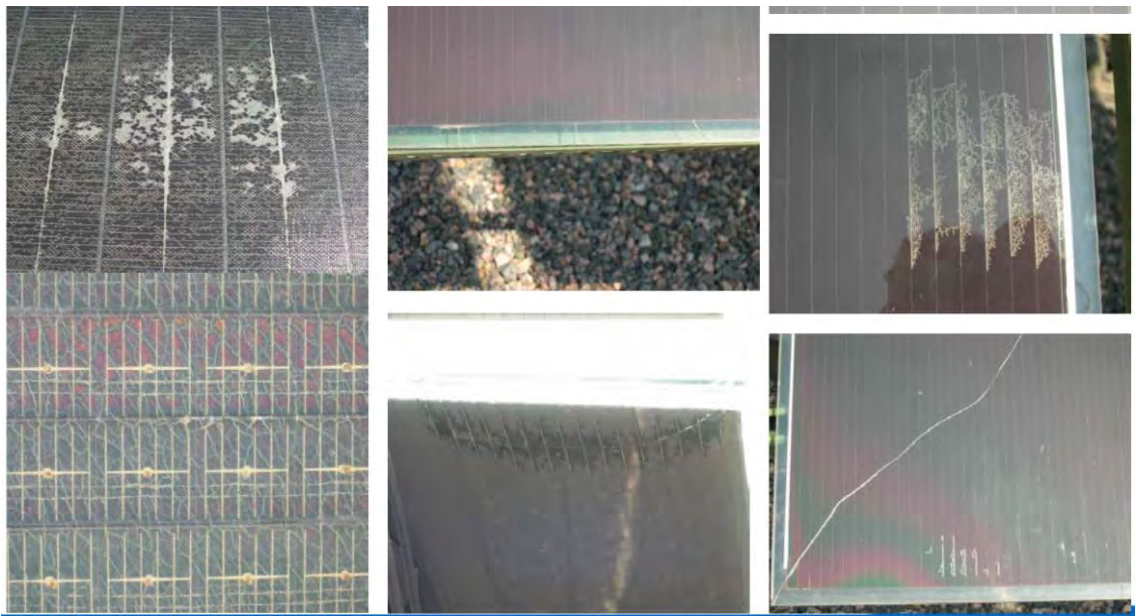


Figure 3-7: Degraded Thin film module at NREL OTF [85]

Proper selection and initial tests of encapsulation materials are, therefore, important. Different encapsulant formulations (e.g., EVA) are essential as these lead to different quality and different PV

performance. Encapsulation methods and processing conditions must be of high quality as these can affect the laminate quality and reliability of PV modules. Adequate accelerated exposure is useful and must be ensured to assess the performance expectation of materials and quality of processed components. The overall module reliability and performance was determined by all component materials and processing factors hence they were carefully determined and chosen.

Proper material selection was therefore carefully carried out to ensure that the developed and modelled 3D PV panel can stand the test of time if it were to be physically built. Supporting material specifications on the selection are referenced in the APPENDICES.

3.6 Meshing of modelled PV panel

Variations in mesh size were explored to determine how large a mesh size could be used without affecting the results. The temperature results in the model of the solar cell were not affected by the mesh size, however this process is important especially in models that are more complex because smaller mesh sizes, generate more accurate results but they have longer computation times. A mesh size of “Normal” was used for these computations, resulting in multiple rows of slices throughout the thickness of the cell.

3.7 Electrical characteristics of the system

The electrical model was carried out in 1D simulation, using Matlab link. This is because the program is a simpler alternative to modelling solar PV cells due to the complexities of modelling the electrical circuit in 3D. Hence, Matlab programing was used in predicting the system’s electrical performance for optimum power output and for the electrical validation. This is treated in details under chapter six of this thesis.

3.8 Chapter conclusion

This Chapter presents the approaches used in determining the effects of 3D structure on two different technologies of solar power generation. The first part considered the effect on CTPV technology and the second part considered the non-concentrated PV technology. In both cases, modelling and simulations were carried out on the systems considered, using COMSOL Multiphysics, version 5.1 in CTPV technology and both the COMSOL Multiphysics and MATLAB/Simulink R2014b for the non-concentrated PV system.

For the CTPV technology, an existing model was re-modelled and the results obtained were validated as expected against the existing built model. Thereafter, new and different CTPV configurations in 2D and 3D models were developed, modelled and simulated as contributions to the existing work.

For the non-concentrated PV, the Sunpower and Yingli PV panels were both modelled, simulated and considered to select a better option of the two for use for further modelling in 3D, study and analysis, using MATLAB/Simulink R2014b for the reasons stated in this Chapter. Sunpower X21- 345 and Yangli YL-260C panels are among the first best ten available PV panels. The validated electrical values obtained from the Yingli panel were used as the input parameters for its 3D modelling and simulation, using COMSOL Multiphysics, version 5.1. The 3D obtained results were analysed and interpreted.

CHAPTER FOUR

MODELLING AND SIMULATION OF THERMAL PHOTOVOLTAIC ENERGY SYSTEM

4.1 Introduction

This chapter first presents various thermal energy technology options available and status update. CTPV energy system is of interest for research because of its huge potential and its fast-growing usage in the international market today. Among many other uses, CTPV is used for heating water for domestic usage, in spaces in residences and in commercial buildings, in solar assisted cooling, the swimming pool, solar-assisted district heating, industrial process heat, desalination, agricultural products and in services such as drying, hatcheries, chick brooders and seed germinators, solar cooking and electric power generation to mention but a few [86]. This chapter also presents the work done on the investigation of the impact of the 3D structure on the CTPV system. Modelling and simulation are essential in the design and development of the CTPV system [42]. An innovative thermal model shall be used to simulate the thermal performance of CTPV modules. For this purpose, the parameters for the materials involved in thermal energy generation were defined and the appropriate physics were applied in the study of various operating conditions that affect the system performance for the two-dimensional system. This model was later used for the developing of the 3D system. This was done in order to establish the conditions at which the thermal PV systems, like any other power generating systems, would maximize the input energy source, radiation and heat transfer in order to improve its efficiency for better performance and improved energy output.

4.2 Concentrating solar thermal energy conversion

Solar thermal energy (STE) exists today as concentrating solar plants (CSP) in parched and semi-parched regions since 2009 [19] and shall be referred to as concentrating solar plants (CSP) in this thesis. This is because the use of concentrators (solar collectors) in generating electricity is crucial. Solar energy radiation can be concentrated to produce heat which can be collected at sufficiently high temperatures to make electricity. The devices used to concentrate the sun's radiation on the PV cells are called concentrating solar collectors (mirrors or lenses) and the radiation is in the form of heat. There are four types available, namely: parabolic dish, parabolic trough collector, power tower (heliostat field focusing on a central receiver) and compact linear Fresnel reflector. These are presented as shown in Figures 4-1(a) to 4-1(d) [42]. The arrows in each of the figures show the path of the sun's heat and how they concentrate on a point on line. Only trough collectors have been deployed in commercial service so far [32, 87]. Four different available types of CSP [87] are briefly described as follows:

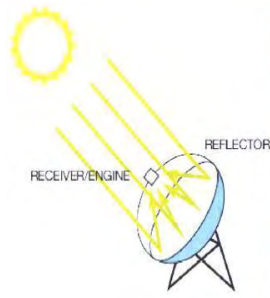


Figure 4-1(a): Parabolic dish

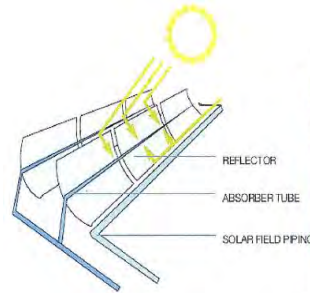


Figure 4-1(b): Parabolic trough

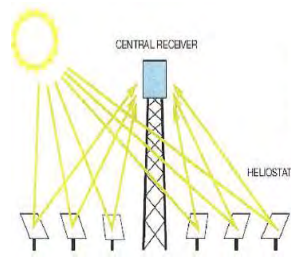


Figure 4-1(c): Central receiver with heliostats

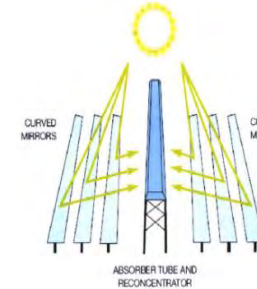


Figure 4-1(d): Linear Fresnel reflector

CTPV is relatively new when compared with PV solar energy, but a steady progress is being made when one considers the generated CSP in the years 2009 and 2013 respectively as contained in Table 4-1. The most developed technology is the parabolic trough, with a recorded use of over 20 years operation in California. The other technology options have only been constructed in the last few years, but look promising as well. For instance, the compact linear Fresnel reflects types are much simpler to build, and are potentially cheaper on a large scale [19].

Table 4-1: Progress in concentrating solar plants (CSP) since 2009 [19]

Description	End Of 2009	End of 2013
Total installed capacity	600 MW	3.6 MW
Annual installed capacity	100 MW	882 MW
Annual investment	USD 1.8 billion	USD 6.8 billion
Number of countries with 50 MW installed	2	5
STE generated during the year	0.9 TWh	5.5 TWh

CSP looks appropriate to be considered as a suitable solar energy option for reducing climate change because it generates electricity and produces no greenhouse gas emissions, hence it could be a key technology. In addition, a CSP plant is flexible and enhances energy security as it has thermal storage ability that ensures firm electric capacities and time-shifting electricity generation. It could also be part of a hybrid plant thus lowering the cost of solar electricity. CSP technology is diverse, ranging from power tower to parabolic trough, Dish-engines and concentrated linear Fresnel reflector (CLFR). The operating characteristics of the different CSP technologies are as presented in Table 4-2. In CSP operation, the working temperatures and towers are increased with a great variety of designs and applications to meet the energy needs in a variety of ways [88].

Unlike in solar PV technologies, CSP plants have the advantage of using steam turbines that will essentially provide all the needed ancillary services. Moreover, they have an intrinsic capacity to store thermal energy to electricity for later conversion. Combining CSP with thermal storage capacity of full-capacity generation that will run for several hours will enable CSP plants to continue production of electricity and with no disturbance even in cloudy conditions, or in the early morning or evening when power demand goes up. The CSP technology in generating electricity in plants presents significant potential for supplying specialized demands such as process heat for industry; heating co-generation, cooling and power; and water desalination.

Table 4-2: Operating characteristics of concentrating solar power technologies [87, 89]

CSP Technology	Concentration Ratio	Tracking Requirement	Operating Temperature	Average, solar to electric efficiency	Unit size Range	Installed Capacity 2009
Power Tower	500-1,000	2-axis heliostats	400-600 ⁰ C	12-18%	30-200 MWe	40 MW
Parabolic Trough	10-100	1-axis reflector	100-400+ ⁰ C	8-12%	30-100 MWe	500 MW
Dish-Engines	600-3,000	2-axis	600-1,500 ⁰ C	15-30%	5-50 kWe	0.5 MW
CLFR	<100	1-axis reflector	100-3000C	<10%	1-50 MWe	5 MW

4.3 Energy analysis of a concentrating thermal photovoltaic system

The working conditions of the CTPV system are primarily influenced by the cell temperature and its efficiency. The illumination characteristics and the construction technology of the cell involved is complex, hence the temperature determination is also a bit complex. Based on some experimental results achieved by [45], equations that could uniquely express the temperature of the cell in terms of the concentration factor C , were arrived at. The cell temperature is expressed as indicated in equation (4.1) [90]:

$$T_c = T_o + \frac{V_{oc}(T_c, C) - V_{oc}(T_o, C_o)}{\beta(C)} \quad (4.1)$$

where the electrical parameters are as defined in the list of Engineering and Mathematical notations.

The knowledge of the parameters in equation (4.1) were empirically obtained from the experimental diagrams of the variables examined by [91]. The open circuit voltages were found to be dependent on the temperature of the cell representing the unknown. This problem was overcome by [45, 92] who deduced a graphical relation where V_{oc} was found to depend only on the concentration factor. Hence V_{oc} is expressed as:

$$V_{oc}(C) = 2.5847 + 0.085283 \cdot \ln(C) \quad (4.2)$$

According to [91], the voltage thermal coefficient also depends on C and it is calculated as:

$$\beta(C) = -0.006424 + 0.00036233 \cdot \ln(C) \quad (4.3)$$

Based on these assumptions, the cell temperature is equal to:

$$T_c = T_o + \frac{V_{oc}(C) - V_{oc}(C_o)}{|\beta(C)|} \quad (4.4)$$

Once the cell temperature is known, the cell efficiency can then be obtained. Similarly, in order to define a theoretical equation between the quantities studied, some experimental diagrams obtained by [91] were used. These show that the efficiency decreases when the concentration factor, $V_{oc}(T_c, C)$, increases at the same cell temperature. Therefore, the cell efficiency is expressed as:

$$\eta_c - \eta_r = \frac{d\eta}{dT} \cdot (T_c - T_r) \quad (4.5)$$

where,

T_r = reference temperature and it is equal to 25°C or 298 K

η_r = reference efficiency corresponding to the concentration factor chosen.

$$\frac{d\eta}{dT} = -0.09167 + 0.005787 \cdot \ln(C)$$

$\frac{d\eta}{dT}$ is only applicable for C factors greater than 30 ($C > 30$) and in accordance to the curves analysed.

4.4 Electrical and thermal energy

According to [88, 93], the electrical energy theoretically produced by a single cell, using a concentration system with biaxial motion, is equal to:

$$P_c = \eta_c \cdot \eta_{opt} \cdot A_c \cdot C \cdot (G_{dir.r} \cdot f) \quad (4.6)$$

where $G_{dir.r}$ represents the direct irradiance previously calculated. Considering a non-ideal tracking system, a factor f of value 0.9 is considered. The optical efficiency of the system with parabolic concentrator mirrors is equal to the expression as stated in equation (4.7) [31]:

$$\eta_{opt} = \tau \cdot \left[\rho + \frac{1}{C} \cdot \left(1 - \frac{p}{0.98} \right) \right] \quad (4.7)$$

where,

τ and ρ represent the transmission and reflectivity coefficients of the mirrors respectively. The value 0.98 is the ratio between the areas of the concentrator and the PV cell.

The electric energy actually delivered by the cell is a function of the power thermal coefficient(k_t). The power thermal coefficient, (k_t), represents a reduction in percentage of the electricity supplied by the system at a given operating temperature and it is given as:

$$k_t = 1 + \sigma_t \cdot (T_c - 25) \quad (4.8)$$

where,

σ_t = temperature coefficient and it is dependent on cell type and manufacturer.

From analysis of many data sheets, the value of σ_t equals to -0.16% has been chosen. Hence, the electrical energy actually delivered by the cell is equal to:

$$P_{c,r} = k_t \cdot P_c \quad (4.9)$$

According to [93], calculating the module electric energy necessitates considering the cells number that develop it and its efficiency (η_{mod}) when fixed to 0.9 This value takes into consideration, the coupling in series of the cells along a line, taking note of the possibility that a cell can operate at a lower efficiency than the nominal one.

Hence, the electrical energy supplied by the module is equal to:

$$P_{mod} = P_{c,r} \cdot n_c \cdot \eta_{mod} \quad (4.10)$$

As a result of the parasitic current losses produced in the module, the obtained value has to be reduced [93]:

Hence:

$$P_{par} = P_{par} \cdot G_{dir,r} A_c \cdot C \cdot n_c \quad (4.11)$$

where,

P_{par} = a loss factor with value equal to 0.023 [93] depending on the radiation.

Considering the inverter efficiency (η_{inv}) fixed at 0.9 [88] and cells connected in series, the actual electric energy provided by module is equal to:

$$P_{mod,r} = (P_{mod} - P_{par}) \cdot \eta_{mv} \quad (4.12)$$

The thermal energy delivered under ideal conditions by the module is then equal to [88] :

$$Q_{th,id} = (1 - \eta_{pv}) \cdot \eta_{opt} \cdot C \cdot (G_{dir,r} \cdot f) \cdot A_c \cdot n_c \quad (4.13)$$

where the overall efficiency (η_{pv}) for the concentrating PV module considers all the losses in the system and it is equal to [93]:

$$\eta_{pv} = \eta_c \cdot \eta_{mod} \cdot k_t \quad (4.14)$$

Furthermore, because of radiative and convective phenomena, its heating and thermal energy dispersion is determined by the solar rays which act on the triple-junction cell [88]:

$$Q_{th,l} = [h_c \cdot (T_c - T_o) + \varepsilon_c \cdot \sigma \cdot (T_c^4 - T_o^4)] A_c \cdot n_c \quad (4.15)$$

where,

$h_c \cdot (T_c - T_o)$ = the convective component

$\sigma \cdot (T_c^4 - T_o^4)$ = the radiative component

ε_c = PV cell emissivity and it is equal to 0.85. The actual thermal energy is the difference between the theoretical total thermal energy and the sum of radiative and convective losses, generally included in the range (1 to 3) % [93].

4.5 Solar thermal electricity – present status

Present trends in STE energy supply and use are unsustainable in terms of economic, environmental and social considerations. There is need for avoidance of energy-related emissions of greenhouse-gas (GHG) that lead to considerable climate change with an average of 6°C global warming. Sustainable and carbon- negligible energy technologies play a vital role in the energy turn-around required to effect this change. Energy Efficiency improvement for the various types of renewable energy would all require widespread improvement in the bid to compete favourably with fossil fuel generated power. It is anticipated that it may be possible to achieve a target of 50% below the present levels of global energy-related CO₂ by 2050 and a global temperature rise limit of 2°C by 2050 [6, 94].

Solar thermal technology (STT) uses the sun's energy, rather than fossil fuels, to generate low-cost, environmentally friendly thermal energy. It focusses the light from the sun to develop heat which is used to run a heat engine, which turns a generator to produce electricity. This is known as concentrated thermal electricity. It is one of those technologies that is generated by CSP [19]. The interesting outcome of this reassessment is that the vision set for STE four years ago, to reach about 11% of global electricity generation by 2050, still remains unchanged – in spite of the increased prospects for PV deployment [94].

4.6 Modelling and simulation of the concentrating thermal photovoltaic module

Generation of CTPV power has been in existence since 2010 and has grown strongly worldwide, although at a slower rate than expected [32]. In CTPV systems, mirrors or lenses are used to concentrate a large area of sunlight, or heat onto a small area in order to generate solar power. The concentrated light is converted to heat that drives a heat engine (which is usually a steam turbine connected to an electrical power generator) before electricity is generated. Modelling and simulation was applied to the development and design of the PV devices for this system. A new thermal model was used to develop the thermal performance of the PV modules. Using the developed model, several studies were performed to evaluate the electrical and thermal performance of the module under heat transfer with surface-to-surface radiation.

4.6.1 Energy conversion process - Brief description

Presently, the conversion efficiency for PV modules lies between 13% and 20% [44], which represents the fraction of the total available photons that are converted into conducting electrons. The remaining absorbed solar radiation by the PV panel that is not converted into useful energy is then converted to heat that increases the panel temperature. Furthermore, an increase in the module temperature brings about decrease in the module efficiency [37]. Hence, the target is to reduce the cell temperature in order to bring about improved conversion efficiency for the PV cells and consequently enhance the PV system performance.

In this Thesis, the performance prediction of the CTPV panel was considered for the radiation and thermal models only. The radiation model [95-97] could be used to estimate the absorbed solar radiation in the PV cells. While different electrical models are necessary in estimating the electrical output of PV

panels under a defined operating condition, thermal modelling is used in determining temperature distribution in the CTPV structure at any given environmental and operating condition. More information on the development of thermal models is available in these referenced materials [69, 98, 99].

An analytical modelling on concentrating solar thermal collectors containing eight PV cells with an equal number of mirrors was effected to validate the already modelled one by COMSOL. Further contributions to this were made by developing and comparing other cases of modelled 2D with six PV cell and equal number of mirrors, ten PV cell and equal number of mirrors and also 3D with eight CTPV cell with equal number of mirror was made to determine the varying performances of different design cases with varying number of PV cells covering the collector area. According to [99], the result of their study revealed that decreasing the fraction of cell-covered area, causes improvement in instantaneous efficiency of the CTPV panel. Further work was undertaken to determine best CTPV operating configuration when the model was later extended to modelling and comparing the performance of 2D and 3D CTPV collector configurations for six PV cells and an equal number of mirrors. For electrical modelling, the validated values in 1D were used as simulating input into the 3D simulation. The accuracy of the model is possible to be improved upon by using the equivalent electric circuit model to determine the electrical performance of the system and by using more detailed expressions for determining the thermal resistances within the system [99, 100]. The effect of model complexity on accuracy forecast was extensively conducted and studied by [101]. The findings proposed that the consequence of including dynamical effects on a day's energy output forecast was not significant, but the deviation in the steady state model increased for short periods of time.

Most of the reviewed literature above related to the 1D analytical thermal model for PV panels with temperature variation involving the thickness only. Although simple 1D models are reasonably accurate for long-term performance forecasts, more complex 2D and 3D models are needed to capture the temperature gradient effect in CTPV collectors. Models of more complex attributes could handle the required complex flow patterns and design optimization tasks [101].

4.7 Modelling and simulation of solar cells

Modelling and simulation of the solar cells and modules was carried out in two parts. The first involved the use of Matlab for the 1D simulation of the electrical model while 2D simulations or even 3D simulations are required for accurate interpretation of electrical and thermal properties of silicon semiconductor devices as well as for achieving accurate results [60]. Some of the numerous simulation tools and solar cell programs developed and used by researchers in various parts of the world for solar cells modelling include SILVACO, TFT and Crosslight, APSYS, Advanced Physical Models of Semiconductor Devices, Synopsys and COMSOL Multiphysics [14, 67].

In this chapter, 2D and 3D numerical models were developed with the use of COMSOL Multiphysics to predict the thermal behaviour of the CTPV system and in addition to calculate the electrical performance of the system such as the output power and system efficiency. Therefore, the performance metrics considered in this work include the PV cell temperature distribution, PV cells efficiency and PV electrical power output.

The basic modelling of COMSOL Multiphysics enabled the researcher as a desktop environment model-builder to get full overview of the model and to access all and solve coupled physics phenomena. It possesses built-in physics interfaces and advanced support for material properties. However, models are built by defining the relevant physical quantities - such as material properties, loads, constraints, sources, and fluxes or by describing the underlying equations. The variables, expressions, or numbers could be directly applied to solid and fluid domains, boundaries, edges, and points independently of the computational mesh. The work done in building the models was carried out on 2D and 3D geometries. In addition, the technical effects of modelling to vary the operating conditions in the CTPV system were studied and results are presented in this Chapter.

4.8 Concentrated thermal photovoltaic modelling

The CTPV was modelled from an existing prototype CTPV system. The same material properties and physics were defined earlier for a similar model built to validate against the existing literature data which were found to be technically the same. The study was further carried out to determine the impact of configuration variations on the system performances such as the CYPV system efficiency and the electrical power output. In addition, a 3D model was developed, modelled, compared and analysed against the 2D model earlier developed and the findings are reported in the later part of this chapter.

The purpose of the CTPV models was to enable its use for calculating the 2D and 3D temperature distributions and they interpreted the results in the CTPV panel. The materials properties involved had to be defined as the temperature distributions depend on the materials in general. The materials involved for this modelling are – the heater, emitter, PV cell type, the mirrors, the insulation attached to the PV cells, and the prevailing environmental conditions.

The PV panel gains energy by absorbing photons from the solar irradiation falling upon it while at the same time, it gives out energy by convection and radiation to the environment from the electrical energy delivered to the electrical load and from the energy drop from the heat exchanger working fluid. The load characteristics determine the operating current–voltage (I–V) point and the electrical power output of the PV panel and consequently the amount of electrical energy taken out of the system. In CTPV systems, radiation heat needs to be maximized in order to step-up efficiency. However, unutilized energy from convection and radiation turned out as heat losses and contributed to the PV cells' increased temperature and these were undesirable combinations [99, 100]. The operating temperature range of PV cells is limited and depends on the type of material used. The efficiency of the PV system is determined by this temperature with a maximum at some temperature above ambient [101]. Solar cells have their temperatures limited to below 80 °C, however, semiconductor materials with high-efficiency could have their temperature raised as high as 1000 °C [64].

For improved system efficiency, it is preferable to use high-efficiency PV cells, but this usage comes at a high cost. Therefore, in order to reduce system costs, the study was carried out with smaller-area PV cells and then mirrors or lenses were utilized to focus the radiation on these PV cells. The use of mirrors or lenses to focus the beams on the PV cells has its limits. If the radiation intensity from the mirrors or lenses is too high, the PV cells could overheat and burn out. Therefore, there is the need to determine accurate system geometry and operating conditions in order to achieve maximum performance and power output at reasonable material costs.

4.9 The implementation of the thermal model, using COMSOL Multiphysics

A CTPV system utilises a concentrating medium to generate electricity from the combustion of fuel and through radiation. Figure 4-2 depicts the general operating principle where the CTPV cell generates electricity from the combustion of fuel and through radiation. The fuel burned from inside an emitting device that radiate heat intensely. The PV cells captured the radiation and converted it to electricity. The efficiency of a CTPV system normally varies between one percent and twenty percent [64]. Radiation losses not converted to electric power would raise the temperature of the PV cells further, hence indicating that PV efficiency is inversely related to the operating temperature. Furthermore, heat transfer through conduction does also bring about increased cell temperature. Hence, the CTPV would not be able to maximize radiation heat transfer for improved efficiency. However, the type of material used determines the PV cell's limited operating temperature. The effect of operating conditions (emitter heat) on the CTPV system efficiency and the temperature of components in the CTPV system was investigated. The heat transfer application which uses surface-to-surface radiation interface was applied.

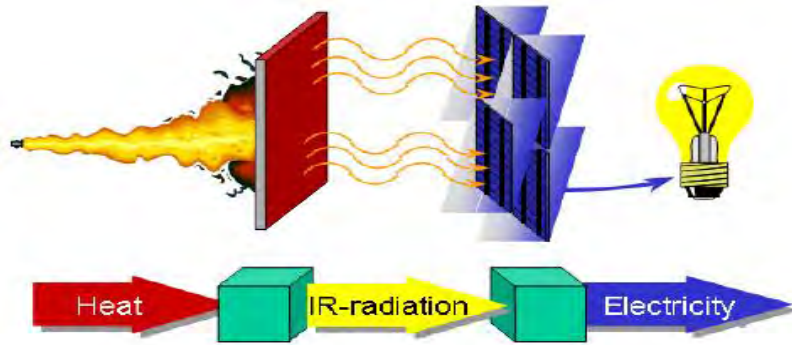


Figure 4-2: Operating principle of a concentrating thermal photovoltaic system [64]

The parameters of the materials of the CTPV system under study is as presented in Figure 4-3. The PV cells were cooled by water on their rear surface (the interface with the insulation) to reduce the temperature. Since there was flow of heat on the different boundaries, conduction was always present. The emitter was simulated with a particular temperature called T_{heater} , on the inner boundary by the model as indicated in Table 4-3. In the boundary condition, radiation (surface-to-surface) was taken into consideration at the outer emitter boundary. The global definition for the PV cell was specified as indicated in Table 4-4. The mirrors were simulated and radiation heat was applied on all boundaries and with a low emissivity to it as indicated in Table 4-5.

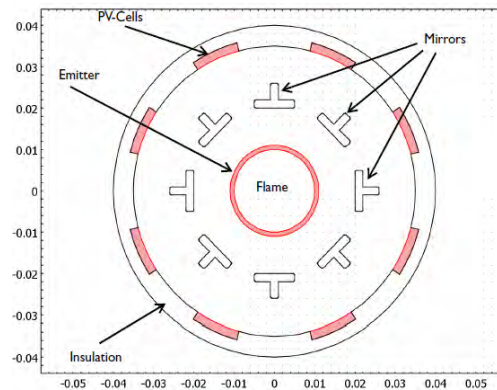


Figure 4-3: Geometry and dimensions of the modelled thermal PV system [64]

Radiation boundary conditions were applied to the inner boundaries of the PV cells and that of the insulation as well. On the other hand, the PV cells have a greater emissivity value than that of the insulation. Furthermore, a fraction of the irradiation was converted to electricity in the PV cells. The heat sinks situated on the PV cells inner boundaries account for a boundary heat source, q , which is defined in equation (4.16) as:

$$q = -G\eta_{pv} \quad (4.16)$$

where,

G = irradiation flux (W/m^2)

η_{pv} is as earlier defined in the list of engineering and mathematical notation. The efficiency of the PV cell depends on the local temperature T in the equation.

4.9.1 Thermal modelling and simulation

The 2D model of the thermal CTPV has already been modelled by COMSOL but the results were validated against COMSOL results. This was carried out by re-developing the 2D CTPV model. The 2D CTPV was first modelled as a circle and the other materials were also modelled as represented and shown in Figure 4-4. The defined geometry, definition, dimensions and meshing were initiated in 2D model using COMSOL Multiphysics as seen in Figure 4-4. Further contributions were made to it in various ways as discussed in this chapter. First, the 3D model of the CTPV was achieved through direct conversion of the 2D model in order to ensure precise translation the same approach in modelling was applied but with an increased number of boundaries and domains in the 3D CTPV. The thermal properties for the various materials used in the model are given in Table 4-5 and these are the same for both the 2D and 3D models.

Table 4-3: Global definition for the heater

Parameters Name	Expression	Value	Description
T_heater	1000 [K]	1000 K	Temperature, emitter inner boundary

Table 4-4: Global definition for the PV Cell

Name	Expression	Unit	Description
eta_pv	if($T < 1600[K]$, $0.2 * (1 - (T/800[K] - 1)^2)$, 0)		Voltaic efficiency, PV cell
q_out	ht.Gm*eta_pv	W/m ²	Electric output power

4.9.2 Materials specifications

The materials described below were used for the modelling and simulation. The emitter was assigned a specific temperature, T_{heater} , on the inner boundary. Radiation was taken into account on all boundaries and a low emissivity was applied for the mirrors. The PV cells were assigned a high emissivity value while the insulation was assigned a low emissivity value. Their references and relevant material properties are appropriately referenced.

Table 4-5: Material properties used in the CTPV modelling [64]

Component	k [W/(m·K)]	ρ (rho) [kg/m ³]	C_p [J/(kg·K)]	ϵ
Emitter	10	2000	900	0.99
Mirror	10	5000	840	0.01
PV Cell	93	2000	840	0.99
Insulation	0.05	700	100	0.1

4.9.3 Governing equations for the heat transfer

The heat transfer equations for solid and fluid domains are as earlier stated in equations (2.32) and (2.33) respectively [13].

The voltaic efficiency of the PV cells, η_{pv} , is a function of the ambient temperature and it is defined as:

$$\eta_{pv} = \begin{cases} 0.2 \left[1 - \left(\frac{T}{800 K} - 1 \right)^2 \right] & T \leq 1600 K \\ 0 & T > 1600 K \end{cases} \quad (4.17)$$

where the electrical parameters are as defined in the list of Engineering and Mathematical notations.

The absorbed solar radiation was partly converted to electrical energy while the remaining unconverted energy raises the temperature of the PV cells. The heat transfer equation of the PV cell layers expressed as an internal heat generation, Q , is related to the electrical efficiency of the PV panel η_{pv} , the front area of the PV panel A_{panel} and the volume of the PV cells in the pane $V_{pc.cell}$. The heat transferred could be determined from the absorbed solar radiation using the equation in (4.18):

$$Q = \frac{(1 - \eta_{pv}) \times S \times A_{panel}}{V_{pc.cell}} \quad (4.18)$$

Using the applied physics application, Heat Transfer with surface-to-surface radiation interface, the influence of operating conditions (flame temperature or emitter heat) on system efficiency and electric output power in a typical CTPV system was investigated and studied. The application also considered the influence of geometry changes on the system such as the number of materials used or the specifications given on these materials. In this Chapter, the effects of varying the number of mirrors used on the temperature distribution, the efficiency and the electrical power output of the CTPV system was investigated and findings and results are presented.

The model simulated the emitter with an assigned temperature, T_{heater} , on the inner boundary. At the outer emitter boundary, the surface-to-surface radiation was applied in the boundary condition. The mirrors were simulated by applying radiation on all boundaries with a low emissivity value. Heat loss by conduction was continually present and considered on the different boundaries. Radiation boundary conditions were considered for both the inner boundaries of the PV cells (with high emissivity) and that of the insulation (with low emissivity) as indicated in Table 4-5.

The heat sink on the inner boundaries of the PV cells simulated water cooling on the PV cells to convert a fraction of the irradiation to electricity instead of heat. This was made possible by accounting for a boundary heat source, q , as defined earlier in equation (2.32) within the ambient temperature as

indicated in equation (4.20). The efficiency of the PV cells, η_{PV} is a function of the local temperature as defined in equation (4.17). The local temperature of 800 K was applied. The PV cell's voltaic efficiency is a function of this temperature and so turned out to have a value of 0.2 at this temperature. This is obvious from its generalized equation in equation (4.17).

At the outer boundary of the PV cells, the convective water cooling was applied by the model to avoid PV cells from over-heating by setting:

$$h = 50W/(m^2 \cdot K) \quad (4.19)$$

$$T_{amb} = 273 K \quad (4.20)$$

At the outer boundary of the insulation, convective cooling was applied with h defined as:

$$h = 5W/(m^2 \cdot K) \quad (4.21)$$

$$T_{amb} = 293 K \quad (4.22)$$

The equations governing the physics for the modelling of the 2D and 3D CTPV systems are presented in Appendix A-4. Although the same material properties and procedural approaches were used for both the 2D and 3D CTPV modelling, as presented in Appendix A-4, different numbers of boundaries and domains were obtained..

4.10 2D modelling and simulation of a CTPV system for optimum performance

The bottom line in any project handling is cost reduction; usually, there is a trade-off between the efficiency of the CTPV system and its cost. Due to high cost of silicon PV cells, smaller area PV cells were utilized and mirrors were then used to focus the radiation from the heat source on these PV cells for greater concentration and intensity. However, there was a limit to how much of these beams could be focused on the PV cells because high radiation intensity could overheat and burn out the PV cells. Therefore, there was the need to optimize system geometry and operating conditions in order to achieve maximum performance (efficiency and power output) at minimum material costs.

Any of the various system parameters could be varied to investigate the variation effect on the CTPV performance output. These variation could be from any of the materials listed in Table 4-5 or the operating conditions such as the emitter heat or the operating temperature in Table 4-3.

In this chapter, modelling and simulation were initially carried out for three different CTPV configurations. The number of the mirrors radiating heat on the PV cells were varied, while all other parameters were fixed. The number of mirrors or lenses (concentrators) are the same with the number of the PV cells receiving the radiation. These three scenarios studied are listed below:

- (a) A CTPV system with eight pairs of mirror and PV cells which was set as the standard and validated.
- (b) A reduction in the pair number of mirror and PV cell used from eight to six.
- (c) An increase in the pair number of mirror and PV cell used from eight to ten.

The mirror/PV cell pair is being referred to as number of mirrors for simplicity. The effect of the variations on the CTPV system configuration was studied on the system efficiency and generated output power. The material properties were defined and used in the simulation as contained in Table 4-5 and it remains the same for each of the cases considered. The summary of domain selection for the selected

materials is presented on Table 4-6 and Geometry statistics for the 2D and 3D CTPV are presented on Table 4-7.

Reports were generated for the stationary temperature distributions, the voltaic efficiency and output power in each of the cases. The findings of the influence of the configuration variation in the 2D CTPV are as presented in Figure 4-4(a, b and c) to Figure 4-7(a, b and c). The comparative analysis of the 2D CTPV system with eight, six and ten mirrors configurations is presented in Table 4-8 as case 1, while the comparative analysis between the 2D CTPV configuration with eight mirrors and 3D CTPV configuration with six mirrors configurations is presented in Table 4-9 as case 2. The summaries of the results for the two cases are given on Table 4-10 and Table 4-11.

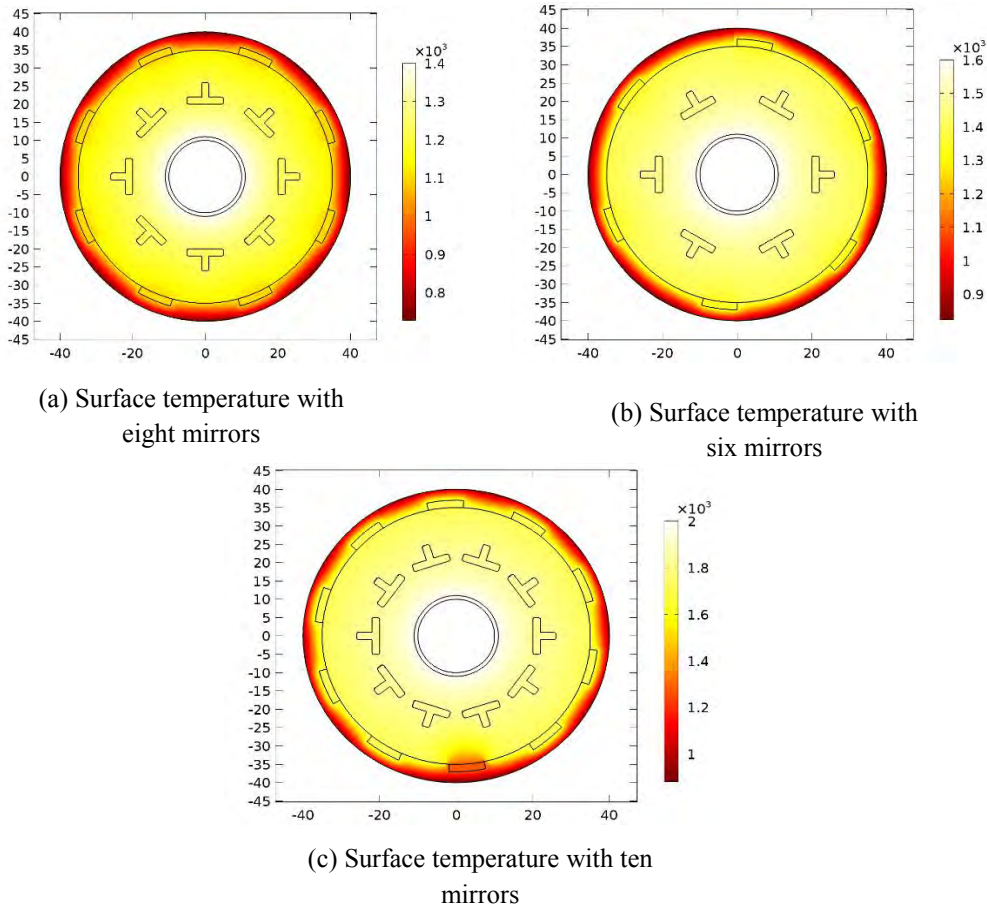


Figure 4-4: Stationary temperature distribution at operating conditions for (a) eight mirrors, (b) six mirrors, and (c) 10 mirrors

Application of heat transfer with surface-to-surface radiation interface was based on the type of energy transfer taking place. In addition, the emitter was simulated with a definite temperature, T_{heater} on the inner boundary. The influence of geometry changes on the system such as the number of materials used or the specifications given of these materials was studied. The application investigated and studied the influence of operating conditions (flame temperature) on system efficiency and electric output power in a typical CTPV system. For all the studies carried out on the various CTPV configurations, the materials selection and specification remain the same.

In order to explore all possibilities and to ensure that the best configuration possible for optimal solar power generation was considered, selected and reported for this work, the 3D CTPV was later

modelled, simulated and compared with the best option (six mirrors) from the 2D CTPV. This is in addition to the three scenarios studied and stated earlier. A full report on the comparative modelling of the 2D and 3D CTPV systems with six mirrors configuration is presented later in section 4.15 of this chapter and the results summary is given on Table 4-12.

In Figure 4-4(a) to Figures 4-4(c) all through to Figure 4-5(a) to Figures 4-5(c) are the comparative analyses of the three different modelled configurations of the 2D CTPV.

Figures 4-4(a, b and c) show the visual temperature distribution (stationary) for the CTPV systems with eight, six and ten mirrors respectively that were subjected to prevailing operating conditions with an emitter temperature of 2,000 K. The structure with eight pairs of mirrors and PV cells was set as the standard since the geometry was initially built with eight pairs of mirrors and PV cells along with the other materials. The results showed that the CTPV system experienced a remarkable temperature distribution that varied almost linearly with the operating conditions.

The temperature distributions graphically represented in Figures 4-5(a, b and c) showed that the PV cells reached temperature values of 1,820 K, 1,880 K and 1700 K for the systems with eight mirrors, six mirrors and ten mirrors respectively. These are significantly higher than their best operating temperature of 780 K, 1,300 K and 1,300 K respectively for the eight mirrors, six mirrors and ten mirrors respectively which would yield system output power of 7.8 kW/m², 31.8 kW/m² and 29.8 kW/m² respectively and at the operating temperature of 1,200 K, 1,600 K, and 1,800 K respectively.

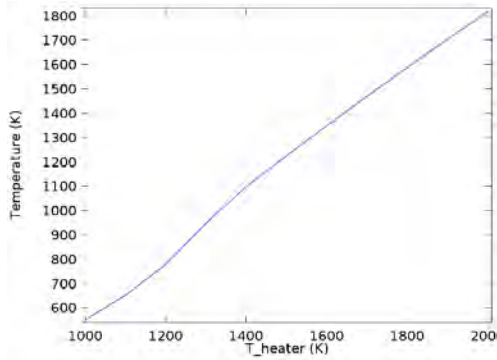


Figure 4-5(a) Temperature for eight mirrors

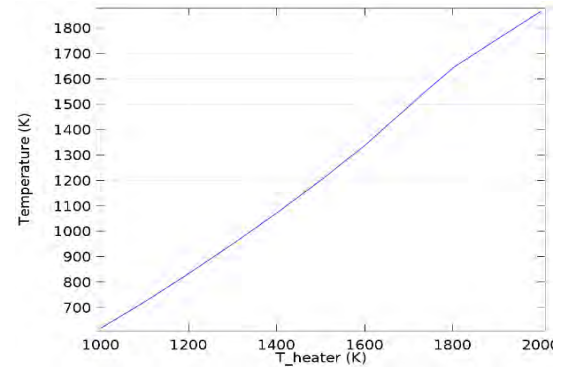


Figure 4-5(b) Temperature for six mirrors

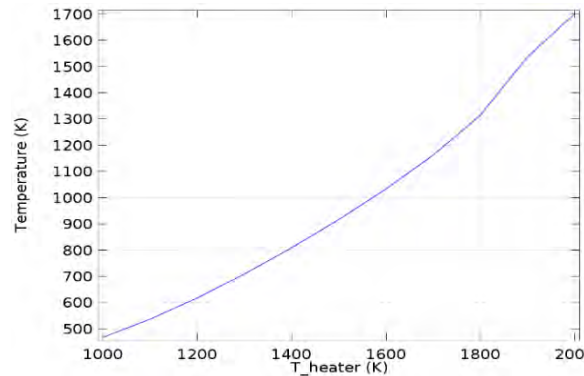


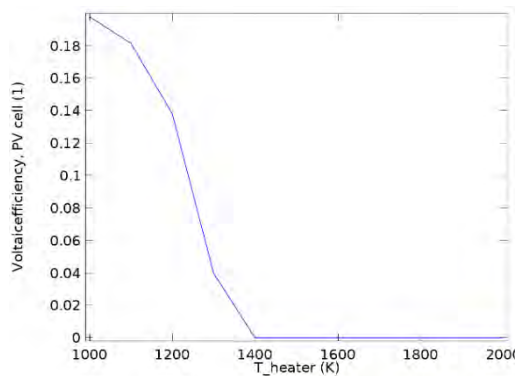
Figure 4-5(c): Temperature for ten mirrors

Figure 4-5: The point graph of the PV cell temperature versus the heater temperature for (a) eight, (b) six, and (c) ten mirrors respectively.

These are significantly higher than their best operating temperature of 780 K, 1,300 K and 1,300 K respectively in (Figures 4-5(a, b and c) for the eight mirrors, six mirrors and ten mirrors respectively which would yield system output power of 7.8 kW/m², 31.8 kW/m² and 29.8 kW/m² respectively in Figures 4-7(a, b and c) and at the operating temperature of 1,200 K, 1,600 K, and 1,800 K respectively in Figures 4-7(a, b and c).

On the other hand, in the 3D model, the maximum PV cell temperature reached was 800 K at the heater temperature of as high as 4,000 K (this is obvious from the graph in Figure 4-9(b). The stationary temperature distribution indicated that the high heater operating temperature was quite safe for the PV cells in 3D CTPV as they did not get overheated as seen in Figure 4-8(n). The maximum efficiency obtained was also about 20% at heater temperature of 2500 K as seen in Figure 4-9(d).

The output power in the 2D model in Figure 4-9(c) was 7.8 kW/m² at 1200 K heater temperature above which the output power drops sharply while that of the 3D model was 2.2 kW/m² at 3600 K and this was fairly stable to heater temperature of about 3800 K as shown in Figure 4-9(d). Figures 4-6 (a, b and c) show the CTPV voltaic efficiency for the eight mirrors, six mirrors and ten mirrors configuration respectively. The efficiency values for each configuration remain constant at almost 20 percent. However, the operating temperature for output power generation for the eight, six and ten mirrors configuration occurred at 1400 K, 1800 K and 2000 K as seen in Figures 4-7(a, b and c).



4-6(a): Voltaic efficiency against temperature for eight mirrors configuration in 2D

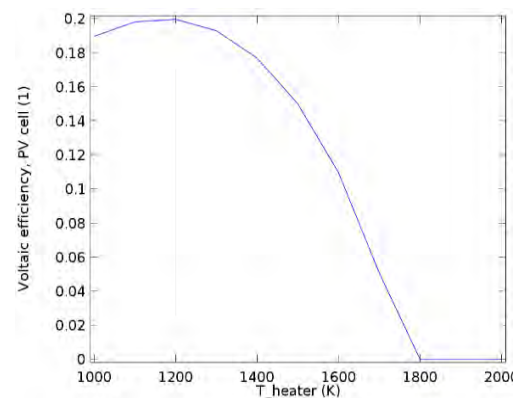
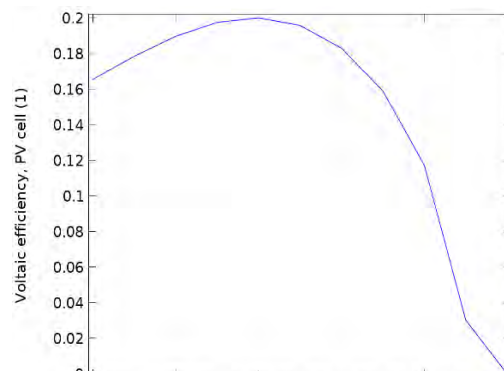


Figure 4-6(b): Voltaic efficiency against temperature for six mirrors configuration in 2D



4-6(c): Voltaic efficiency against temperature for ten mirrors configuration in 2D

Figure 4-6: Plot showing the voltaic efficiency against temperature for 2D CTPV configuration with (a) eight mirrors, (b) six, (c) ten mirrors

Above each of these stated operating temperatures, their output power would begin to drop sharply and eventually come to zero at 1,400 K, 1,800 K and 2,000 K for the eight mirrors, six mirrors and ten mirrors respectively in each case as shown in Figures 4-7(a, b and c) and their PV efficiency would collapse to zero accordingly. These graphs present the operating temperature, T_{heater} , at which the system attained the maximum electric power output for the system with eight mirrors, six mirrors and ten mirrors respectively.

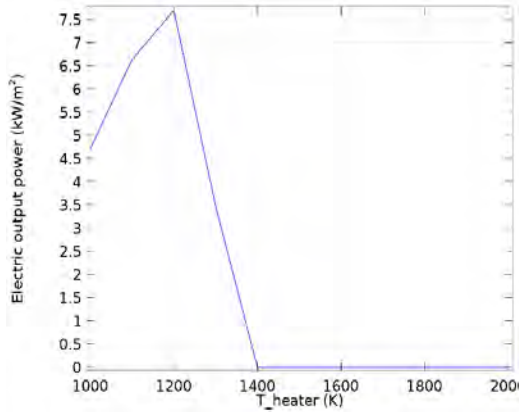


Figure 4-7(a): Electric output power against temperature of 2D CTPV configuration with eight mirrors

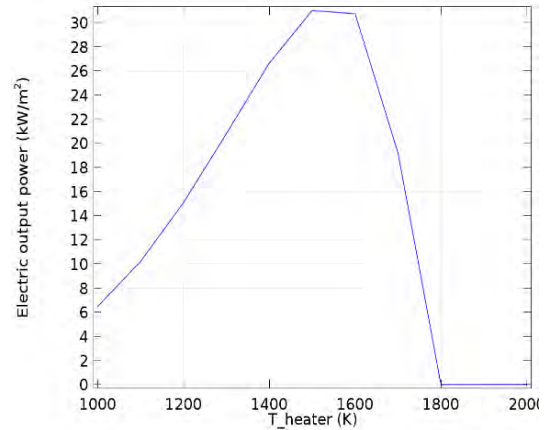


Figure 4-7(b): Electric output power against temperature of 2DCTPV configuration with six mirrors

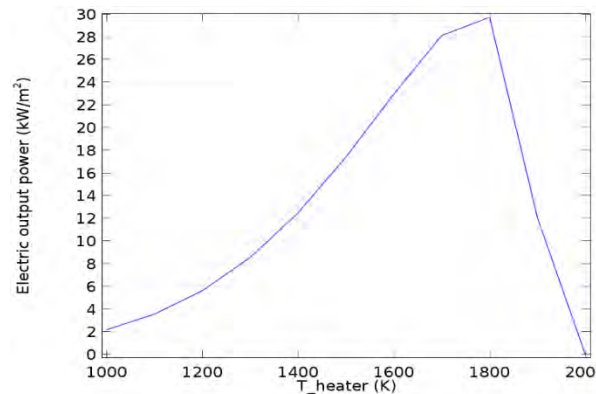


Figure 4-7(c): Electric output power against temperature of 2D CTPV configuration with ten mirrors

Figure 4-7: Plot showing the electric output power against the heater temperature for the CTPV with (a) eight mirrors, (b) six mirrors, and (c) ten mirrors

4.11 3D Thermal modelling and simulation of a CTPV system for optimum performance

COMSOL Multiphysics engineering software was used to develop the 3D CTPV model to study the thermal and electrical performances of the system. This ensured that the modelling parameters for 2D and the 3D of the TPV could be compared directly one to the other. Notwithstanding the geometric differences between the 2D and 3D structures, they were characterised by the same material definitions and properties.

Then modelling in 3D was carried out for the domains, boundaries, edges and vertices of the structure. The materials parameters for the insulation, PV cells, mirror and emitter remained the same as earlier stated in Table 4-5. However, the number of points generated for the domain, boundaries, edges and points in the 3D modelling were more than what are available in 2D geometry as indicated in Table 4-6. Table 4-6 shows the various materials geometries modelled with their dimensions, using the appropriate materials properties as defined earlier in Table 4-5, while their geometry statistics are presented in Table 4-7. Domain selections were necessary and developed for all the solid materials used in the modelling, namely: Insulation, PV Cells, mirrors, emitters and the Air domains and boundaries. The selections are useful in the implementation of materials settings and boundary conditions.

The comparative models for the 2D and 3D configurations with eight PV cells and corresponding number of mirrors are presented in Figure 4-8(a to m). The comparative analysis of the study on 2D CTPV and 3D CTPV geometries are presented in Table 4-9 and the summary of the results is given on Table 4-11.

Table 4-6: The summary of domain selection for the selected materials

Materials	2D Modelling		3D Modelling	
	Domains Selection	Number of Points	Selection	Number of Points
Insulation	1	1	1	1
PV Cells	2, 3, 8, 9, 12, 13, 17, and 18	8	2, 3, 8, 9, 14, 15, 19, and 20	8
Mirrors	5–7, 10, 11, and 14–16	8	5–7, 12, 13, and 16–18	8
Emitter	19	1	10	1
Air	4 and 20	2	4 and 10	2

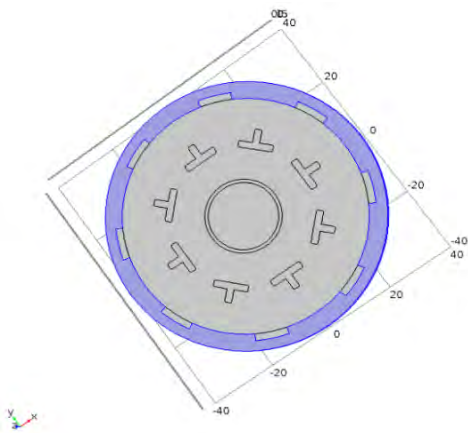
Table 4-7: Geometry statistics of two-dimensional and three-dimensional geometries

2D Geometry		3D Geometry	
Description	Value	Description	Value
Space dimension	2	Space dimension	3
Number of domains	20	Number of domains	20
Number of boundaries	184	Number of boundaries	224
Number of edges	Not applicable	Number of edges	544
Number of vertices	176	Number of vertices	352

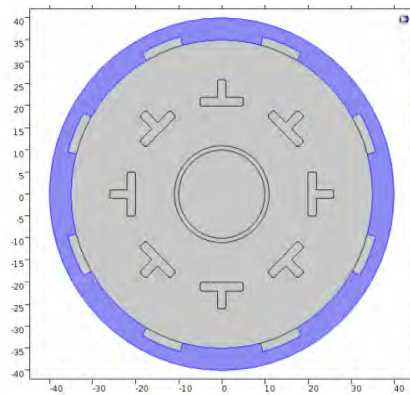
Physics determination and selection was carried out for the 3D model in order to mesh and simulate the models. The materials physics application was chosen from both COMSOL library and user-definition. The same materials selection and definitions were used for both the 2D and 3D models, likewise, the same physics on selected materials applied for the 2D and 3D models. The applicable default physics selected in the modelling and simulation was heat transfer with surface-to-surface radiation. This was because the heat radiation and transfer variations that took place in these models were best described by this physics. The summary of which is as presented in Appendix A-4.

4.12 Comparison of the 2D and 3D models for the CTPV system

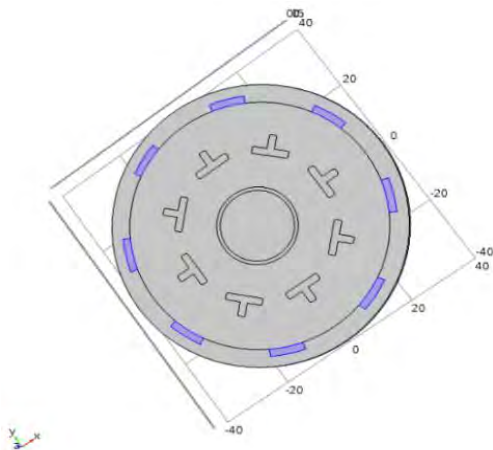
The geometric statistics between the modelled 2D and 3D CTPV systems are summarised in Table 4-7. The various boundary selections for the 2D and 3D were not the same in number. For the 3D model, the various points on the x, y and z axes were considered and taken while only the x and y planes are considered for the 2D model. The boundary selections are important in the required physics application for the modelling and simulation. These were successfully carried out for successful simulation. The comparative analysis of the modelled 2D and 3D CTPV systems are illustrated in Figures 4-8(a to u).



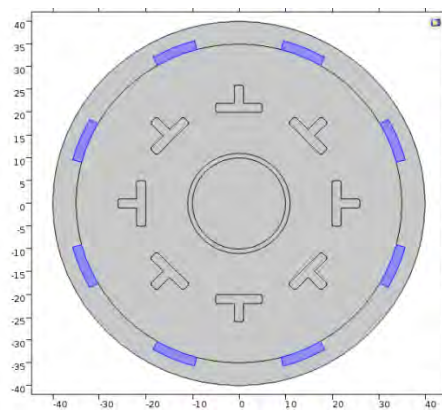
Figures 4-8(b): Modelled insulation for 3D CTPV geometry with eight mirrors



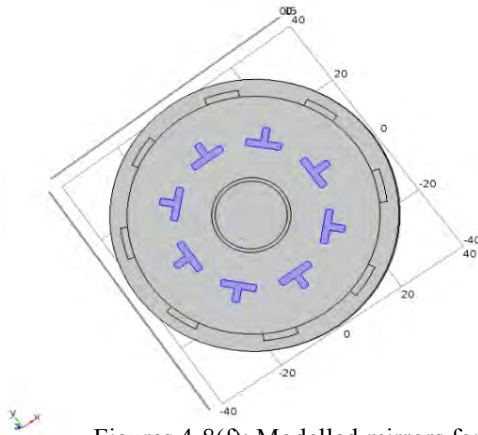
Figures 4-8(a): Modelled insulation for 2D CTPV geometry with eight mirrors



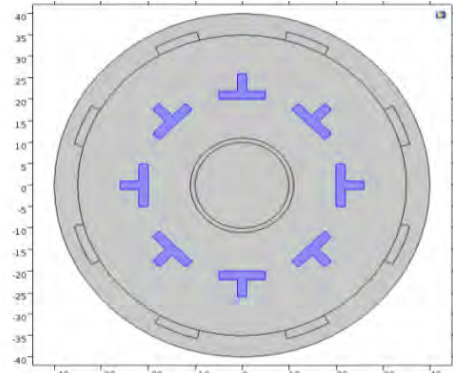
Figures 4-8(d): Modelled PV cells for 3D CTPV geometry with eight mirrors



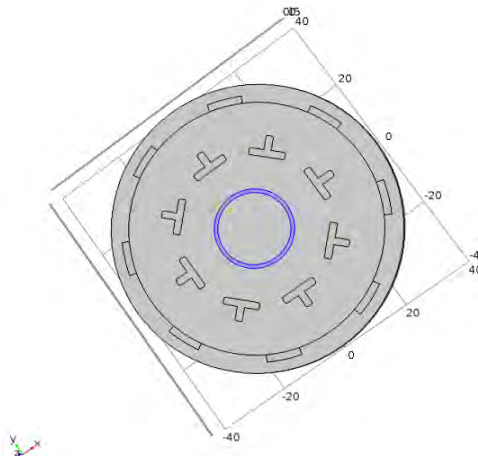
Figures 4-8(c): Modelled PV cells for 2D CTPV geometry with eight mirrors



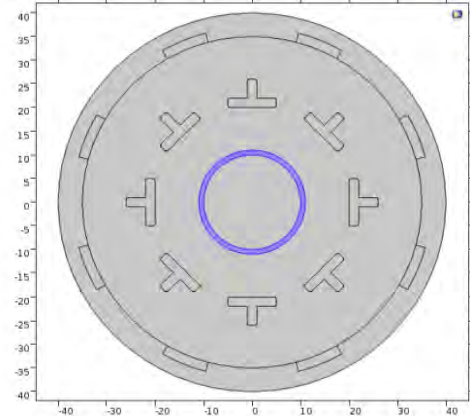
Figures 4-8(f): Modelled mirrors for 3D CTPV geometry with eight mirrors



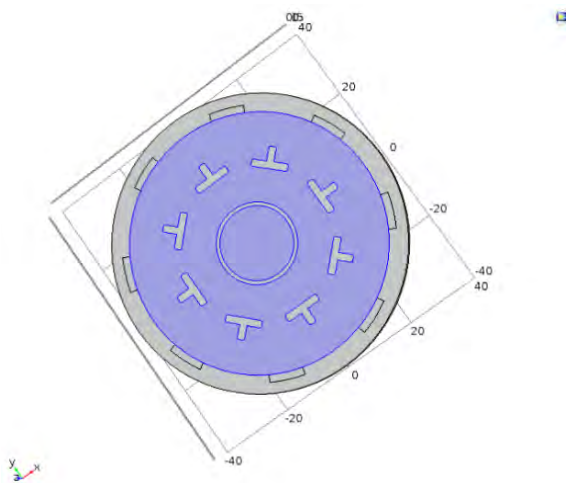
Figures 4-8(e): Modelled mirrors for 2D CTPV geometry with eight mirrors



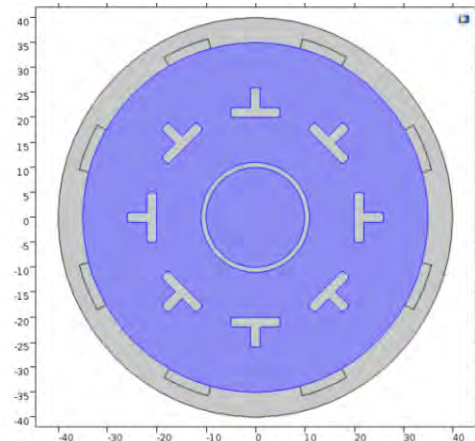
Figures 4-8(h): Modelled emitter for 3D CTPV geometry with eight mirrors



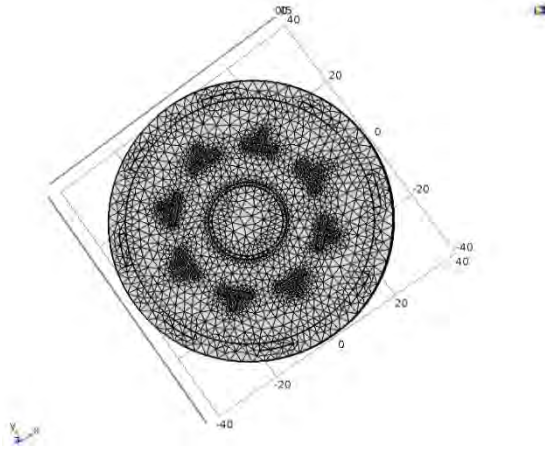
Figures 4-8(g): Modelled emitter for 2D CTPV geometry with eight mirrors



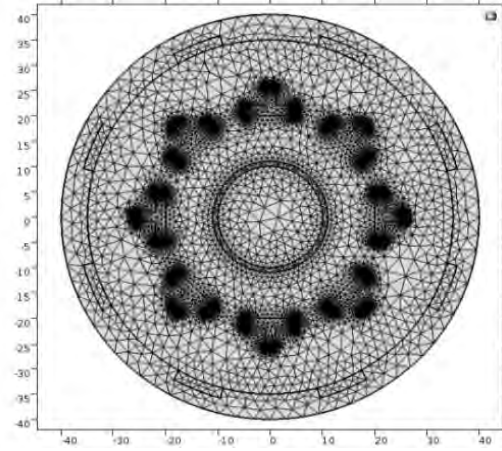
Figures 4-8(j): Modelled air for 3D CTPV geometry with eight mirrors



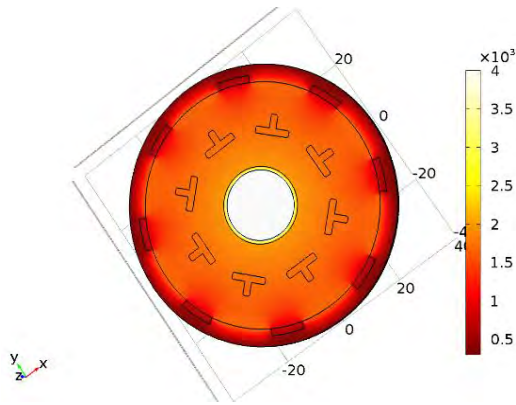
Figures 4-8(i): Modelled air for 2D CTPV geometry with eight mirrors



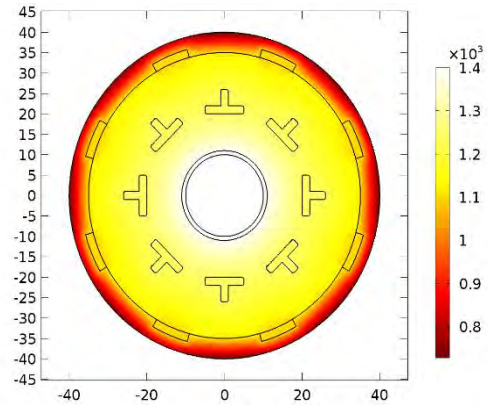
Figures 4-8(l): Meshed result of 3D CTPV thermal PV system with eight mirrors



Figures 4-8(k): Meshed result of 2D CTPV thermal PV system with eight mirrors



Figures 4-8(n): Stationary temperature distribution of modelled 3D CTPV system with eight mirrors



Figures 4-8(m): Stationary temperature distribution of modelled 2D CTPV system with eight mirrors

The stationary temperature distribution of modelled 2D CTPV and 3D CTPV systems are shown in Figure 4-8(m) and Figure 4-8(n) respectively while their meshing results are indicated in Figures 4-8(k) and Figures 4-8(l) respectively. The graphical results obtained for the 2D and 3D simulations are as shown in Figure 4-9(a to f). All edges were defined and captured for the 3D geometry while definitions for edges were not applicable for the 2D geometry.

Comparative analysis of the 1D graphs between the 2D and 3D CTPV systems for eight mirrors/PV cells are as presented in the Figures 4-9(a to f) below:

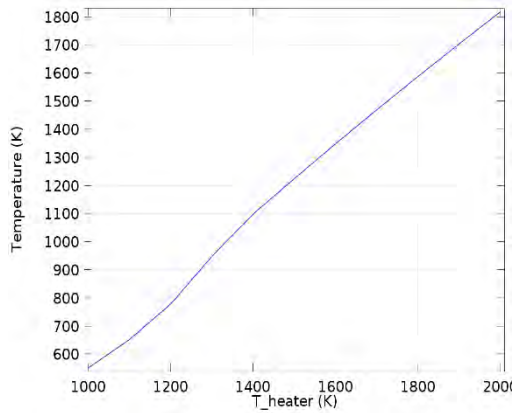


Figure 4-9(a): Point graph - temperature in a 2D CTPV for eight mirrors

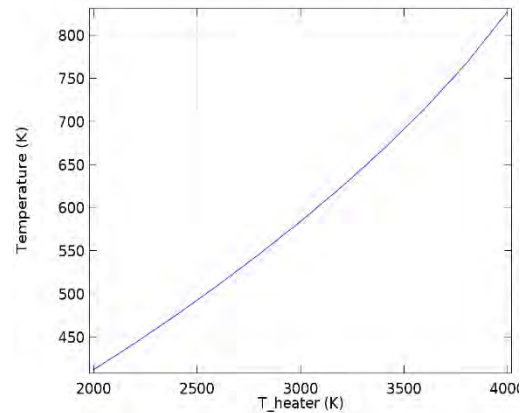


Figure 4-9(b): Point graph - temperature in a 3D CTPV for eight mirrors

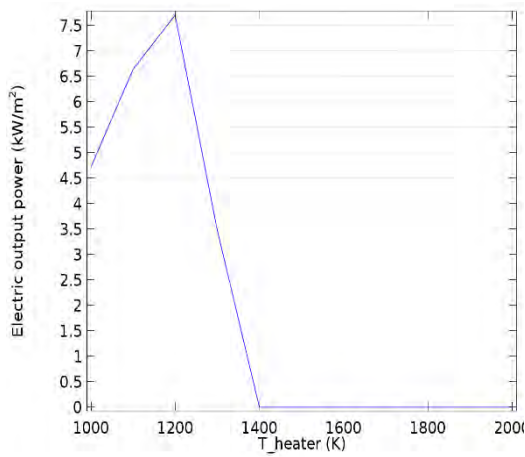


Figure 4-9(c): Electric power output versus temperature in a 2D CTPV for eight mirrors

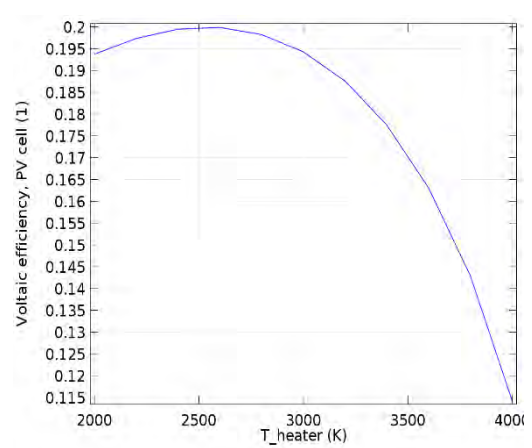


Figure 4-9(d): Voltaic efficiency versus temperature in a 2D CTPV for eight mirrors

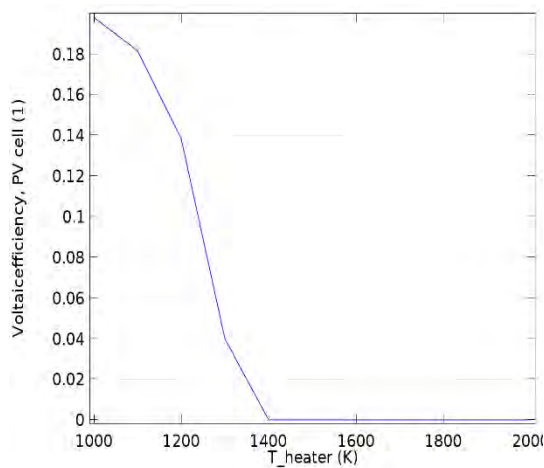


Figure 4-9(e): Voltaic efficiency versus temperature in a 2D CTPV for eight mirrors

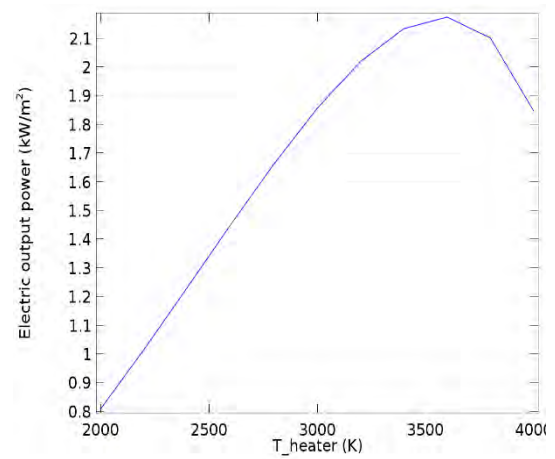


Figure 4-9(f): Electric power output versus temperature - in a 2D CTPV for eight mirrors

4.13 Results and Discussions

Study Case 1 is the comparative analysis of the 2D CTPV Geometry with different number of PV cells/mirrors pairs, simply referred to as ‘number of mirrors’.

Table 4-8: Results of comparative analysis of the 2D CTPV geometry with different number of mirrors

CTPV system with Eight mirrors	CTPV system with Six mirrors	CTPV system with Ten mirrors
<p>In Figure 4-6(a), the operating temperature (T_{heater}) was 1,400 K. This was appreciably higher than its (heater) maximum temperature of 1,200 K, above which the CTPV system’s efficiency would begin to decline and eventually become zero. The PV cells experienced a temperature distribution from 500 K to a temperature of approximately 1,800 K.</p> <p>Increasing the operating temperature above 1,200 K as in Figures 4-7(a) would begin to drop the output power of the CTPV system (7.8 kW/m²) sharply and eventually this would drop to zero at an operating temperature of 1,400 K and above as seen in Figures 4-7(a).</p> <p>The optimum operating temperature (for the heater) at which the CTPV system achieved maximum electric power output is 1200 K. At this temperature, the PV cells would reach a temperature of approximately 780 K, which they could withstand without any problem as shown in</p>	<p>In Figure 4-6 (b), the operating temperature (T_{heater}) was 1,800 K. This was appreciably higher than its (heater) maximum temperature range of 1,500 K and 1,600 K, above which the CTPV system’s efficiency would begin to decline and eventually become zero. The PV cells experienced a temperature distribution from 600 K to a temperature of approximately 1,900 K.</p> <p>Increasing the operating temperature above 1,600 K in Figures 4-7(b) would begin to drop the output power of the CTPV system (7.6 kW/m²) sharply and eventually this would drop to zero at an operating temperature of 1,800 K and above as seen in Figures 4-7(b).</p> <p>The optimum operating temperature (for the heater) at which the CTPV system achieved maximum electric power output is 1600 K. At this temperature, the PV cells would reach a temperature of approximately 1,300 K, which they could withstand without any problem as</p>	<p>In Figure 4-6 (c), the operating temperature (T_{heater}) was 2,000 K. This was appreciably higher than its (heater) maximum temperature of 1,800 K, above which the CTPV system’s efficiency would begin to decline and eventually become zero. The PV cells experienced a temperature distribution from 450 K to a temperature of approximately 1,700 K.</p> <p>Increasing the operating temperature above 1,800 K in Figures 4-7(c) would begin to drop the output power of the CTPV system (7.8 kW/m²) sharply and eventually this would drop to zero at an operating temperature of 2,000 K and above as seen in Figures 4-7(c).</p> <p>The optimum operating temperature (for the heater) at which the CTPV system achieved maximum electric power output is 1800 K. At this temperature, the PV cells would reach a temperature of approximately 1,300 K, which they could withstand without any problem as</p>

Figure 4-5(a). Hence, the best operating condition (emitter temperature) and the PV cells temperature for optimal output power (7.8 kW/m ²) were 1,200 K and 780 K respectively. Any system operation outside these temperature ranges would only be a waste of resources as the output power would become zero. This stage needs to be avoided. The optimal efficiency obtained was 19.8%	shown in Figure 4-5(b). Hence, the best emitter (operating condition) temperature and the PV cells temperature for optimal output power (31.8 kW/m ²) were 1,600 K and 1,300 K respectively. Any system operation outside these temperature ranges would only be a waste of resources as the output power would become zero. The optimal efficiency obtained was 19.8%	shown in 4-5(c). Hence, the best emitter (operating condition) temperature and the PV cells temperature for optimal output power (29.8 kW/m ²) were 1,800 K and 1,300 K respectively. Any system operation outside these temperature ranges would only be a waste of resources as the output power would become zero. The optimal efficiency obtained was 19.8%
---	---	--

Study Case 2 is the comparative analysis of 2D CTPV configuration with eight mirrors and 3D CTPV configuration with six mirrors.

Table 4-9: Results of comparative analysis of 2D CTPV with eight mirrors and 3D CTPV with six mirrors

2D Geometry of the CTPV system with Eight mirrors	3D Geometry of the CTPV system with Six mirrors
As contained in Figure 4-9(a), the operating temperature (T_{heater}) of the 2D CTPV system was 1,400 K. The PV cells experienced a temperature distribution from 500 K to a temperature of approximately 1,800 K (Figure 4-9(a)). This was appreciably higher than its (heater) maximum temperature of 1,200 K, above which the CTPV system's efficiency would begin to decline and eventually become zero. Increasing the operating temperature above 1,200 K as in Figure 4-7m would begin to drop the output power of the CTPV system (7.8 kW/m ²) sharply and eventually drop to zero at operating temperature of 1,400 K and above – refer to Figure 4-8(t).	As contained in Figure 4-9(b), the performance of the 3D CTPV system was not stable until the operating temperature (T_{heater}) was raised to 4,000 K. The PV cells experienced a temperature distribution from 400 K to a temperature of approximately 850 K (Figure 4-9(b)). This was much lower than its (heater) maximum temperature range of about 3,600 K. This is obvious from the stationary temperature distribution graph in Figure 4-8q, where the graph showed that, apart from the operating condition (heat source at the centre of the module) where the temperature was about 4,000 K, the rest of the CTPV system was very low in temperature at about just 500 K. The operating temperature had to be raised to about 3,600 K before appreciable and steady generated output power was obtained. Increasing the operating temperature above the 3,600 K in

<p>The optimum operating temperature (for the heater) at which the CTPV system achieved maximum electric power output is 1200 K. At this temperature, the PV cells would reach a temperature of approximately 780 K, which they could withstand without any problem as illustrated in Figure 4-9(c). Hence, the best operating condition (emitter temperature) and the PV cells temperature for optimal output power (7.8 kW/m²) were 1,200 K and 780 K respectively. Any system operation outside these temperature ranges would only be a waste of resources as the output power would become zero. This stage needs to be avoided.</p> <p>The optimal efficiency obtained was 19.8%.</p>	<p>Figure 4-9(d), would begin to drop the output power of the CTPV system (2.2 kW/m²) gradually to a much higher heater temperature before it would eventually drop to zero at an unknown operating temperature.</p> <p>The optimum operating temperature (for the heater) at which the CTPV system achieved maximum electric power output was 3,600 K. At this temperature, the PV cells would reach a temperature of approximately 715 K which looks very favourable for the PV operation. However, the operating temperature for the emitter heat is unexpectedly very high and attaining such a high temperature could be uneconomical.</p> <p>The optimal efficiency obtained was a bit higher than the 2CTPV - at about 20% and well-rounded for a longer period and this indicates sustainability but for a lower output power.</p>
--	---

Table 4-10: Case one summary of the results of 2D CTPV modelling with different mirror configurations

Parameters	CTPV with Eight Mirrors	CTPV with Six Mirrors	CTPV with Ten Mirrors
Subjected operating condition (Emitter temperature)	1,400 K	1,800 K	2,000 K
Heater temperature range for the operation	1,000 K to 2,000 K	1,000 K to 2,000 K	1,000 K to 2,000 K
Best operating condition (Best Emitter temperature)	1,200 K	1,600 K	1,800 K
Attained PV cells temperature	1,820 K	1,880 K	1,700 K
Best PV cells temperature	780 K	1,300 K	1,300 K
Output power	7.8 kW/m ²	31.8 kW/m ²	29.8 kW/m ²
CTPV system attained efficiency	19.8 %	19.8%	19.8%
Percentage temperature deviation (increase)	133%	45.0%	31.0%
Percentage temperature deviation (increase) on operating condition (emitter)	16.7%	12.5 %	11.1%

Table 4-11: Case two summary of the results on 2D and 3D CTPV modelling with eight mirrors

Parameters	2D Geometry of CTPV system	3D Geometry of CTPV system
Subjected operating condition (emitter temperature)	1,400 K	4,000 K
Heater temperature range for the operation	1,000 K to 2,000 K	2,000 K to 4,000 K
Operating condition (emitter temperature) for maximum output power	1,200 K	3,600 K
Attained PV cells temperature	1,820 K	850 K
PV cells temperature for optimal output power	780 K	715 K
Output power	7.8 kW/m ²	2.2 kW/m ²
CTPV system attained efficiency	19.8 %	19.9%
Percentage temperature deviation	133% (increase)	45.0% (decrease)

4.14 Findings and analysis of simulations of modelled CTPV different configurations

The results obtained for the 2-D CTPV modelling and simulation, with a varying number of PV cells and mirrors are as expressed graphically in Figures 4-4(a, b and c) to Figures 4-7(a, b and c) (a, b and c). The analysis was made and summarised as shown in Table 4-8. Based on the summary given on Table 4-10, in all cases, the CTPV system attained fairly the same efficiency value of 19.8%. The output power generated was 7.8 kW/m², 31.8 kW/m² and 29.8 kW/m² for the eight mirror, six mirror and ten mirror configurations respectively. The attained temperature deviation are 133%, 45.0% and 31.0% respectively for each case. Hence, the CTPV configuration with eight mirrors has the least generated output power and highest temperature deviation and so it is the least suitable. The option for consideration was between the six mirrors and the ten mirror configurations. Studies carried out have revealed that the lower the temperature increase, the better for the PV cells in order to avoid over-heating and damage to the PV cells. Based on these reasons, the ten PV cells/mirrors had the least temperature rise, which is obviously preferable.

However, it was considered necessary to model and simulate the eight mirror configuration in 3D to determine its effects on the CTPV system performance. The summary of the findings is captured on Table 4-1.

Based on the analysis made from Table 4-11, for the Comparative analysis of 2D and 3D CTPV modelling with eight mirrors, the 2D configuration (eight mirror) will require lower emitter temperature to generate output power of 7.8 kW/m² which is greater when compared with the 3D configuration (eight mirror) with power output of about 2.2 kW/m². Although, the 2D configuration generated higher output power but its attained PV cell temperature is higher which translate to about 133% heat increase. This is not good for the configuration as it will soon burn out. In the case of 3D configuration, there is no heat generated but the operating cost is high and at very low power output, hence the operation will not be

economical. Therefore, further investigations are needed to be carried out for best optimal operating conditions.

However, the six PV cells/mirrors configuration generated the highest power output of the three configurations. In addition, the six mirror configuration utilized the least numbers of mirrors and the PV cells out of the three configurations, ultimately translating to reduced material costs for the operation. However, it is known in PV technology that temperature increase in the system generates heat which must be avoided. The high temperature conditions and the abrupt nature of the efficiency and power output graphs are suggestive that the operation of the CTPV system with six PV cells/mirrors may eventually not be sustainable.

The results obtained for the comparative 2D and 3D simulations for six mirror configuration are expressed graphically in Figures 4-11(a and b) to Figures 4-12(a and b) and Figures 4-13(a and b) and summarised in Table 4-12. For the 2D model, the heater temperature was operated between 1000 K and 2000 K at PV cell temperature range of 600 K and 1800 K as shown in Figure 4-11(a). For the 3D model, the heater temperature was between 2000 K and 4000 K at PV cell temperature range of 450 K and 850 K as shown in Figure 4-11(b). As the upper plot in Figure 4-11(a) for the 2D model shows, the PV cells reached the temperature of approximately 1800 K, while that of 3D in Figure 4-11(b) was at PV temperature of about 850 K. The PV temperature in 2D was significantly higher than their normal maximum operating temperature of 1400 K, above which their PV efficiency would become zero as seen Figure 4-12(a and b). The maximum PV efficiency attained was about 19.8% in both cases.

From the analysis of these results, modelling the thermal PV system in 2D, the six mirror configuration would obviously be able to deliver more power output than going for the 3D, eight mirrors configuration, but care must be taken to ensure that the Heater temperature of 1200 K is not exceeded. The CTPV system attained the same efficiency value of 19.8%. In order to determine the operation that would yield the best or optimum performance, major consideration needs to be given to the temperature issue. One of the attributes of the 3D modelling is the ability to reveal the temperature distribution in a system. Since the 2D with six mirrors was the best among the various tests carried out, then it was considered necessary to model further and simulate the 3D configuration of the 2D six mirrors to see what difference it could make to the options on the ground.

4.15 Comparison of 2D and 3D six mirror configurations of the CTPV system

The CTPV with six mirrors configuration was then modelled and simulated in 3D. The same procedure for the previous ones was followed, using the same material properties. Further detailed comparative analysis of the various segments of the modelled six mirrors 2D and 3D CTPV systems are not considered again here since comparison of various modelled works has already been extensively covered in this Chapter and also in order to maintain a sizeable work-load limitation. However, the COMSOL simulated work for the 3D six mirrors alongside with other modelled configurations are included in the Appendices for perusal and further reference. In the Figure 4-8(a to u), the plots for 2D and 3D six mirror configuration plots show visual temperature distributions (stationary).

The comparative analysis of the 2D and 3D CTPV systems with six mirrors/PV cells is as presented in Figure 4-10(a) and Figure 4-10(b).

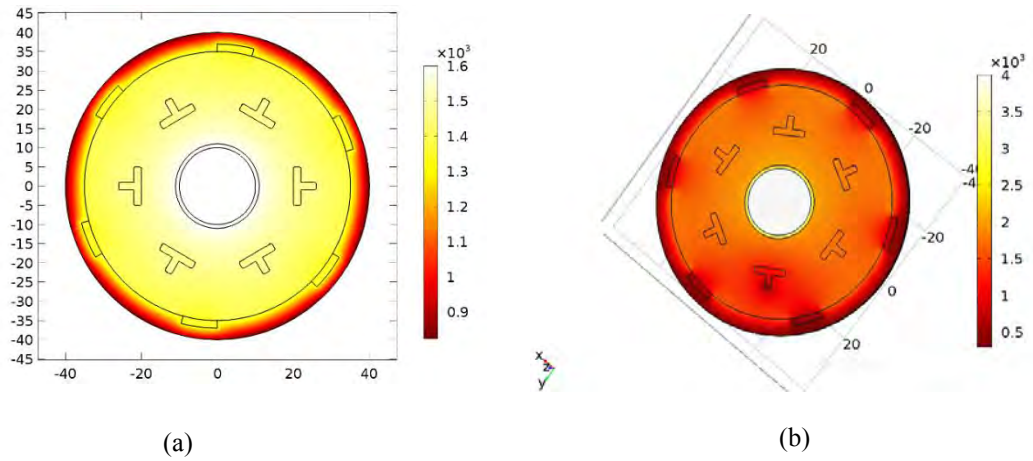


Figure 4-10(a): Temperature distribution of modelled 2D CTPV with six mirrors

Figure 4-10(b): Temperature distribution of modelled 3D CTPV with six mirrors

The two different geometries, 2D and 3D for the CTPV system with six mirrors were developed and subjected to prevailing operating conditions. The emitter temperature reached for the 2D was 2,000 K and that of the 3D was 4000 K. This is to enable further investigations as to the best CTPV structure that could give the optimum solar generated output power. The results showed that the CTPV system experienced a remarkable temperature distribution that varied almost linearly with the operating conditions and the type of system configuration place.

The temperature distribution graphs showed that the 2D CTPV with six mirrors reached temperature values of about 1,880 K and that of the 3D CTPV with six mirrors reached 900 K. The temperature at which the output power is reached is 1600 K for the 2D and at 3400 K for the 3D configuration. The comparative analysis of Point temperature of the 2D and 3D CTPV systems with six mirrors/PV cells are as presented Figure 4-11(a) and Figure 4-11(b).

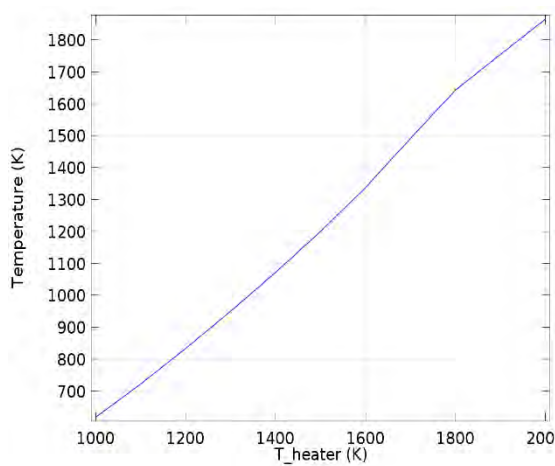


Figure 4-11(a): Point temperature of modelled 2D CTPV with six mirrors

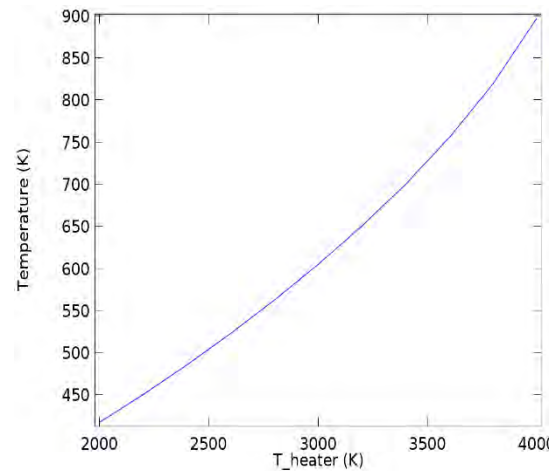


Figure 4-11(b): Point temperature of modelled 3D CTPV with six mirrors

The temperature values of the PV cells are significantly higher than their best operating temperature of 1,300 K and 700 K respectively for the 2D and 3D, six mirror configurations which would yield a system output power of 31.8 kW/m², 2.28 kW/m².

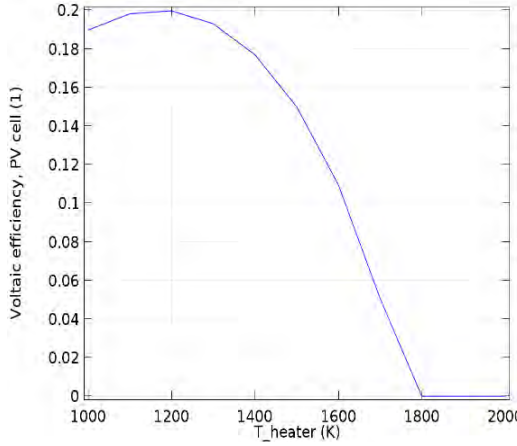


Figure 4-12(a): Voltaic efficiency against temperature of modelled 2D CTPV with six mirrors

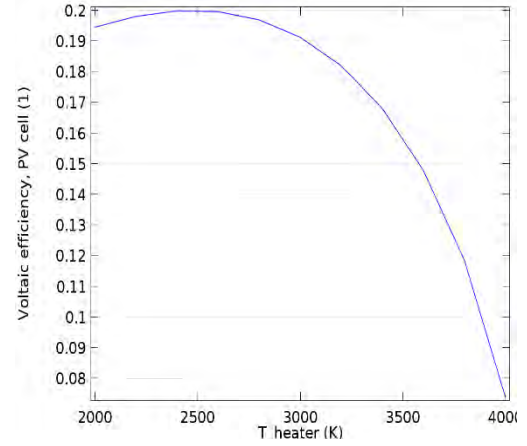


Figure 4-12(b): Voltaic efficiency against temperature of modelled 3D CTPV with six mirrors

Figures in 4-10(a) and Figures in 4-10(b) show the 3D CTPV six mirrors configuration respectively. The efficiency values for each configuration remain constant at almost 20 percent in Figure 4-12(a) and Figure 4-12(b). The efficiency distribution graph for the 3D six mirrors appeared better distributed with a wider range of sustainability than that of the 2D six mirrors.

The operating temperature for output power generation for the 2D and that of the 3D occurred at 1600 K and 3400 K above which the temperature efficiency would begin to drop sharply for the 2D and gradually for the 3D, until it gets to 1800 K and becomes zero for the 2D and to 4000 K for the 3D before it too becomes zero.

The Electric output power graphs present the operating temperature, T_{heater} , at which the system attained the maximum electric power output for the system with 2D and 3D, six mirrors respectively.

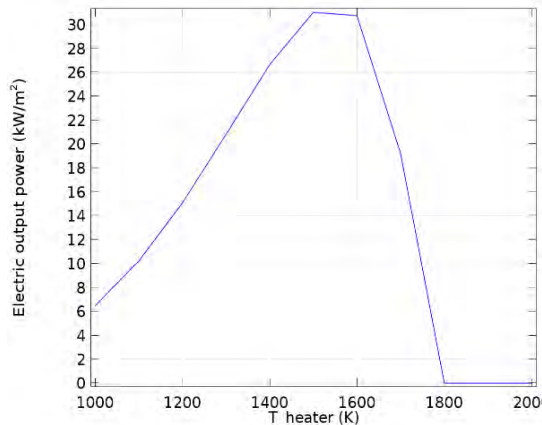


Figure 4-13(a): Electric output power against temperature of modelled 2D CTPV with six mirrors

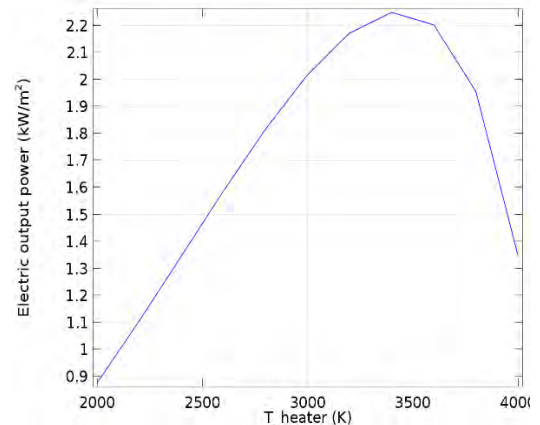


Figure 4-13(b): Electric output power against temperature of modelled 3D CTPV with six mirrors

Comparative analysis of the electric output power against temperature of the 2D and 3D CTPV configurations system performances with six mirrors.

Table 4-12: Summary of the results on 2D and 3D CTPV modelling with six mirrors

Parameters	2D Geometry, six mirror CTPV system	3D six mirror CTPV system
Subjected operating condition (emitter temperature)	1,200 K	2,500 K
Heater temperature range for the operation	1,000 K to 2,000 K	2,000 K to 4,000 K
Operating condition (emitter temperature) for maximum output power	1,600 K	3,400 K
Attained PV cells temperature	1,900K	900 K
PV cells temperature for optimal output power	1,300 K	700 K
Output power	31.8 kW/m ²	2.29 kW/m ²
CTPV system attained efficiency	19.8 %	19.9%
Percentage temperature deviation (increase)	133% (increase)	45.0% (decrease)

From the foregoing, the stationary temperature distribution indicate that the high heater operating temperature was quite safe for the PV cells in 3D CTPV six mirrors as they did not get overheated as seen in Figure 4-10(b). The maximum efficiency obtained was also about 20% at heater temperature of 2500 K as seen in Figure 4-12(b). The output power in the 2D model in Figure 4-13(a) was 31.8 kW/m² at 1200 K heater temperature above which the output power drops sharply while that of the 3D model was 2.28 kW/m² at 3400 K and was fairly stable to heater temperature of about 3800 K as shown in Figure 4-13(b). The efficiency and output power for the 2D, six mirrors is much higher but its sustainability even for a short period is not guaranteed while the output power for the 3D, six mirrors is less but the system performance will be more sustainable for a longer period because the PV cells operate in safer conditions.

4.16 Chapter conclusion

In conclusion, the choice of 3D thermal modelling with six mirror configuration appears more desirable over the 2D six mirror configuration which was considered the best in the previous analysis because the 3D six mirror configuration appears more favourable to contributing and impacting favourably on solar power generation in a sustainable manner and therefore it is preferred. This decision is based on the simple fact that the design focus is to obtain optimum power output that can be sustained over time. The benefit of this thermal modelling is that it can shortcut the prototype development time, optimize the operating conditions for the finalized TPV device and eliminate undue operational cost. It could also serve as a reference for Researchers who are interested in thermal solar energy and for Stakeholders who want to invest or work in this field. The choice of 3D thermal modelling over that of 2D modelling with the same number of mirrors (six) is more favourable to contributing and impacting positively on solar power generation in a sustainable manner. The benefit of this thermal modelling is that it can shortcut the prototype development time, optimize the operating conditions for the finalized TPV device and eliminate undue unsustainable projects. It could also serve as a reference for Researchers who are interested in thermal solar energy and for stakeholders who want to invest or work in this field.

CHAPTER FIVE

THE EFFECT OF HEIGHT IN INCORPORATING THE 3DPV STRUCTURE FOR OPTIMUM SOLAR POWER GENERATION

5.1 Introduction

In solar energy systems, incorporating 3D technology in solar power generation takes advantage of the 3D nature of the biosphere so that energy collection occurs in a volume, contrary to what is commonly obtained in a planar or flat photovoltaic panel. 3DPV technologies are capable of generating more power from the same base area when compared to the conventional flat solar panels. This chapter discusses methodologies for computation and analysis of the effect of height per unit volume compared with a plain surface arrangement and the obtained results are discussed. The results showed a remarkable increase in the energy generated by the 3DPV structure over the 3D planar structures.

5.2 Present status of solar power generation

Solar power is a major energy source capable of making a substantial contribution to fulfilling the world's future energy requirements. According to literature from [30, 50, 102, 103], the average cost of commercial PV modules stands at an average of about R28.25Wp to R37.37Wp. At present, PV energy costs less than 1% of what it used to be but in spite of impressive drops in PV system costs, the levelised cost of electricity (LCOE) of PV remains high. As at 2011, the LCOE for residential systems without storage and with assumption of a 10% cost of capital was in the range R3.74 and R9.72/kWh. With the addition of electricity storage added, the cost range increases to R5.38 and R10.61/kWh. Still in 2011, for thin-film systems, the LCOE of current utility-scale was estimated to be between R3.89 and R8.82/kWh. The cost for the crystalline solar PV system is higher [25]. For the PV solar energy conversion technology to be affordable and for BiPV technology to become economically attractive for building applications, then this cost must be brought down to nothing more than R14.95Wp [76]. This can only be made possible if the appropriate solar energy conversion technology is employed [51] and a solar incentive program and net metering is implemented [104]. Different types of solar cells are available for use for energy conversion technology; however, crystalline silicon (Si) dominates around 90% of the current PV market [20]

Convectional PV modules have relatively low energy density and this is worsened by the fact that the output of the devices is dependent on the latitude of the installation and the weather conditions of the location; besides, the peak insolation hours available in most locations is limited [10] [105]. In achieving the energy conversion target, the use of low-cost base material, optimal device design, and affordable device- processing technology is vital [54]. Conventionally, for low-scale solar energy generation, flat PV panels are installed in residential and commercial rooftop installations. In cases where the rooftop is impracticable for use or the plants are too large for roof-mounting, solar modules can also be placed on the ground, either as a fixed mount or as a tracking mount that follows the sun to orient the PV modules.

Other options include mounting as structures that create covered parking or that provide shade as window awnings. This is often used in multifamily or commercial applications [104].

There is the need for establishing improved technology in order to optimize power generation per installation area. For more effective use of the sunlight energy, the number of hours the solar cells are in trajectory with the sun for peak power generation can be lengthened by incorporating sun-trackers. However, tracking has the disadvantages of introducing additional cost. It also requires larger space for operation thereby causing interference with other panels and possible shading and it is also subjected to occasional maintenance periods and other disruptions. Furthermore, it is not suitable for residential or commercial installations due to its bulky moving parts [4, 106]. However, it is still being used because its price has reduced considerably [41]. A tracking system can be more cost efficient if the cost of its tracker is less than total costs of that system by a factor of $(T_c - 1)/T_c$ where T_c is tracking factor which tends to unity as it improves the output power generated and this varies from location to location [4]. In addition, it can generate more energy with less solar panels, lower electrical device ratings and smaller structure on about the same land area. Nevertheless, there is the need for improved technology for solar energy optimization.

5.3 Three dimensional nature of photovoltaic (3DPV) structure

The 3DPV technology is a new technology in PV energy generation that mimics the pattern found in the nature of structures that collect sunlight in 3D [51, 54, 55]. Three main physical reasons underlying the advantages of collecting light in 3D are the multiple orientations of the absorbers that allow for the effective capturing of off-peak sunlight, the avoidance of inter-cell shading, and the re-absorption of light reflected within the 3D structure [4, 50, 51]. These benefits enable the measured generated energy densities (energy per base area) to be higher by a factor of 2 to 20, than the stationary flat PV panels. 3DPV is a new approach for achieving optimum solar energy that will yield cost-effective, more reliable and a most economically friendly alternative energy source [50, 107].

3DPV technology utilizes the 3D nature of the dimensional structures such as the spherical or cubic system to absorb power in the entire volume of that material. Hence, power is measured in Watts per unit volume as against per area measurement as it is the case with planar or 2D systems. Furthermore, the impact of height in system efficiency for the 3DPV is remarkable [4, 55, 107]. Some of the research work carried out on this technology is briefly discussed in this chapter.

5.3.1 Solar energy generation in 3D

According to the Massachusetts Institute of Technology (MIT), it has been established that 3DPV structures can increase the generated energy density in a linear proportion to the structure height, for a given day and location. The optimum shape of the 3D structures was derived using computer simulations such as genetic algorithms (GA) for optimizing the generated output energy. These 3D structures include a cubic box open at the top, a funnel-like shaped cubic box, a sphere, a parallelepiped or any other 3D shape that in principle is found capable of doubling the daily energy density. 3DPV structures were found to lessen some of the variability inherent to solar PV as they provide a more regular source of solar energy generation at all latitudes. They are found capable of doubling the number of peak power

generation hours as they intensely reduce the seasonal, latitude and weather variations of solar energy generation when compared to a flat panel design [4, 11, 50].

5.3.2 3DPV module assembly by Fibonacci number

3DPV technology by Fibonacci number method involves the arrangement of the individual solar cells of the 3DPV module in a leaf-like manner. The arrangement revealed that such a modular design has the benefits of enabling each solar cell to receive the reflected light from the other cells thereby maximizing power generation per installation area. It also enables solar cells to be stacked in a vertical configuration, which enhances the doubling of daily energy density [4, 55].

Another research group, carried out a test on a 3DPV module whose configuration was based on Fibonacci numbers. The simulation results revealed that the power generation characteristics of the solar cells depend on the shape and spacing of the solar cells for most effective use of sunlight energy [8, 51, 55].

5.3.3 Spherical silicon solar technology

Accurate 3D technology has been found to enable innovative and improved device design, which can result in overall cost-effectiveness, improved material processing and system utilization [54, 58]. Of particular interest is the spherical Si solar technology (SSST), which has been found to be efficient and quite inexpensive. It utilizes low-cost Silicon (Si) feedstock for its fabrication process which is simple and inexpensive [108]. In addition, self-supporting 3D shapes are discovered to develop new schemes for PV installation and to increase energy density which can facilitate the use of inexpensive thin film materials in area-limited applications. Hence, harnessing solar energy in three dimensions can open new avenues towards Terawatt scale generation[50].

5.3.4 3D Nanopillar-based cell modules

In recent years, much progress has been made in developing PV that can potentially be mass deployed. An example of this is in the use of 3D Nanopillar-based cell modules, with the emphasis on reduced solar cells cost by using novel device structures and materials processing for enabling acceptable efficiencies. In this regard, the highly regular, single-crystalline nanopillar array of optically active semiconductors can be directly grown on aluminium substrates, which are configured as solar modules. An example of this is the CdTe/CdS PV structure that incorporates three-dimensional, single-crystalline *n*-CdS nanopillars which is embedded in polycrystalline thin films of *p*-CdTe, to enable high absorption of light and efficient collection of the carriers. Various experiments and modelling have proved the potency arising from the geometric configuration of this approach to enable enhanced carrier collection efficiency on both rigid and flexible substrates of the highly versatile nanopillars solar modules [59].

5.4 Effect of height in the Fibonacci method of 3DPV generation

The Fibonacci method of employing the PV module (FPM), utilizes numbers to attain the height spacing for improved adsorption of solar energy [8, 51, 55]. The Fibonacci numbers are manifested in all spheres of life. They are present in the leaf or petal arrangement of most plants as seen in Figure 5-1.

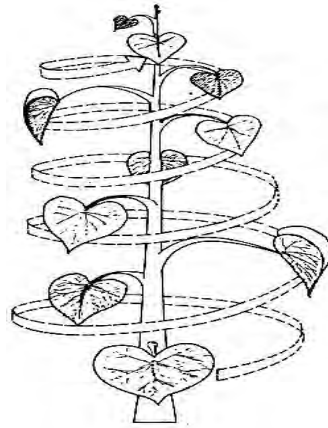


Figure 5-1: Leaf arrangement on plants by phyllotaxis [57]

It has been stated that the reason often presented in such arrangements, is to maximize the amount of light received on the space allotted for each leaf or petal on the plant [54, 55, 106].

In a similar fashion, a mass of silicon with an expanded surface can absorb the solar radiation in layers of its crystallized molecules. Conversely, the leaves are not usually arranged on a flat surface, but spread in the whole volume of a plant. This is synonymous with why the trees tend to grow vertically to access most of the solar rays in a given volume. Solar panels can also be arranged in a similar fashion and the solar energy considered in terms of Watt-hours per unit volume. However, to install the PV panels on a tall structure is more tedious and costly than laying them down on the ground. That notwithstanding, depending on price of land, the arrangement of the solar equipment on a raised structure could be more cost-effective. Another advantage of a vertical arrangement is the possibility of rotating Fibonacci solar panels in order to track the sun for a higher efficiency [51, 54, 107].

The manifestations of the Fibonacci numbers and the golden ratio are apparently endless and can be found throughout nature in the forms and designs of many plants and animals. The Fibonacci sequence can be perceived in nature in the spirals of a sunflower's seeds and the shape of a snail's shell. These numbers have also been used in various ways in works of Architecture, Art and Music for centuries. The numbers have been of use in medicine, science and engineering. In particular, the numbers are widely used in engineering applications including computer data structures and in sorting algorithms, financial engineering, audio compression, architectural engineering and solar energy application [109-112]. The numbers highlight the order and mathematical complexity of the natural world. [57].

Although 3DPV solar power installations are not common yet, one such installation, using a FPM approach already exists in Ontario, Canada as seen in Figure 5-2. The solar-powered tree of about 0.5 kW is installed at Tourism London, Wellington Rd, Ontario Canada and it is funded by an Ontario Power Authority. This solar-powered tree is 7 meters tall and has 27 leaves, each producing power [113].



Figure 5-2: A 500 Watts solar-powered tree at tourism London, Ontario Canada [113]

5.5 3DPV structure effect on solar radiation intensity

The generated solar energy density is a function of the solar intensity called irradiance and it is measured in W/m^2 . Many parameters determine the intensity of solar radiation such as latitude, season, altitude, geographical conditions, atmospheric pressure, humidity, time of day, and some other extra-terrestrial effects such as solar storms. On a clear day, the intensity of solar radiation is at its maximum around noon and decreases towards dusk. However, 3DPV structures have been found to nearly double the number of peak hours available for solar energy generation and provide a measured increase in the energy density by a factor of about 2 to 20 without the use of sun tracking in the case of cloudy weather. The structures are also found able to reduce the large variability in solar energy generation with latitude and season contrary to what is obtained in the case of planar solar configuration [4, 51, 55, 57]. The solar radiation received on the surface of the material is proportional to the power absorbed in the entire volume of the 3DPV structure.

5.6 Energy per unit volume

Generally, some level of physical mass is required for energy of any sort to be absorbed and this energy is found to be proportional to the volume and density of that material [4, 50, 51].

Mathematically, the material surface is two-dimensional while the physical objects are three-dimensional. It is proper to consider energy in the volume, as well as energy on the surface, in the context of solar energy. For energy per unit volume consideration, it is assumed that some solar collectors are effectively arranged within any three dimensional structure such as a cube with arbitrary dimensions f , g , h facing northerly with the x , y , z -axes. Hence, the cube volume, V , is also considered as a vector V with three assigned components below:

$$\begin{cases} V_x = gh \\ V_y = fh \\ V_z = fg \end{cases} \quad (5.1)$$

These components are assumed to be proportional to the cube's three faces on which the solar beams radiate on the top, front and east or west at any given time.

The solar irradiance is considered a vector with variable components proportional to the absolute values of x, y, z components. Hence, solar power, P , going into the cube as indicated earlier can be extended and interpreted as the scalar product of the volume and irradiance vectors.

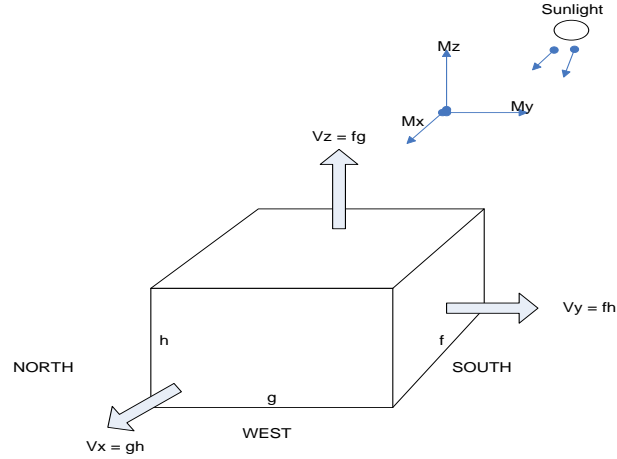


Figure 5-3: Solar irradiance components to a cube [4]

5.7 Computation of solar energy in three-dimensions

In order to analyse the energy absorbed by the cube, the authors considered the cube volume and the vector components of the surfaces. In Figure 5-3, with dimensions f, g, h standing northwest with the x, y, z – axes as shown. As earlier stated, the cube volume, V , was considered a vector \underline{V} , with three components as given in equation (5.1). These components of the volume vector were exposed to the solar beam radiation.

Considering that the solar irradiance is also a vector, with variable components proportional to the absolute values of x, y, z given by equation (5.1). It would imply that the solar power going into the cube of a solar tree can be expressed as:

$$P = \underline{V} \cdot \underline{I} \quad (5.2)$$

where,

$$\begin{aligned} P_x &= ghI [\cos(\beta)\cos(\theta)] \\ P_y &= fhI [\sin(\alpha)\sin(\beta)\cos(\theta) - \cos(\alpha)\sin(\theta)] \\ P_z &= fgI [\cos(\alpha)\sin(\beta)\cos(\theta) + \sin(\alpha)\sin(\theta)] \end{aligned} \quad (5.3)$$

Total power is the vectorial sum of the components, such that:

$$P_{Tot} = P_x + P_y + P_z \quad (5.4)$$

The value of irradiance and the angles β and θ are functions of time as described above. The module of irradiance M , which is defined as the average irradiance in any location at a certain latitude α , is introduced in equation (5.5). For the purpose of computation, M value applied here is taken as 62% for location latitude of -29.8833 (South).

Then,

$$Avg[cos(\beta)cos(\theta)] = Avg[sin(\beta)cos(\theta)] = 0.62$$

$$Avg[sin(\beta)] = 0 \text{ and } f, g, h = 1$$

The module of irradiance for Durban is assumed here as 0.62 for the month of January and it is utilized here as a parameter of average irradiance at the latitude (α) -29.8833 (South). This is specified by the three components below:

$$\begin{aligned} M_x &= 0.62I \\ M_y &= 0.62I \sin(\alpha) \\ M_z &= 0.62I \cos(\alpha) \end{aligned} \tag{5.5}$$

and

$$M = M_x + M_y + M_z$$

The average value of available solar power obtained within the volume is the scalar product of volume vector V and module of irradiance, M as indicated:

$$P_{avg} = V \cdot M \tag{5.6}$$

Hence,

$$P_{Avg} = \begin{cases} P_{x-Avg} = ghIM_x \\ P_{y-Avg} = fhIM_y \\ P_{z-Avg} = fgIM_z \end{cases} \tag{5.7}$$

and

$$P_{Tot-Avg} = P_{x-Avg} + P_{y-Avg} + P_{z-Avg} \tag{5.8}$$

Dimensions f, g, h in these equations are the effective dimensions where 100 percent of the solar energy is absorbed. However, real dimensions of the occupied space are “ n ” times larger; and n relates to the efficiency η of the collectors. The efficiency of the PV panels is assumed to be 16 percent, therefore, n is 2.5 in this case. This was found useful in the optimization programming carried out on these two different solar panels’ installation configurations.

The efficiency of a solar power system depends on how it collects solar energy. In order to determine the solar irradiance in volume, it was assumed the solar panel was effectively arranged within a cube as shown in Figure 5-4. From equation 5.4, more energy could enter a volume as compared to entering through a surface such that:

$$P_{Tot} > P_x, P_y, P_z \tag{5.9}$$

The main concept of measuring energy per unit volume is that solar collectors get more irradiance when elevated from the horizontal position as seen in Figure 5-5 to the vertical position as seen in Figure 5-4.

The solar cell efficiency depends on the collectivity factor, c , which is defined as the ratio of the collected solar energy to the maximum solar energy available in an effective volume occupied by the solar system installed in an area and at a certain height. The amount of solar energy generated is a function of the collectivity factor and this was found to be in direct proportion to the height.

In this chapter, the author compared the results obtained on the power (Watts) generated with this tree-level arrangement (3D) in Figure 5-4, with the Power (Watts) generated by its equivalent co-planer

arrangement (2D) in Figure 5-5 and the data were run using the Matlab program and the results were plotted and analysed as shown in Figures 5-6, 5-7 and 5-8.

5.7.1 3D Configuration of the solar panel

In order to estimate the effect of height, a 10 kW solar array was assumed for the multilevel fixed structure as shown in Figure 5-4. The effective volume dimensions occupied by the tree-level system were assumed as $f = 3.5$; $g = 2.5$ and $h = 3$ meters. The index of the real dimensions of the occupied space by the PV panel, n , is assumed as 2.5, the assumed irradiation I , was 678 W/m^2 for the solar panels installed at a tilted angle of 50° towards the South.

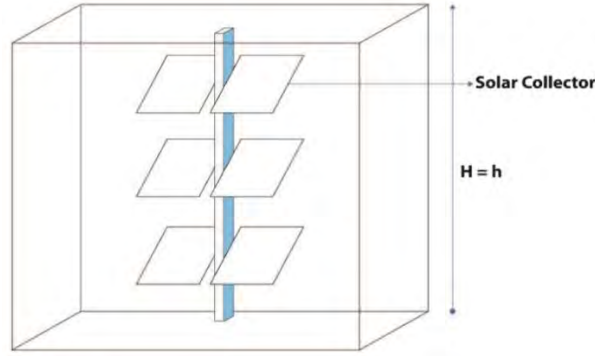


Figure 5-4: Multilevel panels arranged as a volume

From equation (5.5), the modules of irradiance of the solar radiation for the 3D and 2D structures were determined for this location as:

$$M_x = 420 \text{ W/m}^2 \quad M_y = 292 \text{ W/m}^2 \quad \text{and} \quad M_z = 302 \text{ W/m}^2 \quad (5.10)$$

These values were used for Modules of irradiance in the Matlab computations as.

$$\begin{aligned} P_{x-Avg} &= ghM_x = 0.62ghI, \\ P_{y-Avg} &= fhM_y = 0.62fhI\sin(\alpha) \\ P_{z-Avg} &= fgM_z = 0.62fgICos(\alpha) \end{aligned} \quad (5.11)$$

5.8 2D Configuration of the solar panel

It was assumed that the elevation, for the 2D arrangement is one-third of the height h , for the 3D structure. In the 2D arrangement, not all the sides are present (as shown in Figure 5-5), hence only the Front and the Top would receive the solar radiation.

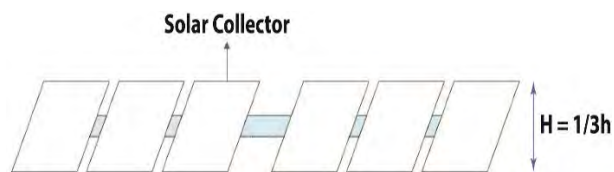


Figure 5-5: Planer (2D) arrangement of solar panels

Hence for the 2D arrangement, the average total power in Watts, is estimated as:

$$P_{Tot-Avg} = P_{y-Avg} + P_{z-Avg} \quad (5.12)$$

where,

$$P_{y-Avg} = fhM_y = +0.62fhI\sin(\alpha)$$

$$P_{z-Avg} = fgM_z = +0.62fgICos(\alpha) \quad (5.13)$$

$$H = 1/3h \quad (5.14)$$

5.9 Results and discussions

The variables derived for the solar power in equations (5.4), (5.7) and (5.11) were used to determine generated powers for the 2D and 3D solar structures for height variation of 1 to 6 meters. The values are as indicated in Table 5-1. The graphs obtained in 2D and 3D cases are linear in shape since the effects of other factors such as weather, seasonal variations such as cloud and rain and temperature are not considered for simplicity.

From Table 5-1, at height of 1 meter, the 2D and 3D solar structures generated output power of 2.983 kW and 4.714 kW respectively (Figures 5-6 and 5-7) while at height 6 meters, the 2D and 3D generated output power are 4.686 kW and 15.08 kW respectively (Figure 5-8). The percentage increase in output power ratio between the 2D and 3D solar structures increases from the minimum height (1 meter) to the maximum height (6 meters) is from 37 % to 69%. This indicates that power generation in 3D improves with increasing height.

Since a linear relationship exists between solar generated energy and the generated output power, it is then true to imply that solar energy generated increases with increasing height. However, this statement may not be true for a solar farm with multiple trees because of the shading effect from the adjacent trees which hinders the absorption of the reflected rays by the PV cells thereby causing a reduction in the generated output power. In order to avoid excessive partial shading of the elements, the solar trees would need to be installed with a relatively large spacing. A new set of equations would need to be applied to accommodate these changes [114].

Table 5-1: Power output data for the 2D and 3D solar installations

Height h (m)	1.000	2.000	3.000	4.000	5.000	6.000
Power (2D) kW	2.983	3.324	3.665	4.005	4.345	4.686
Power (3D) kW	4.714	6.786	8.859	10.93	13.00	15.08

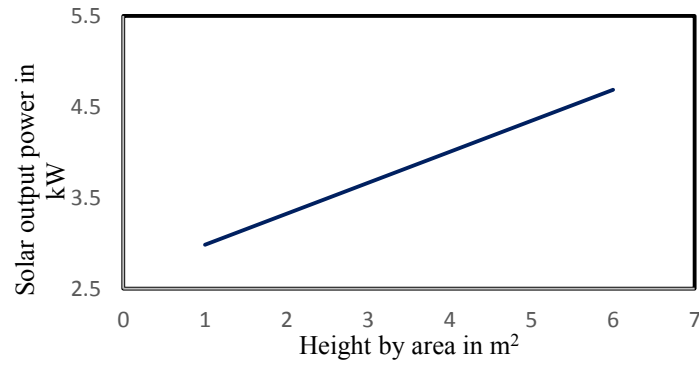


Figure 5-6: Energy optimization by 'area' in a planar system

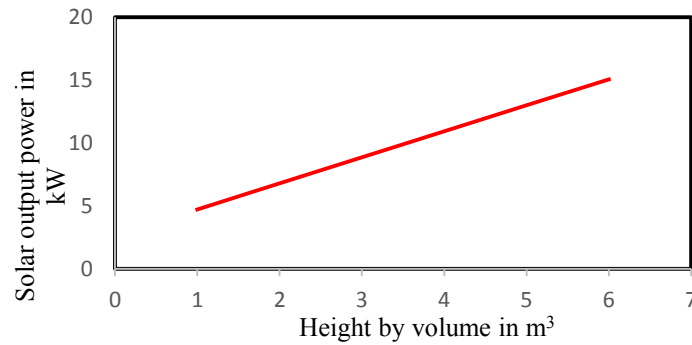


Figure 5-7: Energy optimization by 'volume' in a 3DPV system

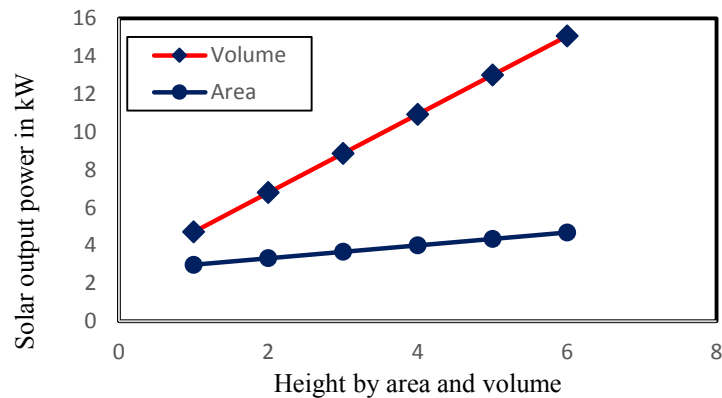


Figure 5-8: Energy optimization by 'volume' in a 3DPV and by area in a planar systems

5.10 Chapter conclusion

In this chapter, the effects of height on solar generated energy and power were analysed and discussed. All other variable parameters, such as weather conditions, time of the day and such like were not considered. The concept of energy-per-unit volume for solar energy was held to be true for solar installations with consideration given to height. Module of Irradiance, M , was found to be a simple and useful tool for establishing the per-unit component for the top, front, and the side surfaces for the irradiance into a unit volume. There was an enhanced power output with the use of the Module of Irradiance. The graphs for the generated power by volume for the 3DPV system and the generated power

by area for the planar system showed a linear relationship between solar panel height and the generated output power. The gradients of the two graphs revealed increased power by the 3DPV structure over the planar structure by 16 percent. This confirms the fact that introducing height to a solar power installation will increase the performance of the solar device. This conclusion is true for a single tree like the one considered in this chapter. However, in situations where more than one tree is used, there is the tendency of experiencing uneven illumination of solar panels composing a 3DPV system due to shading by other solar cells. Consequently, the power output decreases progressively as a result of parasitic dark currents which are believed to be in the masked cells thereby reducing the overall voltage and current and ultimately reducing the maximum power output of the array. In order to mitigate the power imbalances resulting from shaded cells, a blocking diode is usually placed in series with every cell to reduce electrical losses and optimize the power output of a 3DPV system [50]. Another way possible to avoid excessive partial shading of the PV cells is for the PV panels to be installed with relatively large spacing. When more solar trees are involved, more complex equations would be required to describe all figurations [114]. These results obtained in this work suggest that utilizing three-dimensional technology in PV solar installation presents interesting opportunities in PV design and improved solar energy generation.

CHAPTER SIX

ONE DIMENSIONAL SIMULATION OF PHOTOVOLTAIC MODULE FOR PERFORMANCE PREDICTION

6.1 Introduction

In order to determine the performance and the impact of 3DPV structure on photovoltaic power generation, it is necessary to first model the PV in 1D. This is to effect the determination of the influence of variation of environmental parameters on PV electrical characteristics. This is done by varying the PV cell parameter while the other parameters are kept constant or fixed. This is made possible by using 1D simulation like MATLAB or any other 1D software such as INSEL, TRNSYS, Solar Advisor Model (SAM), DDSCAD PV, Solar Pro, PV Professional, SolarGIS, 3TIER and PVGIS to mention but a few [115]. In this work, MATLAB R2014b was used.

In this Chapter, a step-by-step development of mathematical modelling, based on a single diode equivalent circuit was used to simulate a PV cell/module under different operating parameters is presented. These steps were used in estimating the five PV parameters and in obtaining the IV characteristic curves of the photovoltaic module with respect to the changes on the parameters such as the environmental parameters (temperature and irradiation), the cell parameters (parasitic resistances – series and shunt resistances) and the ideality factor. Using a Shockley diode equation, the simulated results were validated and compared with the manufacturers' specifications at standard temperature and pressure (STD) and these figures are presented. These results are based on the best commercially available PV modules namely: a Sunpower 345W X21-Series solar panel with 96 cells as contained in the Appendix and Yingli Mono 260 Series PV panel with 60 cells, also contained in the Appendix. The simulated results in both cases were analysed and matched with the manufacturers' specifications. The findings under various conditions helped in the choice of the panel chosen for the 3D design of the most current, accurate, efficient and the best available at present..

6.2 1D Modelling of photovoltaic module/performance analysis determination

The study, development, design, modelling and analysis of a PV power system and its components from conception to delivery are complex and require adequate understanding of physics selection and its application on the geometry in order to meet up with quality service delivery. Furthermore, since solar energy generation is time and season-variant, adequate care needs to be taken into consideration for accurate PV model production for optimal power generation [116]. The developing and modelling of PV modules presented in this work and their performance prediction involved the initial use of 1D simulation approach that involved the use of an efficient PV configuration module based on single diode equivalent circuit and using Matlab/Simulink. The cell parameters obtained in the simulated modules were compared against the manufacturers' specifications. The compared results include R_s , R_{sh} , I_{sc} , V_{oc} , and N , these abbreviations are as earlier defined in the list of Engineering and Mathematical notation. Furthermore, the performance of the simulated modules under variation of series resistance, ideality factor, irradiation and temperature was also analysed.

Two different types of the best among the PV modules were simulated and analysed. This was done to screen further between these two, the more suitable PV that has better manufacturers' specifications, capable of generating improved and better output power. The two panels considered were Yingli Mono 260 Series PV panel with 60 cells which was taken from the group of the conventional panels while the other one was a commercial PV module - a Sunpower 345W X21-Series solar panel with 96 cells which was taken from among the recent technology. This is done for performance comparison purposes. In the Figure 6-1(a) to Figure 6-4(b) is the comparison between Sunpower X21- 345 and Yangli YL260C panels.



Figure 6-1(a): Image of Sunpower X21- 345 PV panel



Figure 6-1(c): Image of Yingli YL260C- PV panel

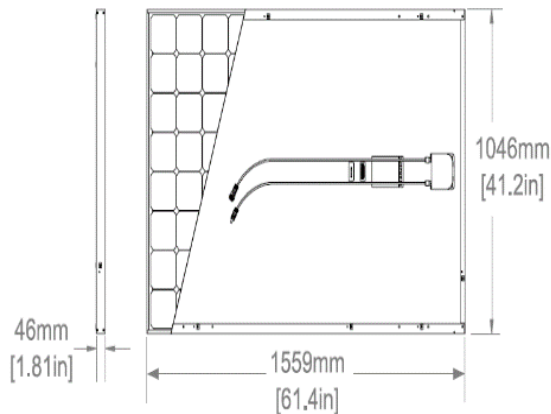


Figure 6-1(b): Dimension (mm) of Sunpower X21 1,559 x 1,046 x 46

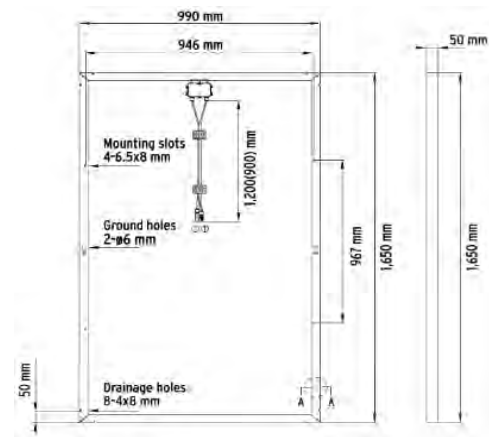


Figure 6-1(d): Dimension (mm) of Yingli PV panel 990 x 1,650 x 50

These selected panels, Sunpower 345W X21-series solar panel and Yingli mono 260 series PV panel were picked as the best among their groups. These are the closest, among the best and the most current and available panels as enlisted in APPENDIX B-1. They are very close in physical, dimension, area of the panel and in electrical properties as shown in in the Appendices, hence they are equivalent and good for comparison.

The purpose of this comparison is to ensure and justify the fact that the best available panel is used for modelling and simulation for determining the effect of 3DPV on the generated output power. This is to ensure that the reports that are generated in this thesis at the end of this work are up to date and most current.

6.3 Mathematical modelling of PV cells and Module

A single diode equivalent circuit was used in 1D modelling of the practical PV cell. More details have been presented on this modelling in Chapters 2 and 3 in accordance with Current-Voltage (IV) relationship of the solar cell. A practical PV cell has equivalent series resistance R_s and a parallel/shunt resistance R_{sh} connected to it in contrast to an ideal PV cell that has only a current source and a reversed-connected diode in parallel to it. The presence of series resistance is brought about as a result of solar cell design defect [117]. Its presence reduces the fill factor FF, while its excessively high values may cause further reduction in the short-circuit current I_{sc} and reduced short circuit current is [118]. On the other hand, the presence of shunt resistance R_{sh} is due to manufacturing defects and its presence causes appreciable power losses. The effect of low shunt resistance is largely severe at low light levels, since the impact of diverted current will be severe on the light-generated current. Furthermore, the impact is also greatly felt at lower voltages where the effective resistance of the solar cell is high [118]. For these reasons and for good modelling results, the values of R_s must tend to zero while that of R_{sh} must tend to infinity [118, 119].

For an ideal PV cell [28]

$$I = I_{ph} - I_d \quad (6.1)$$

Shockley diode equation is:

$$I_d = I_s \left[\exp\left(\frac{qV}{NkT}\right) - 1 \right] \quad (6.2)$$

For a practical cell

$$I = I_{ph} - I_d - I_{sh} \quad (6.3)$$

and

$$I_{sh} = \left[\frac{V + IR_s}{R_{sh}} \right] \quad (6.4)$$

Hence:

$$I = I_{ph} - I_s \left[\exp\left(\frac{qV}{NkT}\right) - 1 \right] - \left[\frac{V + IR_s}{R_{sh}} \right] \quad (6.5)$$

In the presence of both series and shunt resistances, the IV curve of the solar cell is described by the equation:

$$I = I_{ph} - I_s \exp\left[\frac{q(V + IR_s)}{NkT}\right] - \left(\frac{V + IR_s}{R_{SH}}\right) \quad (6.6)$$

where, all electrical parameters are as defined in the list of Engineering and Mathematical notations.

The series resistance, R_s is more dominant in operation when PV is in the voltage source region. R_{sh} is related to diode reverse voltage current and it is more dominant in operation when PV is in the current source region. The reverse saturation current, I_s , was determined by considering open circuit

condition where (when) $I_{cell} = 0$ and at short circuit condition where (when) $I_{cell} = I_{sc}$. This implies that I_{sc} is equal to light generated current I_{ph} given by [67]:

$$I_s = \left[\frac{I_{sc}}{\left(\frac{V_{oc}}{e(NkT)} - 1 \right)} \right] \quad (6.7)$$

6.3.1 Consideration for environmental and cell parameters in PV modelling

These considerations fall into two categories and their effects are as described below:

a. Effect of Temperature and Irradiation variations on the PV cell or panel.

The effects of environmental parameters, namely: temperature and solar irradiation on the performances of the PV system were investigated. Increase in solar radiation intensity increases the photovoltaic current, I_{ph} while increase in operating temperature, T_{op} , decreases the open circuit voltage and consequently the generated power output [120]. The photovoltaic current, I_{ph} is related to the temperature and solar irradiation in Equation (6.7) and according to [67]:

$$I_{ph} = (G_k)[I_{sc} + K_i(T_{op} - T_{ref})] \quad (6.8)$$

The variation in solar radiation reaching the ground is caused by some factors such as the distance travelled by the irradiation, time and season variations, climatic conditions, apparent motion of the sun and tropospheric conditions [121]. All these variants affect the PV module performance. Hence the light generated current in Equation (6.7) can be re-written as [36, 116]:

$$I_{ph} = \left[\frac{I_r}{100} \right] [I_{sc} + K_i(T - T_{ref})] \quad (6.9)$$

$$I_s(T) = I_s \left(\frac{T}{T_{ref}} \right)^3 \exp \left[\frac{E_g}{NV_t} \left(\frac{T}{T_{ref}} - 1 \right) \right] \quad (6.10)$$

$$V_{oc} = V_t \ln \left(\frac{I_{ph}}{I_s} \right) \quad (6.11)$$

It implies that the photovoltaic current, I_{ph} is a linear function of ambient irradiation, G in W/m^2 . As G increases, so also I_{ph} increases. The symbol K_1 is the change in panel short circuit current, ΔI_{sc} per $^{\circ}C$, at temperatures that differ from 25 $^{\circ}C$ or 298 K. The value of K_1 increases as the operating temperature deviates further from the standard temperature of 25 $^{\circ}C$ or 298 K, that is at a temperature where [66]

$$T \neq T_{ref} \text{ (25 C or 298 KC)}$$

As the operating temperature, T_{op} increases, the open circuit voltage decreases, indicating the inverse relationship between the operating temperature of the PV cell, T_{op} (in Kelvin) and the open circuit voltage, V_{oc} [37]. At standard test conditions of irradiation value, $G = 1 \text{ KW/m}^2$, air mass, $AM = 1.5$ and operating temperature, $T_{op} = 25 \text{ }^{\circ}C$ or 298 K, the photovoltaic current equals the short circuit current, meaning that:

$$I_{ph} = I_{sc} \quad (6.12)$$

As the cell temperature increases, the fill factor, FF, decreases, the open circuit voltage, V_{oc} also decreases linearly and short circuit current, I_{sc} increases slightly and the PV cell becomes less efficient. These conditions need to be avoided in good PV cell modelling. On the contrary, as the irradiation increases, the open circuit voltage, V_{oc} increases logarithmically, the short circuit current, I_{sc} increases

linearly and the PV cell becomes more efficient. This condition needs to be upheld in good PV cell modelling [122].

Equation (6.11) represents the greatest current value condition [66]. The variation in the incident light intensity on a solar cell alters all solar cell parameters, inclusive of the followings: the short-circuit current, the open-circuit voltage, the FF, the efficiency and the impact of series and shunt resistances. These are essential PV cells parameters used in characterising the PV cells.

b. Effect of Cell Parameters variation on the PV cell or panel

The cell parameters determined included the parasitic resistance (R_s and R_{sh}) and N . The presence of R_s is due to solar cell design defects while R_{sh} presence is due to manufacturing defects [66] and this is a major concern for power losses in solar power generation. Hence, in PV modelling, the parasitic resistance needs to be made as close as possible to the ideal condition whereby R_s is as close as possible to 0 and R_{sh} is as close as possible to infinity [66, 119].

The ideality factor is associated with the carriers' mobility across the junction. If mobility process is purely diffusion, then $N = 1$ and N is equal to 2, if mobility is mainly due to recombination in the depletion region. So, $1 \leq N \leq 2$ and N is a function of solar cell material and is independent of solar irradiation, G . The carriers recombination in the depletion region is unfavourable and not desired, so as the value of N tends to 1 is most desirable.

In this work, some pre-defined manufacturers' specifications were obtained from Yingli mono 260 series PV panel and Sunpower 345W X21-series solar panel as indicated on Tables 6-1 and 6-2. These values are $V_{oc} = 38.6$ V, $I_{sc} = 8.91$ A for Yingli PV panel and $V_{oc} = 68.2$ V, $I_{sc} = 6.39$ A for Sunpower solar panel and were used along with Equations (6.12) and (6.12) to obtain the values of R_s and R_{sh} for both panels. Furthermore, these values were used and varied in line with equations (6-13) and (6-14) to obtain the varying values of G_1 , T_{op} , and N . The calculated data from the manufacturers' Yingli mono 260 series PV panel and Sunpower 345W X21-series solar panel are presented in Tables 6.1 and 6.2 and these were used for evaluating against the simulated models.

6.4 Matlab modelling of a PV Module

The mathematical model of the PV module was implemented using MATLAB/Simulink R2014b. The PV nature or electrical behaviour is non-linear as evident from its characteristic equations. The manufacturers' specifications in standard test conditions, were used to determine and predict the behavioural patterns of the $I-V$, $P-V$ graphs for varying temperature T , irradiation G , series resistance R_s , parallel/shunt resistance R_{sh} , and ideality factor N . Some information was obtained from the PV manufacturer's datasheet such as open circuit voltage V_{oc} , the short circuit current I_{sc} , maximum power current I_{mp} , maximum power voltage V_{mp} .

The series resistance (R_s) lower and upper limits were determined from [28] as:

$$R_s < \frac{0.1 \times V_{oc}}{I_{sc}} \quad (6.13)$$

and

$$R_{sh} > \frac{10 \times V_{oc}}{I_{sc}} \quad (6.14)$$

Hence in Table 6-1, the values of series and shunt resistances for both PV panels Sunpower 345W X21-Series Solar and Yingli Mono 260 Series PV panel were determined using these equations.

Table 6-1: Establishing the series and shunt resistances for Sunpower and Yingli PV Panels

	$R_s < \frac{0.1 \times V_{oc}}{I_{sc}}$	$R_{sh} > \frac{10 \times V_{oc}}{I_{sc}}$
Sunpower 345W X21-Series, $V_{oc} = 68.2 \text{ V}$, $I_{sc} = 6.39 \text{ A}$	$R_s < 1.07$	$R_{sh} > 106.73$
Yingli Mono 260 Series PV panel, $V_{oc} = 38.6 \text{ V}$, $I_{sc} = 8.91 \text{ A}$	$R_s < 0.43$	$R_{sh} > 43.32$

For the Sunpower 345W X21-Series PV panel, the value for R_s must not be greater than 1.07Ω and the value for R_{sh} must not be less than 106.73Ω . On the other hand, for the Yingli Mono 260 Series PV panel, R_s must not be greater than 0.43Ω and R_{sh} must not be less than 43.32Ω . These were taken into consideration for the 1D modelling, hence these values of R_s and R_{sh} were set as the boundary conditions for generating the I-V and P-V simulation curves.

The essential cells parameters used in characterising the PV panels were the short circuit current, I_{sc} , open circuit voltage, V_{oc} , fill factor, FF and Efficiency, η . The fill factor, FF could combine (I_{sc}) and (V_{oc}) to determine the solar cell maximum power [123], such that:

$$FF = \frac{\text{Maximum power from the solar cell}}{\text{Product of } (I_{sc}) \text{ and } (V_{oc})} \quad (6.15)$$

$$FF = \frac{\text{Product of voltage and current at maximum power conditions}}{\text{Product of Open circuit voltage } V_{oc} \text{ and Short circuit current } I_{sc}} = \frac{V_{mp} I_{mp}}{V_{oc} I_{sc}} \quad (6.16)$$

This is the geographical rectangular area under the IV, PV graphs and a good PV cell must have a FF value greater than 0.7, such that $FF > 0.7$.

Similarly, the maximum theoretical FF of a solar cell can be obtained at the turning point. Hence, the power can be differentiated with respect to the voltage to obtaining FF. Equating the turning point to Zero gives a maximum point.

This implies that:

$$\frac{d(IV)}{dV} = 0, \text{ not bothering with the calculation steps involved, the eventual equation yields:}$$

$$FF = \frac{V_{oc} - \ln(V_{oc} + 0.72)}{V_{oc} + 1} \quad (6.17)$$

Equation (6.17) indicates that a higher voltage will yield correspondingly higher FF value. A good PV cell must have $FF > 0.7$. As the cell temperature increases, the fill factor, FF, decreases, the open circuit voltage, V_{oc} decreases linearly and short circuit current, I_{sc} increases slightly and the PV cell then becomes less efficient. These conditions need to be avoided in good PV cell modelling.

The performance of solar cells from one to the other is rated by the cell's efficiency. Efficiency is the PV cell's effective attribute of the ratio of the solar cell energy output to the solar irradiation falling upon it. The spectrum and intensity of the incident light (sun) and the solar cell temperature, all affect the cell's efficiency, and hence the operating condition of the solar cell must be carefully controlled when

determining its efficiency in order to enable performance comparison of one device to the other. For control purposes, all terrestrial solar cells are measured under standard conditions of Air mass (AM) of 1.5 and temperature of 25 °C or 298 K. The case is different for space of satellite applications.

According to [28, 66], the module efficiency is the ratio of the maximum power to the irradiation and it is defined in Equation (6.18) as:

$$\eta = \text{Efficiency} = \frac{\text{Maximum output power}}{\text{Incident light power}} = \frac{P_m}{EA_c} \quad (6.18)$$

The output power of the cell/module, P is given as:

$$P = V * I$$

$$\text{From equation, } P_{max} = V_{oc} I_{sc} FF \quad (6.19)$$

The efficiency is defined as

$$\eta = \frac{V_{oc} I_{sc} FF}{P_{in}} \quad (6.20)$$

where the parameters are as earlier defined and

$$P_{in} = \text{input power for efficiency calculation} = 1 \text{ KW/m}^2 \text{ or } 1000\text{mW/cm}^2$$

6.5 Simulation and results

SunPower X21-Series-345 PV panel and Yingli Mono 260 Series PV panel were simulated for various operating conditions and PV parameters as presented in Table 6-2 to Table 6-13 and in Figure 6-2 to Figures 6-12(a,b,c and d). The results for each case of the panel was analysed and matched with the manufacturers' specifications. The derived and calculated data from the simulated models for each of the panels respectively at STC are presented on Table 6-12 to Table 6-14 for the SunPower X21-Series-345 PV panel and Table 6-15 to Table 6-17 for Yingli Mono 260 Series PV panel. The data on these referenced Tables were compared in Table 6-18 and used to evaluate the simulation results. The results under various conditions helped in the choice of the panel chosen for the 3D modelling and simulation of the most current, accurate, efficient and the best presently available and the validated electrical parameters were used as the input for the simulation of the 3D modelling of the panel.

Table 6-2: 1D Simulation of SunPower X21-series-345 solar panel for series resistance

Variation in series resistance (R_s)	V_{mp} (V)	P_m (W)	I_{mp} (A)	module efficiency (%)	fill factor (FF)
0.20	58.2686	335.8250	5.7634	20.59	0.77
0.40	57.6365	328.5790	5.7009	20.15	0.75
0.60	54.7947	321.7241	5.8714	19.73	0.74
0.80	56.3019	313.5383	5.5689	19.23	0.72
1.00	55.6134	305.9164	5.5008	18.76	0.70

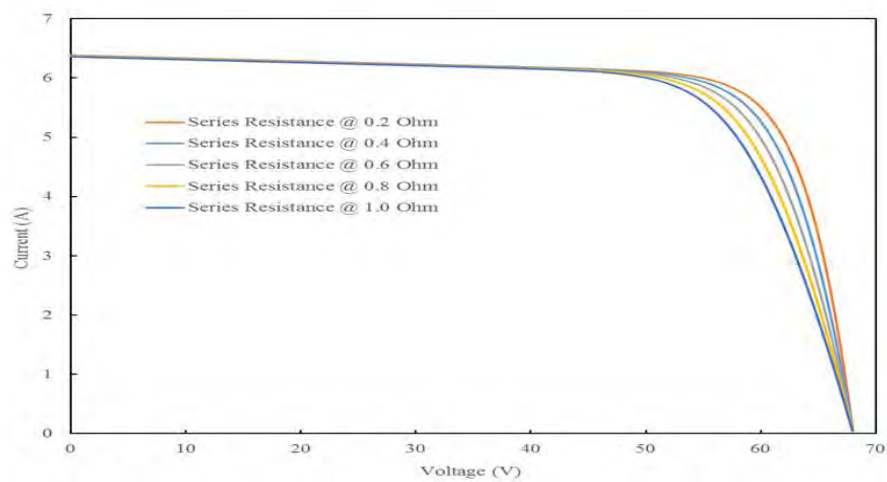


Figure 6-2(a): I-V Characteristics for series resistance (R_s) variation for SunPower PV panel

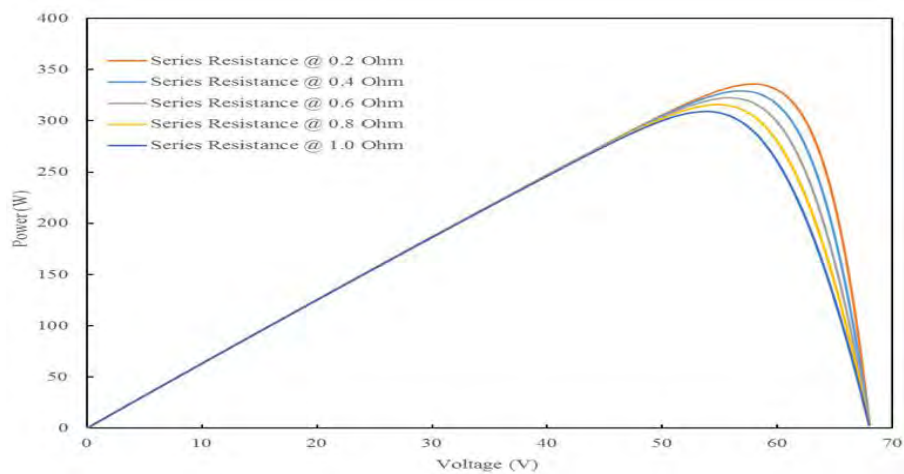


Figure 6-2(b): P-V Characteristics for series resistance (R_s) variation for SunPower PV panel

From the graphs on varying series resistance on SunPower X21-series-345 solar panel, it is seen that for both the I-V and P-V graphs, there is little or no effect of varying series resistance on the different curves but as the voltage increases to about 45V, the effect on the curves become significant and the curves are separated out.

Table 6-3: 1D Simulation of Yingli Mono PV 260 Series 60 solar panel for series resistance

Varying series resistance (R_s)	V_{mp} (V)	P_m (W)	I_{mp} (A)	module efficiency (%)	fill factor (FF)
0.20	31.8313	260.5710	8.1860	15.95	0.76
0.40	30.9262	245.9632	7.9532	15.06	0.72
0.60	29.9775	231.1053	7.7093	14.15	0.67
0.80	26.0411	217.9951	8.3712	13.35	0.63
1.00	25.3874	207.1872	8.1610	12.68	0.60

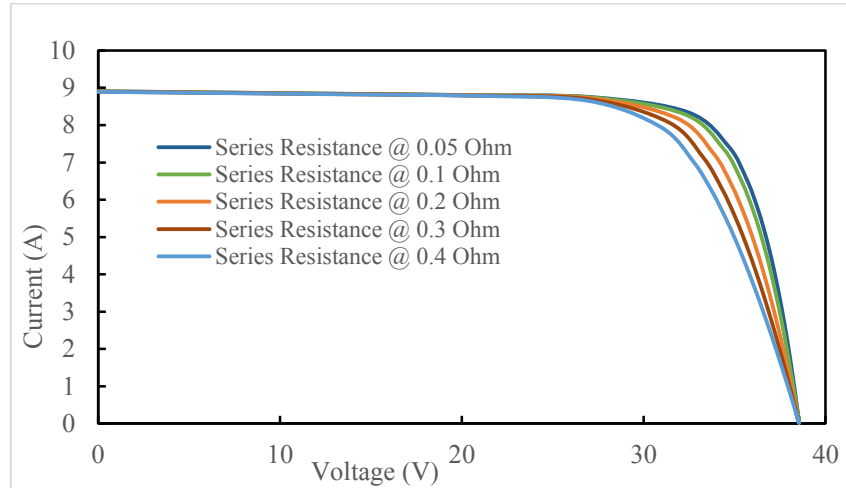


Figure 6-3(a): I-V Characteristics for series resistance (R_s) variation for Yingli PV panel

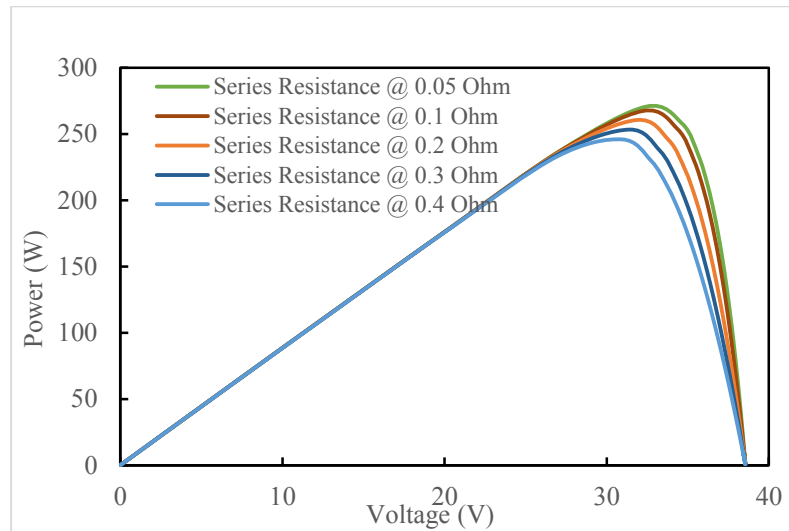


Figure 6-3(b): P-V Characteristics for series resistance (R_s) variation for Yingli PV panel

From the graphs on varying series resistance on Yingli Mono PV 260 Series 60 solar panel, it can be observed that for both the I-V and P-V graphs, there is little or no effect of varying series resistance on the different curves but as the voltage increases to about 25V, the effect on the curves become significant and the curves are separated out.

Table 6-4: 1D simulation of SunPower X21-Series-345 solar panel for shunt resistance

Variation in shunt resistance (Rsh)	V_{mp} (V)	P_m (W)	I_{mp} (A)	module efficiency (%)	fill factor (FF)
200	58.2686	335.8250	5.7634	20.59	0.77
400	58.9183	343.3559	5.8277	21.06	0.79
600	56.8106	345.8322	6.0875	21.21	0.79
800	56.9441	347.4596	6.1018	21.31	0.80
1000	57.0233	348.4271	6.1103	21.37	0.80

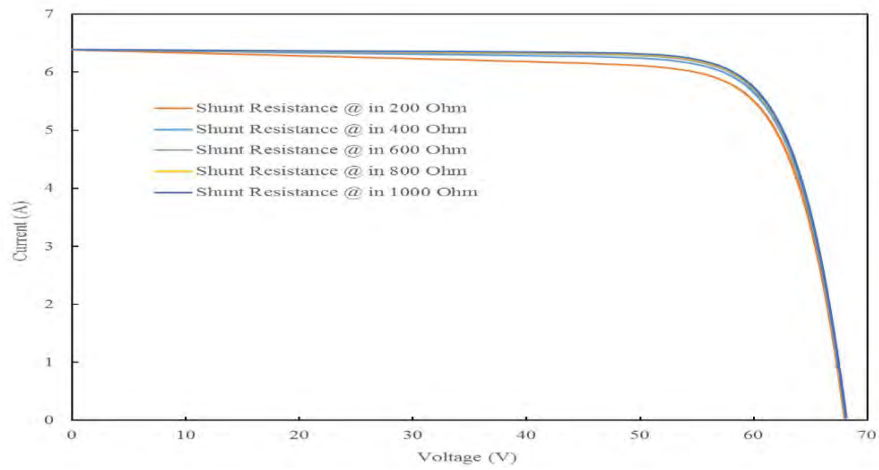


Figure 6-4(a): I-V Characteristics for shunt resistance (Rsh) variation for SunPower panel

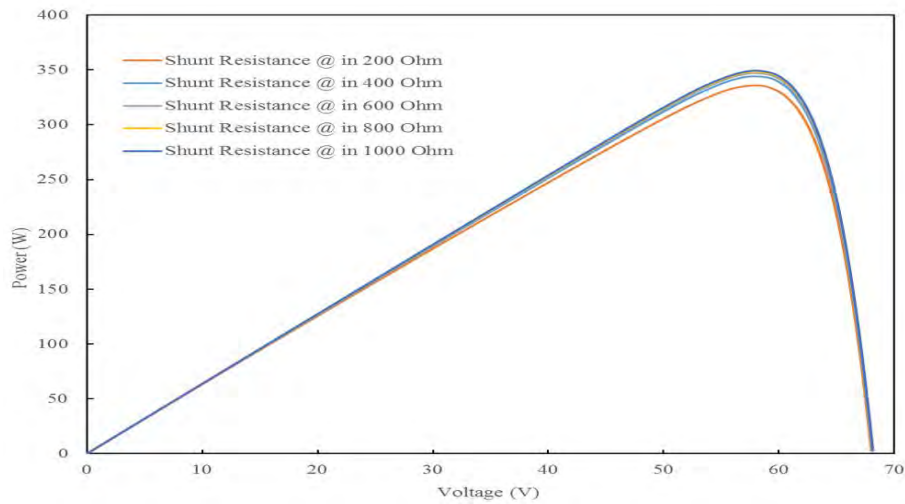


Figure 6-4(b): P-V Characteristics for shunt resistance (Rsh) variation for SunPower panel

From the above two graphs, it can be observed that the curves on SunPower X21-Series-345 solar panel are as close as possible to each other, indicating that the influence of variation in shunt resistance is almost insignificant. However, the effect is experienced slightly at voltage range of $40V \leq V \leq 65V$. This is an improvement over what is obtainable in Yingli Mono PV 260 Series c-60 solar panel.

Table 6-5: 1D Simulation of Yingli Mono PV 260 Series c-60 solar panel for shunt resistance

Variation in shunt resistance (Rsh)	V_{mp} (V)	P_m (W)	I_{mp} (A)	module efficiency (%)	fill factor (FF)
200	31.8313	260.5710	8.1860	15.95	0.76
400	31.9733	262.9012	8.2225	16.09	0.76
600	32.0195	263.6616	8.2344	16.14	0.77
800	32.0424	264.0387	8.2403	16.16	0.77
1000	32.0561	264.2640	8.2438	16.18	0.77

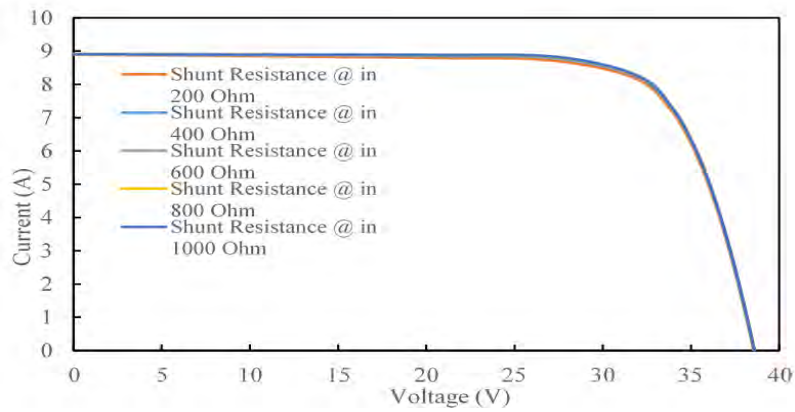


Figure 6-5(a): I-V Characteristics for shunt resistance (Rsh) variation for Yingli panel

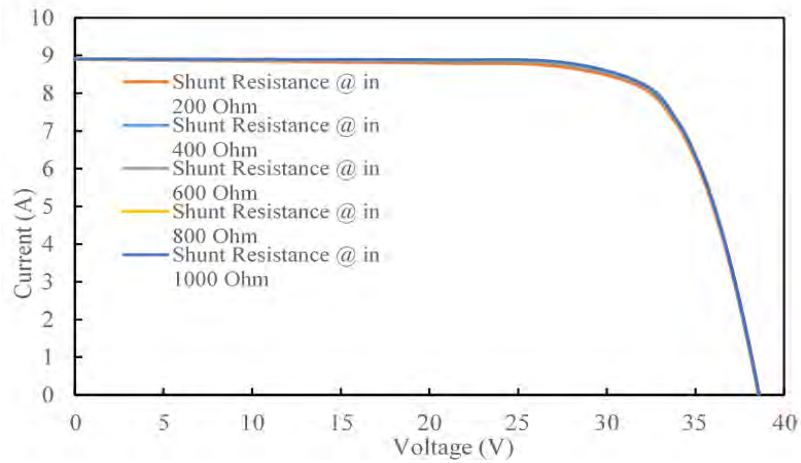


Figure 6-5(b): I-V Characteristics for shunt resistance (Rsh) variation for Yingli panel

From the above two graphs, it can be observed that the curves on Yingli PV solar panel are as close as possible to each other, indicating that the influence of variation in shunt resistance is almost insignificant. However, the varying shunt resistance effect is less significant here. Hence, the curves stayed more closely together than what was observed with the SunPower X21-Series-345 solar panel.

Table 6-6: 1D Simulation of the SunPower X21-Series-345 solar panel for Ideality factor

Variation in Ideality factor (n)	V_{mp} (V)	P_m (W)	I_{mp} (A)	module efficiency (%)	fill factor (FF)
1.20	56.6707	335.8250	5.6054	20.59	0.73
1.35	57.7169	329.4961	5.7088	20.21	0.76
1.50	57.1845	323.4460	5.6562	19.83	0.74
1.65	56.6707	317.6597	5.6054	19.48	0.73
1.80	56.1744	312.1196	5.5563	19.14	0.72

The input power for efficiency calculations is 1 kW/m^2

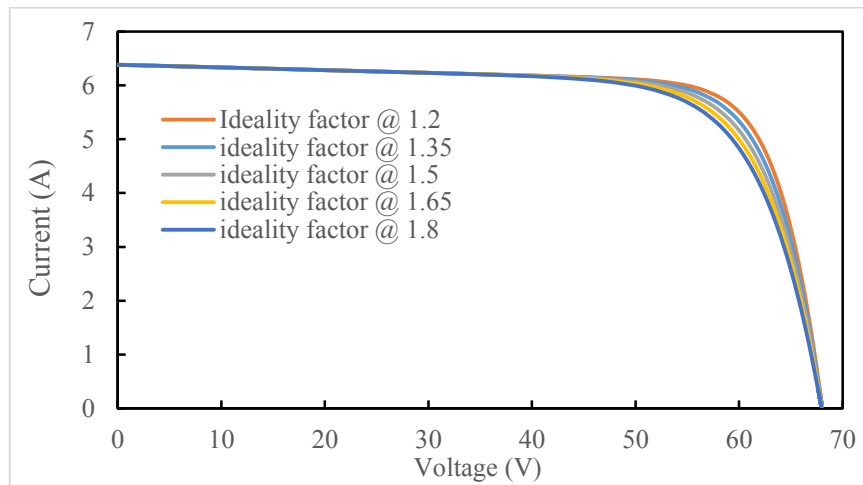


Figure 6-6(a): I-V Characteristics for ideality (N) variation for SunPower PV panel

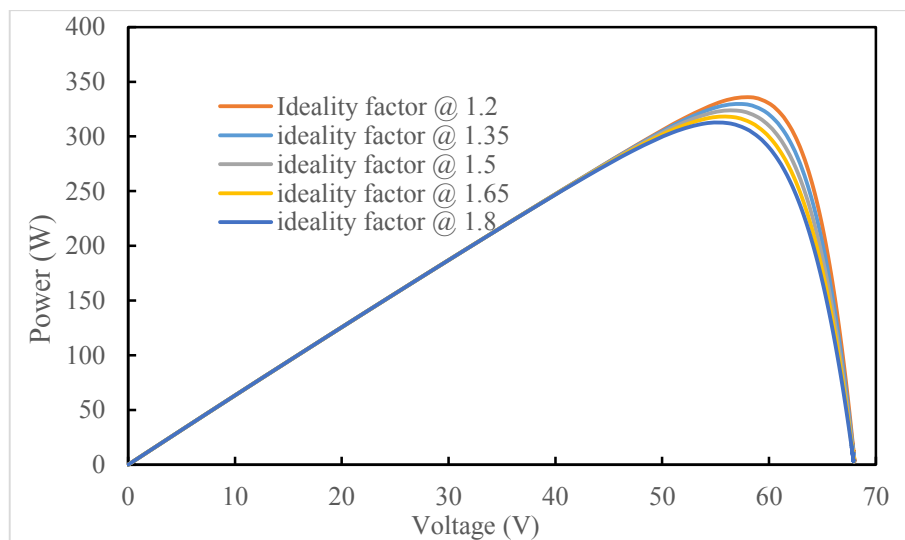


Figure 6-6(b): P-V Characteristics for ideality (N) variation for SunPower PV panel

Table 6-7: 1D Simulation of the Yingli Mono PV 260 Series 60 solar panel for Ideality factor

Variation in Ideality factor (n)	V_{mp} (V)	P_m (W)	I_{mp} (A)	module efficiency (%)	fill factor (FF)
1.20	31.8313	260.5710	8.1860	15.95	0.76
1.35	31.5047	255.2521	8.1020	15.63	0.74
1.50	31.1913	250.1981	8.0214	15.32	0.73
1.65	30.8899	245.3868	7.9439	15.02	0.71
1.80	30.5997	240.7974	7.8693	14.74	0.70

The input power for efficiency calculations is 1 kW/m²

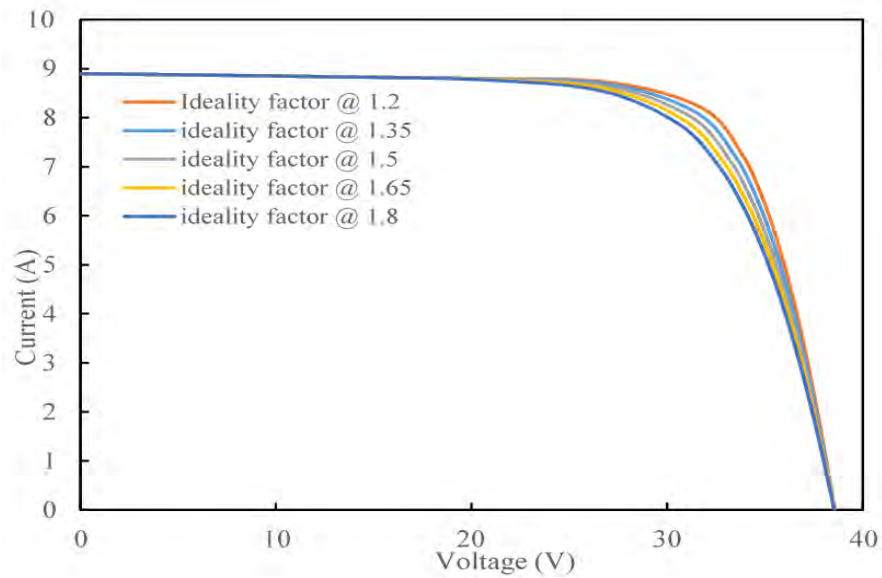


Figure 6-7(a): I-V Characteristics for ideality (N) variation for Yingli PV panel

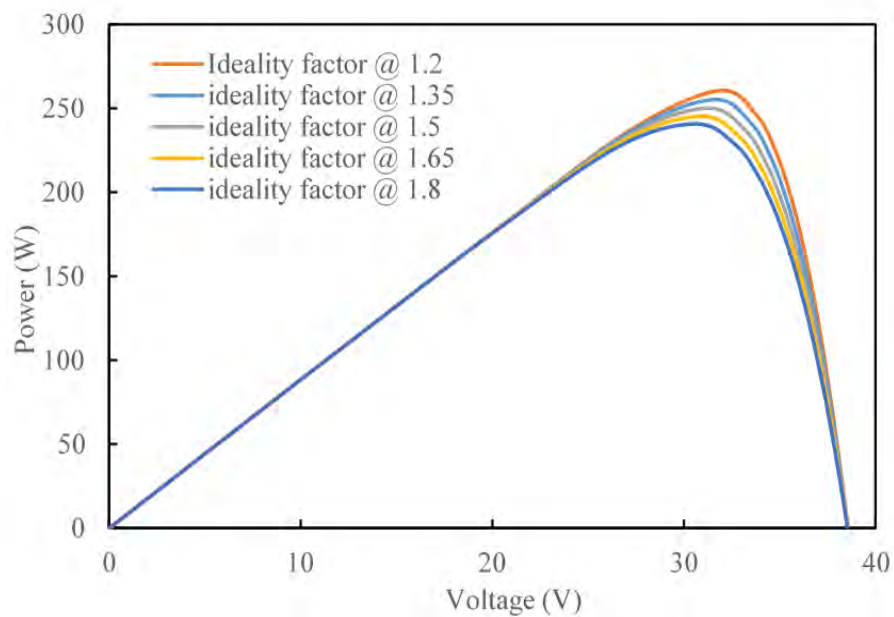


Figure 6-7(b): P-V Characteristics for ideality (N) variation for Yingli PV panel

Table 6-8: 1D Simulation of the SunPower X21-Series-345 solar panel for Temperature variation

Variation in PV cell temperature (Tc)	V _{mp} (V)	P _m (W)	I _{mp} (A)	module efficiency (%)	fill factor (FF)
298.15	58.2686	335.8250	5.7634	20.59	0.77
308.18	58.2762	335.9132	5.7642	20.60	0.77
318.15	58.2793	335.9486	5.7645	20.60	0.77
328.15	58.2786	335.9411	5.7644	20.60	0.77
338.15	56.0102	336.1564	6.0017	20.61	0.77
348.15	56.0683	336.8539	6.0079	20.66	0.77
358.15	56.1189	337.4626	6.0133	20.69	0.77

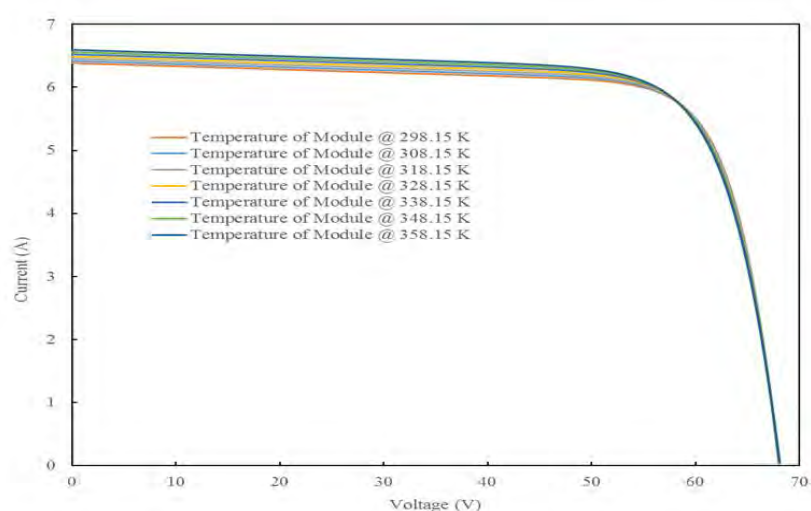


Figure 6-8(a): I-V Characteristics for temperature variation for SunPower PV panel

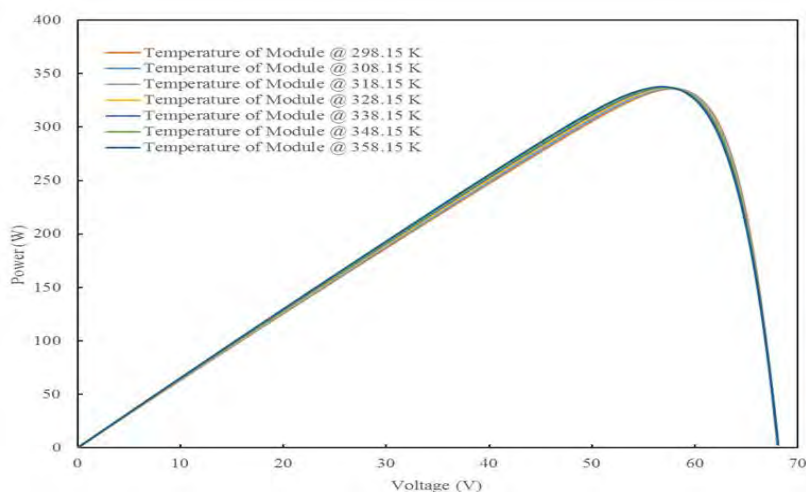


Figure 6-8(b): P-V Characteristics for temperature variation for SunPower PV panel

From the above I-V and P-V graphs, it can be observed that the curves on the SunPower PV panel are as close as possible to each other, indicating that the influence of Temperature variation has almost no effect on them. Hence, the varying Temperature effect is of little or no significance here.

Hence, the curves stayed more closely together than what was observed with the Yingli Mono PV 260 Series c-60 solar panel.

Table 6-9: 1D Simulation of Yingli Mono PV 260 Series c-60 solar panel for Temperature variation

Variation in PV cell temperature (Tc)	V _{mp} (V)	P _m (W)	I _{mp} (A)	module efficiency (%)	fill factor (FF)
298.15	31.8313	260.5710	8.1860	15.95	0.76
308.18	31.6493	257.5999	8.1392	15.77	0.75
318.15	31.4622	254.5635	8.0911	15.58	0.74
328.15	31.2703	251.4678	8.0417	15.39	0.73
338.15	31.0739	248.3187	7.9912	15.20	0.72
348.15	30.8732	245.1211	7.9396	15.01	0.71
358.15	30.6684	241.8798	7.8869	14.81	0.70

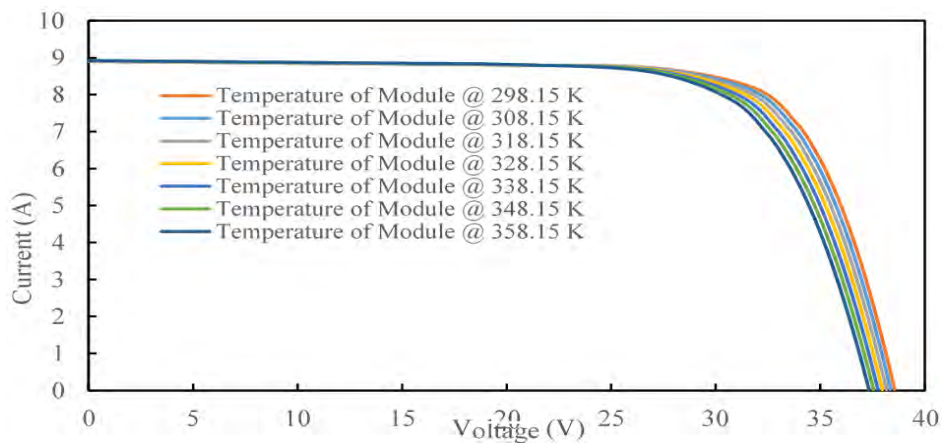


Figure 6-9(a): I-V Characteristics for temperature variation for the Yingli PV panel

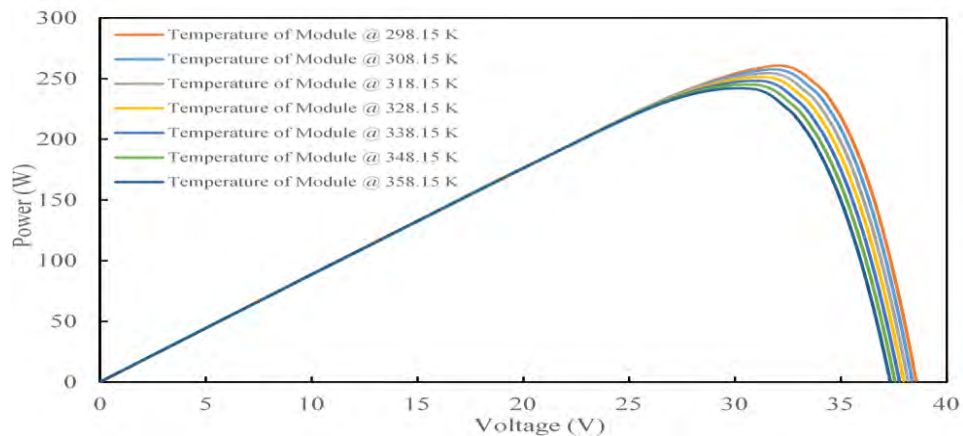


Figure 6-9(b): P-V Characteristics for temperature variation for the Yingli PV panel

From the above I-V and P-V graphs, it can be observed that for the Yingli PV panels, the curves are as close as possible to each other in the lower voltage range, indicating that the influence of Temperature variation has almost no effect on them at low voltage. However, at higher voltage of about

28V upwards, the effect of temperature is predominant as reflected in the curves as the curves separated out.

Table 6-10: 1D Simulation of the SunPower X21-Series-345 solar panel for irradiation variation

Variation in Irradiation (G)	V_{mp} (V)	P_m (W)	I_{mp} (A)	module efficiency (%)	fill factor (FF)
600	57.2492	191.5596	3.3461	19.58	0.44
700	56.4160	227.3631	4.0301	19.92	0.52
800	57.2769	263.6493	4.6031	20.21	0.60
900	57.1085	299.5448	5.2452	20.41	0.69
1000	58.2686	335.8250	5.7634	20.59	0.77

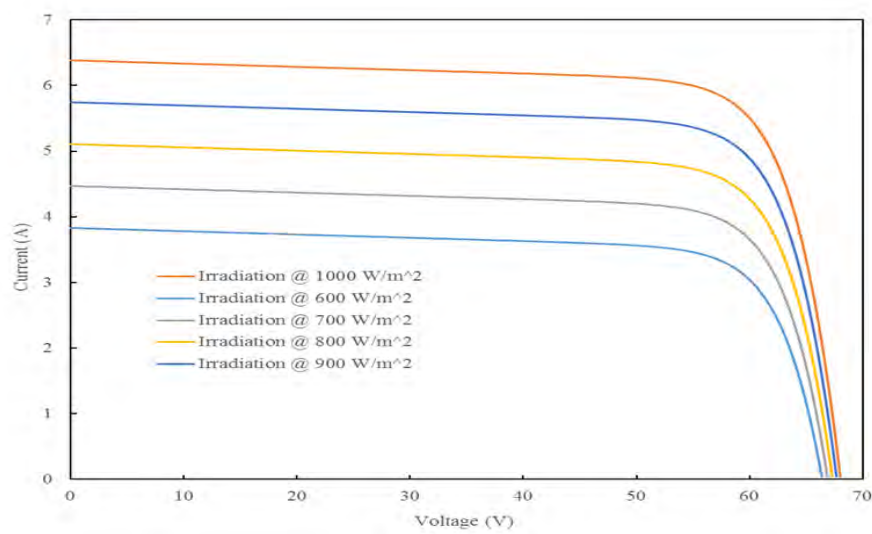


Figure 6-10(a): I-V Characteristics for irradiation (G) variation for the SunPower PV panel

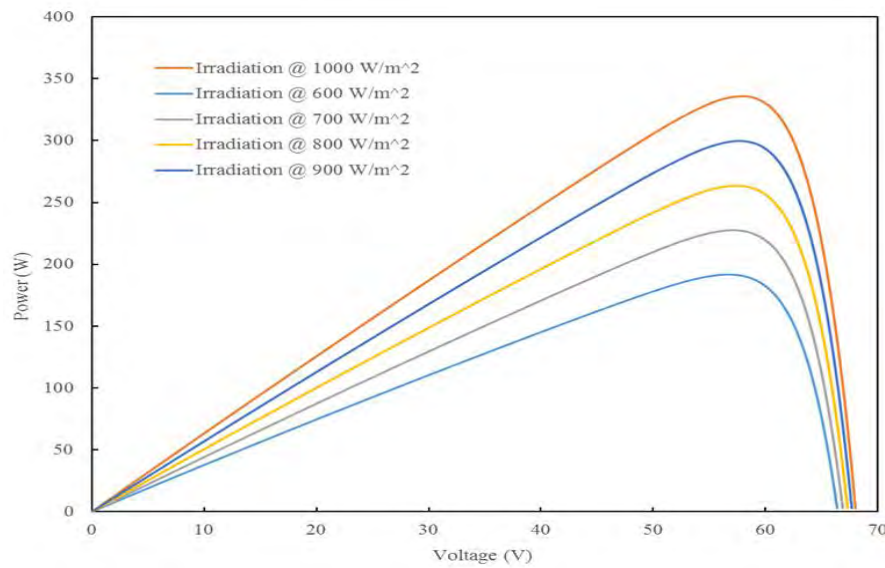


Figure 6-10(b): P-V Characteristics for irradiation (G) variation for the SunPower PV panel

Table 6-11: 1D Simulation of the Yingli Mono PV 260 Series 60 solar panel for irradiation variation

Variation in Irradiation (G)	V_{mp} (V)	P_m (W)	I_{mp} (A)	module efficiency (%)	fill factor (FF)
600	30.9891	154.3529	4.9809	15.75	0.45
700	31.3113	180.0909	5.7516	15.75	0.52
800	31.0566	206.7016	6.6556	15.82	0.60
900	32.7847	230.3455	7.0260	15.67	0.67
1000	31.8313	260.5710	8.1860	15.95	0.76

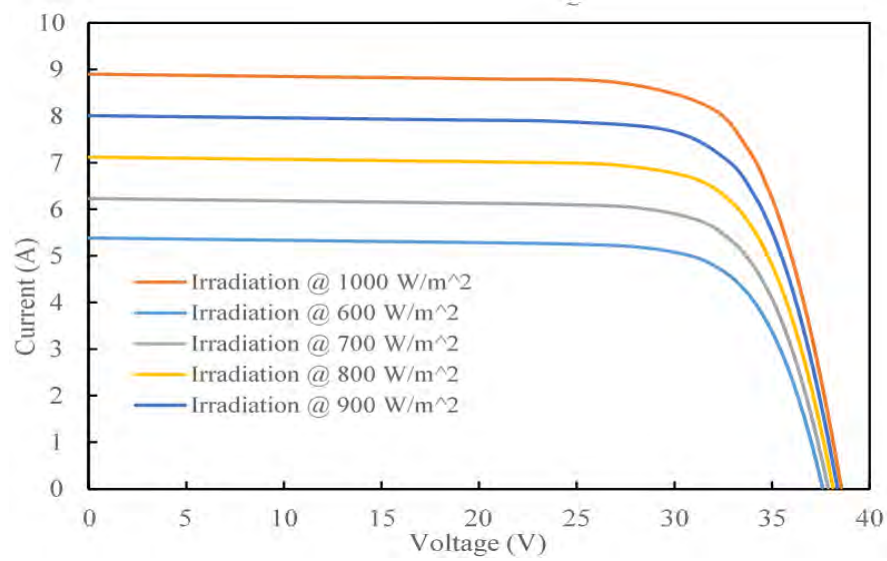


Figure 6-11(a): I-V Characteristics for irradiation (G) variation for the Yingli PV panel

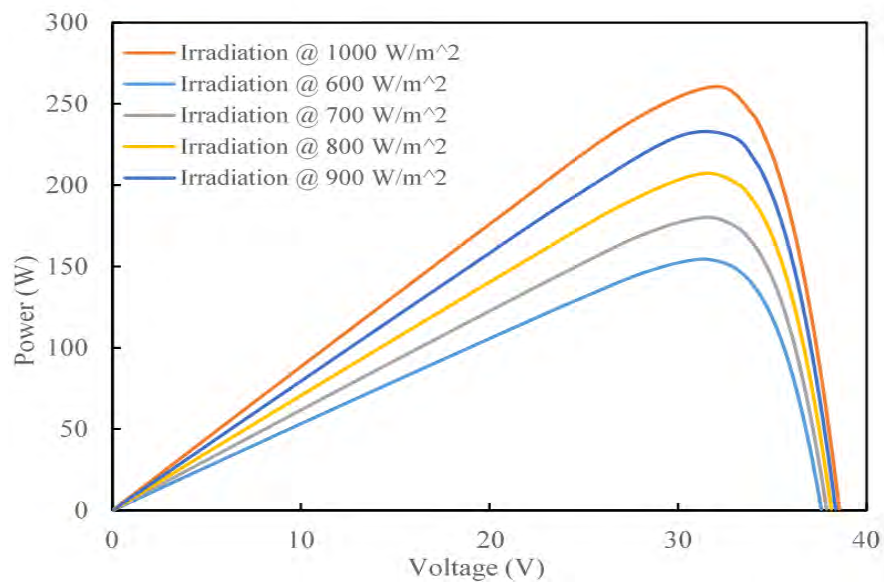


Figure 6-11(b): P-V Characteristics for irradiation (G) variation for the Yingli PV panel

Based on the 1-D simulation results generated for the Sunpower_X21-Series-345 W Solar Panel, the optimum operating parameters derived are as stated in Table 6-12.

Table 6-12: Derived optimum operating parameters for the SunPower X21-Series panel at STC

Various parameters	Value	Unit
Solar Irradiance (G)	1000	W/m ²
Cell-operating temperature	25	°C
Series resistance (R _s)	0.2	ohm
Shunt resistance (R _{sh})	1000	ohm
Ideality factor (n)	1.35	
Air Mass (AM)	1.5	
Band-gap energy of the cell (E _g)	1.17	eV
Diode ideality factor	1.35	
Number of cells in the PV panel	96	
Area of cell (A)	1.63	m ²
Open-Circuit Voltage (V _{oc})	68.2	V
Short -Circuit Current (I _{sc})	6.39	A
Current-Temp, Coefficient, (K _i)	3.5	mA/°C
Voltage-Temp, Coefficient, (K _v)	-167.4	mV/°C

Table 6-13: Validated electrical parameters for the SunPower X21-Series-345 solar panel at STC

Parameters	Calculated Values	Rated value in Datasheet	Unit	% Deviation
Nominal Power (P _{nom})	342.3	345.0	W	-0.8
Peak Voltage (V _{mpp})	56.5	57.3	V	-1.4
Peak Current (I _{mpp})	6.06	6.02	A	0.6
Average Panel Efficiency	20.99	21.5	%	-2.4

Table 6-14: The 345 W Sunpower_X21-Series- solar panel at STC

PV cell temperature @ STC (K)	V _{mp} (V)	P _m (W)	I _{mp} (A)	module efficiency (%)	fill factor (FF)
298.15	56.5208	342.3131	6.0564	20.99	0.79

Based on the 1-D simulation results generated for the Yingli Mono PV 260 Series 60 c-Si Solar Panel, the optimum operating parameters derived are as stated in Table 6-15.

Table 6-15: Derived optimum PV operating parameters for the Yingli Mono PV 260 Series 60 c-Si solar panel at STC

Other parameters	value	unit
Solar Irradiance (G)	1000	W/m ²
Cell-operating temperature	25	°C
Series resistance (R _s)	0.2	ohm
Shunt resistance (R _{sh})	200	ohm
ideality factor (n)	1.2	ohm
Air Mass (AM)	1.5	
Band-gap energy of the cell (E _g)	1.17	eV
number of cells in a PV panel	60	
Area of module (A)	1.63	m ²
Open-Circuit Voltage (V _{oc})	38.6	V
Open-Circuit Current (I _{sc})	8.91	A
Current Temp, Coeff, (I _{sc})	0.04	%/ K
Cell dimension in size	156*156	mm

Table 6-16: Validated electrical parameters for the Yingli Mono PV 260 Series 60 c-Si solar panel

Parameters	Calculated Values	Rated value in Datasheet	Unit	% Deviation
Power Output at STC	260.6	260.0	W	0.2
Peak Voltage (V _{mpp})	31.8	30.8	V	3.3
Peak Current (I _{mpp})	8.19	8.46	A	-3.2
Module Efficiency	15.95	15.9	%	0.3

Table 6-17: The Yingli 260 Series 60 c-Si, Monocrystalline solar panel at STC

PV cell temperature @ STC (K)	V _{mp} (V)	P _m (W)	I _{mp} (A)	Module efficiency (%)	fill factor (FF)
298.15	31.8313	260.5710	8.1860	15.95	0.76

The above parameters in Table 6-15 and Table 6-16 were used as material specification for the 3D solar panel modelling and simulation.

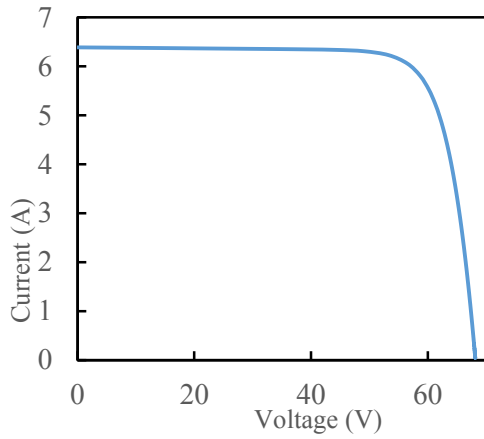


Figure 6-12(a): I-V characteristic for modelled SunPower solar panel @ STC

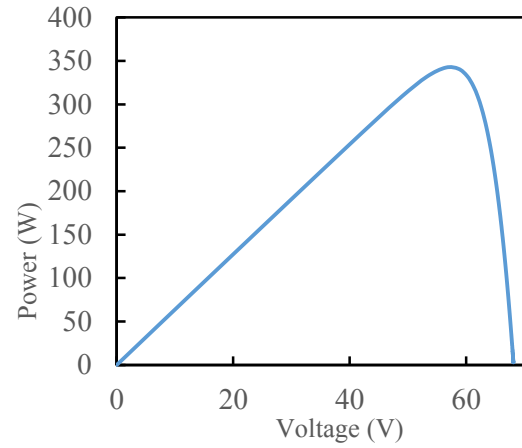


Figure 6-12(b): P-V characteristic for modelled SunPower solar panel @ STC

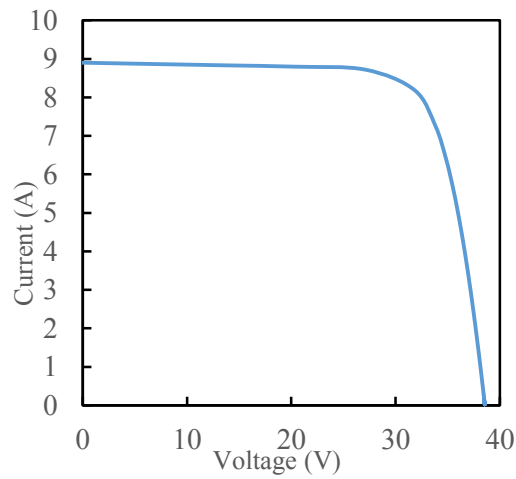


Figure 6-12(c): I-V characteristic for modelled Yingli solar panel @ STC

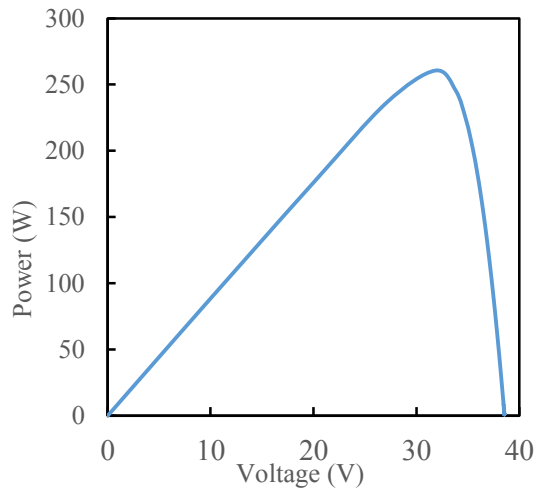


Figure 6-12(d): I-V characteristic for modelled Yingli solar panel @ STC

In 6-13 and Table 6-16 are the calculated/validated parameters under Standard Test Conditions (STC) of 1000 W/m^2 irradiance, AM 1.5, 25°C for the SunPower X21-Series-345 PV panel and the Yingli Mono 260 Series PV panel respectively. These two Tables are brought together to form Table 6-18 for easy comparison and analysis. From the analysis, comparatively, from Table 6-18, the Sunpower 345W X21-Series PV panel has higher values of V_{mp} , P_m , efficiency and fill factor than those obtained for the Yingli Mono 260 Series PV panel, except for the value of I_{mp} which is higher than that obtained for the Sunpower 345W X21-Series PV panel. However, this was not the case because the Sunpower 345W X21-Series PV panel prototype found in solidworks site was encapsulated as a domain (an entity), thus making it difficult for meshing the different segments of the panel, while that of the Sunpower 345W X21-Series PV panel has independent segments and hence easier to mesh. Hence, the preference of the Yingli Mono 260 Series PV panel over the Sunpower 345W X21-Series PV panel.

Table 6-18: Compared calculated/validated values for the SunPower and the Yingli PV panels

Sunpower 345W X21-Series PV	PV cell temperature @ STC (K)	V_{mp} (V)	P_m (W)	I_{mp} (A)	module efficiency (%)	fill factor (FF)
	298.15	56.5208	342.3131	6.0564	20.99	0.79
Yingli Mono 260 Series 60 Panel	PV cell temperature @ STC (K)	V_{mp} (V)	P_m (W)	I_{mp} (A)	Module efficiency (%)	fill factor (FF)
	298.15	31.8313	260.5710	8.1860	15.95	0.76

In Figures 6-12(a and b) and Figures 6-12(c and d), the I-V and P-V characteristics Graphs were generated for the SunPower and Yingli solar panels respectively at Standard Test Conditions (STC). The I-V graphs between the two panels showed that the current generated for the SunPower PV panel was maintained at about 6.5 Amperes constant, for maximum voltage of 50 Volts while that generated by the Yingli PV panel was constant at 9 Ampere for maximum voltage of 30 Volts and then both started to decline beyond this voltages and eventually came to zero at a voltage beyond 68 Volts and 38 Volts respectively. Likewise, the P-V graphs showed continuous linear plot with positive gradient for the case of the SunPower panel. The P-V graph for the SunPower panel initially increased linearly with greater positive gradient to a voltage value of about 58 Volts and maximum output power of 350 Watt, thereafter abruptly dropped to zero value and consequently experienced a drop in output power; whereas that of the Yingli panel experienced continuous increase to a voltage value of about 33 Volts and maximum output power of 260 Watt.

Although the electrical values obtained for the SunPower PV Panel were more favourable than the electrical parameters for the Yingli PV panel on technical grounds, the electrical specification for the Yingli PV panel were, however, adopted and used as the input parameters for the 3-D PV modelling, based on the explanations given earlier in Chapter 6.

6.6 Conclusion

The two PV panels were simulated in 1D, generating the graphs as indicated in Figure 6-2 to Figures 6-12(a, b, c and d). The cell parameters, G_1 , T_{op} , R_s , R_p and N which to a large extent affect the PV panel performance were determined the V_{mp} , studied intensively.

These ideal conditions were also specified in the data sheets for the SunPower X21-Series-345 PV panel and the Yingli Mono 260 Series PV panel. Every manufacturer tends to manufacture their systems as close as possible to the ideal conditions. Hence, the behaviour of PV panels with deviation from the ideal situation and the effects of such changes were studied, analysed as reflected in this work. The results obtained in this situation were used as defined parameters for the design, modelling and simulation of the 3-D PV system in order to carry out the environmental parameters (temperature distribution, efficiency and power output) and to predict its optimum operating performance.

CHAPTER SEVEN

THREE-DIMENSIONAL MODELLING AND SIMULATION OF PHOTOVOLTAIC ENERGY SYSTEM

7.1 Introduction

This chapter consists of two parts. The first part presents 1D modelling of the electrical part of the PV module which was fully implemented in Chapter 6 with a generalized photovoltaic simulation model using MATLAB/GUI interface.

This chapter contains the second part of the modelling which was the development of a thermal model to simulate the performance prediction of the PV module. The purpose of the thermal model is to determine the 3D temperature distribution in the PV panel. This temperature distribution is affected by various factors such as the type of materials used for the PV module, the type of PV cell, the panel configuration, the electrical load connected to the PV system and the prevailing environmental conditions [44]. Thermal modelling of PV panels reveals the strong correlation between module temperature distribution and electrical characteristics of the PV panel [65]. Studies were performed on this developed model to evaluate its thermal performance under different environmental and operating conditions with air cooling. Two PV models, Sunpower X31-345 series panel and the Yingli 260 series panel, were studied in order to select a suitable model for PV device implementation as contained in the manufacturers' lists. See the Appendix. Their manufacturers' data sheet values were used in evaluating their I-V, P-V behavioural characteristics. The Yingli PV panel was eventually selected based on the reasons earlier stated in Chapter 6 and its validated electrical parameters and structural specifications are now being used in this Chapter as the input electrical parameters and dimensions for the 3D modelling and simulation aspect of this work. The 3D simulation was preferred for use on the PV thermal modelling because 1D simulations are usually inadequate for conventional geometry solar cells, especially at high solar intensities and for semiconductor materials that are not well formed. Although 1D models are simpler and sufficiently accurate for long term performance predictions, nevertheless, more complex 2D and 3D models are required for better and more accurate PV performance prediction. At high intensities, many high efficiency cell designs require 2D simulations or even 3D simulations for correct interpretation of 2D/3D finite element analysis of temperature, efficiency, and power, thermal properties of compound and silicon semiconductor devices and for more accurate PV performance prediction. Only such 2D and 3D models can effectively handle such complex flow patterns and design optimization tasks [13, 50]. Contrary to previous approaches that have been used for solar PV performance prediction, this thesis has utilized a 3D approach in predicting the solar performances as they relate to its efficiency and generated output power.

The 3D simulations involve system ability to handle complex problems involving the use of increasingly large solution space and a correspondingly efficient system of adequate ram, speed and capacity. In order to achieve accurate 3D results, this 3DPV model was developed in COMSOL Multiphysics to study and predict the performances of the Yingli 260 series PV system. The materials and the Physics were determined, selected and defined by using COMSOL Multiphysics which allowed for the full coupling of the different physics interfaces. The physical boundaries were also defined for each simulation in accordance with real values and conditions.

7.2 The need for PV modules design, modelling and optimization

It is necessary that solar cells, modules or systems undergo modelling and simulation. This is required in order to study the effects of weather variation on system performance, to be able to optimize design performance, to and meet target reliability and to achieve improved PV efficiency. These are also necessary in order to address some of the challenges facing the PV industry. Some of these challenges include low efficiency and generated output power due to the losses through radiation, convection, resistive drops and poor weather conditions experienced by a typical PV system. Furthermore, modelling and simulation of solar cells and modules have been found to make possible the prediction of manufacturing yields, thus resulting in lowering production costs [9, 13, 54].

The performance prediction of the PV panel was carried out in the radiation model, the thermal model and the electrical model. The radiation & thermal models were used for calculating the solar radiation absorbed and the temperature distributions in the PV cells. The electrical models were used to determine the electrical output of PV panels under any given operating condition. These electrical values determined were used as the electrical input parameters for the 3D modelling. Most of the available literature and even the items referenced in this thesis dealt more with 1D and 2D analytical models for PV panels with temperature variation only. The 3D modelling is able to generate the thermal behaviour of the PV panel and it enables the calculation of the three dimensional temperature distribution in the PV panel. Modelling of PV panels in 3D is a relatively new technology compared with 1D and 2D modelling therefore much work has not been carried out on it.

7.3 Three-dimensional (3D) modelling of the PV panel system

The 3D model of the solar panel was developed in COMSOL Multiphysics to simulate the 3D temperature distribution in the PV panel. The required geometry for each simulation was developed, the material properties were defined and selected based on values from the COMSOL materials library and literature. The materials selected for modelling and the prevailing environmental conditions, to a large extent, affect the temperature distribution in the PV module [13]. Depicted in Figure (7-1) is an hypothetical PV panel used to illustrate the various modes of energy transfer in the PV panel which involve energy transfer through radiation losses (incoming and outgoing) and convection. The panel energy increases by absorbing incoming solar radiation while on the other hand, there was energy loss from it to the environment by convection and radiation. The operating current–voltage (I–V) point and the electrical power output of the PV panel were determined by the amount of electrical energy that is taken out of the system and is found to be a function of the load characteristics. This has been earlier determined in Chapter six where the electrical parameters were determined at a reference condition which was translated to the operating condition or input parameters for the 3D modelling of the PV panel. These input parameters are as presented in Table 7-1.

Table 7-1: Electrical parameters from 1D modelling of the Yingli 260 series PV panel as input parameters for the 3D modelling of the same PV panel

Name	Expression	Value	Description
W_PVCell	156[mm]	0.156 m	PV cell width
W_Panel	5*W_PVCell	0.78 m	Width of eight PV cells
H_PV	46[mm]	0.046 m	PV panel thickness
T_Amb	298.15[K]	298.15 K	Ambient air temperature
T_Init	298.15[K]	298.15 K	Initial cell temperature
T_Room	298.15[K]	298.15 K	Room temperature
Emissivity	0.6	0.6	Emissivity of Silicon
HX_Silicon	10.52 [W/(m ² *K)]	10.52 W/(m ² *K)	Silicon/air heat transfer coefficient
PVEFF0	0.159	0.159	PV cell efficiency at room temperature
PVdeg	0.0045 [1/K]	0.0045 1/K	PV cell degradation with temperature
Q_Sun	1000[W/m ²]	1000 W/m ²	Sun incident radiation
A	1.11[m ²]	1.11 m ²	Area of PV panel
P_in	Q_Sun*A	1110 W	Power in
V_mpp	31.83[V]	31.83 V	Max output voltage at max. power point
I_mpp	8.186[A]	8.186 A	Max output current at max. power point
V_pv	0.056[m ³]	0.056 m ³	Volume of the PV panel

The temperature distribution illustrating the various modes of energy transfer in the PV panel involve energy transfer in form of heat loss. All three methods of heat transfer are involved in a practical PV panel. Heat is transferred within the PV cell structure through conduction, it is transferred to the PV panel surroundings by both free and/or forced convection and the PV experiences radiation losses (incoming and outgoing) through conduction and convection. Heat loss by conduction to the panel framework structure is neglected here due to the small area of contact points. The heat transfer in a PV is as shown below in Figure 7-1:

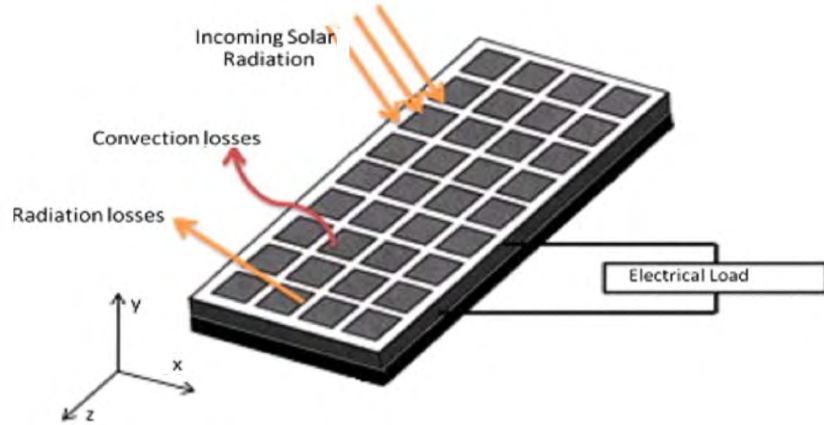


Figure 7.1: Sources of heat loss in a PV device [13]

All the three different types of heat loss sources mentioned are involved in the modelling. So the physics selected from COMSOL Multiphysics was heat transfer with surface-to-surface radiation. This involved fluid and multiple domains. The fluid could be either liquid or air. In this work, the type of fluid considered was air. The materials involved for the PV in this section of the work were silicon, encapsulant (polyester) and air and their properties were defined based on values from the COMSOL materials library and literature. Each item of material has a separate solid domain in the PV panel. The geometry needed for each simulation was developed, the material properties were defined based on their real values.

7.3.1 Details of the modelled thermal PV system

The PV panel type used in this modelling was a 40 cells Yingli panel made up of 8 by 5 cells c-Si, Monocrystalline silicon cells with material properties as described in Table 7-1. The component of the Yingli PV panel consisted of seven different materials made up of the PV cell, two runs of fingers across the silicon surface, tempered glass front cover, top and bottom encapsulation materials made up of ethylene vinyl acetate (EVA), the rear cover material made up of laminated polymer plastic and finally the frame holding it and made up of robust anodized aluminium alloy. However, the PV panel was imported from Solidworks using livelink, so most of these materials were unified as a domain thus making it difficult for their separation for modelling and meshing purposes. The PV cells and the back-cover polyester were able to be separated for modelling and meshing.

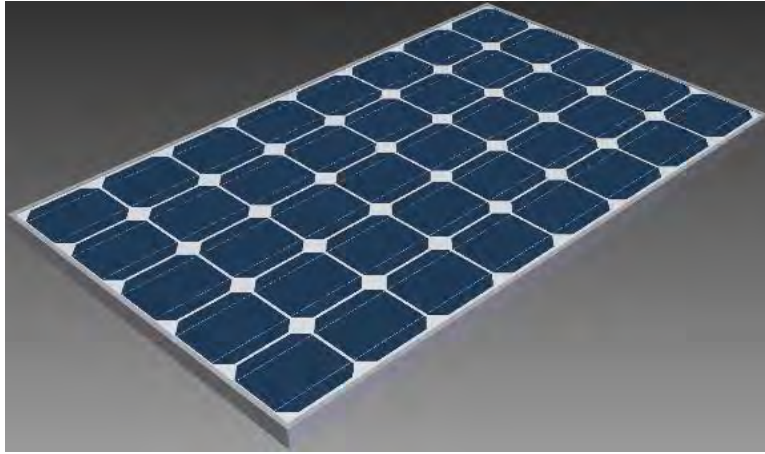


Figure 7-2: The Yingli YL260C-30b panel

The initial proposed and modelled PV panel was the Yingli Mono 260 Series PV panel with 60 cells as presented in Chapter six of this work. The Yingli panel type with 60 cells has to be exchanged for the type with 40 cells due to modelling challenges encountered. The computer used for the modelling could not successfully run the modelling due to the large size of the file. The details of the system CPU used for all the modelling and simulation works for this thesis was a Windows 10 DELL LAPTOP with Intel(R) Core(TM) i7-4712HQ CPU @ 2.30GHz, 4 cores, 16.0 GB RAM, 64-bit x 64-based processor. The 40 cells Yingli PV has the same material and electrical properties as the 60 cells counterpart, so it was a good and acceptable replacement to use. Similarly, with the 40 cells Yingli PV, running the simulation was not achieved even after having run it for days at a stretch. This problem was overcome by starting the simulation with just one PV cell. The running was successful. Then the number of cells were increased to three and finally to five cells, the results of which is presented in this work. These 5 cells represent the solar cells receiving the solar irradiation and if the modelling could be right for one cell, it would then work for as many cells as receive the solar irradiation. Therefore, the Yingli PV panel studied consisted of 5 PV cells arranged in a 1x5 rectangle as shown in Figure 7-3.

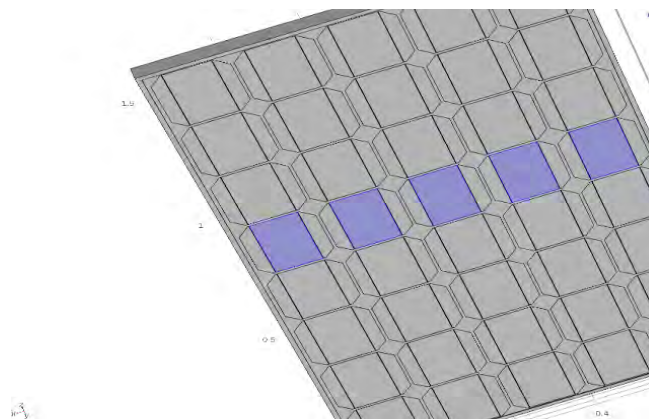


Figure 7-3: 3D modelled Yingli of 5 cells arranged in a 1x5 rectangle

The solution time for the successful modelling and simulation for the 3D PV panel was 352625 seconds, representing 4 days, 1 hour, 57 minutes, 5 seconds. The simulation details and results are contained in the Appendices.

7.3.2 Implementation of solar thermal PV panel model in COMSOL Multiphysics

The geometry needed for the simulation was developed, the material properties were defined based on values from the COMSOL materials library and literature – these are attached under the Appendices. The model consists of five different materials making up of the PV cell, with two runs of fingers across the silicon surface, tempered glass front cover, top and bottom encapsulation materials made up of EVA, the rear cover material made up of laminated polymer plastic and finally the frame holding it and made up of robust anodized aluminium alloy. The rendering for the Yingli PV panel in Figure 7-2 was obtained from Solidworks using livelink and by design, most of these materials were in one entity as a domain, making it difficult for their separation for modelling and meshing purposes. Only the PV cells and the back-cover polyester could be separated for modelling and meshing. The thermal properties for the two materials used in the modelling are as given in Table 7-1.

7.3.3 Physics and materials selection and applicable boundary conditions

The physics selection determines what parameters should be solved-for and also defines the physical boundaries of the simulation. The geometry needed for each simulation was developed with COMSOL in three space dimension. For the PV panel alone, the total number of domains developed was 122 with a total number of 927 boundaries. The identified number of edges were 2036 while the number of vertices were 1356. The physics selection defined the parameters solved for, and the physical boundaries of the simulation. The physics applied was heat transfer in solids with surface-to-surface radiation and the application of the same was activated and used for simulation in this study. If different physics interfaces were used, COMSOL allows for the full coupling of these interfaces. Furthermore, the physical boundaries were also defined for each simulation in line with their real values and conditions.

The materials involved were silicon, polyester encapsulant and air as a coolant and their properties were defined based on values from the COMSOL materials library and literature.

Table 7-2: Modelled material properties for 3D modelling and simulation

Material	Layer	Thermal Conductivity (W/m K)	Specific Heat Capacity (J/kg K)	Density (kg/m ³)
Silicon	Solar cell	130	700	2329
Polyester	Bottom cover	0.5	1250	1300
Air		$k(T[1/K])$	$C_p(T[1/K])$	$\rho(pA[1/Pa], T[1/K])$

Air was part of the domain for simulation. The following expressions defined the properties of air and determined the behaviour of the air cooling system. Heat capacity at constant pressure is temperature dependent- and it is expressed as $C_p(T[1/K])$ with the unit given as $[J/(kg \cdot K)]$. The density is pressure dependent and it is expressed as $\rho(pA[1/Pa], T[1/K])$ with the unit given as $[kg/m^3]$. The Thermal conductivity is temperature- dependent and is expressed as $k(T[1/K])$ with the unit given as $[W/(m \cdot K)]$.

7.3.4 Theory and governing equations

The materials properties and the physics were determined, defined and selected by the Author from COMSOL physics library and developed in 3D geometry as earlier described. This allowed for the full coupling of the different physics interfaces. The physical boundaries were also defined for each simulation in accordance to actual values and conditions.

The heat transfer equation with surface to surface radiation for the solid domain are expressed as:

$$\rho_i C_{p,i} \frac{\partial T_{i(x,y,z)}}{\partial t} = \nabla \cdot (q_i) + Q_i \quad i=1,2,3,\dots,n \quad (7-1)$$

$$\rho C_p \frac{\partial T}{\partial t} + \rho C_p u \cdot \nabla T(x,y,z) = \nabla \cdot (q) + Q_{vh} \quad (7-2)$$

Heat loss by conduction in Equation (7-2) is defined as:

$$q = k_{cond} \nabla T$$

According to [79] In a steady state, the heat transfer is at equilibrium and heat loss is zero, then the heat equation is given in Equation (7-3) as:

$$\nabla \cdot (k \nabla T) = 0 \quad (7-3)$$

Heat loss in the form of long-wave radiation was generated from the panel surface. This heat loss by longwave radiation was calculated in from Equation (7-4) [79] as:.

$$-n \cdot q = \varepsilon \sigma [(T_{amb})^4 - T^4] \quad (7-4)$$

The quantity of energy being converted into electric power in the PV cell is a function of the PV cell efficiency, η , as shown below in Equation [7-5], and it is given as:

$$q_{heat} = q_{rad} \cdot (1 - \eta_{pv}) \quad (7-5)$$

The electrical output efficiency of the PV panel, η_{pv} , is expressed in terms of its reference temperature efficiency, the temperature and thermal coefficient of the PV [79] as:.

$$\eta_{pv} = \eta_{Tref} [1 - \beta_{ref} (T_{pv} - T_{ref})] \quad (7-6)$$

This electrical output efficiency, η_{pv} , of the PV panel could also be expressed in terms of the power output of the PV panel, its surface area and the solar irradiance upon it [69] as given in Equation (7-7) as:

$$\eta_{pv} = \frac{V_{mp} \cdot I_{mp}}{Q_{rad} \cdot A} \quad (7-7)$$

In Equation 7-6, the PV cell efficiency at reference condition T_{ref} was given as 25⁰ C or 298⁰ K, the output power by irradiation, Q_{rad} was given as 1000 W/m² and β_{ref} was the PV thermal coefficient. A constant ambient temperature of 298.15 K was used throughout all test cases.

The panel thermal efficiency, η_{thrm} is the product of the incident power, E_{in} , and the thermal energy removed by the coolant (air). This is expressed by [79] as:

$$E_{in} = Q_{rad} \cdot A \quad (7.8)$$

$$E_{air} = m_{air} C_{pair} \cdot (T_{out} - T_{in}) \quad (7.9)$$

Combining Equations (7.8) and Equation (7.9) gives the thermal efficiency as:

$$\eta_{thrm} = \frac{E_{air}}{E_{in}} \quad (7-10)$$

From Equation (7-6), the average of the efficiency of the PV panel was obtained from the solution data of COMSOL for each iteration and at the completion of the simulation, the total input energy converting to the electrical energy was calculated as:

$$E_{pv} = \dot{\eta}_{pv} \cdot E_{in} \quad (7-11)$$

From equation (7-11), the total efficiency of the PV panel is then calculated as:

$$\eta_{tot} = \frac{(E_{air} + E_{pv})}{E_{in}} \quad (7-12)$$

7.3.5 The variables to be determined as the output

The variables to be determined as the electrical output are the PV cell efficiency, thermal efficiency, electrical efficiency, voltaic efficiency and the electrical output power. They are described and defined as contained and indicated in Table 7-3.

Table 7-3: Geometric entries for output variables to be determined

Name	Expression	Unit	Description
PVEFF	PVEFF0*(1 - PVdeg*(T - T_Init))		PV cell efficiency temp. dependence
Q_Heat	Q_Sun*(1 - PVEFF)	kW/m ²	Sun's energy converted to heat
ThermEFF	(V_mpp*I_mpp)/(Q_Sun*A)		Thermal efficiency
EFF_Net	PVEFF + ThermEFF		Overall efficiency
q_out	ht.Gm*eta_pv	kW/m ²	Electrical output power
eta_pv	if(T<368.15 [K] , 0.159*(1 - (T / 298.15 [K] - 1)^2), 0.15)		Voltaic efficiency, PV cell

The models for the simulations were developed as earlier explained in section 7.3.3. The models are tested conditions that could be integrated into standard operating conditions for predicting the PV performance outcome based on literature and experience. Once the initial model was tested to be working properly, further modifications were made to investigate material and atmospheric conditions dependencies.

7.3.6 Material composition description

The solar cells were fortified together in a vacuum lamination process with 40 cells wired into a unit panel size. The cells were sandwiched between two encapsulants, comprising a backsheet on the bottom for structural rigidity and a frontsheet atop the panel, often glass, on top of that. The sandwiched cells were placed into the laminator and the air removed from it through a vacuum application.

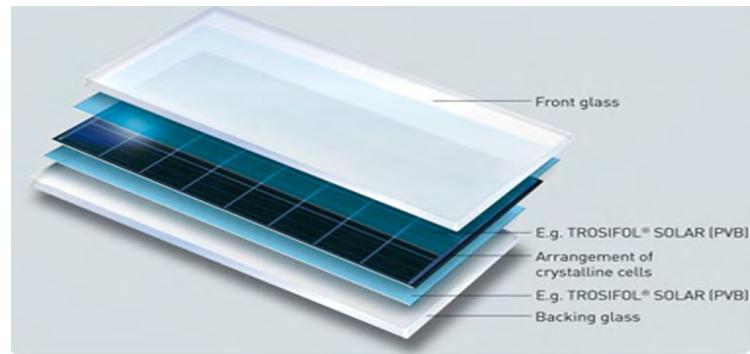


Figure 7-4 : Principle of a crystalline module assembly [124]

The laminator was subjected to heating up the cells so as to melt the top and bottom encapsulants which secured the PV cells in place as indicated in Figure 7-4. Upon their process completion and exit, a frame and junction box were fixed to complete the panel. The choice of materials selected for use on the PV panels was done in such a manner that would ensure a better tolerance for weather and high resistance to UV discolouring. The PV films, though transparent, are tough enough to ensure provision of high resistance to chemicals and harsh weather conditions, exhibit highly non-flammability, highly flexibility and good insulating properties. More details on materials properties selection are provided in Chapter 3.

7.3.7 Meshing

Meshing is necessary in order to correctly resolve the physics of the modelled work and to generate an accurate solution. The mesh size is chosen from one of the predefined mesh sizes under general physics. The mesh types available range from the 2D mesh which are the triangle and the quadrilateral to the 3D mesh which are the tetrahedron, quadrilateral pyramid, triangular prism, and hexahedron. In Figure 7-5(a) to Figure 7-5(c) are the generated results obtained for different mesh types applied on the different parts of the PV cell.

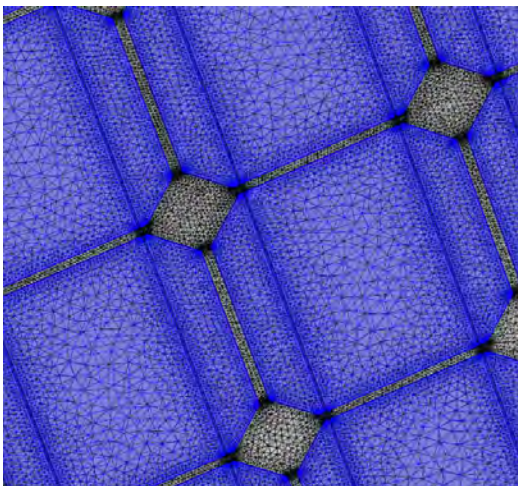


Figure 7-5a: Free tetrahedral meshing of PV cell

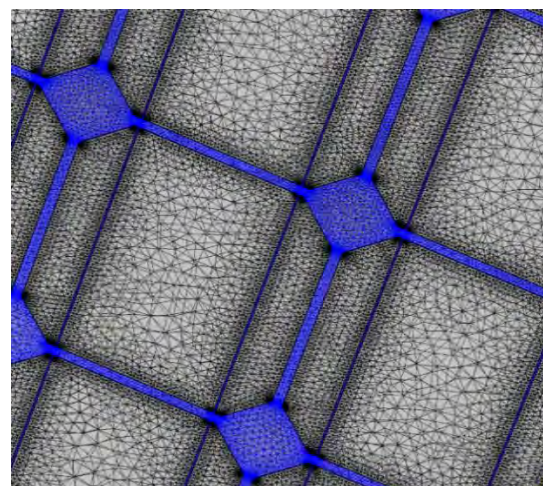


Figure 7-5b: Normal meshing of PV fins

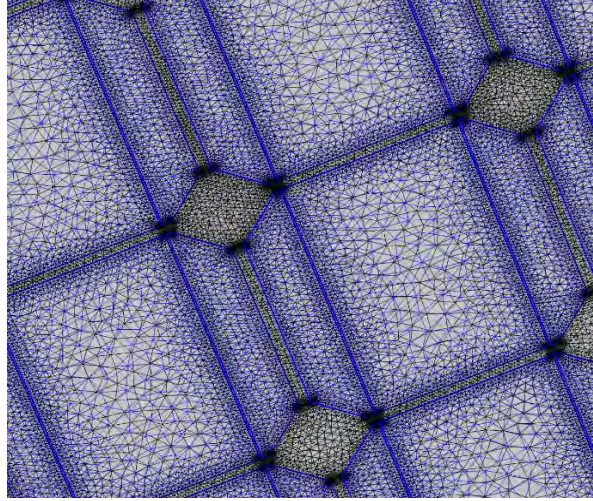


Figure 7-5c: Extra-fine meshing of PV edges

These mesh types were chosen from the predefined mesh sizes under general physics in COMSOL tool bar. The mesh type employed was user defined and ranged from extremely coarse mesh size to normal and then extremely fine mesh size.

The PV cells were meshed with coarse size tetrahedral elements and triangular elements, the custom mesh was operated on the PV Fins mesh while extremely fine was applied to the PV edges. The mesh was made much coarser in the wider regions like the PV cells and finer at the narrow regions like in the PV edges as shown in Figures 7-5(a, b and c).

7.4 Model validation

The modelled 3D Yingli PV panel was validated against the 1D model. The thermal model obtained was used to predict the standard operating conditions of the Yingli PV 260 series monocrystalline PV panel and to compare with the validated values obtained in the 1D simulation. The validated values of the input to the model are as given in Table 6-18 of Chapter six of this thesis.

7.5 Results and discussion

Using the developed and validated model, a study was conducted to see the impact of three-dimensional photovoltaic structure on solar power generation. The standard testing conditions (STC) were considered for the operating and environmental conditions for the standard case of 1000 W/m^2 absorbed radiation, 25°C or $298 \text{ }^\circ\text{K}$ ambient temperature and for cooling air equal to 0.05 m/s and $298 \text{ }^\circ\text{K}$ were used. The effects of atmospheric factors such as ambient temperature, solar irradiance, efficiency and electric output power on the performance of the Yingli PV panel were studied. The reports on the generated 3D results are given below:

7.5.1 Effect of ambient temperature on panel performance

Ambient temperature is one of the important environmental factors that affects PV performance. In Figure 7-6(a,b and c), different 3D plots of temperature distribution in the cells of the Yingli PV panel with air cooling are shown.

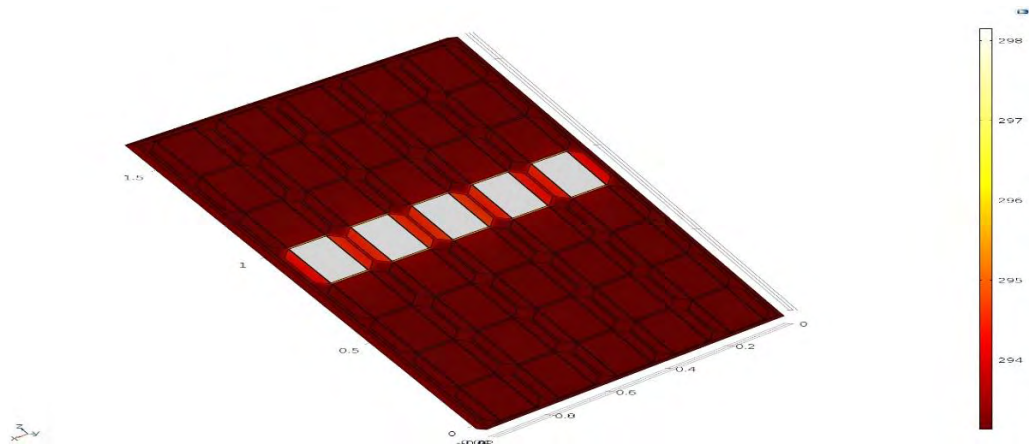


Figure 7-6a: 3D Solar PV 40 cells @ 298.15 K

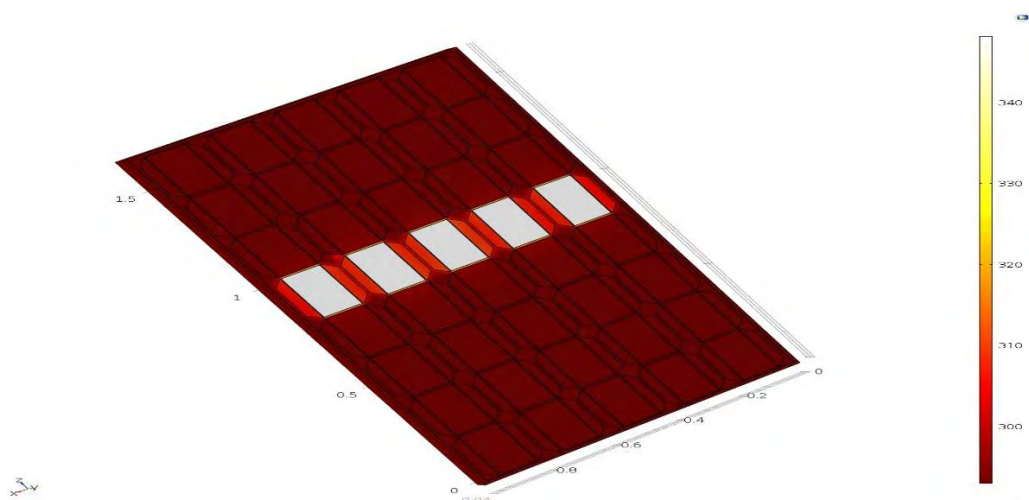


Figure 7-6b: 3D Solar PV 40 cells @ 348.15 K

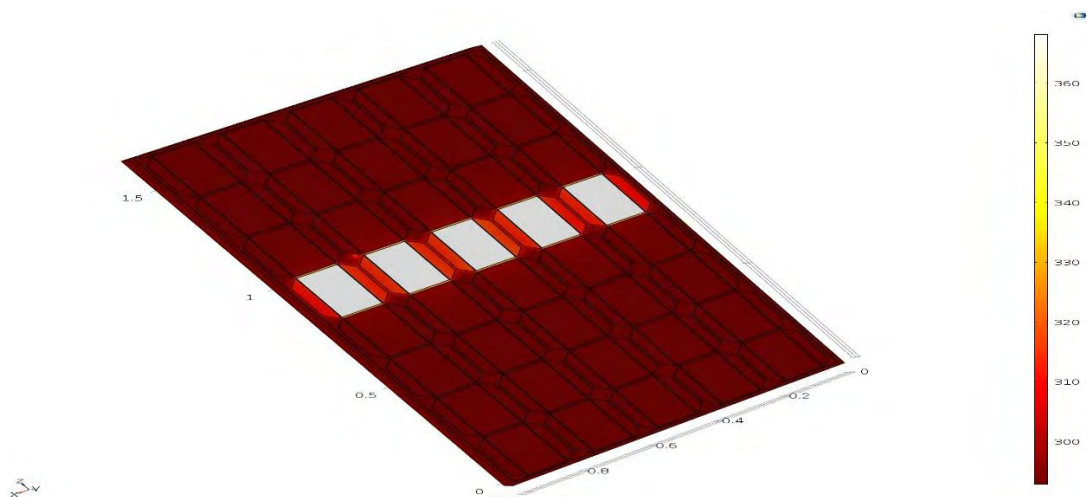


Figure 7-6c: 3D Solar PV 40 cells @ 368.15 K

Figure 7-6(a, b and c): 3D Solar PV 40 cells @ varying temperature

The phenomenon is seen by the visual plots in Figure 7-6(a, b and c) and the generated plot extracted from the COMSOL solution in Figure 7-7. The energy applied to the PV cell is the sum of the amount of energy converted to heat and the amount of energy converted into electric power in the PV

panel. The amount of energy generated as heat is directly proportional to the panel's operating temperature. The higher the panel temperature is, the greater will be the heat generated by the PV.

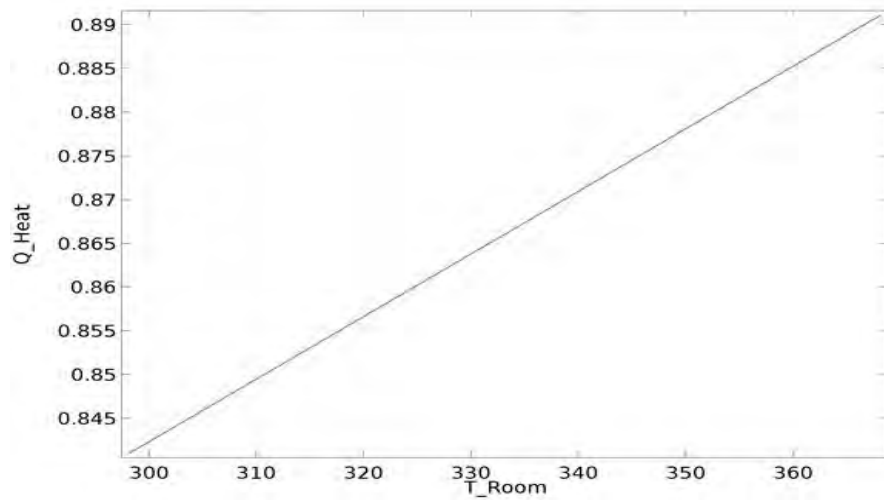


Figure 7-7: Sun's energy converted to heat (kW/m²)

In Figure 7-8, the effect of temperature on the PV cell efficiency was determined by making a plot of the PV cell efficiency against the operating temperature. It is shown from the plot that the PV cell efficiency is inversely related to the operating temperature. The PV cell efficiency is the fraction of the irradiation (sun's input energy) that is converted to useful energy while the remaining unwanted energy is lost in form of heat. The more the untapped energy, the more the heat, the higher the PV cell temperature becomes. The highest efficiency of the PV cell was about 16% and was obtained at the room temperature of about 298⁰ K.

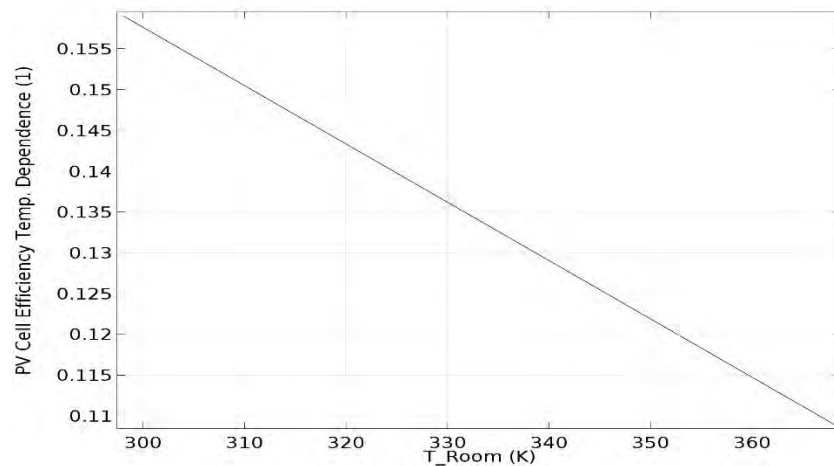


Figure 7-8: PV cell efficiency temperature dependence

In Figure 7-9, the plot of thermal efficiency is made against the temperature of the PV panel. The thermal efficiency is a measure of the extent to which energy added by heat is converted to network output. The thermal efficiency was found to be constant at about 23.5% and affected by change in PV cell operating temperature.

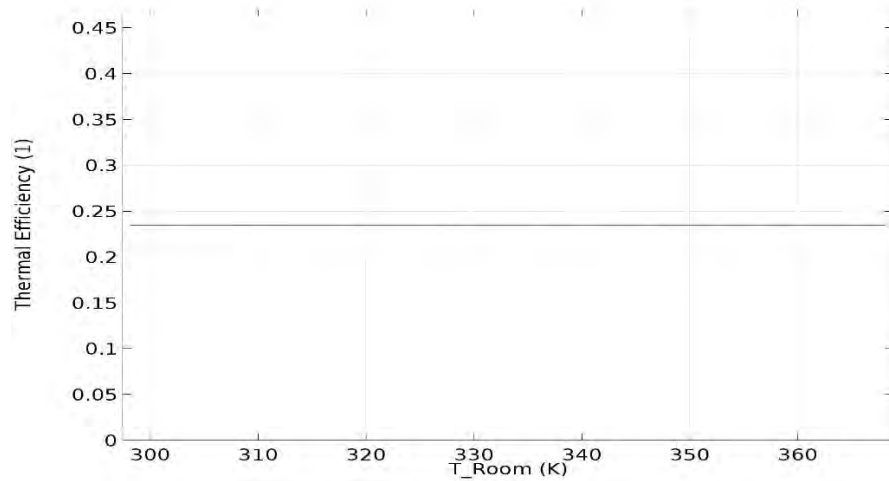


Figure 7-9: Thermal efficiency

The PV cell electrical efficiency is illustrated in Figure 7-10. It is directly related to the PV panel temperature, the thermal coefficient which is a constant and its efficiency at reference temperature. In Figure 7-10, the PV panel efficiency is maximum around the room temperature of 298⁰ K and gradually

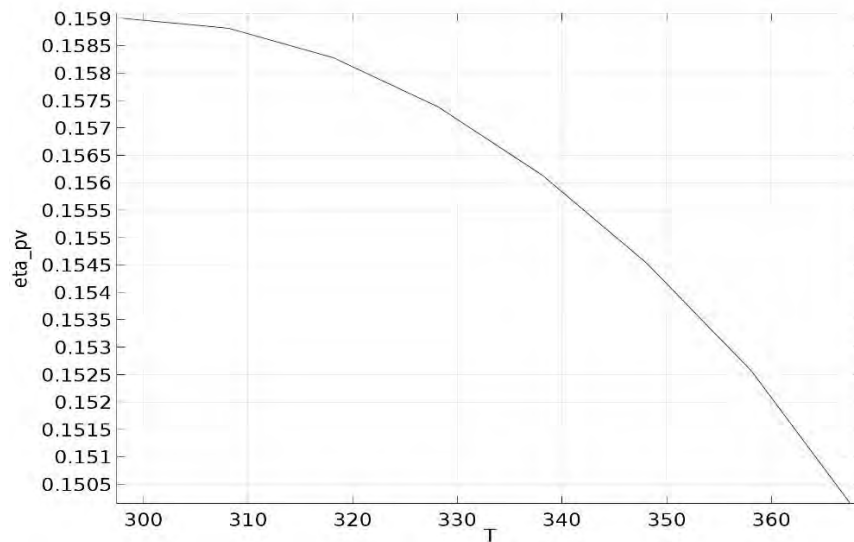


Figure 7-10: Voltaic efficiency

decreases with temperature until it reaches the temperature value 368⁰ K above which the temperature reduces to zero. The maximum PV panel electrical (voltaic) efficiency obtained was 15.9%.

The PV panel overall efficiency plot is illustrated in Figure 7-11. This is the overall efficiency of the PV panel. The overall efficiency reached was about 39.5% and was obtained at room temperature of about 298⁰ K. The overall efficiency decreases with temperature and will eventual become zero about operating temperature of about 370⁰ K.

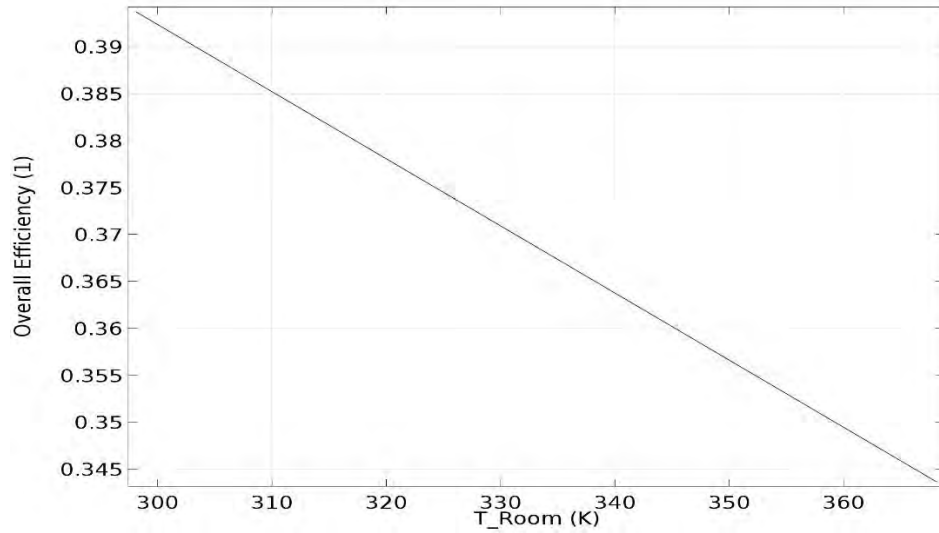


Figure 7-11: Overall efficiency

The PV panel electrical power output is shown in Figure 7-12. The maximum electrical power output reached was 1.045 kW/m² at the room temperature 298⁰ K. The higher the operating temperature, the lower the amount of electrical power output that would be generated.

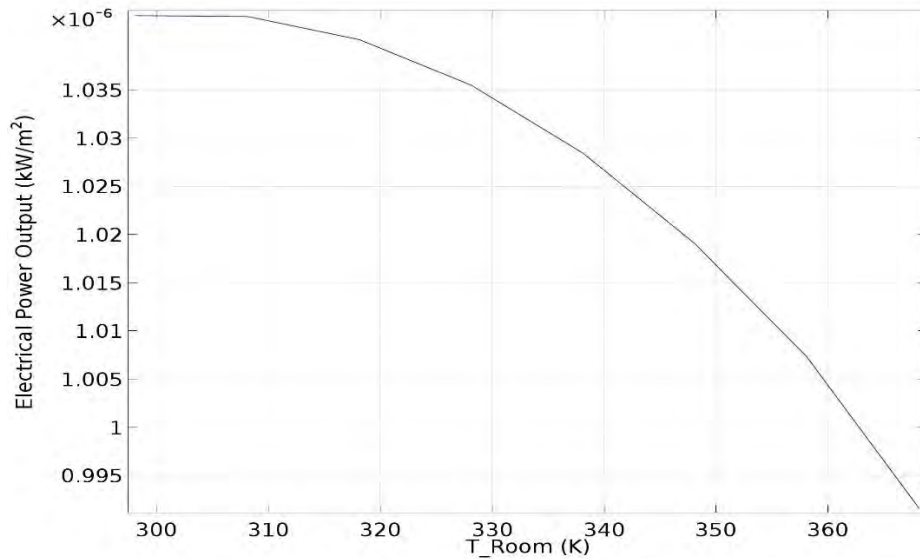


Figure 7-12: Electric output power (kW/m²)

7.6 Conclusions

A 3D thermal model of the Yingli PV panel was successfully modelled and simulated using the engineering software, COMSOL Multiphysics, Version 5.1. The simulation results enabled the prediction of the electrical performance of the modelled PV panel. The 3D modelling and simulation generated both the 3D thermal results which made possible the analysis and prediction of the temperature distribution of the PV structure. The simulation result also generated its 1D plots that revealed the electrical behaviour of the PV panel under study. These were used in validating the 1D graphs obtained in the 1D simulation. The obtained results were as expected.

CHAPTER EIGHT

SUMMARY AND CONCLUSION

8.1 Conclusion

This thesis focused on the two most established and commercialized methods of solar power generation by the PV method. The first method, the CTPV system, considered heat as the energy source and utilised concentrating mirrors to focus generated heat on the PV cells while the second method, the non-concentrated PV system, considered sun's radiation as the energy source and focused directly on the PV cells without the use of any concentrator. COMSOL Multiphysics, Version 5.1 was used for the 3D and non-3D modelling and simulation of both systems - the CTPV and the PV systems considered in this thesis. However, modelled PV systems in 3D in both cases of the study, were able to operate with minimal temperature influence on the system operation. In both cases of the study, 3D PV structure revealed through temperature distribution on the system operation, that temperature increase with increasing irradiation was common and experienced in both study cases of solar power generation. In the course of the research work, it was established that 3D simulation is about the completeness of the design criteria of the PV cells/modules with adequate consideration being given to their performance optimisation and minimisation of material variation or degradation on module performance in order to achieve optimised system performance and improved efficiency. 3D cell/panel simulation is able to reveal the temperature distribution of the system under study and enables the optimization of light absorption and PN-junction design for improved cell efficiency. 3D modelling has been able to eliminate temperature increase in the cells lattice structure in line with the expectation of reducing unprofitable/unwanted heat in the structure of the PV cell or module in the two study cases of the CTPV and non-concentrated solar PV systems. The normal cell design was subjected to early validation, ensuring the development of optimised PV cells, modules and arrays.

For the CTPV system, in order to arrive at the best operating condition, modelling and simulations were carried out on five different configurations. The 2D modelling and simulation was first carried out among three different configurations with eight mirrors, six mirrors and ten mirrors. Furthermore, the 3D modelling and simulation was carried out between the six mirrors and the eight mirrors. The 2D configuration with best performance was six mirrors with emitter heater temperature 1,600 K and PV cell temperature 1,300 K, generating optimal output power 31,800 W/m² and optimal efficiency of 19.8 per cent. The attained percentage temperature increase on the PV cell temperature was 45 per cent. This 2D configuration with six mirrors was then re-modelled in 3D in order to study the effect. There was an improvement on the performance of the 3D configuration over the 2D configuration with same number of mirrors (six). The 3D optimum performance curve could not be obtained until the heater temperature of about 4,000 K was reached and the expected output power was low but its graph was better normally distributed, indicating more sustainability than the output power generated in its 2D counterpart. From the 2D configuration to 3D configuration, there was a reduction in the attained PV temperature deviation from 45% to 28.6⁰ K, representing a further 36.4% reduction from the 2D configuration to 3D configuration. In line with expectation, the effect of temperature increase was less with the 3D

configuration than that of the 2D configuration of the same number of mirrors. In solar power systems, the effect of temperature needs to be minimized as much as possible. Contrary to expectation, the output power for the 3D was low ($2,290 \text{ W/m}^2$) and the operating heater temperature at which the 3D configuration began to yield output results was higher (about $4,000 \text{ K}$) but this high temperature was not a threat to the PV cells temperature and the efficiency was slightly improved upon at 19.9 per cent.

For the non-concentrated PV solar panel, the Yingli panel was eventually used to develop, model and study to predict the operational performance of the solar PV panel. The Yingli PV panel was used because it is one of the highly ranked PV panels. It could be more readily developed and modelled and the manufacturer's specifications were available for validation. The 1D and 3D modelling and simulations were used to study and determine the effects of the PV cell variables such as G , T_{op} , R_s , R_{sh} and N , which affect the operation performance of the PV panel being studied. The ideal conditions obtained for maximum power generation favourably compared with the specified manufacturer's values. The 3DPV simulation revealed the 3D temperature distribution of the Yingli PV panel was well defined as illustrated in the generated temperature distribution plots. The 1D COMSOL generated plots on sun's energy converted, the temperature dependence of the PV cell, the efficiency and the electrical output power. The results of these were in agreement with the earlier obtained results from 1D simulation and the manufacturer's specifications. Each manufacturer of PV panels tends to produce their system under ideal conditions as validated in this work. The thesis has been able to reveal and predict the performance behaviour of the panel under study.

The work done in this thesis is therefore sufficient to address the research questions raised at the beginning of this thesis as follows:

1. 3D complex design and fabrication could be realized and incorporated for sustainable installation at a global level for optimum power generation through the use of appropriate engineering software for developing, modelling and simulation exercises to pre-define the expected operating parameter that will meet the operational specifications and subjected to further research work for improvement.
2. 3DPV has impacted positively on the efficiency and power generated in comparison to the planar method of roof or ground installation because 3D configuration is able to predict the thermal behaviour of which its interpretation and adaptation into design systems is able to explore the space in greater dimensions, absorb more of the otherwise reflected rays, calculate and predict the electrical performances of the PV systems. This is evident from the numbers of domain and boundary formations for the 2D and 3D geometry building of any of the modelled systems carried out in this thesis. 3D model can handle complex flow patterns and design optimisation tasks.
3. Temperature increase is known to mitigate against solar energy generation with the planar configuration. The work done in this thesis has been able to show that 3DPV structure has a better temperature distribution than the planar configuration. The negative temperature distribution in 3D is therefore less than what is obtained in 2D or any other configuration.

8.2 Recommendation for further research

For the CTPV system, the temperature distribution in 3D study on solar systems has revealed that the effect of temperature rise is minimal and the heat loss is reduced compared with the non-3D system. It is then expected that this should result in improved output power generation. Therefore, further study needs to be carried out to determine the cause of the system's high operating temperature and unexpectedly lower output power generated.

Other questions requiring future research work are:

How has 3DPV impacted on the seasonal and latitudinal variation of solar energy generation particularly at night and in the cloudy season?

What are the effects of wind and gravitational pull on the 3DPV structures and how could these effects be minimized or prevented?

What are the cost implications and economic benefits of the use of 3DPV structures over the use of planar configurations?

REFERENCES

- [1] S. G. Daniel Yergin, Daniel Bachman, John Larson, Ted Lyman, Nancy Meyer and Jan Randolph, "Energy for Economic Growth - The Oxygen of the Economy," *World's Economic Forum*, 2012.
- [2] E. Martinot and J. Sawin, "Renewables global status report. Renewables 2012 Global Status Report, REN21," ed, 2012.
- [3] M. Sarraf, B. Rismanchi, R. Saidur, H. W. Ping, and N. A. Rahim, "Renewable energy policies for sustainable development in Cambodia," *Renewable and Sustainable Energy Reviews*, vol. 22, pp. 223-229, 2013.
- [4] M. Yahyavi, M. Vaziri, and S. Vadhva, "Solar energy in a volume and efficiency in solar power generation," in *Information Reuse and Integration (IRI), 2010 IEEE International Conference on*, 2010, pp. 394-399.
- [5] S. D. Foroudastan and O. Dees, "Solar power and sustainability in developing countries," in *Proceedings of the international conference on renewable energy for developing countries*, 2006.
- [6] C. J. Dai Qinghui, "Improving the efficiency of solar photovoltaic power generation in several important ways," *IET Conference Publications*, pp. 1-3, 2009 2009.
- [7] N. M. Maricar, E. Lee, H. K. Lim, M. F. Sepikit, M. R. M. Maskum, M. F. Ahmad, *et al.*, "Photovoltaic solar energy technology overview for Malaysia scenario," in *Power Engineering Conference, 2003. PECon 2003. Proceedings. National*, 2003, pp. 300-305.
- [8] L. T. Seiji Suzumoto¹, Toshiaki Yachi¹, "Output Power Characteristics of a Three-Dimensional Photovoltaic Module Using Fibonacci Number Composition," *IEEE*, p. 7, 2012.
- [9] W. De Soto, S. Klein, and W. Beckman, "Improvement and validation of a model for photovoltaic array performance," *Solar energy*, vol. 80, pp. 78-88, 2006.
- [10] N. F. Marco Bernardi, Jin H. Wan, Rachelle Villalon and Jeffrey C. Grossman, "Solar Energy Generation in Three Dimensions," *The Royal Socieity of Chemistry*, pp. 1-5, 2012.
- [11] B. Myers, M. Bernardi, J. C. Grossman, "Three-Dimensional Photovoltaics," *American Institute of Physics*, vol. 96, pp. 071902 - 071902-3, 2010.
- [12] A. Gupta, A. Khare, A. Shrivastava, "Modeling of Solar Photovoltaic Module and Effect of Variation of Insolation Using Matlab/Simulink," *International Journal of Electrical, Electronics and Computer Engineering* 3(1): 126-131(2014), pp. 126-131, 2014 2014.
- [13] M. Usama Siddiqui, A. F. M. Arif, L. Kelley, and S. Dubowsky, "Three-dimensional thermal modeling of a photovoltaic module under varying conditions," *Solar Energy*, vol. 86, pp. 2620-2631, 2012.
- [14] A. Bayoumi, M. Abdelaziz, and M. M. Abdelhameed, "Modeling and simulation of Photovoltaic/Thermal hybrid system," in *Computer Engineering & Systems (ICCES), 2013 8th International Conference on*, 2013, pp. 127-132.
- [15] S. Suzumoto, L. Tayo, T. Yachi, "Output Power Characteristics of a Three-Dimensional Photovoltaic Module Using Fibonacci Number Composition," *IEEE Journal*, p. 7, 2012.

- [16] G. K. Singh, "Solar power generation by PV (photovoltaic) technology: A review," *Energy*, vol. 53, pp. 2013.
- [17] P. Valera, A. Esteban, M. de los Reyes Carrillo, R. Osuna, P. Menna, R. Gambi, P. Helm, M. Grottko, M. Geyer, F. Dodon, J. Monedero, A. Lugo, M. Romero, F. Chenlo, M. Alonso, M. Sanchez, J. Artigas and A. Fresneda, "Solar Energy: Comparative Analysis of Solar Technologies for Electricity Production," *Proceedings of 3rd World Conference on*, (vol. 3, pp. 2482-2485). IEEE Osaka, Japan, 2003.
- [18] H. Garg, *Solar energy: fundamentals and applications*: Tata McGraw-Hill Education, 2000.
- [19] A. Marcucci, H. Turton, "Solar Energy Perspectives in Renewable Energy," in *Renewable Energy Technologies*, ed. Printed in Luxembourg by Imprimerie Centrale: IEA Publications, 2011, p. 1.
- [20] J. Ellis and K. Tréanton, "Recent trends in energy-related CO₂ emissions," *Energy Policy*, vol. 26, pp. 159-166, 1998.
- [21] Y. Chu, "Review and comparison of different solar energy technologies," *Global Energy Network Institute (GENI), San Diego, CA*, 2011.
- [22] L. M. Peter, "Towards sustainable photovoltaics: the search for new materials," *Philosophical Transactions of the Royal Society A: Mathematical, Physical and Engineering Sciences*, vol. 369, pp. 1840-1856, 2011.
- [23] P. Denholm, E. Drury, R. Margolis, and M. Mehos, "Chapter 10 - Solar Energy: The Largest Energy Resource," in *Generating Electricity in a Carbon-Constrained World*, ed Boston: Academic Press, pp. 271-302, 2010.
- [24] T. Markvart, *Solar electricity*. vol. 6: John Wiley & Sons, 2000.
- [25] D. Gielen, "Renewable energy technologies: Cost analysis series," *Solar Photovoltaics*, vol. 1, p. 52, 2012.
- [26] I. Suárez, M. M. Prieto, and F. J. Fernández, "Analysis of potential energy, economic and environmental savings in residential buildings: Solar collectors combined with microturbines," *Applied Energy*, vol. 104, pp. 128-136, 2013.
- [27] R. K. Akikur, R. Saidur, H. W. Ping, and K. R. Ullah, "Comparative study of stand-alone and hybrid solar energy systems suitable for off-grid rural electrification: A review," *Renewable and Sustainable Energy Reviews*, vol. 27, pp. 738-752, 2013.
- [28] P. Savitha, M. Shashikala, and K. Puttabuddhi, "Modelling of Photovoltaic Cell/Module under Environmental Disturbances using MATLAB/Simulink," *International Journal of Engineering Trends and Technology (IJETT)*, vol. 9, 2014.
- [29] N. Tanaka, "Technology roadmap-solar photovoltaic energy," *International energy agency report. Paris/France*, 2010.
- [30] A. Sahay, V. Sethi, and A. Tiwari, "A Comparative Study of Attributes of Thin Film and Crystalline Photovoltaic Cells," *International Journal of Mechanical, Civil, Automobile and Production Engineering*, vol. vol. 3 No. 7, p. 4, 2013.
- [31] M. Brogren, "Optical efficiency of low-concentrating solar energy systems with parabolic reflectors," 2004.

- [32] M. Hoeven, "Solar Thermal Electricity - Technology Roadmap", *International Energy Agency*, pp. 52, 2014.
- [33] G. Dzimano, "Modeling of photovoltaic systems" PhD diss., The Ohio State University, 2008.
- [34] B. Padmanabhan, D. Vasileska, D. K. Schroder, and D. Mamaluy, "Modeling of solar cells," *Arizona State University*, 2008.
- [35] F. M. González-Longatt, "Model of photovoltaic module in Matlab," *II CIBELEC*, vol. 2005, pp. 1-5, 2005.
- [36] M. Eteiba, E. El Shenawy, J. Shazly, and A. Hafez, "A Photovoltaic (Cell, Module, Array) Simulation and Monitoring Model using MATLAB?/GUI Interface," *International Journal of Computer Applications*, vol. 69, 2013.
- [37] E. Skoplaki and J. Palyvos, "On the temperature dependence of photovoltaic module electrical performance: A review of efficiency/power correlations," *Solar energy*, vol. 83, pp. 614-624, 2009.
- [38] K. Hussein, I. Muta, T. Hoshino, and M. Osakada, "Maximum photovoltaic power tracking: an algorithm for rapidly changing atmospheric conditions," *IEE Proceedings-Generation on*, vol. 142, pp. 59-64, 1995.
- [39] M. Edouard and D. Njomo, "Mathematical Modeling and Digital Simulation of PV Solar Panel using MATLAB Software", *International Journal of Emerging Technology and Advanced Engineering*, 3(9), pp. 24-32, 2013.
- [40] C. R. Sullivan and M. J. Powers, "A high-efficiency maximum power point tracker for photovoltaic arrays in a solar-powered race vehicle," in *Power Electronics Specialists Conference, 1993. PESC '93 Record., 24th Annual IEEE*, pp. 574-580, 1993.
- [41] S. Philipps, A. Bett, K. Horowitz, and S. Kurtz, "Current Status of Concentrator Photovoltaic (CPV) Technology," *National Renewable Energy Laboratory (NREL)*, Golden, CO.2015.
- [42] H. L. Zhang, J. Baeyens, J. Degreè, and G. Cacères, "Concentrated solar power plants: Review and design methodology," *Renewable and Sustainable Energy Reviews*, vol. 22, pp. 466-481, 2013.
- [43] M. Grätzel, "Conversion of sunlight to electric power by nanocrystalline dye-sensitized solar cells," *Journal of Photochemistry and Photobiology A: Chemistry*, vol. 164, pp. 3-14, 2004.
- [44] S. Armstrong and W. Hurley, "A thermal model for photovoltaic panels under varying atmospheric conditions," *Applied Thermal Engineering*, vol. 30, pp. 1488-1495, 2010.
- [45] C. Renno and F. Petit, "Energy Analysis of a Concentrating Photovoltaic Thermal (CPV/T) System," *Energy Science and Technology*, vol. 6, pp. 53-63, 2013.
- [46] M. Grätzel, "Photovoltaic and photoelectrochemical Conversion of Solar Energy," *Philosophical Transactions of the Royal Society A: Mathematical, Physical and Engineering Sciences*, vol. 365, pp. 993-1005, 2007.
- [47] N. Ulapane, S. Abeyratne, P. Binduhewa, C. Dhanapala, S. Wickramasinghe, and N. Rathnayake, "A simple software application for simulating commercially available solar panels," *arXiv preprint arXiv:1401.5162*, 2014.

- [48] C. G. Miller and J. G. Pohl, "Three-Dimensional Tracking Solar Energy Concentrator and Method for Making Same", *United State Patent No. 4,046,462*, 1977.
- [49] B. J. Huang, W. Z. Ton, C. C. Wu, H. W. Ko, H. S. Chang, R. H. Yen, *et al.*, "Maximum-power-point tracking control of solar heating system," *Solar Energy*, vol. 86, pp. 3278-3287, 2012.
- [50] M. Bernardi, N. Ferralis, J. H. Wan, R. Villalon, and J. C. Grossman, "Solar energy generation in three dimensions," *Energy & Environmental Science*, vol. 5, pp. 6880-6884, 2012.
- [51] T. Suto and T. Yachi, "Power-generation characteristics of an FPM by simulation with shadow-effect analysis," in *Photovoltaic Specialists Conference (PVSC), 2011 37th IEEE*, pp. 001881-001886, 2011,
- [52] G. Aglietti, T. Markvart, A. Tatnall, and S. Walker, "Solar power generation using high altitude platforms feasibility and viability," *Progress in Photovoltaics: Research and Applications*, vol. 16, pp. 349-359, 2008.
- [53] B. Myers, M. Bernardi, and J. C. Grossman, "Three-dimensional photovoltaics," *Applied Physics Letters*, vol. 96, pp. 071902-071902-3, 2010.
- [54] M. Gharghi, B. Hua, G. Stevens, and S. Sivoththaman, "Three-dimensional modeling and simulation of p-n junction spherical silicon solar cells," *Electron Devices, IEEE Transactions on*, vol. 53, pp. 1355-1363, 2006.
- [55] A. Yuji and T. Yachi, "A novel photovoltaic module assembled three-dimensional," in *Photovoltaic Specialists Conference (PVSC), 2010 35th IEEE*, pp. 002811-002816, 2010.
- [56] B. Myers, M. Bernardi and J. C. Grossman. Bryan Myers, "Three-Dimensional Photovoltaics," *American Institute of Physics*, vol. 96, pp. 071902 - 071902-3, 2010.
- [57] A. Grigas, "The Fibonacci Sequence: Its History, Significance, and Manifestations in Nature," 2013.
- [58] J. Szlufcik, S. Sivoththaman, J. Nlis, R. P. Mertens, and R. Van Overstraeten, "Low-cost industrial technologies of crystalline silicon solar cells," *Proceedings of the IEEE*, vol. 85, pp. 711-730, 1997.
- [59] S. Neale, K. Yu, M. Wu, J.W. Ager and A. Javey, "Three-dimensional nanopillar-array photovoltaics on low-cost and flexible substrates," *Nat Mater*, vol. 8, pp. 648-653, 08/print 2009.
- [60] B. Kuhlmann, A. G. Aberle, R. Hezel, and G. Heiser, "Simulation and optimization of metal-insulator-semiconductor inversion-layer silicon solar cells," *Electron Devices, IEEE Transactions on*, vol. 47, pp. 2167-2178, 2000.
- [61] X. Xiaoli, L. Qiushuang and Z. Yunbo, "A Study on All-Weather Flexible Auto-tracking Control Strategy of High-Efficiency Solar Concentrating Photovoltaic Power Generation System," in *Intelligent Systems (GCIS), 2010 Second WRI Global Congress on*, 2010, pp. 375-378, 2010.
- [62] R. P. Collins, "Hybrid Solar Panel Efficiency Optimization with a Labyrinth Fin Arrangement," Rensselaer Polytechnic Institute, 2013.
- [63] AB, COMSOL, "COMSOL Multiphysics User's Guide, Version 4.3", COMSOL AB., Stockholm, Sweden, 2012.

- [64] AB, COMSOL, "Thermo-Photo-Voltaic Cell," Application Library path: Heat_Transfer_Module/Thermal_Radiation/tpv_cell, COMSOL Multiphysics User's Guide, Version 5.1, Ed., ed, p. 22, 2015.
- [65] M. Eteiba, E. El Shenawy, J. Shazly, and A. Hafez, "A Photovoltaic (Cell, Module, Array) Simulation and Monitoring Model using MATLAB®/GUI Interface," *International Journal of Computer Applications*, Vol. 69, pp. 14-28, 2013.
- [66] P. Shivananda, "A Photovoltaic Panel Model in Matlab/Simulink," *ResearchGate*, p. 6, 2013.
- [67] M. G. Villalva and J. R. Gazoli, "Comprehensive approach to modeling and simulation of photovoltaic arrays," *Power Electronics, IEEE Transactions on*, vol. 24, pp. 1198-1208, 2009.
- [68] B. Alsayid and J. Jallad, "Modeling and simulation of photovoltaic cells/modules/arrays," *International Journal of Research and Reviews in Computer Science (IJRRCS)*, vol. 2, pp. 1327-1331, 2011.
- [69] H. Teo, P. Lee, and M. N. A. Hawlader, "An active cooling system for photovoltaic modules," *Applied Energy*, vol. 90, pp. 309-315, 2012.
- [70] C. Honsberg and S. Bowden, "Module Materials", Internet: "<http://pveducation.org/pvcdrom/modules/module-materials>", available as at May 15, 2016.
- [71] T. Rahman and K. Fobelets, "Efficient tool flow for 3D photovoltaic modelling," *Computer Physics Communications*, vol. 193, pp. 124-130, 2015.
- [72] N. Peter, O. E. Kabu, K. Stephen and D. Anthony, "3D finite element method modeling and simulation of the temperature of crystalline photovoltaic module", *International Journal of Research in Engineering and Technology*, vol. 04, pp. 7, 2015.
- [73] T. Senjyu, D. Hayashi, N. Urasaki, and T. Funabashi, "Optimum configuration for renewable generating systems in residence using genetic algorithm," *Energy Conversion, IEEE Transactions on*, vol. 21, pp. 459-466, 2006.
- [74] A. Sinhaa and P. Bajpai, "Swarm intelligence based optimal sizing of solar PV, fuel cell and battery hybrid system," in *Proc. of International Conference on Power and Energy Systems Lecture Notes in Information Technology*, pp. 467-473, 2012.
- [75] J. Cepeda, S. Birla, J. Subbiah, and H. Thippareddi, "A Practical Method to Model Complex Three-Dimensional Geometries with Non-Uniform Material Properties Using Image-based Design and COMSOL Multiphysics®," in *COMSOL conference, Boston*, 2013.
- [76] S. Shaari, "Photovoltaics in the built environment: an application for Malaysia," 1998.
- [77] J. H. Wan, "Geometric modeling and optimization in 3D solar cells: implementation and algorithms," Massachusetts Institute of Technology, 2014.
- [78] N. A. Ahmed and M. Miyatake, "A novel maximum power point tracking for photovoltaic applications under partially shaded insolation conditions," *Electric Power Systems Research*, 78(5) pp. 777-784, 2008.
- [79] B. J. Fontenault and E. Gutierrez-Miravete, "Modeling a Combined Photovoltaic-Thermal Solar Panel," in *Comsol Conference, Boston, MA*, pp. 1-8, 2002.
- [80] M. C. Lux-Steiner, "Non-conventional Semiconductor materials for solar cells", *Springer Proceedings in Physics*, vol. 54, pp. 420-431, 1991.

- [81] DuPont, "Interactive: What makes up a Solar Panel?", "<http://www.dupont.com/products-and-services/solar-photovoltaic-materials/what-makes-up-solar-panel.html>", available as at 15 May 2016.
- [82] R. A. Allaire and P. L. Bocko, "Fracture behavior and Intrinsic Strength of FPD Substrate - Technical Information Paper," *SID International Symposium Digest of Technical Papers*, vol. 27, Society of Information Display, pp. 933-936, 2004.
- [83] Technical Glass "7059/7059F Low Alkaline Barium-borosilicate Glass", "<http://www.pgo-online.com/intl/katalog/7059.html>", *Prazisions Glas & Optik GmbH, Germany*, available as at 15 May, 2016.
- [84] J. Pern, "Module Encapsulation Materials, Processing and Testing," National Renewable Energy Laboratory of the U.S. Department of Energy, Ed., pp. 33, 2008.
- [85] A. A. Adeyanju and K. Manohar, "Assessment of Solar Thermal Energy Technologies in Nigeria," in *Green Technologies Conference (IEEE-Green), 2011 IEEE*, pp. 1-6, 2011.
- [86] A. D. Greenhut, "Modeling and analysis of hybrid geothermal-solar thermal energy conversion systems," Massachusetts Institute of Technology, 2009.
- [87] G. Mittelman, A. Kribus and A. Dayan, "Solar cooling with concentrating photovoltaic/thermal (CPVT) systems," *Energy Conversion and Management*, vol. 48, pp. 2481-2490, 2007.
- [88] J. Tester, R. Dippio, R. Field, C. Augustine, K. Frey, and H. Thorsteinsson, "Utilization of low-enthalpy geothermal fluids to produce electric power," *Final Report Project*, vol. 1, 2008.
- [89] A. Luque, G. Sala and J. Arboiro, "Electric and thermal model for non-uniformly illuminated concentration cells," *Solar Energy Materials and Solar Cells*, vol. 51, pp. 269-290, 1998.
- [90] M. Steiner, J. F. Geisz, D. J. Friedman, W. J. Olavarria, A. Duda and T. E. Moriarty, "Temperature-dependent measurements of an inverted metamorphic multijunction (IMM) solar cell," in *Photovoltaic Specialists Conference (PVSC), 2011 37th IEEE*, pp. 002527-002532, 2011.
- [91] H. Cotal, C. Fetzer, J. Boisvert, G. Kinsey, R. King, P. Hebert and N. Karam, "III-V multijunction solar cells for concentrating photovoltaics," *Energy & Environmental Science*, vol. 2, pp. 174-192, 2009.
- [92] A. Kribus, D. Kaftori, G. Mittelman, A. Hirshfeld, Y. Flitsanov, and A. Dayan, "A miniature concentrating photovoltaic and thermal system," *Energy Conversion and Management*, vol. 47, pp. 3582-3590, 2006.
- [93] W. Grasse, C. Tyner, and A. Steinfeld, "International R & D collaboration in developing solar thermal technologies for electric power and solar chemistry: The solarPACES program of the International Energy Agency (IEA)," *Le Journal de Physique IV*, vol. 9, pp. Pr3-9-Pr3-15, 1999.
- [94] T. M. Klucher, "Evaluation of models to predict insolation on tilted surfaces," *Solar energy*, vol. 23, pp. 111-114, 1979.
- [95] R. Perez, R. Stewart, C. Arbogast, R. Seals, and J. Scott, "An anisotropic hourly diffuse radiation model for sloping surfaces: description, performance validation, site dependency evaluation," *Solar energy*, vol. 36, pp. 481-497, 1986.

- [96] D. Reindl, W. Beckman, and J. Duffie, "Evaluation of hourly tilted surface radiation models," *Solar Energy*, vol. 45, pp. 9-17, 1990.
- [97] A. Tiwari and M. Sodha, "Performance evaluation of hybrid PV/thermal water/air heating system: a parametric study," *Renewable energy*, vol. 31, pp. 2460-2474, 2006.
- [98] S. Dubey and G. Tiwari, "Thermal modeling of a combined system of photovoltaic thermal (PV/T) solar water heater," *Solar Energy*, vol. 82, pp. 602-612, 2008.
- [99] F. Sarhaddi, S. Farahat, H. Ajam, A. Behzadmehr, and M. M. Adeli, "An improved thermal and electrical model for a solar photovoltaic thermal (PV/T) air collector," *Applied Energy*, vol. 87, pp. 2328-2339, 2010.
- [100] H. Zondag, D. D. De Vries, W. Van Helden, R. Van Zolingen, and A. Van Steenhoven, "The thermal and electrical yield of a PV-thermal collector," *Solar energy*, vol. 72, pp. 113-128, 2002.
- [101] J. Duckworth, M. Gleason, N. Grue, P. Gray-Hann, D. Heimiller, D. Hettinger, J. Leyshon, A. Lopez, G. Maclaurin, M. Mooney and B.J. Roberts, "Dynamic Maps, GIS Data, & Analysis Tools", Internet: "<http://www.nrel.gov/gis/solar.html>", National Renewable Energy Laboratory, (May 2012, 2012). Renewable Energy Technologies: Cost Analysis Series. *Solar Photovoltaics*, 1(4/5), 52, available as at 15 May, 2016.
- [102] G. Russell, "Third-Generation Photovoltaic Technology - The Potential for Low-Cost Solar Energy Conversion," *The Journal of Physical Chemistry Letters*, pp. 2, 2010.
- [103] F. Economy, "Energy Efficiency and Renewable Energy", "www.fueleconomy.gov/feg/byfueltype.htm", US Department of Energy. Washington DC., USA ed 2008:, available as at 15, May 2016.
- [104] G. S. Aglietti, S. Redi, A. R. Tatnall and T. Markvart, "High altitude electrical power generation," *WSEAS Transactions on Environment and Development*, vol. 4, pp. 1067-1077, 2008.
- [105] O. A. Mafimidiwo and A. K. Saha, "Improving Solar Energy Generation Through the Use of Three Dimensional Photovoltaics Technology", in *Proceedings of the Southern African Universities Power Engineering Conference*, University of KwaZulu-Natal, ISBN: 978-1-868840-619-7, pp 294-300, 2014.
- [106] G. S. Aglietti, S. Redi, A. R. Tatnall, and T. Markvart, "Harnessing high-altitude solar power," *Energy Conversion, IEEE Transactions on*, vol. 24, pp. 442-451, 2009.
- [107] M. Gharghi, H. Bai, G. Stevens, and S. Sivothythaman, "Three-dimensional modeling and simulation of pn junction spherical silicon solar cells," *Electron Devices, IEEE Transactions on*, vol. 53, pp. 1355-1363, 2006.
- [108] J. Zou, R. K. Ward, and D. Qi, "A new digital image scrambling method based on Fibonacci numbers," in *Circuits and Systems, ISCAS'04. Proceedings of the 2004 International Symposium on*, pp. III-965-8 Vol. 3, 2004.
- [109] A. D. Belegundu and T. R. Chandrupatla, "Optimization concepts and applications in engineering", Cambridge University Press, 2011.
- [110] A. Stakhov, "The Generalized Principle of the Golden Section and its applications in mathematics, science, and engineering," *Chaos, Solitons & Fractals*, vol. 26, pp. 263-289, 2005.

- [111] T. Koshy, "Fibonacci and Lucas numbers with applications", John Wiley & Sons, vol. 51, 2011.
- [112] City of London, "Corporate Energy Conservation and Demand Management (CDM) Plan," Available at:
<http://www.london.ca/residents/Environment/Energy/Documents/2014%20CDM%20Plan%20final.pdf>," available as at 15 May, 2016.
- [113] D. Sampatakos, "Development of three dimensional PV structures as shading devices for a Decentralized Facade Unit of the Future," TU Delft, Delft University of Technology, 2014.
- [114] K. S. Dinesh, V. Varsha and P. S. Anil, "Review and Analysis of Solar Photovoltaic Softwares," *International Journal of Current Engineering and Technology*, pp. 725-731, 2014.
- [115] P. Savitha, M. Shashikala, and K. Puttabuddhi, "Modelling of 250WP Photovoltaic module and its performance analysis using MATLAB/SIMULINK," in *Proceedings of IRF International Conference, Bangalore*, pp. 34-40, 2014.
- [116] K. Instruments, "Making IV and CV Measurements on Solar/Photovoltaic Cells Using the Model 4200-SCS Semiconductor Characterization System," *Keithley Application Note Series*, 2007.
- [117] P. Shivananda, "A photovoltaic panel model in Matlab/Simulink," *ResearchGate*, pp. 6, 2013.
- [118] J. A. Ramos-Hernanz, J. J. Campayo, J. Larranaga, E. Zulueta, O. Barambones, J. Motrico, U. F. Gamiz and I. Zamora, "Two photovoltaic cell simulation models in Matlab/Simulink," *International Journal on Technical and Physical Problems of Engineering, (IJTPE)*, vol. 4, no. 1, pp. 45-51, 2012.
- [119] M. Ibrahim, K. Sopian, W. R. W. Daud, M. A. Alghoul, M. Yahya, M. Y. Sulaiman and A. Zaharim, "Solar chemical heat pump drying system for tropical region," *WSEAS Transactions on Environment and Development*, vol. 5, pp. 404-413, 2009.
- [120] L. Wong and W. Chow, "Solar radiation model," *Applied Energy*, vol. 69, pp. 191-224, 2001.
- [121] G. Tina and R. Abate, "Experimental verification of thermal behaviour of photovoltaic modules," in *Electrotechnical Conference, MELECON, The 14th IEEE Mediterranean*, pp. 579-584, 2008.
- [122] P. Savitha, M. Shashikala, and K. Puttabuddhi, "Modelling of 250WP Photovoltaic module and its performance analysis using MATLAB/SIMULINK," in *Proceedings of IRF International Conference, Bangalore*, pp. 34-40, 2014.
- [123] B. Koll, "More solar module encapsulation with PVB film", "Glassonweb" Available at:
www.glassonweb.com/articles/article/567/," available as at 15 May, 2016.

APPENDIX A

APPENDIX A-1: COMSOL generated report on 2D CTPV system with 6 mirrors configuration

Parameter

Name	Expression	Value	Description
T_heater	1000 [K]	1000 K	Temperature, emitter inner boundary

Variables

Name	Expression	Unit	Description
eta_pv	if($T < 1600$ [K] , $0.2 * (1 - (T / 800$ [K] - 1) ²), 0)		Voltaic efficiency, PV cell
q_out	ht.Gm*eta_pv	W/m ²	Electric output power

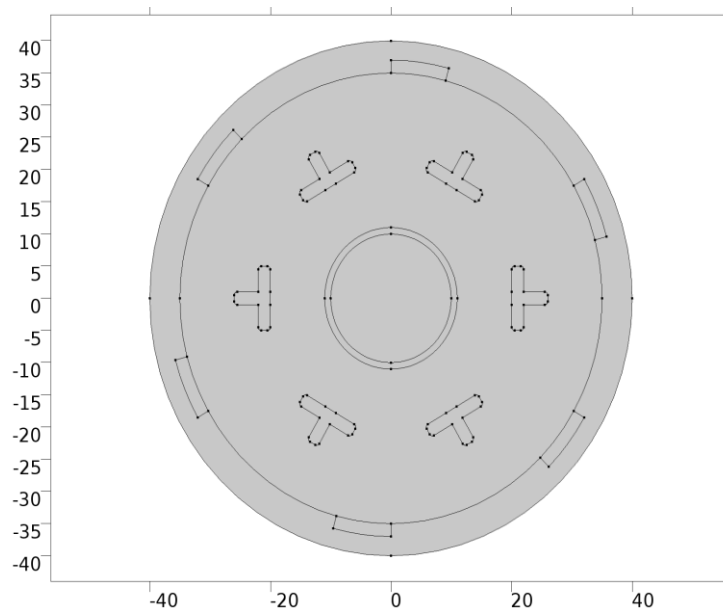


Figure A-1.1: Geometry of the concentrated thermal photovoltaics system in two-dimension

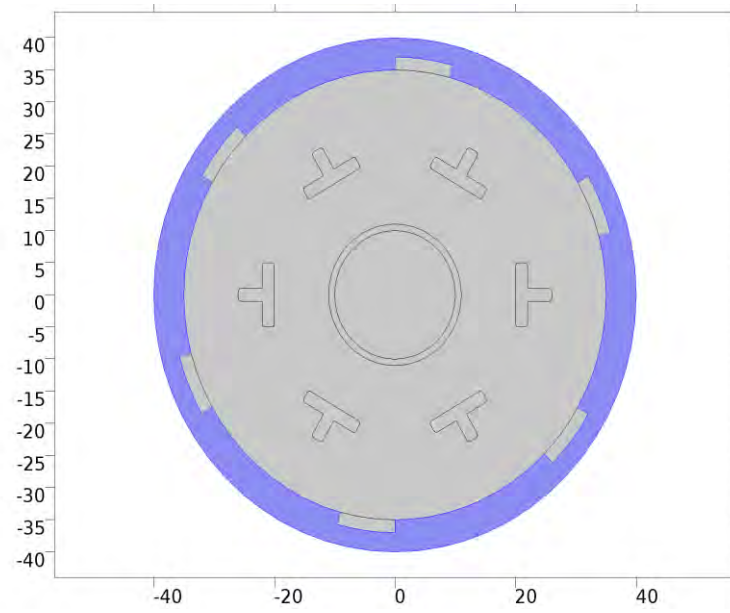


Figure A-1.2: Geometry of the modelled 2D CTPV system with six cells and insulation around the PV cells.

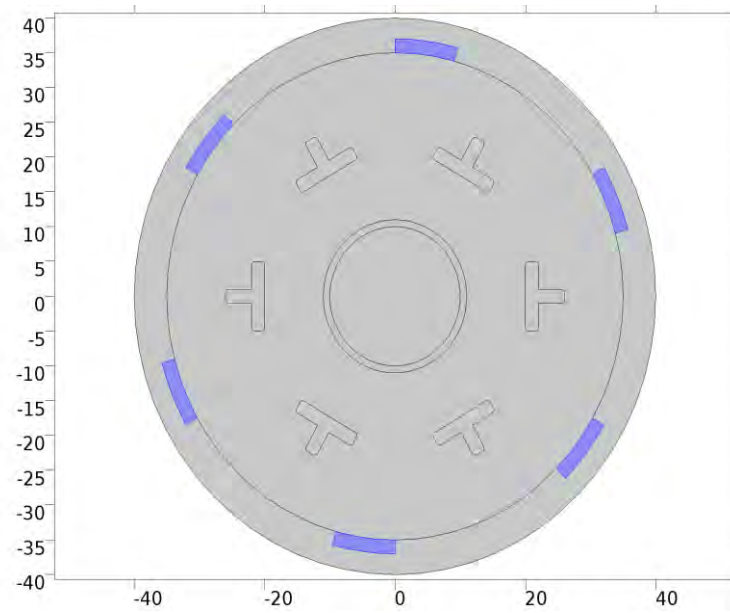


Figure A-1.3: Geometry of the modelled 2D CTPV system showing the PV cells (six in number)

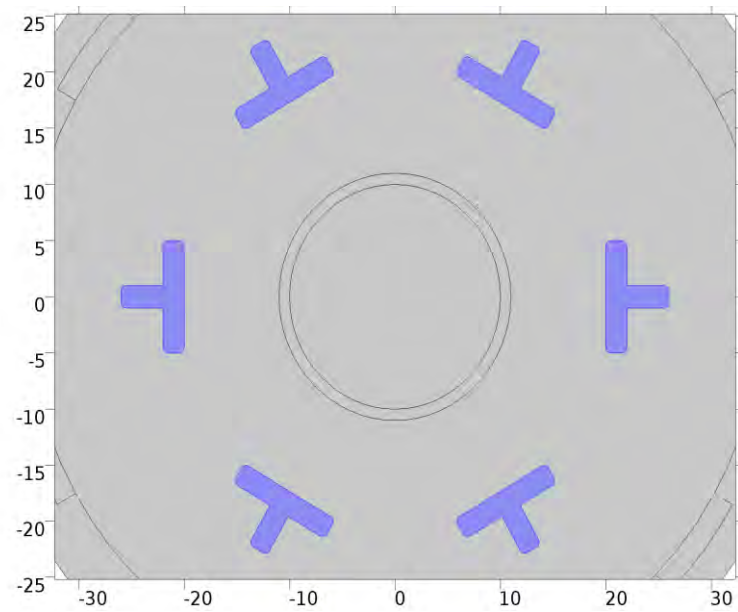


Figure A-1.4: Geometry of the modelled 2D CTPV system showing the mirrors (six in number)

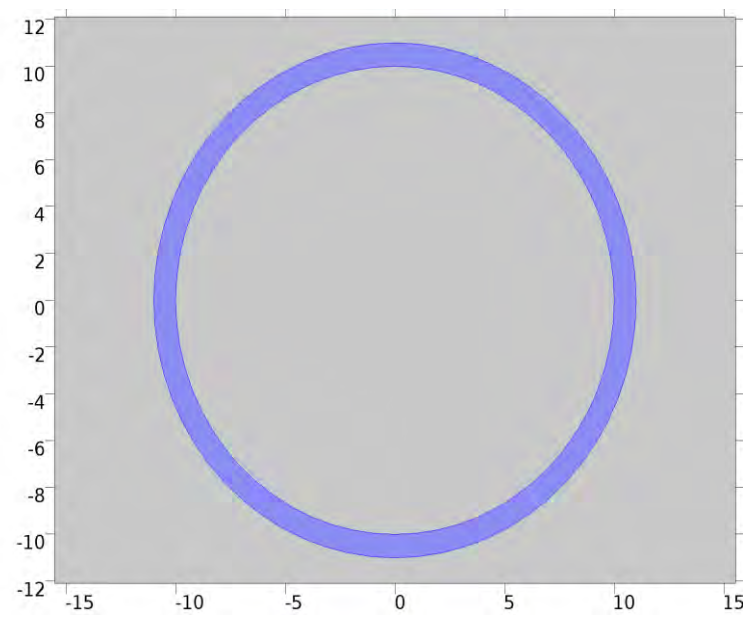


Figure A-1.5: Geometry of the modelled emitter for the 2D CTPV system

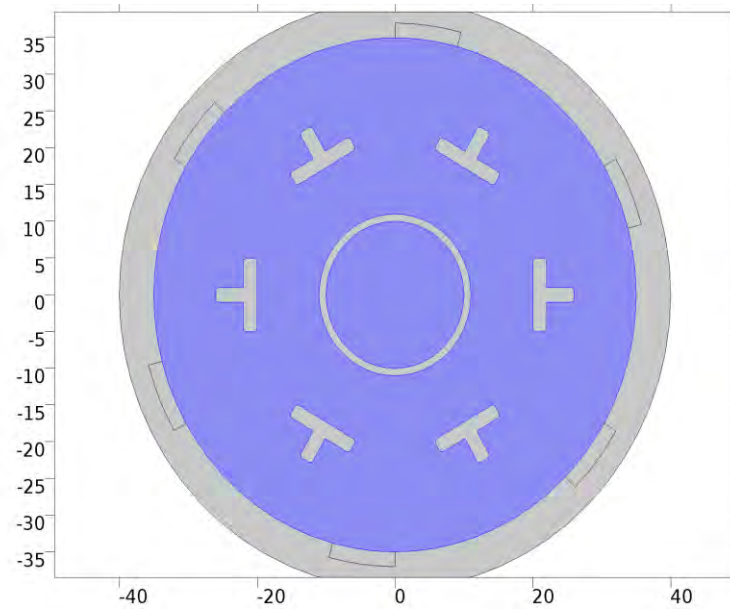


Figure A-1.6: Geometry of the modelled air for emitter cooling in a 2D CTPV system with six mirrors.

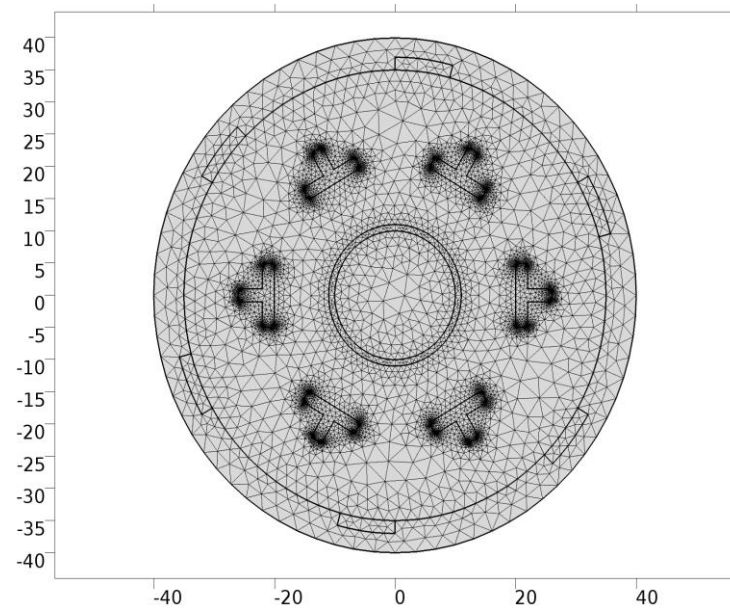


Figure A-1.7: Geometry of the meshing of various domains in CTPV system.

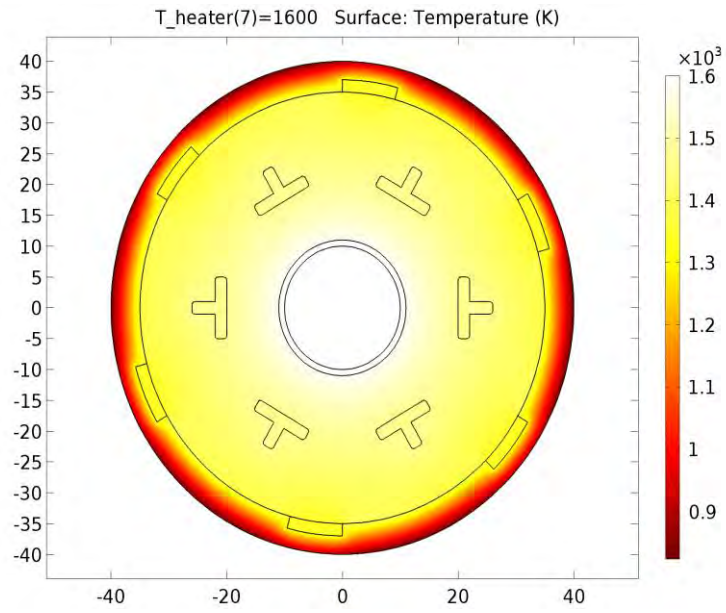


Figure A-1.8: Stationary temperature distribution of modelled 2D CTPV system with six mirrors/PV cells .

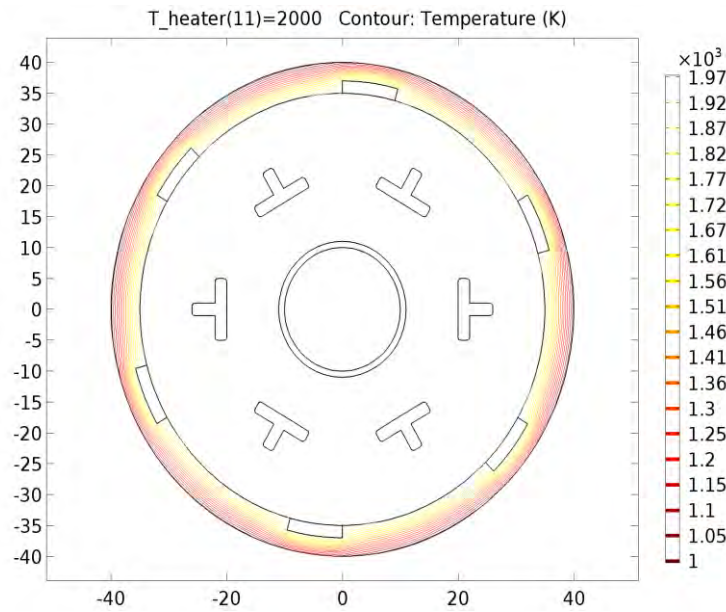


Figure A-1.9: The isothermal contours in 2D geometry with six mirrors and PV cells.

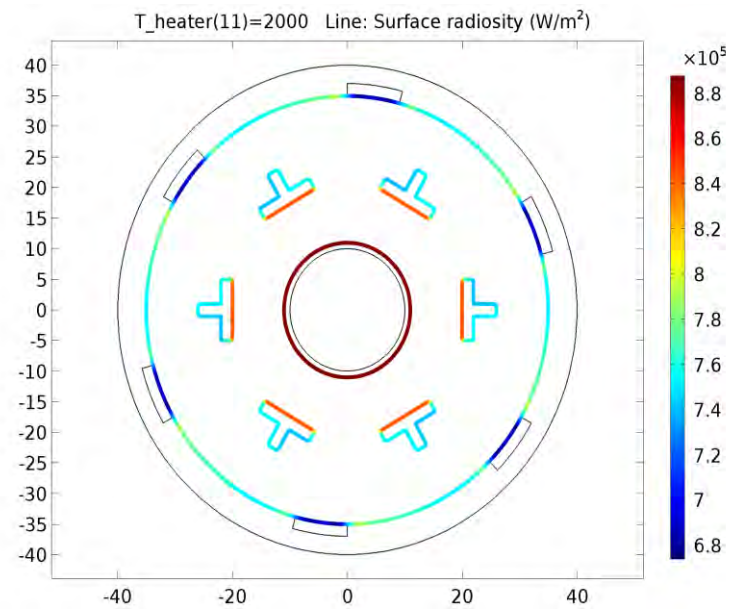


Figure A-1.10: Line surface radiosity of the modelled 2D, six mirrors CTPV system.

APPENDIX A-2: COMSOL generated report on 2D CTPV system with 10 mirrors configuration



Date	Oct 13, 2015 3:00:02 PM
------	-------------------------

Parameter

Name	Expression	Value	Description
T_heater	1000 [K]	1000 K	Temperature, emitter inner boundary

Variables

Name	Expression	Unit	Description
eta_pv	if($T < 1600$ [K] , $0.2 * (1 - (T / 800$ [K] - 1) ²), 0)		Voltaic efficiency, PV cell
q_out	ht.Gm*eta_pv	W/m ²	Electric output power

Geometry 1

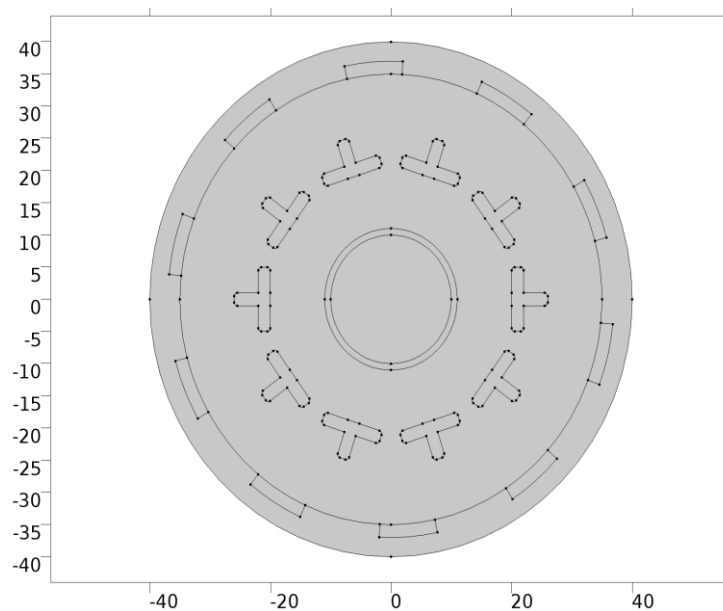


Figure A-2.1: Geometry of the concentrated thermal photovoltaics system in two-dimensions

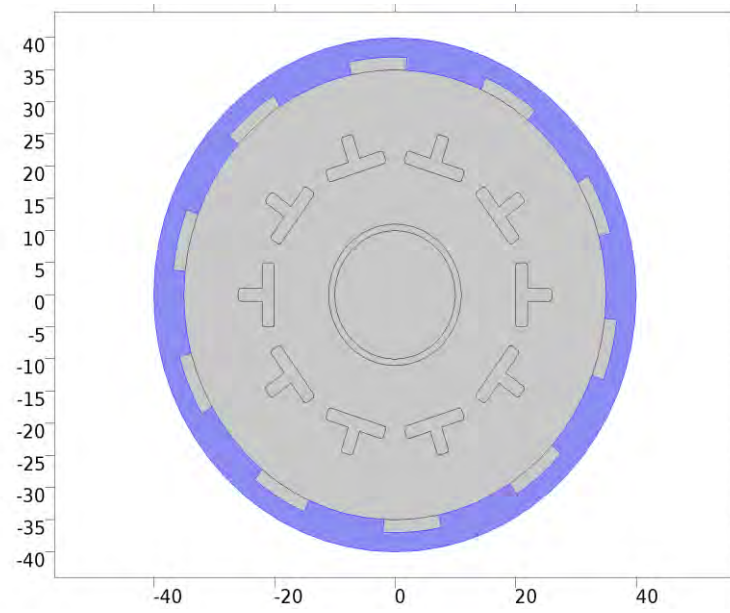


Figure A-2.2: Geometry of 2D CTPV system with ten cells and insulation around the PV cells.

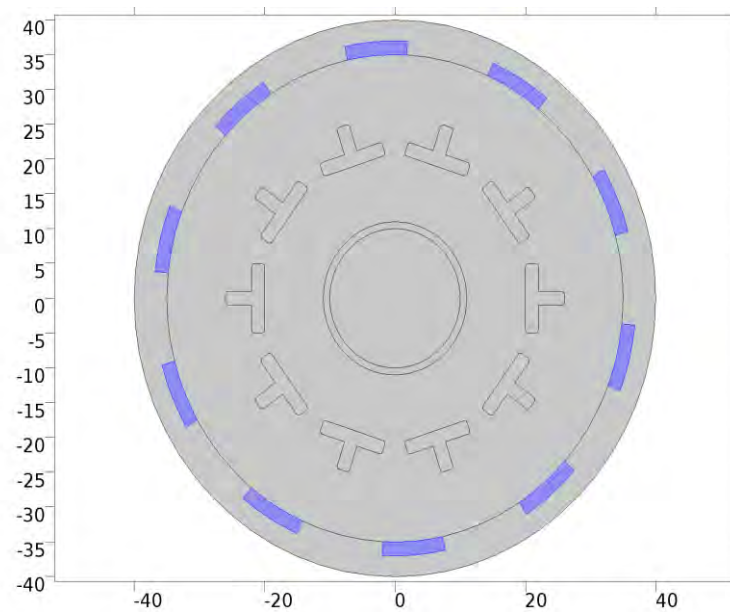


Figure A-2.3: Geometry of 2D CTPV system showing the PV cells (ten in number)

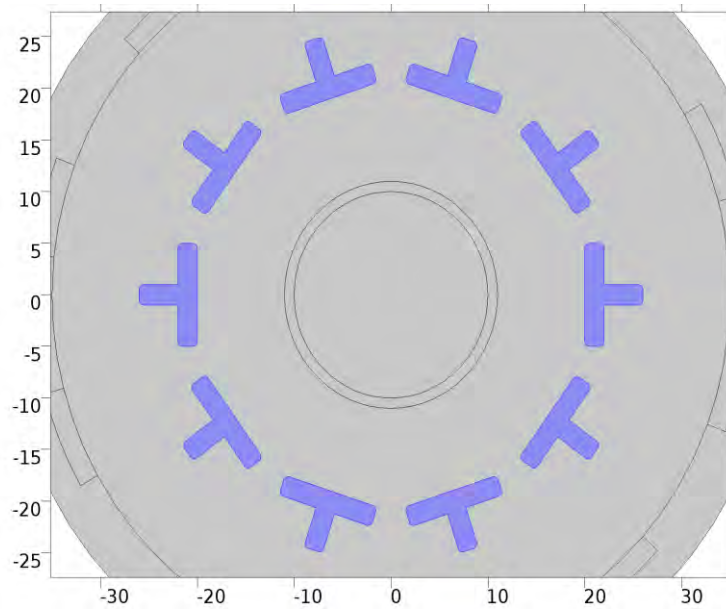


Figure A-2.4: Geometry of the 2D CTPV system showing the mirrors (ten in number)

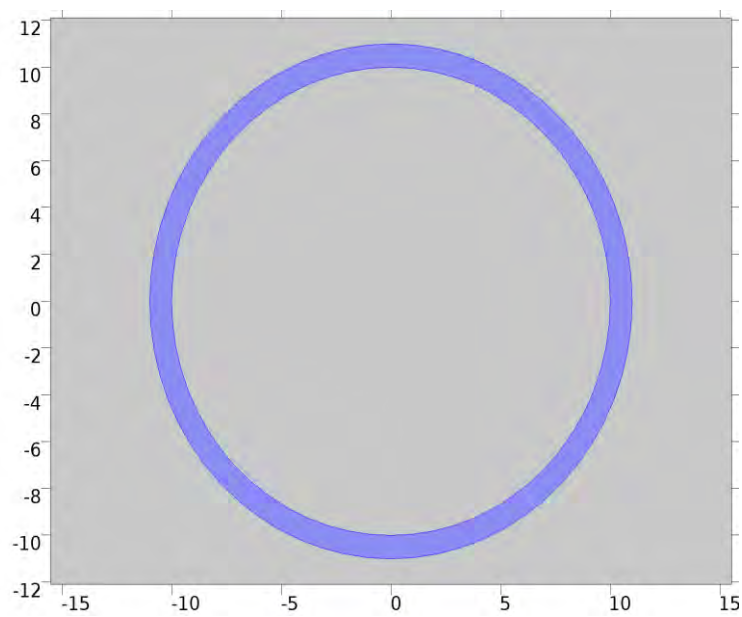


Figure A-2.5: Geometry of the emitter for the thermal photovoltaics system

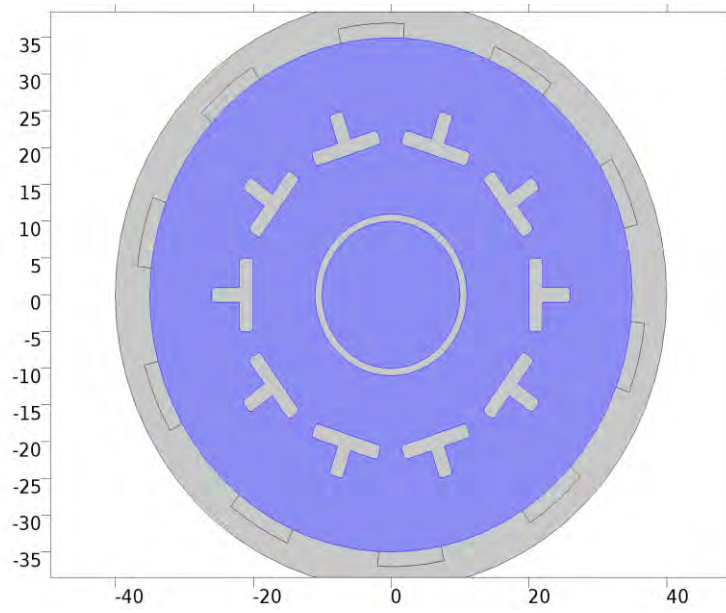


Figure A-2.6: Geometry of the air for cooling in the emitter and around the mirrors in a 2D CTPV system

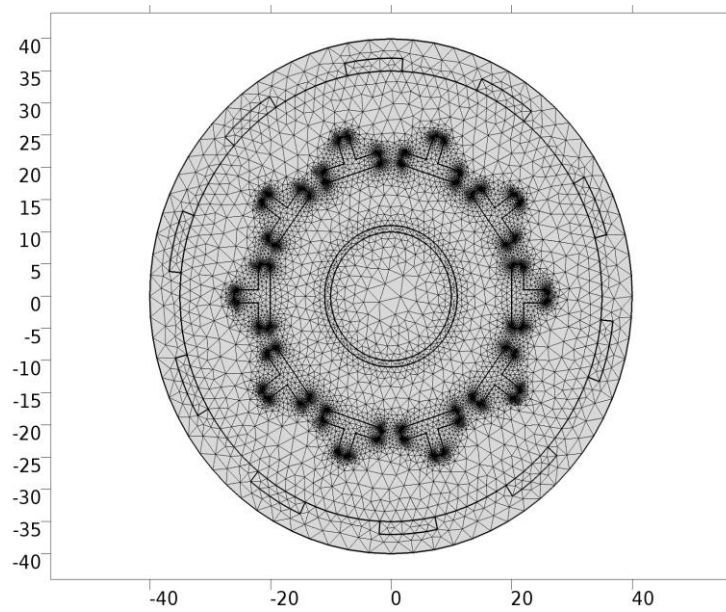


Figure A-2.7: Geometry of the meshing of various domains in 2D CTPV system with ten mirrors.

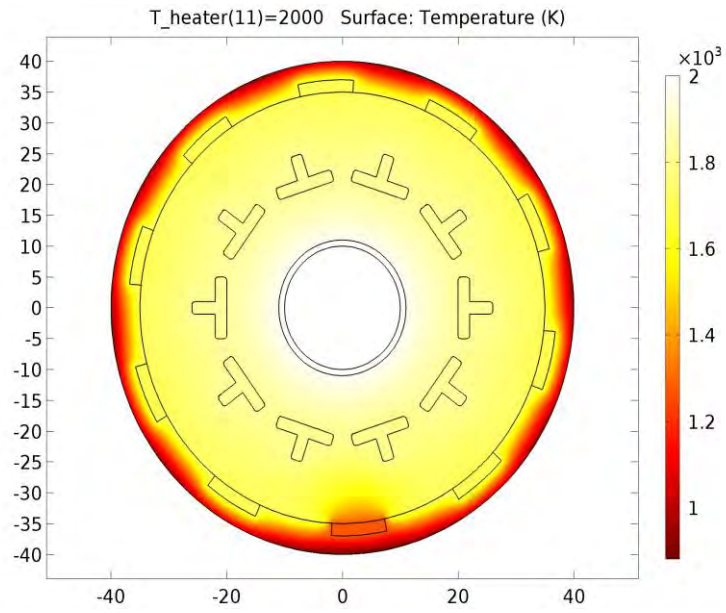


Figure A-2.8: Stationary temperature distribution of modelled 2D CTPV system with ten mirrors/PV

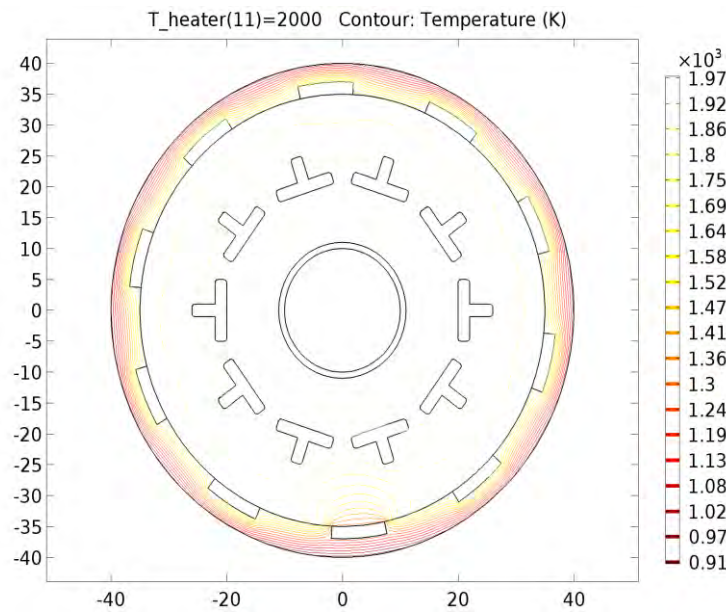


Figure A-2.9: The isothermal contours in 2D geometry with ten mirrors and PV cells

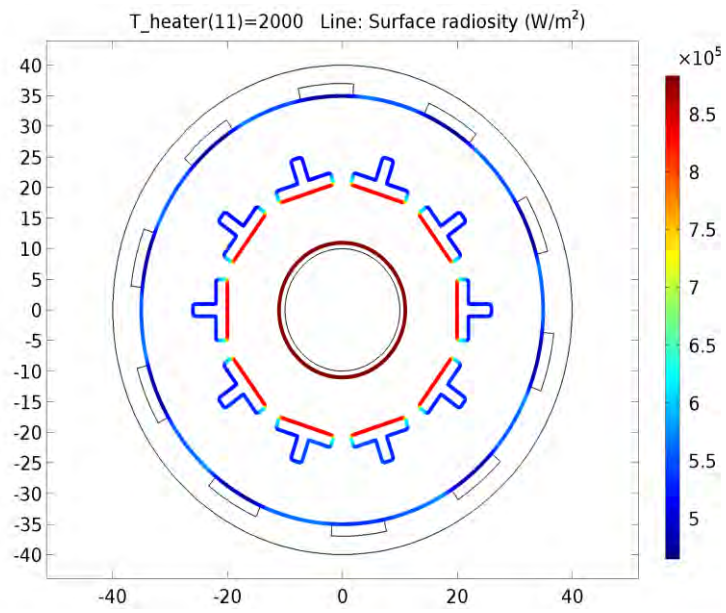


Figure A-2.10: Line surface radiosity of the modelled 2D CTPV system with ten pair mirrors/PV cells

APPENDIX A-3: COMSOL generated report on 3D CTPV system with 8 mirrors configuration



Parameter

Name	Expression	Value	Description
T_heater	2000 [K]	2000 K	Temperature, emitter inner boundary

Variables

Name	Expression	Unit	Description
eta_pv	$\text{if}(T < 1000[\text{K}], 0.2 * (1 - (T/500[\text{K}] - 1)^2), 0)$		Voltaic efficiency, PV cell
q_out	ht.Gm*eta_pv	W/m ²	Electric output power

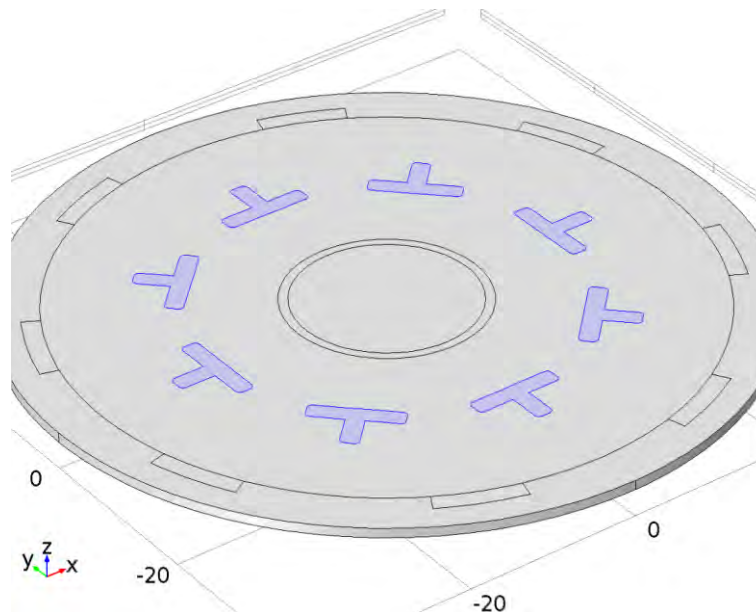


Figure A-3.1: Geometry of modelled 3D CTPV system showing the mirrors (eight in number)

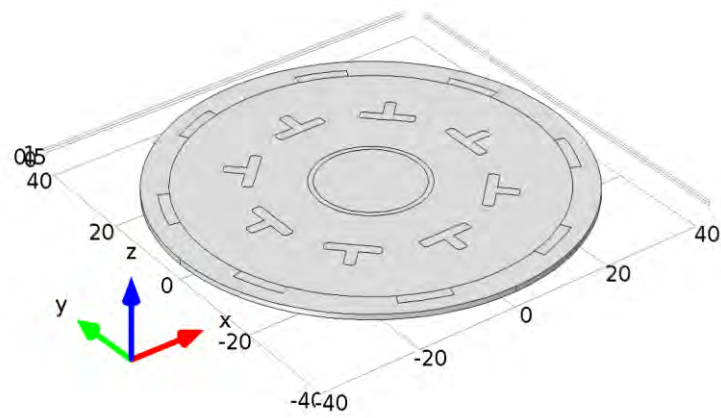


Figure A-3.2: Geometry of the modelled 3D CTPV system

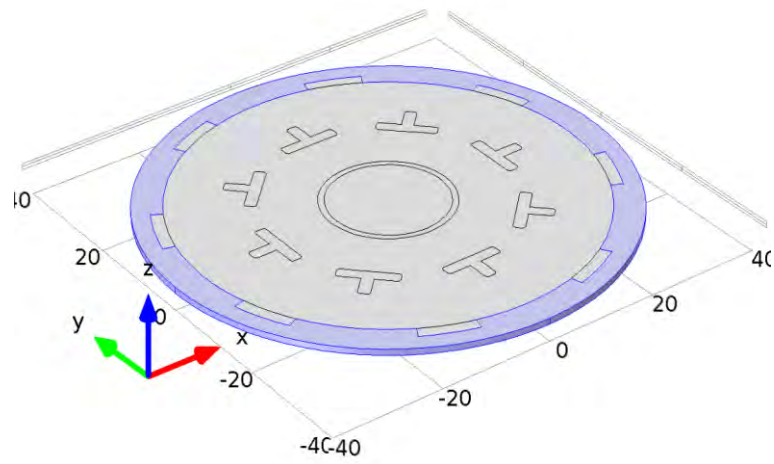


Figure A-3.3: Geometry of insulation of modelled 3D CTPV system in three-dimension

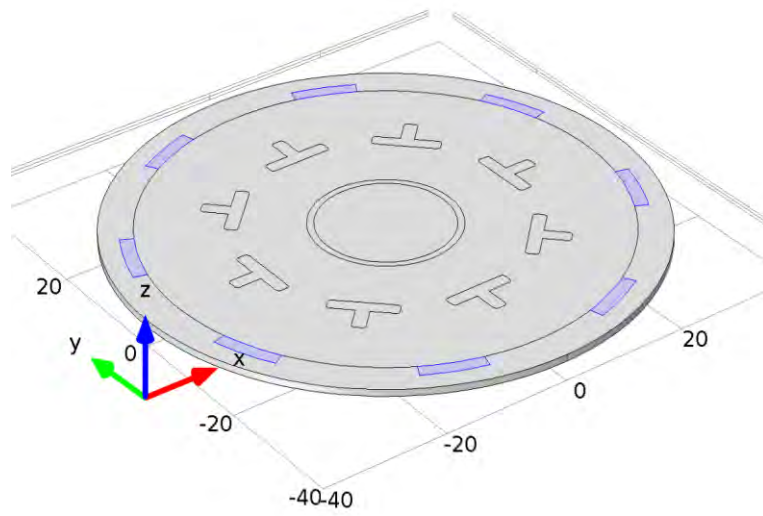


Figure A-3.4: Geometry of modelled 3D CTPV system

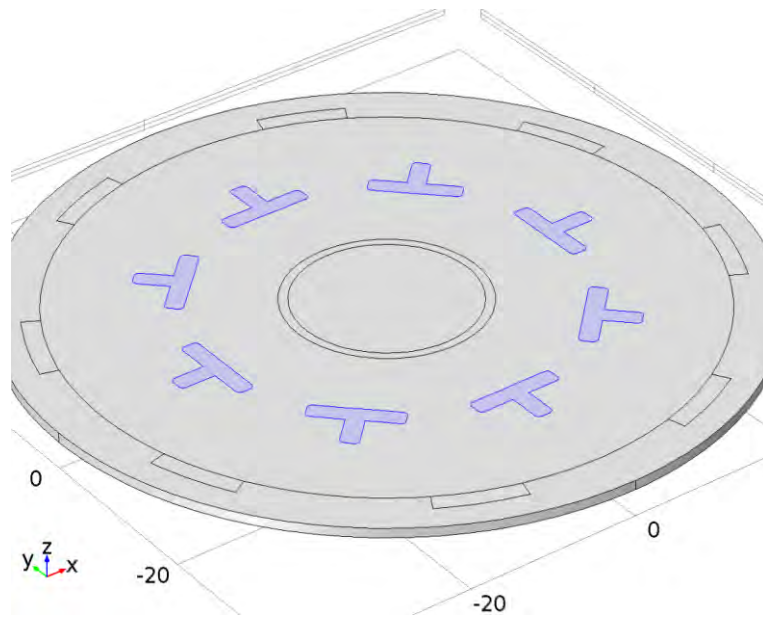


Figure A-3.5.: Geometry of the modelled 3D CTPV system showing the mirrors (eight in number)

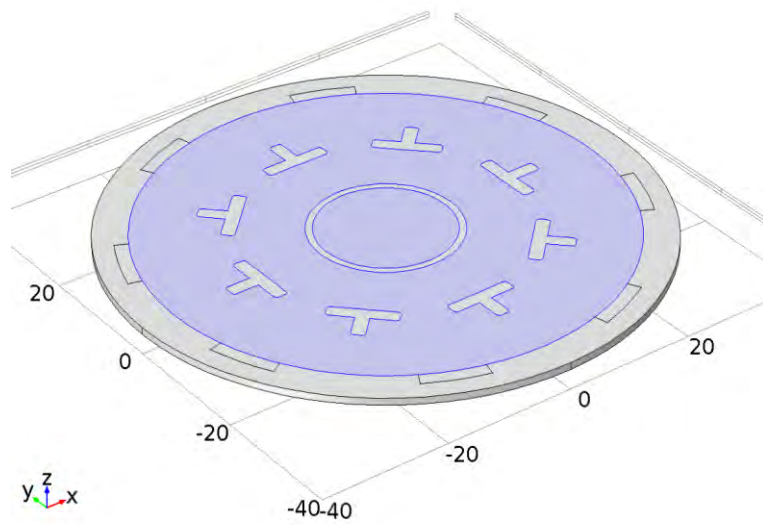


Figure A-3.6.: Geometry of the modelled 3D CTPV system showing the modelled air/fluid area

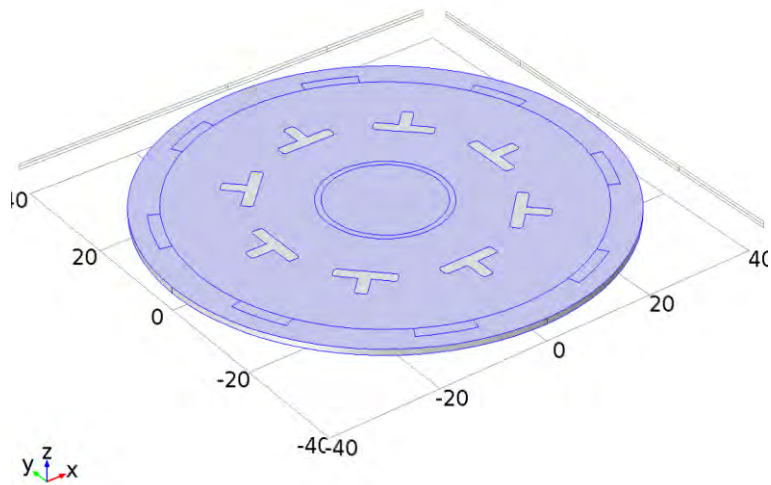


Figure A-3.7.: Geometry of the modelled CTPV system showing the modelled insulation

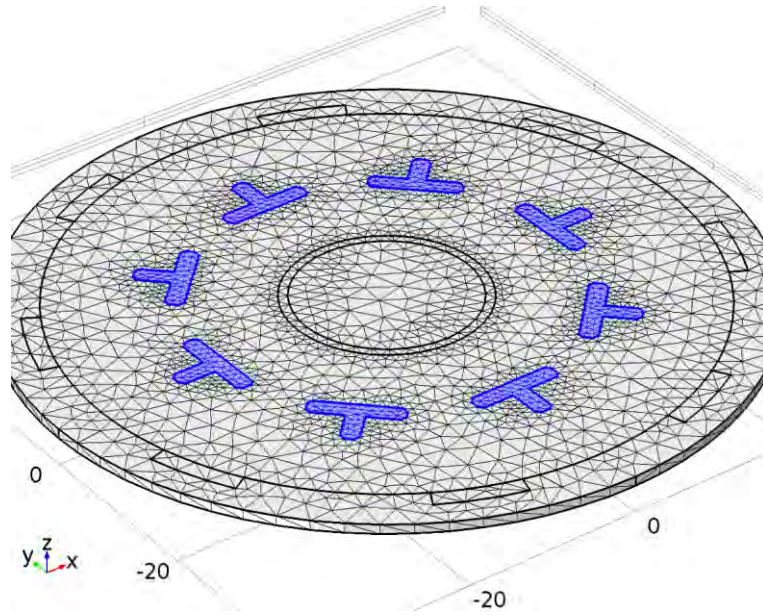


Figure A-3.8: Geometry of the meshed mirrors in the 3D CTPV system with eight mirrors

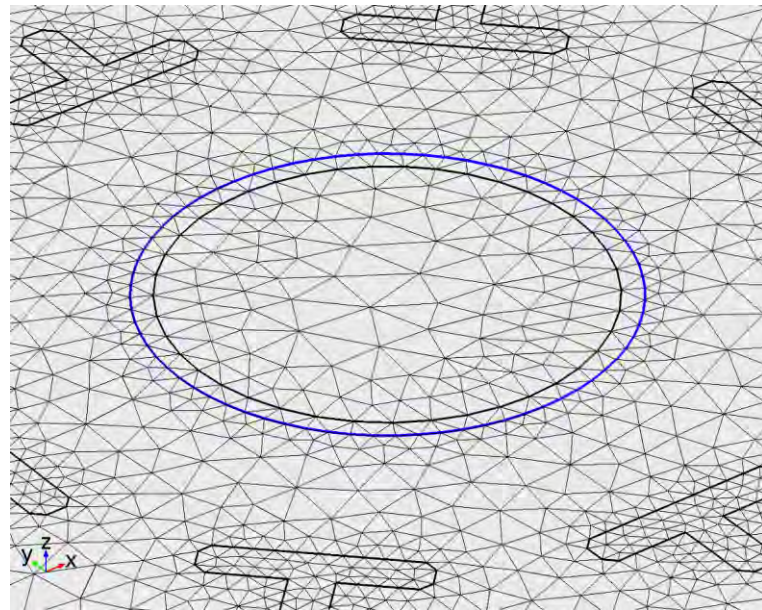


Figure A-3.9: Geometry of the meshed emitter in the 3D CTPV system with eight mirrors

Stationary Solver 1 in Solution 1 started at 25-Sep-2015 08:57:25.
Continuation solver
Nonlinear solver
Number of degrees of freedom solved for: 31957 (plus 30342 internal DOFs).

Continuation parameter T_heater = 2000.
Nonsymmetric matrix found.
Scales for dependent variables:
Temperature (compl.T): 21
Surface radiosity (compl.ht.J): 4.1e+002
Orthonormal null-space function used.

Iter	SolEst	ResEst	Damping	Stepsize	#Res	#Jac	#Sol	LinErr
LinRes								
1	56	2e+004	0.0100000	56	2	1	2	4.3e-
010 5.5e-015								
2	8.2	1.9e+004	0.0680977	8.5	3	2	4	2.3e-
010 5.7e-015								
3	9.8	1.8e+004	0.0295835	10	4	3	6	4.3e-
010 7.2e-015								
4	5.6	1.7e+004	0.0677666	5.9	5	4	8	3.5e-
010 8.1e-015								
5	5.2	1.6e+004	0.0568881	5.5	6	5	10	3.4e-
010 8.4e-015								
6	3.4	1.5e+004	0.0998460	3.7	7	6	12	2.9e-
010 8.1e-015								
7	2.5	1.3e+004	0.1250558	2.8	8	7	14	1.6e-
010 7.9e-015								
8	1.4	1.2e+004	0.2336303	1.7	9	8	16	8.1e-
011 4.9e-015								
9	0.55	1.5e+004	0.4684395	0.88	10	9	18	3.7e-
011 2.3e-015								
10	0.042	8.8e+003	1.0000000	0.36	11	10	20	3.8e-
011 1.2e-015								
11	0.00022	83	1.0000000	0.026	12	11	22	7.4e-
011 1.2e-015								

Continuation parameter T_heater = 2200.

Iter	SolEst	ResEst	Damping	Stepsize	#Res	#Jac	#Sol	LinErr
LinRes								
1	0.0056	3.2e+005	1.0000000	0.13	14	12	24	6e-
011 1.2e-015								
2	9.7e-006	1.2	1.0000000	0.0051	15	13	26	6.9e-
011 1.2e-015								

Continuation parameter T_heater = 2400.

Iter	SolEst	ResEst	Damping	Stepsize	#Res	#Jac	#Sol	LinErr
LinRes								
1	0.0042	2.2e+007	1.0000000	0.12	17	14	28	6.5e-
011 1.1e-015								
2	5.8e-006	0.94	1.0000000	0.0038	18	15	30	6.1e-
011 1.2e-015								

Continuation parameter T_heater = 2600.

Iter	SolEst	ResEst	Damping	Stepsize	#Res	#Jac	#Sol	LinErr
LinRes								
1	0.0033	3.4e+007	1.0000000	0.11	20	16	32	6.2e-
011 1.2e-015								
2	3.5e-006	0.75	1.0000000	0.003	21	17	34	5.5e-
011 1.2e-015								

Continuation parameter T_heater = 2800.

Iter	SolEst	ResEst	Damping	Stepsize	#Res	#Jac	#Sol	LinErr
LinRes								
1	0.0027	4.8e+007	1.0000000	0.097	23	18	36	5.7e-
011	1.1e-015							
2	2.4e-006	0.62	1.0000000	0.0025	24	19	38	8.4e-
011	1.1e-015							

Continuation parameter T_heater = 3000.

Iter	SolEst	ResEst	Damping	Stepsize	#Res	#Jac	#Sol	LinErr
LinRes								
1	0.0024	7e+007	1.0000000	0.089	26	20	40	4.7e-
011	1.2e-015							
2	1.8e-006	0.49	1.0000000	0.0023	27	21	42	4.6e-
011	1.2e-015							

Continuation parameter T_heater = 3200.

Iter	SolEst	ResEst	Damping	Stepsize	#Res	#Jac	#Sol	LinErr
LinRes								
1	0.0023	1.1e+008	1.0000000	0.082	29	22	44	4.1e-
011	1.2e-015							
2	1.7e-006	0.38	1.0000000	0.0022	30	23	46	3.7e-
011	1.3e-015							

Continuation parameter T_heater = 3400.

Iter	SolEst	ResEst	Damping	Stepsize	#Res	#Jac	#Sol	LinErr
LinRes								
1	0.0024	2e+008	1.0000000	0.077	32	24	48	2.9e-
011	1.2e-015							
2	2.3e-006	0.28	1.0000000	0.0023	33	25	50	1.3e-
011	1.8e-015							

Continuation parameter T_heater = 3600.

Iter	SolEst	ResEst	Damping	Stepsize	#Res	#Jac	#Sol	LinErr
LinRes								
1	0.0026	6e+008	1.0000000	0.072	35	26	52	2.3e-
011	1.4e-015							
2	4.2e-006	0.19	1.0000000	0.0027	36	27	54	1.3e-
011	2.5e-015							

Continuation parameter T_heater = 3800.

Iter	SolEst	ResEst	Damping	Stepsize	#Res	#Jac	#Sol	LinErr
LinRes								
1	0.0032	4.5e+008	1.0000000	0.069	38	28	56	1.2e-
011	1.6e-015							
2	9.1e-006	0.21	1.0000000	0.0033	39	29	58	2.3e-
011	2.1e-015							

Continuation parameter T_heater = 4000.

Iter	SolEst	ResEst	Damping	Stepsize	#Res	#Jac	#Sol	LinErr
LinRes								
1	0.0042	1.7e+008	1.0000000	0.068	41	30	60	6e-
012	1.6e-015							
2	2.5e-005	0.52	1.0000000	0.0045	42	31	62	2.1e-
011	2.3e-015							

Stationary Solver 1 in Solution 1: Solution time: 232 s (3 minutes, 52 second s)

Physical memory: 1.48 GB, Virtual memory: 1.58 GB

Plot Groups

Temperature (ht)

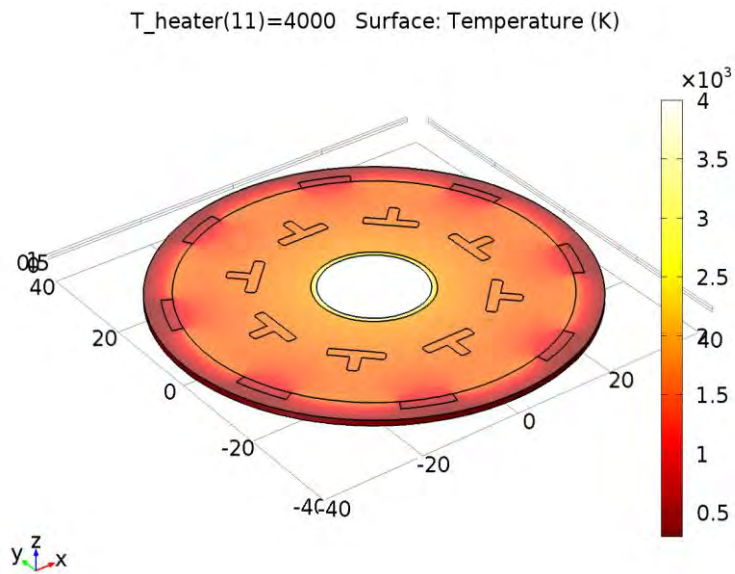


Figure A-3.10: Stationary temperature distribution of modelled 3D CTPV system with eight mirrors

Isothermal Contours (ht)

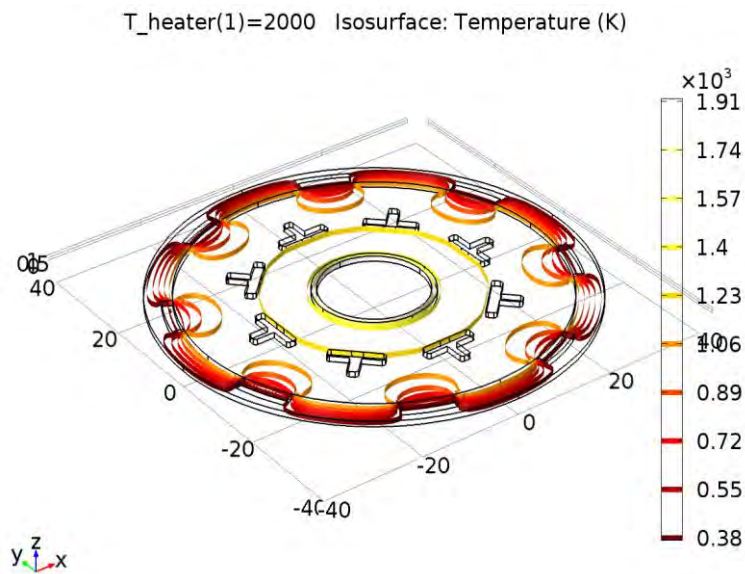


Figure A-3.11: Line surface isothermal of the modelled 3D, CTPV system with eight mirrors/PV cells

Radiosity (ht)

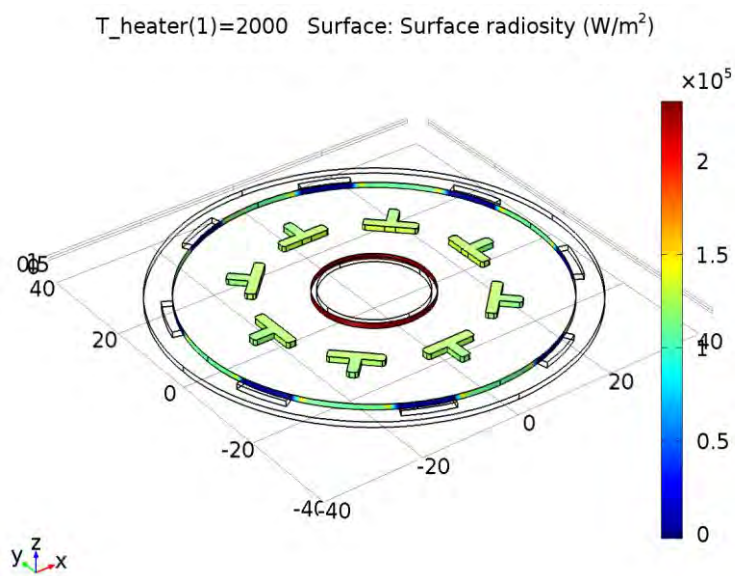


Figure A-3.12: Line surface radiosity of the modelled 3D, CTPV system with eight mirrors/PV cells.

APPENDIX B

APPENDIX B-1: Top 50 solar PV module efficiency

List of Top 50 solar PV high module efficiency				
	Company	Module Efficiency	Module Type	Cell Efficiency
1	Sunpower	20.40%	E20 / 333 SOLAR PANEL	22.80%
2	AUO Solar	19.50%	PM318B00	
3	Sanyo Electric	19.00%	HIT-N240SE10	21.60%
4	Jiawei	18.30%	JW-S100	21.01%
5	Crown Renewable Energy	18.30%	Summit 100LM	
6	JA Solar	16.84%	JAM5(L)-72-215/SI	19.10%
7	Trina Solar	16.40%	TSM-210DC80	18.10%
8	CNPV Solar	16.20%	CNPV-105M	18.80%
9	Yingli Solar	16.20%	Panda 265 Series	18.50%
10	Jetion	16.20%	JT315SAc	18.30%
11	LG Solar	16.20%	LG260S1C	
12	China Sunergy	16.06%	CSUN205-72M	19.00%
13	ET Solar	16.06%	ET-M572205 205W	18.94%
14	Hareon Solar	16.06%	HR-205W	18.80%
15	Suniva	16.00%	Optimus 260	19.20%
16	Siliken	16.00%	SLK60M6L 260Wp	
17	Topray	15.80%	SLSM-180D 305W	
18	FVG	15.75%	FVG 84-125 230W	17.90%
19	Group Dmegc Magnetics	15.73%	DM255-M156-6	18.00%
20	Sunrise Solartech	15.70%	SR-M572200-1	18.50%
21	Suntech	15.70%	PLUTO200-Ade	19.00%
22	Jinko Solar	15.67%	JKM-200M (R165)	18.25%
23	Risen	15.66%	SYP200S-M	
24	Frankfurt CS Solar	15.66%	FS 200W MON	
25	Chaori	15.66%	CRM200S 125M-7	
26	Eopllly New Energy	15.66%	125M/72-200	
27	Era Solar	15.66%	ESPSA 200	
28	CETC	15.60%	ZKX-200D-24	18.00%
29	Silfab	15.60%	SLA255M	
30	Topsola	15.53%	TSM60-156M	17.82%
31	Bisol	15.40%	BMO/25	17.20%
32	Hanwha SolarOne	15.30%	SF160	16.50%
33	Astronergy	15.30%	CHSM5612M 195	
34	DelSolar	15.30%	D6M_B3A-WT series 250	
35	Perlight	15.27%	PLM-250/24	18.00%
36	JMS Solar	15.27%	JMS-CS 180M 195	
37	Mage Solar	15.25%	Mage Powertec Plus 255/5 MR	17.80%
38	Solon	15.24%	SOLO Black 230/07	
39	PV Power Technologies	15.12%	SM-240MH0	
40	Renesola	15.06%	JC245S-24/Bb	
41	Schüco	14.90%	SPV 210 SMAU-1	
42	Aleo Solar	14.90%	S19.245	
43	Eging	14.90%	EGM 190	

	Company	Module	Module Type	Cell Efficiency
44	Astom	14.88%	ASH190m-72	
45	Sun Earth Solar Power	14.88%	Sun Earth M 190W	
46	Hyundai	14.80%	HiS-S215 SF	
47	Win Win Precision	14.73%	WSP-245M6	
48	Kioto Photovoltaics	14.72%	KPV 220 M	
49	Sharp Solar	14.70%	NU-U240F2	
50	Solar-Fabrik	14.70%	Premium L-Mono 245	

APPENDIX B-2: YINGLI MONO 260 SERIES SOLAR PANEL

SOLAR PV ELECTRICAL SPECIFICATIONS



Yingli Mono 260 Series



YL260C-30b YL255C-30b YL250C-30b YL245C-30b



Yingli Solar High Efficiency Monocrystalline Module

ABOUT YINGLI SOLAR

- » The first renewable energy company and the first Chinese company to sponsor FIFA World Cup™
- » Publicly listed on the New York Stock Exchange (NYSE: YGE)
- » One of the leading fully vertically integrated PV manufacturers in the world
- » The first Chinese company to receive Social Accountability System SA 8000 Certification

HIGH PERFORMANCE

- » Industry leading in-house manufacturing of polysilicon, ingots, wafers, cells and modules ensures tight control of our material and production quality.
- » Combined with high transmission glass, high efficiency monocrystalline solar cells deliver module efficiency of up to 15.9%, reducing installation costs and maximizing the kWh output per unit area.
- » Power tolerance of +/-3% minimizes PV system mismatch losses.

QUALITY & RELIABILITY

- » Robust aluminum frames ensure maximum mechanical load up to 5,400Pa
- » Manufactured in our new state-of-the-art production line
- » Manufacturing facilities certified by TÜV Rheinland to ISO 9001:2008, ISO 14001:2004 and BS OHSAS 18001:2007

* In compliance with our Warranty Terms and Conditions

WARRANTIES

- » 5-year limited product warranty*
- » Limited power warranty*: 10 years at 90% of the minimal rated power output, 25 years at 80% of the minimal rated power output

QUALIFICATIONS AND CERTIFICATES

» ISO 9001:2008, ISO 14001:2004, BS OHSAS 18001:2007, SA 8000







www.yinglisolar.com




Official Sponsor of the 2010 FIFA World Cup™

Yingli Mono 260 Series

ELECTRICAL PARAMETERS

Electrical parameters at STC (1,000 W/m², 25°C, AM 1.5 according to EN 60904-3)

Module type		YL245C-30b	YL250C-30b	YL255C-30b	YL260C-30b
Power output	[W]	245.0	250.0	255.0	260.0
Power output production tolerances	[%]	+/- 3	+/- 3	+/- 3	+/- 3
Module efficiency	[%]	15.0	15.3	15.6	15.9
Voltage at P _{max} , V _{mp}	[V]	30.4	30.5	30.6	30.8
Current at P _{max} , I _{mp}	[A]	8.07	8.20	8.33	8.46
Open circuit voltage V _{oc}	[V]	38.1	38.1	38.2	38.6
Short circuit current I _{sc}	[A]	8.59	8.71	8.85	8.91
Limiting reverse current I _r	[A]			20	
Max. system voltage	[V]			1,000 VDC	

Electrical parameters at NOCT (800 W/m², AM 1.5, wind velocity 1m/s, Tamb 20°C)

NOCT (Nominal Operating Cell Temperature)	[°C]			46 +/- 2	
Voltage at P _{max} , V _{mp}	[V]	27.5	27.6	27.7	27.8
Current at P _{max} , I _{mp}	[A]	6.48	6.58	6.68	6.79
Open circuit voltage V _{oc}	[V]	35.1	35.1	35.2	35.5
Short circuit current I _{sc}	[A]	6.92	7.02	7.13	7.18

Thermal characteristics

Temperature coefficient beta of I _{sc}	[%/K]			+ 0.04	
Temperature coefficient alpha of V _{oc}	[%/K]			- 0.33	
Temperature coefficient gamma of P _{mp}	[%/K]			- 0.45	

MECHANICAL PARAMETERS

Dimensions (length [mm] / width [mm] / thickness [mm])		1,650 / 990 / 50
Frame height [mm]		50
Weight [kg]		19.5
Front cover (material / thickness [mm])		Tempered Glass, 3.2mm
Cell type (quantity / technology / dimensions)		60 / c-Si, Monocrystalline / 156 x 156
Encapsulation materials		Ethylene Vinyl Acetate (EVA)
Rear cover (material)		Laminated Polymer Plastic
Frame (material)		Robust Anodized Aluminum Alloy

Junction box, cable & connector configuration

		Configuration is available with 2 different connector types
Junction box (protection degree)		IP65
Junction box dimensions (length / width / thickness [mm])		151 / 122 / 25
Positive cable & negative cable (length [mm] / cable cross-section [mm ²])		1,200(900) / 4.0
Connector (type / protection degree)	05-i / IP67	MC / MC4 / IP67

OPERATING CONDITIONS

Operating temperature [°C]	- 40 to + 85
Max. wind load / Max. snow load [Pa]	2.4K / 5.4K
Reduction of efficiency from an irradiance of 1,000 W/m ² to 200 W/m ² (T _{module} = 25 °C) according to EN 60904-1	5%

PACKAGING

Number of modules per box	20
Box size (length / width / depth [mm])	1,700 / 1,150 / 1,190
Box Gross weight in kg	427
Boxes per pallet	1

* The data does not refer to a single module and they are not part of the offer, they serve for comparison only to different module types.

Subject to modifications and errors

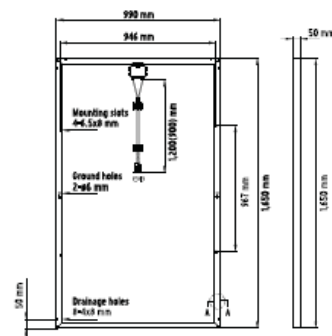
Yingli Green Energy Holding Co. Ltd.
commerce@yinglisolar.com
0086 - (0)312 - 8929802

www.yinglisolar.com



Electrical equipment, check with your installer

Before installation, please check the installation manual provided with the product.



MANUFACTURER'S SPECIFICATION OF THE MODELLED SOLAR PANEL

Electrical specification of the modelled Yingli Mono 260 Series PV solar panel

Module type	YL260C-30b
Power output [W]	260.0
Power output production tolerances [%]	+/-3
Module efficiency [%]	15.9
Voltage at P_{max} , V_{mpp} [V]	30.8
Current at P_{max} , I_{mpp} [A]	8.46
Open circuit voltage V_{oc} [V]	38.6
Short circuit current I_{sc} [A]	8.91
Limiting reverse current I_r [A]	20
Max. system voltage [V]	1,000 VDC
Maximum Series Fuse rating	15 A
Temperature Coefficient of P_{mpp}	-0.45% / °C
Temperature Coefficient of V_{oc}	-0.33% / °C
Temperature Coefficient of I_{sc}	0.06% / °C

APPENDIX B-3: SUNPOWER SOLAR PV ELECTRICAL SPECIFICATIONS



SunPower® X-Series Residential Solar Panels | X21-335-BLK | X21-345

More than 21% Efficiency

Ideal for roofs where space is at a premium or where future expansion might be needed.

Maximum Performance

Designed to deliver the most energy in demanding real world conditions, in partial shade and hot rooftop temperatures.^{1,2,4}

Premium Aesthetics

SunPower® Signature™ Black X-Series panels blend harmoniously into your roof. The most elegant choice for your home.



Maxeon® Solar Cells: Fundamentally better. Engineered for performance, designed for durability.

Engineered for Peace of Mind

Designed to deliver consistent, trouble-free energy over a very long lifetime.^{3,4}

Designed for Durability

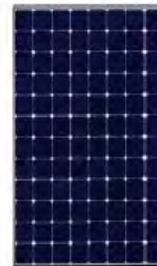
The SunPower Maxeon Solar Cell is the only cell built on a solid copper foundation. Virtually impervious to the corrosion and cracking that degrade Conventional Panels.³

Same excellent durability as E-Series panels.
#1 Rank in Fraunhofer durability test.⁹
100% power maintained in Atlas 25+ comprehensive Durability test.¹⁰

Unmatched Performance, Reliability & Aesthetics



SIGNATURE™ BLACK
SPR-X21-335-BLK



SPR-X21-345



Highest Efficiency⁵

Generate more energy per square foot

X-Series residential panels convert more sunlight to electricity producing 38% more power per panel,¹ and 70% more energy per square foot over 25 years.^{1,2,3}

Highest Energy Production⁶

Produce more energy per rated watt

High year one performance delivers 8-10% more energy per rated watt.² This advantage increases over time, producing 21% more energy over the first 25 years to meet your needs.³





SunPower® X-Series Residential Solar Panels | X21-335-BLK | X21-345

Sunpower Offers The Best Combined Power And Product Warranty



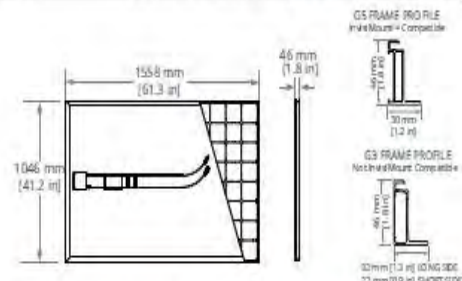
Electrical Data	
	SPR-X21-335-BLK SPR-X21-345
Nominal Power (P _{nom}) ¹¹	335 W 345 W
Power Tolerance	+5/-0% +5/-0%
Avg. Panel Efficiency ¹²	21.0% 21.5%
Rated Voltage (V _{mpp})	57.3 V 57.3 V
Rated Current (I _{mpp})	5.85 A 6.02 A
Open-Circuit Voltage (V _{oc})	67.9 V 68.2 V
Short-Circuit Current (I _{sc})	6.23 A 6.39 A
Max. System Voltage	600 V UL & 1000 V IEC
Maximum Series Fuse	15 A
Power Temp. Coef.	-0.30% / °C
Voltage Temp. Coef.	-167.4 mV / °C
Current Temp. Coef.	3.5 mA / °C

REFERENCES:

- 1 All comparisons are SPR-X21-345 vs. a representative conventional panel; 250W, approx. 1.6 m², 15.3% efficiency.
- 2 Typically 8-10% more energy per watt, BSW/ENR Engineering "SunPower Yield Report," Jan 2013.
- 3 SunPower 0.25%/yr degradation vs. 1.0%/yr conv. panel; Campeau, Z. et al. "SunPower Module Degradation Rate," SunPower white paper, Feb 2013; Jordan, Dirk "SunPower Test Report," NREL, Q1 2015.
- 4 "SunPower Module 40-Year Useful Life" SunPower white paper, May 2015. Useful life is 99 out of 100 panels operating at more than 70% of rated power.
- 5 Highest of over 3,200 silicon solar panels, Photon Module Survey, Feb 2014.
- 6 1% more energy than E-Series panels, 8% more energy than the average of the top 10 panel companies tested in 2012 (151 panels, 102 companies), Photon International, Feb 2013.
- 7 Compared with the top 15 manufacturers' SunPower Warranty Review, May 2015.
- 8 Some restrictions and exclusions may apply. See warranty for details.
- 9 X-Series same as E-Series, 5 of top 8 panel manufacturers tested in 2013 report, 3 additional panels in 2014; Ferrara, C., et al. "Fraunhofer IZD Durability Initiative for Solar Modules: Part 2," Photovoltaics International, 2014.
- 10 Compared with the non-stress-tested control panel, X-Series same as E-Series, tested in Atlas 25+ Durability test report, Feb 2013.
- 11 Standard Test Conditions (1000 W/m² irradiance, AM 1.5, 25° C). NREL calibration Standard: SOMS current, IACCS FF and Voltage.
- 12 Based on average of measured power values during production.
- 13 Type 2 fire rating per UL1709/2013, Class C fire rating per UL1703/2002.
- 14 See sales person for details.

Tests And Certifications	
Standard tests ¹³	UL1703 (Type 2 Fire Rating), IEC 61215, IEC 61730
Quality Certs	ISO 9001:2008, ISO 14001:2004
EHS Compliance	RoHS, OHSAS 18001:2007, lead free, REACH SVHC-155, PV Cycle
Sustainability	Cradle to Cradle (eligible for LEED points) ¹⁴
Ammonia test	IEC 62716
Desert test	10.1109/PVSC.2013.6744437
Salt Spray test	IEC 61701 (maximum severity)
PID test	Potential-Induced Degradation free: 1000V ⁹
Available listings	UL, CEC, TUV, MCS, FSEC

Operating Condition And Mechanical Data	
Temperature	-40°F to +185°F (-40°C to +85°C)
Impact resistance	1 inch (25mm) diameter hail at 52 mph (23 m/s)
Appearance	Class A+
Solar Cells	96 Monocrystalline Maxeon Gen III
Tempered Glass	High transmission tempered Anti-Reflective
Junction Box	IP-65, MC4 Compatible
Weight	41 lbs (18.6 kg)
Max load	G5 Frame: Wind: 62 psf, 3000 Pa, 305 kg/m ² front & back Snow: 125 psf, 6000 Pa, 611 kg/m ² front
	G3 Frame: Wind: 50 psf, 2400 Pa, 244 kg/m ² front & back Snow: 112 psf, 5400 Pa, 550 kg/m ² front
	Frame Class 1 black anodized (highest AAMA rating)



G5 frames have no mounting holes. Please read the safety and installation guide.

Document # 504828 Rev E ATR, US

See <http://www.sunpower.com/facts> for more reference information.
For more details, see extended datasheet: www.sunpower.com/datasheets.

©May 2015 SunPower Corporation. All rights reserved. SUNPOWER, the SUNPOWER logo, MAXEON, and SIGNATURE are trademarks or registered trademarks of SunPower Corporation. Specifications included in this datasheet are subject to change without notice.

SUNPOWER®

APPENDIX B-4: YINGLI SOLAR PANEL SIMULATION REPORT

Name	Expression	Value	Description
W_PVCell	156[mm]	0.156 m	PV Cell Width
W_Panel	5*W_PVCell	0.78 m	Width of Eight PV Cells
H_PV	46[mm]	0.046 m	PV Panel Thickness
T_Amb	298.15[K]	298.15 K	Ambient Air Temperature
T_Init	298.15[K]	298.15 K	Initial Cell Temperature
T_Room	298.15[K]	298.15 K	Room Temperature
Emissivity	0.6	0.6	Emissivity of Silicon
HX_Silicon	10.52 [W/(m ² *K)]	10.52 W/(m ² ·K)	Silicon/Air Heat Transfer Coefficient
PVEFF0	0.159	0.159	PV Cell Efficiency at Room Temperature
PVdeg	0.0045 [1/K]	0.0045 1/K	PV Cell Degradation with Temperature
Q_Sun	1000[W/m ²]	1000 W/m ²	Sun Incident Radiation
A	1.11[m ²]	1.11 m ²	Area of PV Panel
P_in	Q_Sun*A	1110 W	Power in
V_mpp	31.83[V]	31.83 V	Max Output Voltage at Max. Power Point
I_mpp	8.186[A]	8.186 A	Max Output Current at Max. Power Point
V_pv	0.056[m ³]	0.056 m ³	Volume of the PV Panel

Variables being investigated – The Modelling/Simulation Expected Output

Name	Expression	Unit	Description
PVEFF	$PVEFF0 \cdot (1 - PVdeg \cdot (T - T_{Init}))$		PV Cell Efficiency Temp. Dependence
Q_Heat	$Q_{Sun} \cdot (1 - PVEFF)$	W/m ²	Sun's Energy Converted to Heat
ThermEFF	$(V_{mpp} \cdot I_{mpp}) / (Q_{Sun} \cdot A)$		Thermal Efficiency
EFF_Net	$PVEFF + ThermEFF$		Overall Efficiency
q_out	$ht.Gm \cdot \eta_{pv}$	W/m ²	Electrical Output Power
η_{pv}	$if(T < 368.15 \text{ [K]}, 0.159 \cdot (1 - (T / 298.15 \text{ [K]} - 1)^2), 0.15)$		Voltaic efficiency, PV cell

Variables of the modelled domains

Name	Expression	Unit	Description	Selection
ht.J0	ht.J	W/m ²	Surface radiosity	Boundaries 19, 21–22, 925
ht.rflux	ht.ds2.rflux	W/m ²	Radiative heat flux	Boundaries 19, 21–22, 925
ht.T	$if(ht.opaqueLayer == 1, if(down(ht.opaque) == 1, ht.Tu, ht.Td), if(down(ht.opaque) == 1, ht.Td, ht.Tu))$	K	Temperature	Boundaries 19, 21–22, 925
ht.epsilon_rad	$subst(0.1, T, at2(x, y, z, ht.T))$	1	Surface emissivity	Boundaries 19, 21–22, 925
ht.Tamb	T	K	Ambient temperature	Boundaries 19, 21–22, 925
ht.G_ext	$ht.G_{ext_u} + ht.G_{ext_d}$	W/m ²	External irradiation	Boundaries 19, 21–22, 925
ht.G_rad	$ht.Gm + ht.Gamb + ht.G_{ext}$	W/m ²	Surface irradiation	Boundaries 19, 21–22, 925
ht.Famb_gp	$root.compl.ht.radGpEval(ht.Famb)$	1	Ambient view factor, Gauss	Boundaries 19, 21–22,

Name	Expression	Unit	Description	Selection
			point evaluation	925
ht.Jinit	$ht.feb(ht.T_{init}) * ht.epsilon_rad + (1 - ht.epsilon_rad) * ht.e_bamb$	W/m ²	Initial surface radiosity	Boundaries 19, 21–22, 925
ht.Jdef	$ht.epsilon_rad * ht.e_b$	W/m ²	Surface radiosity expression	Boundaries 19, 21–22, 925
ht.e_b	$ht.feb(ht.T)$	W/m ²	Blackbody emissive power	Boundaries 19, 21–22, 925
ht.e_bamb	$ht.feb(ht.T_{amb})$	W/m ²	Ambient blackbody emissive power	Boundaries 19, 21–22, 925
ht.Gamb	$ht.F_{amb} * ht.e_bamb$	W/m ²	Ambient irradiation	Boundaries 19, 21–22, 925
ht.alpha_rad	$ht.epsilon_rad$	1	Absorptivity	Boundaries 19, 21–22, 925
ht.rho_r	$1 - ht.epsilon_rad$	1	Reflectivity	Boundaries 19, 21–22, 925
ht.J_plot	$try_catch(ht.J, NaN)$	W/m ²	Surface radiosity	Boundaries 19, 21–22, 925
ht.Ju_plot	$try_catch(J_u, NaN)$	W/m ²	Upside radiosity	Boundaries 19, 21–22, 925
ht.Jd_plot	$try_catch(J_d, NaN)$	W/m ²	Downside radiosity	Boundaries 19, 21–22, 925
ht.ds2.rflux	$-ht.J_{def} + ht.epsilon_rad * ht.G_rad$	W/m ²	Radiative heat flux	Boundaries 19, 21–22, 925

Shape functions

Name	Shape function	Unit	Description	Shape frame	Selection
ht.J	Lagrange (Linear)	W/m ²	Surface radiosity	Material	Boundaries 19, 21–22, 925

Weak expressions

Weak expression	Integration frame	Selection
$(ht.J_{def} - ht.J + (1 - ht.\epsilon_{rad}) * ht.G_{rad}) * test(ht.J)$	Material	Boundaries 19, 21–22, 925
$ht.ds2.rflux * test(ht.T) * ht.Pc$	Material	Boundaries 19, 21–22, 925

Diffuse Surface 3

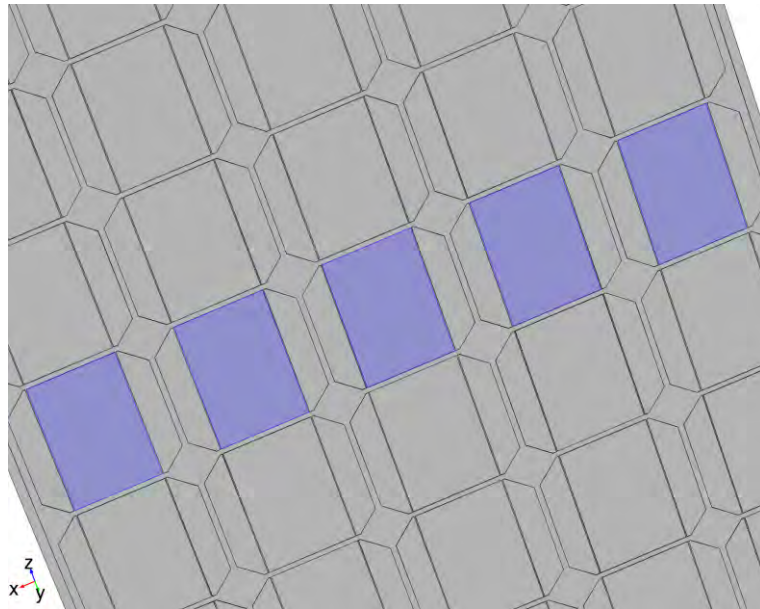


Figure B-4: Diffuse surface geometry of modelled 3D PV system with 5 PV cells.

Variables of the modelled domains in Yingli solar PV panel

Name	Expression	Unit	Description	Selection
ht.J0	ht.J	W/m ²	Surface radiosity	Boundaries 134, 310, 486, 662, 838
ht.rflux	ht.ds3.rflux	W/m ²	Radiative heat flux	Boundaries 134, 310, 486, 662, 838
ht.T	if(ht.opaqueLayer==1,if(down(ht.opaque)==1,ht.Tu,ht.Td),if(down(ht.opaque)==1,ht.Td,ht.Tu))	K	Temperature	Boundaries 134, 310, 486, 662, 838
ht.epsilon_rad	subst(0.6,T,at2(x,y,z,ht.T))	1	Surface emissivity	Boundaries 134, 310, 486, 662, 838
ht.Tamb	T	K	Ambient temperature	Boundaries 134, 310, 486, 662, 838
ht.G_ext	ht.G_ext_u+ht.G_ext_d	W/m ²	External irradiation	Boundaries 134, 310, 486, 662, 838
ht.G_rad	ht.Gm+ht.Gamb+ht.G_ext	W/m ²	Surface irradiation	Boundaries 134, 310, 486, 662, 838
ht.Famb_gp	root.comp1.ht.radGpEval(ht.Famb)	1	Ambient view factor, Gauss point evaluation	Boundaries 134, 310, 486, 662, 838
ht.Jinit	ht.feb(ht.Tinit)*ht.epsilon_rad+(1-ht.epsilon_rad)*ht.e_bamb	W/m ²	Initial surface radiosity	Boundaries 134, 310, 486, 662, 838
ht.Jdef	ht.epsilon_rad*ht.e_b	W/m ²	Surface radiosity expression	Boundaries 134, 310, 486, 662, 838
ht.e_b	ht.feb(ht.T)	W/m ²	Blackbody emissive power	Boundaries 134, 310, 486, 662, 838
ht.e_bamb	ht.feb(ht.Tamb)	W/m ²	Ambient blackbody emissive power	Boundaries 134, 310, 486, 662, 838
ht.Gamb	ht.Famb*ht.e_bamb	W/m ²	Ambient irradiation	Boundaries 134, 310, 486, 662, 838

Name	Expression	Unit	Description	Selection
ht.alpha_rad	ht.epsilon_rad	1	Absorptivity	Boundaries 134, 310, 486, 662, 838
ht.rho_r	1-ht.epsilon_rad	1	Reflectivity	Boundaries 134, 310, 486, 662, 838
ht.J_plot	try_catch(ht.J,NaN)	W/m^2	Surface radiosity	Boundaries 134, 310, 486, 662, 838
ht.Ju_plot	try_catch(Ju,NaN)	W/m^2	Upside radiosity	Boundaries 134, 310, 486, 662, 838
ht.Jd_plot	try_catch(Jd,NaN)	W/m^2	Downside radiosity	Boundaries 134, 310, 486, 662, 838
ht.ds3.rflux	-ht.Jdef+ht.epsilon_rad*ht.G_rad	W/m^2	Radiative heat flux	Boundaries 134, 310, 486, 662, 838

Selection

Geometric entity level	Boundary
Selection	Boundaries 134, 310, 486, 662, 838

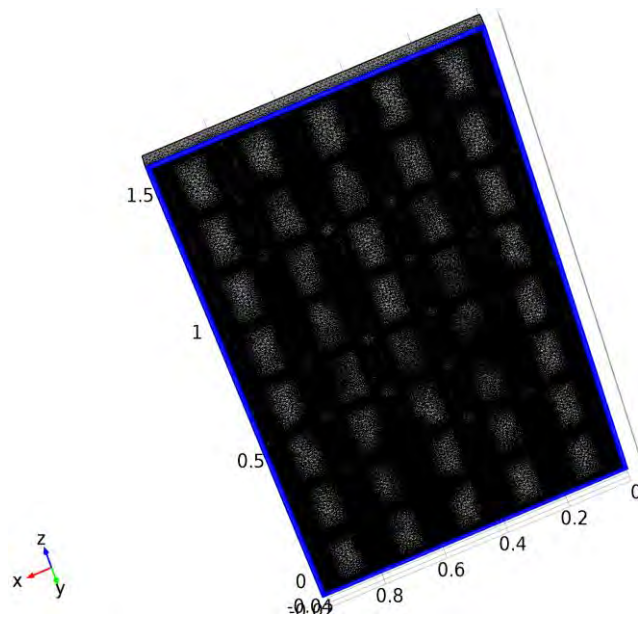
Settings

Description	Value
Heat source	General source
Boundary heat source	User defined
Boundary heat source	-q_out
Source position	Layer

Variables

Name	Expression	Unit	Description	Selection
ht.Qbtot	ht.bhs1.Qb	W/m ²	Total boundary heat source	Boundaries 134, 310, 486, 662, 838
ht.bhs1.Qb	subst(-q_out,T,at2(x,y,z,ht.bhs1.Tvar))	W/m ²	Boundary heat source	Boundaries 134, 310, 486, 662, 838
ht.bhs1.Tvar	0.5*(ht.Tu+ht.Td)	K	Temperature	Boundaries 134, 310, 486, 662, 838
ht.bhs1.ntfluxInt	ht.bhs1.intExtBnd(ht.ntflux*ht.bhs1.varIntSpa)	W	Total net heat rate	Global
ht.bhs1.ntefluxInt	ht.bhs1.intExtBnd(ht.nteflux*ht.bhs1.varIntSpa)	W	Total net energy rate	Global
ht.bhs1.ntfluxInt_u	ht.bhs1.intIntBnd(ht.ntflux_u*ht.bhs1.varIntSpa)	W	Total net heat rate, upside	Global
ht.bhs1.ntefluxInt_u	ht.bhs1.intIntBnd(ht.nteflux_u*ht.bhs1.varIntSpa)	W	Total net energy rate, upside	Global
ht.bhs1.ntfluxInt_d	ht.bhs1.intIntBnd(ht.ntflux_d*ht.bhs1.varIntSpa)	W	Total net heat rate, downside	Global
ht.bhs1.ntefluxInt_d	ht.bhs1.intIntBnd(ht.nteflux_d*ht.bhs1.varIntSpa)	W	Total net energy rate, downside	Global
ht.bhs1.Tave	if(ht.bhs1.intBnd(ht.bhs1.varIntSpa*ht.rho*ht.Cp*(ht.ux*ht.nx+ht.uy*ht.ny+ht.uz*ht.nz))==0,ht.bhs1.intBnd(ht.bhs1.varIntSpa*T)/ht.bhs1.intBnd(ht.bhs1.varIntSpa),ht.bhs1.intBnd(ht.bhs1.varIntSpa*ht.rho*ht.Cp*T*(ht.ux*ht.nx+ht.uy*ht.ny+ht.uz*ht.nz))/ht.bhs1.intBnd(ht.bhs1.varIntSpa*ht.rho*ht.Cp*(ht.ux*ht.nx+ht.uy*ht.ny+ht.uz*ht.nz)))	K	Weighted average temperature	Global

Meshing - PV Cell



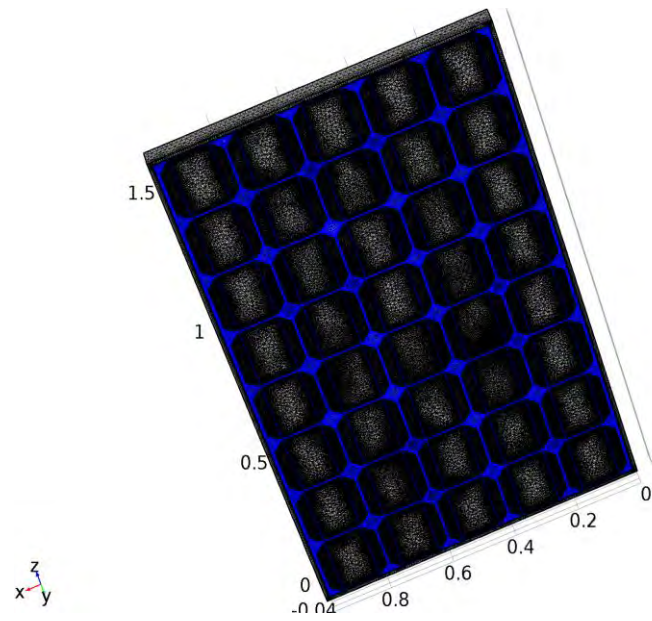
B-4: Meshing of the 3D modelled Yingli PV solar panel.

Settings

Description	Value
Maximum element size	0.016
Minimum element size	0.0014
Curvature factor	0.3
Resolution of narrow regions	0.5
Resolution of narrow regions	Off
Maximum element growth rate	1.3
Custom element size	Custom

PV Fins (size3) - Selection

Geometric entity level	Boundary
Selection	Boundary 20



B-4: Meshing of the fins of the 3D modelled Yingli PV solar panel.

Stationary Solver 1 in Solution 1 started at 29-Apr-2016 03:02:12.
Continuation solver
Nonlinear solver
Number of degrees of freedom solved for: 3005111 (plus 2683152 internal DOFs)
.

Continuation parameter T_Room = 298.15.
Nonsymmetric matrix found.
Scales for dependent variables:
Temperature (compl.T): 2.9e+002
Surface radiosity (compl.ht.J): 1.5e+006
Orthonormal null-space function used.

Iter	SolEst	ResEst	Damping	Stepsize	#Res	#Jac	#Sol	LinIt	L
inErr	LinRes								
1	3.7	8e+007	0.0100000	3.7	2	1	2	2	
0.037	0.0012								
2	1.9	2e+004	0.1000000	2.1	3	2	5	7	0.
00014	2.4e-006								
3	0.00071	2.8e+002	1.0000000	0.42	4	3	8	10	
0.093	0.0018								
4	1.6e-								
009	0.19	1.0000000	0.00071	5	4	11	45	0.12	0.01
4									

Continuation parameter T_Room = 308.15.

Iter	SolEst	ResEst	Damping	Stepsize	#Res	#Jac	#Sol	LinIt	L
inErr	LinRes								
1	5.9e-								
006	21	1.0000000	0.0034	8	5	15	63	0.11	0.001
4									

Continuation parameter T_Room = 318.15.

Iter	SolEst	ResEst	Damping	Stepsize	#Res	#Jac	#Sol	LinIt	L
inErr	LinRes								
1	5e-								
006	7.7	1.0000000	0.0081	11	6	19	89	0.1	0.003
8									

Continuation parameter T_Room = 328.15.

Iter	SolEst	ResEst	Damping	Stepsize	#Res	#Jac	#Sol	LinIt	L
inErr	LinRes								
1	1.4e-								
005	32	1.0000000	0.0071	14	7	23	123	0.094	0.01
2									

Continuation parameter T_Room = 338.15.

Iter	SolEst	ResEst	Damping	Stepsize	#Res	#Jac	#Sol	LinIt	L
inErr	LinRes								
1	0.00087	2e+002	1.0000000	0.0094	17	8	27	157	
0.099	0.016								

Continuation parameter T_Room = 348.15.

Iter	SolEst	ResEst	Damping	Stepsize	#Res	#Jac	#Sol	LinIt	L
inErr	LinRes								
1	0.054	1.4e+004	0.0010000	0.051	23	9	34	172	1.6
e-011	6.2								
2	0.045	1.4e+004	0.0031199	0.045	24	10	36	175	
0.018	6.9								

3	0.055	1.4e+004	0.0038737	0.055	25	11	38	177	1.1
e-013	16								
4	0.083	1.4e+004	0.0062394	0.085	26	12	40	179	1.6
e-006	27								
5	1.8	1.5e+004	0.0010000	1.7	27	13	42	181	5.8
e-013	1.3e+002								
6	0.45	1.9e+006	0.0066319	0.45	28	14	44	183	2.6
e-013	2.6								
7	0.49	1.9e+006	0.0055687	0.5	29	15	46	205	
0.098	0.013								
8	0.35	1.9e+006	0.0174639	0.36	30	16	48	208	
0.12	0.015								
9	0.26	1.6e+006	0.1746386	0.32	31	17	51	210	0
.0056	0.12								
10	0.56	1.5e+006	0.0174639	0.57	32	18	53	222	
0.11	0.0023								
11	0.28	1.5e+006	0.0607394	0.3	33	19	56	228	
0.017	0.01								
12	0.15	1.2e+006	0.2308518	0.19	34	20	58	232	
0.042	0.069								
13	0.14	1.1e+006	0.0684906	0.15	36	21	61	235	
0.081	0.3								
14	0.35	1.1e+006	0.0069848	0.33	37	22	63	237	3.8
e-006	1.6								
15	0.21	1.4e+007	0.0698476	0.23	38	23	65	239	4.7
e-014	1								
16	0.17	3.6e+007	0.0226292	0.17	40	24	68	242	0.
00071	19								
17	12	3.6e+007	0.0022629	12	41	25	70	253	
0.089	0.32								
18	3.9	3.6e+007	0.0132122	4	42	26	72	255	7.7
e-011	1.8								
19	5.1	4e+007	0.0013212	12	43	27	74	257	1.2
e-007	5.1								
20	3.9	4e+007	0.0011296	3.9	44	28	76	297	
0.11	0.039								
21	2.4	4e+007	0.0015444	2.4	45	29	78	318	
0.12	0.0052								
22	4.8	3.9e+007	0.0010000	4.8	46	30	80	326	
0.073	0.0058								
23	4.1	3.9e+007	0.0011734	4.1	47	31	82	328	
0.039	0.02								
24	2.2	3.9e+007	0.0014770	2.2	48	32	84	346	
0.12	0.0051								
25	2.6	3.9e+007	0.0147704	2.7	49	33	86	348	
0.027	0.02								
26	2	3.8e+007	0.0085183	2	50	34	88	368	
0.11	0.0048								
27	2.6	3.8e+007	0.0058017	2.6	51	35	90	380	
0.12	0.0041								
28	0.81	3.8e+007	0.0090990	0.82	52	36	92	400	
0.12	0.0027								
29	0.69	3.7e+007	0.0138427	0.7	53	37	94	409	
0.12	0.0064								
30	0.69	3.6e+007	0.0430986	0.73	54	38	96	418	
0.05	0.0053								
31	0.72	3.4e+007	0.0430986	0.75	56	39	99	421	
0.019	0.039								

32	1	3.4e+007	0.0027616	1	58	40	102	426	0
.0042	0.076								
33	1	3.4e+007	0.0010000	1	59	41	104	427	
0.013	0.087								
34	1	3.4e+007	0.0027367	1	60	42	106	429	2.9
e-014	0.11								
35	3.3	3.4e+007	0.0010000	3.3	61	43	108	438	
0.057	0.023								
36	2.1	3.4e+007	0.0096145	2.2	62	44	110	440	
0.095	0.035								
37	1.4	3.3e+007	0.0096145	1.4	64	45	113	444	
0.084	0.13								
38	0.48	3e+007	0.0961449	0.53	65	46	115	447	0
.0089	1.1								
39	0.69	3e+007	0.0096145	0.81	66	47	117	449	5.7
e-007	5.6								
40	5.6	3e+007	0.0010000	5.6	67	48	119	452	
0.12	9.5								
41	33	3e+007	0.0010000	33	68	49	121	468	
0.087	0.14								
42	13	3e+007	0.0018967	13	69	50	123	474	
0.038	0.076								
43	4.1	3e+007	0.0189674	4.1	70	51	125	476	0
.0019	0.35								
44	4.6	3e+007	0.0020466	4.6	72	52	128	480	
0.016	8								
45	3.5	2.9e+007	0.0056288	3.5	73	53	130	482	1.3
e-015	10								
46	20	3e+007	0.0010000	20	74	54	132	490	
0.006	85								
47	22	3.5e+007	0.0010000	22	75	55	134	495	0
.0023	2.1e+002								

Continuation parameter T_Room = 340.65.

Iter	SolEst	ResEst	Damping	Stepsize	#Res	#Jac	#Sol	LinIt	L
inErr	LinRes								
1	0.0091	1.4e+003	1.0000000	0.06	78	57	139	515	
0.098	0.019								
2	0.0019	1.4e+002	1.0000000	0.013	79	58	142	530	
0.098	0.0059								
3	0.00037	4.6	1.0000000	0.0038	80	59	145	549	
0.076	0.0014								

Continuation parameter T_Room = 345.65.

Iter	SolEst	ResEst	Damping	Stepsize	#Res	#Jac	#Sol	LinIt	L
inErr	LinRes								
1	0.029	4.6e+003	1.0000000	0.26	83	60	149	579	
0.1	0.0017								
2	0.0039	1.5e+003	1.0000000	0.012	84	61	152	592	
0.059	0.0036								
3	0.00094	2.2e+002	1.0000000	0.0061	85	62	155	598	
0.046	0.0046								

Continuation parameter T_Room = 348.15.

Iter	SolEst	ResEst	Damping	Stepsize	#Res	#Jac	#Sol	LinIt	L
inErr	LinRes								
1	0.0045	2.3e+005	1.0000000	0.053	88	63	159	608	
0.057	0.0014								

2	0.003	1.1e+005	1.0000000	0.011	89	64	162	614
0.034	0.0025							
3	0.0023	3.5e+004	1.0000000	0.0079	90	65	165	620
0.027	0.0026							
4	0.0019	1.1e+004	1.0000000	0.0063	91	66	168	626
0.024	0.002							
5	0.0018	3.7e+003	0.9987456	0.0056	92	67	171	632
0.021	0.0014							
6	0.0019	1.3e+003	0.9061683	0.0053	93	68	173	638
0.016	0.00088							
7	0.0017	4.5e+002	0.9043539	0.0052	94	69	176	643
0.018	0.0022							
8	0.00072	79	1.0000000	0.0043	95	70	179	648
0.031	0.0063							

Continuation parameter T_Room = 349.4.

Iter	SolEst	ResEst	Damping	Stepsize	#Res	#Jac	#Sol	LinIt	L
inErr	LinRes								
1	0.0022	1.6e+005	1.0000000	0.0076	98	71	183	657	
0.026	0.0035								
2	0.0019	8.1e+004	0.9965928	0.0062	99	72	186	662	
0.024	0.0022								
3	0.0017	2.7e+004	1.0000000	0.0054	100	73	189	668	
0.02	0.001								
4	0.0017	9.1e+003	0.9517579	0.005	101	74	191	674	
0.017	0.0011								
5	0.0014	2.7e+003	0.9502275	0.0047	102	75	194	678	
0.12	0.0089								
6	0.00043	3.8e+002	1.0000000	0.0032	103	76	197	684	
0.042	0.0092								

Continuation parameter T_Room = 350.025.

Iter	SolEst	ResEst	Damping	Stepsize	#Res	#Jac	#Sol	LinIt	L
inErr	LinRes								
1	0.0016	3.4e+004	1.0000000	0.0055	106	77	201	693	
0.024	0.0011								
2	0.0014	1.4e+004	0.9888190	0.0048	107	78	204	698	
0.024	0.0033								
3	0.00058	2.2e+003	1.0000000	0.0036	108	79	207	704	
0.032	0.0059								

Continuation parameter T_Room = 351.275.

Iter	SolEst	ResEst	Damping	Stepsize	#Res	#Jac	#Sol	LinIt	L
inErr	LinRes								
1	0.002	1.6e+005	1.0000000	0.0065	111	80	211	713	
0.034	0.0033								
2	0.0017	8e+004	1.0000000	0.0055	112	81	214	719	
0.026	0.0013								
3	0.0015	2.6e+004	1.0000000	0.0048	113	82	217	725	
0.022	0.00041								
4	0.0017	1.1e+004	0.8348808	0.0043	114	83	219	730	
0.015	0.00088								
5	0.0012	2.7e+003	1.0000000	0.0047	115	84	222	735	
0.023	0.0047								
6	0.00023	2.9e+002	1.0000000	0.0024	116	85	225	742	
0.051	0.012								

Continuation parameter T_Room = 351.9.

Iter	SolEst	ResEst	Damping	Stepsize	#Res	#Jac	#Sol	LinIt	L
inErr	LinRes								
1	0.0014	1.1e+004	1.0000000	0.0052	119	86	229	751	
0.024	0.0031								
2	0.00061	2.4e+003	1.0000000	0.0038	120	87	232	757	
0.029	0.0046								

Continuation parameter T_Room = 353.15.

Iter	SolEst	ResEst	Damping	Stepsize	#Res	#Jac	#Sol	LinIt	L
inErr	LinRes								
1	0.002	1.7e+005	1.0000000	0.0066	123	88	236	766	
0.039	0.0033								
2	0.0017	8.4e+004	1.0000000	0.0057	124	89	239	772	
0.03	0.0013								
3	0.0015	2.8e+004	1.0000000	0.0048	125	90	242	778	
0.024	0.0004								
4	0.0017	1.1e+004	0.8429184	0.0043	126	91	244	783	
0.015	0.00059								
5	0.0012	3.1e+003	0.9871648	0.0044	127	92	247	787	
0.12	0.021								
6	0.00035	3.7e+002	1.0000000	0.0028	128	93	250	793	
0.039	0.0069								

Continuation parameter T_Room = 353.775.

Iter	SolEst	ResEst	Damping	Stepsize	#Res	#Jac	#Sol	LinIt	L
inErr	LinRes								
1	0.0016	2.3e+004	1.0000000	0.0053	131	94	254	802	
0.027	0.0013								
2	0.0013	8.3e+003	1.0000000	0.005	132	95	257	807	
0.027	0.005								
3	0.00029	9.1e+002	1.0000000	0.0026	133	96	260	813	
0.053	0.0084								

Continuation parameter T_Room = 355.025.

Iter	SolEst	ResEst	Damping	Stepsize	#Res	#Jac	#Sol	LinIt	L
inErr	LinRes								
1	0.0017	4.8e+004	1.0000000	0.0056	136	97	264	822	
0.054	0.0017								
2	0.0015	2.4e+004	1.0000000	0.0049	137	98	267	828	
0.03	0.0007								
3	0.0014	7.3e+003	0.9507957	0.0045	138	99	270	832	
0.12	0.023								
4	0.00048	1e+003	1.0000000	0.0033	139	100	273	838	
0.044	0.0056								

Continuation parameter T_Room = 357.525.

Iter	SolEst	ResEst	Damping	Stepsize	#Res	#Jac	#Sol	LinIt	L
inErr	LinRes								
1	0.0024	2.5e+005	1.0000000	0.0073	142	101	277	848	
0.12	0.0092								
2	0.0023	1.4e+005	0.9180930	0.0066	143	102	279	854	
0.076	0.0012								
3	0.0017	4.4e+004	1.0000000	0.0058	144	103	282	860	
0.08	0.00036								
4	0.0015	1.4e+004	1.0000000	0.0048	145	104	285	866	
0.04	0.0004								
5	0.0015	5e+003	0.9484756	0.0043	146	105	287	872	
0.021	0.0005								

6	0.0017	2e+003	0.8270721	0.0042	147	106	289	876
0.11	0.03							
7	0.001	4.6e+002	1.0000000	0.0044	148	107	292	881
0.02	0.004							
8	0.00013	39	1.0000000	0.0019	149	108	295	888
0.076	0.015							

Continuation parameter T_Room = 358.15.

Iter	SolEst	ResEst	Damping	Stepsize	#Res	#Jac	#Sol	LinIt	L
inErr	LinRes								
1	0.001	3.8e+003	1.0000000	0.0048	152	109	299	897	
0.029	0.003								
2	0.0001	4.6e+002	1.0000000	0.0017	153	110	302	905	
0.097	0.02								

Continuation parameter T_Room = 360.65.

Iter	SolEst	ResEst	Damping	Stepsize	#Res	#Jac	#Sol	LinIt	L
inErr	LinRes								
1	0.0017	7.1e+003	1.0000000	0.006	156	111	306	915	
0.071	0.003								
2	0.0015	3.8e+003	1.0000000	0.005	157	112	309	920	
0.056	0.0037								
3	0.00074	7.5e+002	1.0000000	0.004	158	113	312	925	
0.09	0.0097								

Continuation parameter T_Room = 365.65.

Iter	SolEst	ResEst	Damping	Stepsize	#Res	#Jac	#Sol	LinIt	L
inErr	LinRes								
1	0.0034	3.1e+005	1.0000000	0.011	161	114	316	936	
0.067	0.0048								
2	0.003	1.5e+005	1.0000000	0.0094	162	115	319	944	
0.07	0.0063								
3	0.0028	5e+004	0.9725283	0.0084	163	116	321	952	
0.033	0.0028								
4	0.0026	1.7e+004	0.9345478	0.0076	164	117	323	958	
0.054	0.0067								
5	0.0021	5.5e+003	0.9913337	0.0067	165	118	326	964	
0.12	0.0048								
6	0.0017	1.8e+003	0.9899366	0.0056	166	119	329	971	
0.032	9.3e-005								
7	0.0015	5.8e+002	1.0000000	0.0047	167	120	332	977	
0.061	0.00088								
8	0.0015	2.1e+002	0.9440710	0.0042	168	121	334	983	
0.028	0.00083								
9	0.0018	89	0.7862639	0.004	169	122	336	988	
0.015	0.00042								
10	0.0014	29	0.9305750	0.0042	170	123	338	992	
0.11	0.028								
11	0.0006	4.7	1.0000000	0.0035	171	124	341	997	
0.03	0.0049								

Continuation parameter T_Room = 368.15.

Iter	SolEst	ResEst	Damping	Stepsize	#Res	#Jac	#Sol	LinIt	L
inErr	LinRes								
1	0.0025	2.7e+005	1.0000000	0.0077	174	125	345	1008	
0.04	0.00097								
2	0.0026	1.6e+005	0.8645696	0.0069	175	126	347	1014	
0.088	0.0037								

3	0.0019	5e+004	1.0000000	0.0063	176	127	350	1021
0.021	0.00035							
4	0.0016	1.6e+004	1.0000000	0.0053	177	128	353	1027
0.095	0.0011							
5	0.0014	5.3e+003	1.0000000	0.0045	178	129	356	1033
0.039	0.0011							
6	0.0017	2.3e+003	0.8029421	0.004	179	130	358	1038
0.014	0.00031							
7	0.0015	8.3e+002	0.8889429	0.0042	180	131	360	1042
0.12	0.034							
8	0.00088	1.7e+002	1.0000000	0.0041	181	132	363	1047
0.019	0.0032							

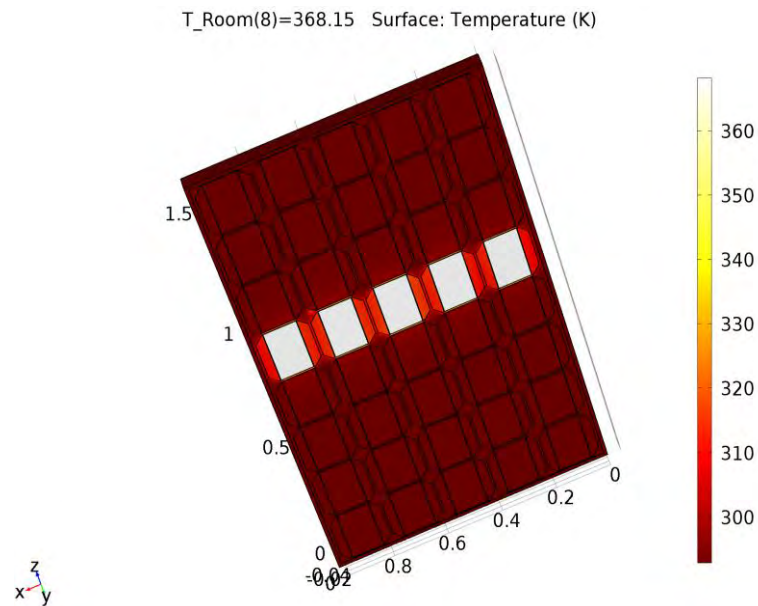
Stationary Solver 1 in Solution 1: Solution time: 352625 s (4 days, 1 hour, 57 minutes, 5 seconds)

Physical memory: 16.22 GB

Virtual memory: 27.1 GB

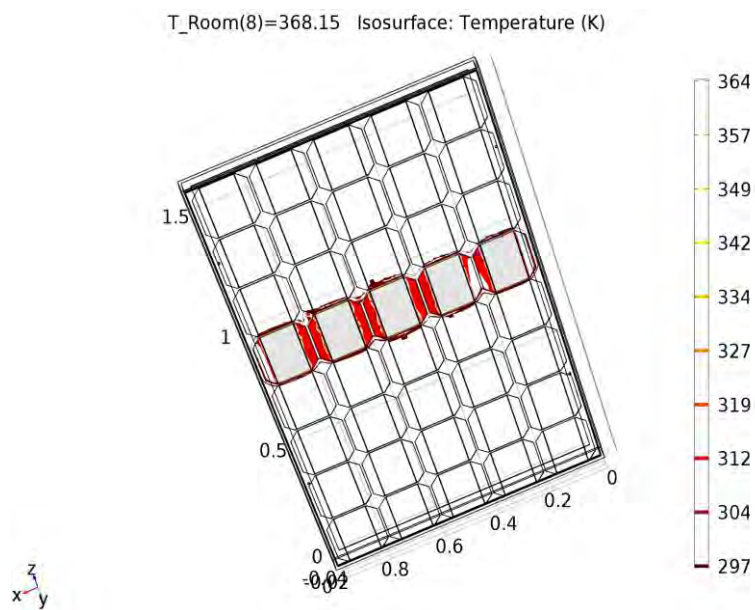
Plot Groups

Temperature (ht)

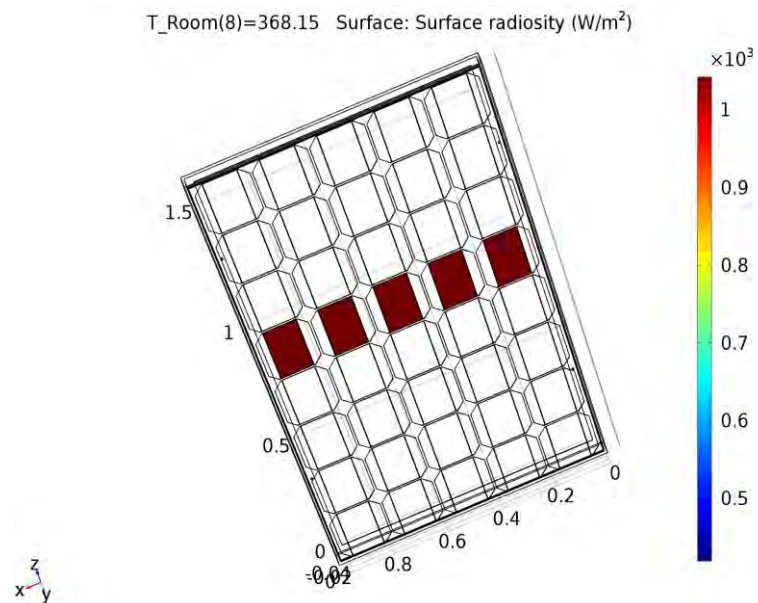


B-4: Temperature distribution in the 3D modelled Yingli PV solar panel, ranging from 300 K to 360 K

Isothermal Contours (ht)



Radiosity (ht)



T_Room(8)=368.15 Surface: Surface radiosity (W/m²) - Upside and downside radiosity (W/m²)

APPENDIX C

PHYSICS DESCRIBING THE THREE DIFFERENT MODES OF HEAT TRANSFER IN THE PV PANEL

The summary of the governing physics is presented in Table 4-6. The various physics were applied in the modelling work and the equations governing the applications are put in tabular form as indicated in Table 4-6. The appropriate physics was applied to various selections such as domains, boundaries, edges and points of the materials used as it was applicable (as indicated in the table). Although the same material properties and procedural approaches were used for both the 2D and 3D CTPV modelling, as presented in Table 4-6, a different number of boundaries and domains were recorded. The generated report with details of the applied physics and other information is contained in the Appendices.

Table C-1: Governing physics for the 2D and 3D CTPV models, using heat transfer with surface-to-surface radiation

Selection	Physics Applied	Applied To	Governing Equation
Domain (Solid Part - Opaque)	Heat Transfer in Solid 1 (Heat Conduction, Solid)	PV cells and Insulation, Mirrors, Emitter and Flame	$\rho C_p u \cdot \nabla T + \nabla \cdot q = Q + Q_{ted}$ $q = -k \nabla T$, $P_A = 1 \quad [atm]$ $k, \rho, C_p =$ values are obtained from materials specifications
Boundaries	Thermal Insulation 1	All (Not Applicable)	$-n \cdot q = 0$
Domain (Solid Part - Opaque)	Heat Transfer in Fluids 1	Air (4)	$\rho C_p u \cdot \nabla T + \nabla \cdot q = Q + Q_p + Q_{vd}$ $q = -k \nabla T$, $P_A = 1 \quad [atm] =$ <i>Absolute Pressure</i> Fluid Type = Gas/Liquid $k, \rho, C_p =$ values are obtained from materials specifications

Boundaries	Diffuse Surface 1 (Surface-to-Surface Radiation)	Mirrors	$-n \cdot q = \varepsilon (G - e_b(T))$ $(1 - \varepsilon)G = J - \varepsilon e_b(T)$ $G = G_m(J) + G_{amb} + G_{ext}$ $G_{amb} = F_{amb} e_b(T_{amb})$ $e_b(T) = n^2 \sigma T^4$ $\varepsilon = User\ defined = 0.01$ <p>Surface radiosity, J_{init} in W/m^2</p>
Boundaries	Heat Flux 1 (Convective heat flux)	Insulation Boundary Outside (These are the outer boundaries of the modelling domain)	$-n \cdot q = q_0$ $q_0 = h \cdot (T_{ext} - T)$ $h = Heat\ transfer\ Coefficient = 5\ W/m^2 \cdot K$ $T_{ext} = External\ Temp. = 293.15\ [K]$ $q_0 = \frac{p_0}{A}$ $= Overall\ heat\ Transfer\ rate$
Boundaries	Diffuse Surface 2 (Surface-to-Surface Radiation)	Insulation Boundary Outside	$-n \cdot q = \varepsilon \sigma (T_{amb}^4 - T^4)$ $T_{amb} = Ambient\ Temperature = 293.15\ [K]$ $\varepsilon = Surface\ emissivity = User\ defined = 0.1$

Boundaries	Diffuse Surface 3 (Surface-to-Surface Radiation)	PV cells connecting links (These are the arc-shaped boundaries connecting the PV cells)	$-n \cdot q = \varepsilon (G - e_b(T))$ $(1 - \varepsilon)G = J - \varepsilon e_b(T)$ $G = G_m(J) + G_{amb} + G_{ext}$ $G_{amb} = F_{amb} e_b(T_{amb})$ $e_b(T) = n^2 \sigma T^4$ $T_{amb} = T \quad [K]$ $\varepsilon = \text{Surface emissivity} = \text{User defined} = 0.1$ <p>Initial Values</p> $J_{init} \quad h_t \cdot J_{init} \quad w/m^2$
Boundaries	Boundary Heat Source 1	PV Cell, Top Surface (These are the outward-facing PV-cell boundaries)	$-n \cdot q = q_0$ $Q_b = \text{User defined}$ $Q_b = 50 \left[\frac{W}{m^2 * k} \right]^*$ $Q_b = \text{Overall heat transfer rate}$ $= \frac{P_b}{A}$
Boundaries	Diffuse Surface 4 (Surface-to-Surface Radiation)	PV Cell, Inner Surface (These are the inward-facing PV-cell boundaries)	$-n \cdot q = \varepsilon (G - e_b(T))$ $(1 - \varepsilon)G = J - \varepsilon e_b(T)$

			$G = G_m (J) + G_{amb} + G_{ext}$ $G_{amb} = F_{amb} e_b (T_{amb})$ $e_b (T) = n^2 \sigma T^4$ $T_{amb} = T \quad [K]$ <p>$\varepsilon = \text{Surface emissivity} = \text{User defined} = 0.99$</p> <p>Initial Values,</p> $J_{init} (h_t \cdot J_{init}) \text{ in } W/m^2$
Boundaries	Boundary Heat Source 2	PV Cell, Inner Surfaces	$-n \cdot q = Q_b$ <p>General Source</p> $Q_b = \text{User defin} = -q_{out} \quad W/m^2$ <p>Overall heat transfer rate, $Q_b = \frac{P_b}{A}$</p>
Boundaries	Diffuse Surface 5 (Surface-to-Surface Radiation)	Emitter Outside Surface (These are the outward-facing emitter boundaries)	$-n \cdot q = \varepsilon (G - e_b(T))$ $(1 - \varepsilon)G = J - \varepsilon e_b(T)$ $G = G_m (J) + G_{amb} + G_{ext}$

			$G_{amb} = F_{amb} e_b (T_{amb})$ $e_b (T) = n^2 \sigma T^4$ $T_{amb} = T \quad [K]$ $\varepsilon = \text{Surface emissivity} =$ <i>User defined</i> = 0.99 $J_{init} = \text{Surface radiosity} =$ $(h_t \cdot J_{init}) \text{ in } W/m^2$
Boundaries	Temperature 1	Emitter Inner boundary (These are the inward facing emitter boundaries).	$T = T_0$ $T_0 = T - T_{heater} \text{ in } [K]$

APPENDIX D

PHYSICS DESCRIBING THE THREE DIFFERENT MODES OF HEAT TRANSFER IN THE PV PANEL

The PV module gains energy from solar irradiation and losses it via convection, conduction and radiation. The heat transfer with fluid-cooled PV modules utilises the application of surface-to-surface radiation because it comprises a fluid and multiple solid domains. The fluid can be water, air or any other applicable fluid. The fluid domains is the applied fluid inside the heat exchanger. Each of the material layers used in the PV module (such as the top cover, the encapsulants, the back sheet and/or any other material used) has its own separate solid domain.

Table D-1: Governing physics for the 3D PV model using heat transfer by surface-to-surface radiation

Governing Equations	Operation Description	Where applicable
$\rho C_p \mathbf{u} \cdot \nabla T + \nabla \cdot \mathbf{q} = Q + Q_{\text{ted}}$ $\mathbf{q} = -k \nabla T$	Heat Transfer by conduction and convection	Solid and fluid domains
$\rho C_p \mathbf{u} \cdot \nabla T + \nabla \cdot \mathbf{q} = Q + Q_{\text{ted}}$ $\mathbf{q} = -k \nabla T$	Heat Transfer by conduction	In Solids 1
$-\mathbf{n} \cdot \mathbf{q} = 0$	Thermal heat loss	In Insulation 1
$\rho C_p \mathbf{u} \cdot \nabla T + \nabla \cdot \mathbf{q} = Q + Q_p + Q_{\text{vd}}$ $\mathbf{q} = -k \nabla T$	Heat Transfer by convection	In Fluids 1
$-\mathbf{n} \cdot \mathbf{q} = \varepsilon(G - e_b(T))$ $(1 - \varepsilon)G = J - \varepsilon e_b(T)$ $G = G_m(J) + G_{\text{amb}} + G_{\text{ext}}$ $G_{\text{amb}} = F_{\text{amb}} e_b(T_{\text{amb}})$ $e_b(T) = \sigma T^4$	Diffuse heat by irradiation	In Surface 1
$-\mathbf{n} \cdot \mathbf{q} = q_0$	Heat Flux 1	Top and bottom layers of the PV module
$-\mathbf{n} \cdot \mathbf{q} = \varepsilon \sigma (T_{\text{amb}}^4 - T^4)$	Radiation loss	In Surface 2
$-\mathbf{n} \cdot \mathbf{q} = \varepsilon(G - e_b(T))$	Diffuse heat by irradiation	In Surface 3

$(1 - \varepsilon)G = J - \varepsilon e_b(T)$ $G = G_m(j) + G_{amb} + G_{ext}$ $G_{amb} = F_{amb} e_b(T_{amb})$ $e_b(T) = \sigma T^4$		
$-\mathbf{n} \cdot \mathbf{q} = Q_b$	Boundary Heat transfer - from Source 1	From the PV to the surrounding medium
$-\mathbf{n} \cdot \mathbf{q} = \varepsilon(G - e_b(T))$ $(1 - \varepsilon)G = J - \varepsilon e_b(T)$ $G = G_m(j) + G_{amb} + G_{ext}$ $G_{amb} = F_{amb} e_b(T_{amb})$ $e_b(T) = \sigma T^4$	Diffuse heat by irradiation	In Surface 4
$-\mathbf{n} \cdot \mathbf{q} = Q_b$	Boundary Heat Source 2	
$-\mathbf{n} \cdot \mathbf{q} = \varepsilon(G - e_b(T))$ $(1 - \varepsilon)G = J - \varepsilon e_b(T)$ $G = G_m(j) + G_{amb} + G_{ext}$ $G_{amb} = F_{amb} e_b(T_{amb})$ $e_b(T) = \sigma T^4$	Diffuse heat by irradiation	In Surface 5
$T = T_0$	Temperature 1	

Where the following symbols are as earlier defined in the LIST OF ENGINEERING AND MATHEMATICAL NOTATION

n = surface normal

ε = surface emissivity

σ = Stefan-Boltzman constant = $5.67 \times 10^{-8} \text{ W/m}^2\text{K}^4$

C_p = Specific heat capacity of the fluid (J/kg K)

k = thermal conductivity of the fluid (W/m K)

ρ = Density of film of the fluid on the front face of the PV module (kg/m^3)

u = velocity of the fluid (m/s)

p = pressure of the fluid (Pa)

μ = dynamic viscosity of the fluid on the front face of the PV module (Pa s)

q = Heat transferred by conduction (W)

Q = Internal Heat Generation (W)

μ_T = Turbulent viscosity (Pa s)

k = Turbulent kinetic energy

T_{pv} = Temperature for the surface of the module

T_{amb} = Ambient temperature

η_{elec} = Efficiency of the PV module

η_{Tref} = PV module efficiency at reference conditions

T_{pv} = Surface temperature of the PV module

β_{ref} = Thermal coefficient of the PV module

G_{amb} = Ambient irradiation (W/m².K)

Q_{vd} = Viscous dissipation ()

F = Geometric factor

F_{amb} = Geometric factor for the ambient

k_{cond} = Thermal conductivity (W/m K)